EBM Experimental Biology and Medicine

Volume 249 | Issue 5

Experimental Biology and Medicine

Chief Editor

Steven Richard Goodman
University of Tennessee Health Science Center, Memphis, USA

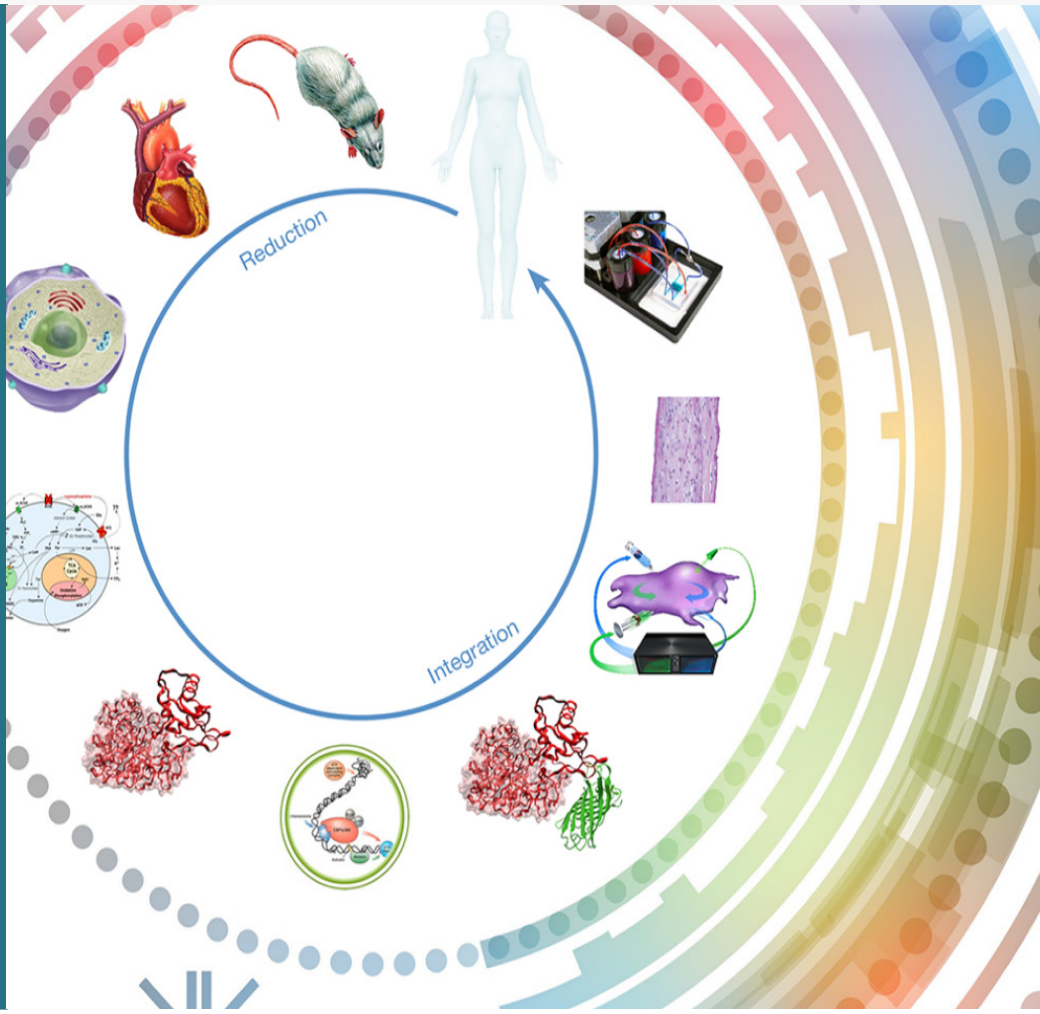

ISBN 978-2-8325-5315-2
DOI 10.3389/978-2-8325-5315-2

frontiers | Publishing Partnerships

SEBM Executive Council

Publication Committee

Society for Experimental Biology and Medicine
3220 N Street NW, #179
Washington DC 20007, USA
Executive Director – ed@sebm.org
Assistant to Editor-in-Chief – bzimmer@sebm.org

www.sebm.org

EBM Experimental Biology and Medicine

Editorial Board

ISSN 1535-3699
ISBN 978-2-8325-5315-2
DOI 10.3389/978-2-8325-5315-2

EBM Experimental Biology and Medicine

2024 | Volume 249 | Issue 5 | ISSN 1535-3699

Table of contents

Pharmacology and Toxicology

Feature

Original Research

Physiology and Pathophysiology

Highlight

Review

Retraction

EBM Experimental Biology and Medicine

TYPE Original Research
PUBLISHED 24 July 2024
DOI 10.3389/ebm.2024.10070

OPEN ACCESS

*CORRESPONDENCE
Mônica Barbosa de Melo,
melomb@unicamp.br

RECEIVED 06 December 2023
ACCEPTED 08 July 2024
PUBLISHED 24 July 2024

CITATION
da Silva Costa SM, Ito MT, da Cruz PRS, De Souza BB, Rios VM, Bertozzo VdHe, Camargo ACL, Viturino MGM, Lanaro C, de Albuquerque DM, do Canto AM, Saad STO, Ospina-Prieto S, Ozelo MC, Costa FF and de Melo MB (2024), The molecular mechanism responsible for HbSC retinopathy may depend on the action of the angiogenesis-related genes *ROBO1* and *SLC38A5*. *Exp. Biol. Med.* 249:10070. doi: 10.3389/ebm.2024.10070

The molecular mechanism responsible for HbSC retinopathy may depend on the action of the angiogenesis-related genes *ROBO1* and *SLC38A5*

Sueli Matilde da Silva Costa[1], Mirta Tomie Ito[1], Pedro Rodrigues Sousa da Cruz[1], Bruno Batista De Souza[1], Vinicius Mandolesi Rios[1], Victor de Haidar e Bertozzo[1], Ana Carolina Lima Camargo[1], Marina Gonçalves Monteiro Viturino[1], Carolina Lanaro[2], Dulcinéia Martins de Albuquerque[2], Amanda Morato do Canto[3], Sara Teresinha Olalla Saad[2], Stephanie Ospina-Prieto[2], Margareth Castro Ozelo[2], Fernando Ferreira Costa[2] and Mônica Barbosa de Melo[1]*

[1]Center for Molecular Biology and Genetic Engineering, State University of Campinas—UNICAMP, Campinas, Brazil, [2]Centro de Hematologia e Hemoterapia, Universidade Estadual de Campinas—UNICAMP, Campinas, Brazil, [3]Departamento de Medicina Translacional, Faculdade de Ciências Médicas, Universidade Estadual de Campinas—UNICAMP, Campinas, Brazil

Abstract

HbSC disease, a less severe form of sickle cell disease, affects the retina more frequently and patients have higher rates of proliferative retinopathy that can progress to vision loss. This study aimed to identify differences in the expression of endothelial cell-derived molecules associated with the pathophysiology of proliferative sickle cell retinopathy (PSCR). RNAseq was used to compare the gene expression profile of circulating endothelial colony-forming cells from patients with SC hemoglobinopathy and proliferative retinopathy (n = 5), versus SC patients without retinopathy (n = 3). Real-time polymerase chain reaction (qRT-PCR) was used to validate the RNAseq results. A total of 134 differentially expressed genes (DEGs) were found. DEGs were mainly associated with vasodilatation, type I interferon signaling, innate immunity and angiogenesis. Among the DEGs identified, we highlight the most up-regulated genes *ROBO1* (log2FoldChange = 4.32, FDR = 1.35E-11) and *SLC38A5* (log2FoldChange = 3.36 FDR = 1.59E-07). *ROBO1*, an axon-guided receptor, promotes endothelial cell migration and contributes to the development of retinal angiogenesis and pathological ocular neovascularization. Endothelial *SLC38A5,* an amino acid (AA) transporter, regulates developmental and pathological retinal angiogenesis by controlling the uptake of AA nutrient, which may serve as metabolic fuel for the proliferation of endothelial cells

(ECs) and consequent promotion of angiogenesis. Our data provide an important step towards elucidating the molecular pathophysiology of PSCR that may explain the differences in ocular manifestations between individuals with hemoglobinopathies and afford insights for new alternative strategies to inhibit pathological angiogenesis.

KEYWORDS

proliferative sickle cell retinopathy, endothelial colony forming cells, transcriptome, differentially expressed genes, angiogenesis

Impact statement

Here we described genes differentially expressed identified in circulant endothelial progenitor cells from SC patients with proliferative retinopathy and their respective functional pathways. Our data, potentially related with sickle cell retinopathy, provide favorable evidence for further studies about molecular mechanisms involved in this complication. Among DEGS identified we highlight the up-regulated genes *ROBO1* and *SLC38A5*. Both genes are known to play important role in angiogenesis. We believe that these genes deserve more attention as an alternative strategy to inhibit pathological angiogenesis, hallmark of PSCR. The identification of new targets to anti-angiogenic therapy is of great interest, particularly in individuals who are resistant to current therapies.

Introduction

Sickle cell retinopathy (SCR) is the major ocular complication of sickle cell disease (SCD), occurring in non-proliferative and proliferative forms. Proliferative sickle cell retinopathy (PSCR) can lead to some degree of visual loss in 5%–20% of affected eyes [1]. This complication results from the aggregation of sickle-shaped red blood cells in the retinal microcirculation, leading to peripheral arterial occlusion, thrombosis, and ischemia, which may be precipitated by hypoxia, acidosis, and hyperosmolarity. Besides being a red blood cell disorder, the pathophysiology of vasoocclusion and tissue ischemia involves inflammation, endothelial cell activation, the presence of procoagulant and proangiogenic molecules and vasculopathy [2].

Vascular occlusion causes ischemic events leading to the release of angiogenic mediators, which may result in retinal neovascularization. The hallmark of PSCR is sea fan formations, new vessels that often assume a frond-like configuration and occur when the neovascularization grows anteriorly from the vascular to avascular retina. These structures may spontaneously regress (20%–60%) by autoinfarction [3]. However, neovascularization can adhere to the inner surface of the retina and the outer surface of the vitreous [4]. Since new blood vessels lack tight junction proteins, plasma can leak into surrounding tissue, including the vitreous, leading to vitreous degeneration and hemorrhage. In addition, the degraded vitreous can contract and pull on the retina, resulting in retinal detachment. Traction retinal detachment involving the macula results in severe vision loss [4].

Although sickle cell anemia (HbSS genotype) has the most severe systemic manifestations, patients with hemoglobin SC disease (HbSC genotype) have the most severe ocular manifestations and an earlier age of onset [2]. The reasons for this discrepancy are unknown. Blood hyperviscosity [5], lower Hb F levels [6] and lower plasma thrombospondin (TSP) levels [7], usually reported in HbSC patients, have been hypothesized to increase the risk for the development of PSCR in these patients.

Retinal neovascularization plays a crucial role in PSCR as well as in other ischemic retinopathies, such as retinopathy of prematurity (ROP) and proliferative diabetic retinopathy (PDR). Many studies in mouse models have shown that there is increased activity of hypoxia-inducible factor 1 (HIF-1) in ischemic retinopathies, causing up-regulation of several hypoxia-regulated genes associated with angiogenesis, including vascular endothelial growth factor (VEGF), essential regulator of angiogenesis and vascular permeability; angiopoietin 2 (ANGPT2), placental growth factor (PlGF), and stromal derived growth factor-1 (SDF-1) among others [4, 8, 9]. Furthermore, extra-cellular signaling pathways such as the Ephrin/Eph receptor, Netrin/UNC receptor and Robo/Slit are involved in the formation of new vessels [10].

Angiogenesis, the growth of new vessels from pre-existing vessels by sprouting endothelial cells, requires the coordinated action of a variety of angiogenic stimulators and inhibitory factors. Although a mouse model of ischemic retinopathy has widely contributed to elucidate the basis of the molecular pathogenesis involved in retinal neovascularization, the literature is still scarce regarding the molecular aspects of PSCR. The aim of the present study was to identify differences in the expressions of molecules produced by endothelial cells that may be associated with the clinical ocular heterogeneity among individuals affected by SC hemoglobinopathy. Identifying molecules associated with PSCR development may help to better elucidate pathogenic mechanisms underlying SCD-induced vision loss and establish new therapeutic targets.

We used RNA-Seq to compare the gene expression profiles of circulating endothelial colony-forming cells (ECFCs) from patients with SC hemoglobinopathy and proliferative retinopathy versus patients without retinopathy. Endothelial colony-forming cells (ECFCs), also called outgrowth endothelial cells or "late" endothelial progenitor cells (EPCs), are the most potent vascular reparative cells type among EPC. These cells are potentially capable of incorporating into foci of physiological or pathological neovascularization [11, 12]. Mouse model studies have provided evidence that ECFCs may play an important role in the regeneration of retinal vasculature and reduction of pathological angiogenesis in a model of ischemic retinopathy [13–15]. Furthermore, to elucidate molecular differences between genotypes, we investigated whether differential expression of the main genes detected in HbSC patients was also observed when HbSS patients, with and without PSCR, were compared. The results presented here, to the best of our knowledge, represent the most comprehensive analysis of comparative gene expression in human EPCs currently available.

Materials and methods

Patients

A total of 10 HbSC and 8 HbSS patients were recruited from the Hematology and Hemotherapy Center, University of Campinas-UNICAMP (Campinas, São Paulo, Brazil). Among the HbSC patients, six had PSCR (Group 1) and four had no retinopathy (Group 2). Among the HbSS patients, four had PSCR (Group 3) and no pathological ophthalmic signs were observed in four (Group 4). Hemoglobinopathy diagnosis was performed through clinical and laboratorial data. Demographic characteristics and hematological parameters were collected (Supplementary Tables S1, S2), as well as clinical data and information on drug therapy (Supplementary Tables S3, S4). It should be emphasized that, in SCD patients under regular blood transfusion therapy (such as in patients with stroke), the peripheral blood samples for isolation of ECFCs were collected immediately before transfusion, at least 15 days after the previous transfusion. All SCD patients in this study were not on hydroxycarbamide (also known as hydroxyurea) therapy or any other disease modifying therapy. After ophthalmic examinations, peripheral blood samples were collected and ECFCs cultures were carried out immediately. Exclusion criteria were malignancy, diabetes mellitus, pregnancy, painful crisis within the 2 weeks before the time of ocular examination, ocular media opacities that precluded fundoscopic examination, hydroxycarbamide therapy and previous eye surgery.

All patients provided written informed consent and the study was approved, in accordance with national guidelines, by the University Ethics Committee.

Ophthalmologic evaluation

All patients in this study underwent a complete ophthalmic examination, which included anterior biomicroscopy, fundus biomicroscopy using 78-diopter lens, indirect fundoscopy with a 20-diopter lens, color fundus photography and fluorescein angiography. The patients were examined by the same ophthalmologist at the Ophthalmology Department of the University of Campinas. In the PSCR groups (1 and 4) patients in stages III, IV and V, according to Goldberg's classification [16], were included with the following ophthalmic features: neovascularized sea fan that occurs at the boundary between the non-vascularized and vascularized zones of the retinal periphery (Stage III), presence of vitreous hemorrhage (Stage IV), tractional or rhegmatogenous retinal detachment (Stage V).

ECFC culture

Cultures of ECFCs were established from peripheral blood samples, according to previously described methods [17, 18]. Peripheral blood (45 mL) was collected in a heparinized solution and samples were processed immediately. The anticoagulated blood was diluted in 2 parts of phosphate-buffered saline solution (PBS) and then added to an equivalent volume of Ficoll-Paque PLUS (GE Healthcare, Uppsala, SE) before centrifugation at 317g for 30 min at room temperature. Mononuclear cells were isolated and washed 3 times with EBM-2 medium (Lonza, Walkersville, MD, United States) and resuspended in EBM-2 medium (Lonza, Walkersville, MD, United States) containing EGM-2 (Endothelial Cell Growth Medium-2) BulletKit™, 10% additional fetal bovine serum (Invitrogen, Carlsbad, CA, United States), 1% penicillin/streptomycin (Invitrogen, Carlsbad, CA, United States) and 1% L-glutamine (Gibco, Life Technologies, Carlsbad, California, United States). Approximately 7×10^6 cells were seeded onto twelve-well flat-bottom tissue culture plates precoated with type 1 rat-tail collagen (Sigma-Aldrich, Saint Louis, MO, United States) and cultured in a humidified incubator at 5% CO_2. After an incubation time of 7–21 days, ECFCs were identified by their typical cobblestone morphology and were evaluated for surface marker expression with a FACSCalibur (BD Bioscience, San. Jose, CA, United States). Results were analyzed using the FlowJo software (Tree Star Inc.). ECFCs were characterized by positive staining for endothelial markers CD31, CD144, CD146, VEGF/KDR; negative or low for endothelial activation antigen, CD34; negative for the myeloid cell marker, CD45, and for the endothelial progenitor marker, CD133.

RNA extraction

After reaching 80%–90% confluence, the ECFCs were harvested using 0.025% trypsin-EDTA. Total RNA was extracted from cells using

Trizol Reagent (Ambion Life Technologies, Carlsbad CA, United States), and a commercial RNeasy mini Kit (Qiagen GmbH, Hilden, Germany), according to the manufacturer's instructions. RNA was treated with DNAse I (Life Technologies, Carlsbad, CA, United States) to remove remaining genomic DNA. The quantity and purity of the extracted RNA were measured using a NanoDrop 2000 spectrophotometer (Thermo Scientific), and RNA integrity was determined using the Bioanalyzer 2100 system (Agilent Technologies).

RNA sequencing and differential gene expression analysis

RNA sequencing (RNA-Seq) was performed on the ECFC samples from SC patients, comprising five patients from Group 1 and three patients from Group 2. RNA libraries were prepared using Illumina TruSeq RNA-Seq v2 kit (Illumina, San Diego, CA, United States) according to manufacturer's protocol. After quality control by Agilent Bioanalyzer (Agilent, Santa Clara, CA), the libraries were submitted to paired-end 100 bp high output sequencing on a HiSeq 2500 instrument. Read quality was assessed by FastQC v0.11.5 [19] and aligned to human genome assembly (GRCh38.88) using STAR version 2.5.2 [20]. Only those reads uniquely mapped to the reference genome were subsequently analyzed.

Differential gene expression analysis was performed using the DESeq2 [21] R package. The FeatureCounts algorithm from Rsubread was used to generate count matrices from reads aligned to the genome [22]. To visualize the overall gene expression levels, a Volcano plot was created with log2FoldChange score and log10 *p*-values through to the EnhancedVolcano package (v1.2.0) [23]. The changes in gene expression levels were considered significant when log2FoldChange were $\geq|+1 \leq|-1|$, and statistical test values (false discovery rate—FDR—adjusted *p*-value) were lower than 0.1. Significance threshold <0.1 was set for Volcano plot to capture highly abundant marginal changes in gene expression. ClustVis [24] was used to build the heatmaps using Pearson's correlation coefficient. *PCAtools* (Principal Component Analysis) [25] of RStudio were used. The relationships between the molecular pathways and ten DEGs selected for validation demonstrated in an alluvium diagram, were performed on the Sankeymatic platform.[1]

Gene ontology (GO) and protein-protein interaction (PPI) network analysis

The PANTHER v14.1 online tool was used to perform enrichment analysis for GO Biological Processes (Fisher's exact test; FDR ≤0.05). All expressed genes (count >5) were used to build the reference list (background) and DEGs with FDR <0.1 were included in the list of analyzed genes.

Cytoscape Network Analysis (v3.8.1) was used to construct and visualize the protein-protein interaction [26]. We used StringApp [27] to search for interactions using UNIPROT IDs [28] of DEGs. The parameters used were confidence score cutoff: 0.4, maximum additional interactors = 0 and load enrichment data. Non-coding genes were excluded before loading the resulting 123 DEGs to StringApp. Additionally, to identify the protein clusters from the overall protein interaction network generated by STRING, we used Markov clustering (MCL) [29] (Granularity parameter, inflation value = 4). Functional enrichment for each cluster and enrichment map (only the gene ontology results) were performed using the following parameters: connectivity cutoff (Jaccard similarity) = 0.4, node cutoff: q-value = 0.05, Style: Q-value FDR and Radial Heat Map. Additionally, we used the Cytohubba plugin to compute different scores for protein nodes and verify the most hub gene [30]. Parameters of cytoHubba were set as follows: Hubba nodes = top 1 node ranked by Degree, display options = check the first-stage nodes and display the shortest path.

Validation by RT-PCR and expression level analysis of DEGs in HbSS patients

The quantitative real-time polymerase chain reaction (qRT-PCR) was used to validate the relative expression patterns obtained by RNA-Seq. Ten genes with log2 fold change $\geq|+1 \leq|-1|$ and FDR ≤ 0.05 were selected: five up-regulated genes, *ROBO1*, *SLC38A5, NNAT, PROX1, SEMA3B* and five down-regulated genes, *CCL2*, *CXCL10*, *GBP5*, *TGFB2* and *OASL*. These genes were selected from functional enrichment analysis due to their association with angiogenesis (FDR 1.59E-02), cell migration (FDR 1.10E-02), cell adhesion (FDR 5.77E-04), immune response (FDR 2.44E-03) and type I interferon signaling pathway (FDR 6.24E-03). To evaluate whether differential expression identified in HbSC patients was also present in HbSS patients, relative expression of these genes was also evaluated in an RNA sample of ECFCs from HbSS patients with (n = 4) and without (n = 4) retinopathy.

Complementary DNA (cDNA) was synthesized from 1 μg of RNA utilizing the RevertAid First Strand cDNA Synthesis Kit (Fermentas), according to the manufacturer's instructions. The cDNA was used as template for real-time qRT-PCR analysis using SYBR green (Applied Biosystems, United States) based detection in an ABI StepOne Plus equipment (Applied Biosystems, Carlsbad, CA). Primer sequences, annealing temperatures and product sizes are provided in Supplementary Table S5. Melting curves were examined to

1 https://sankeymatic.com/

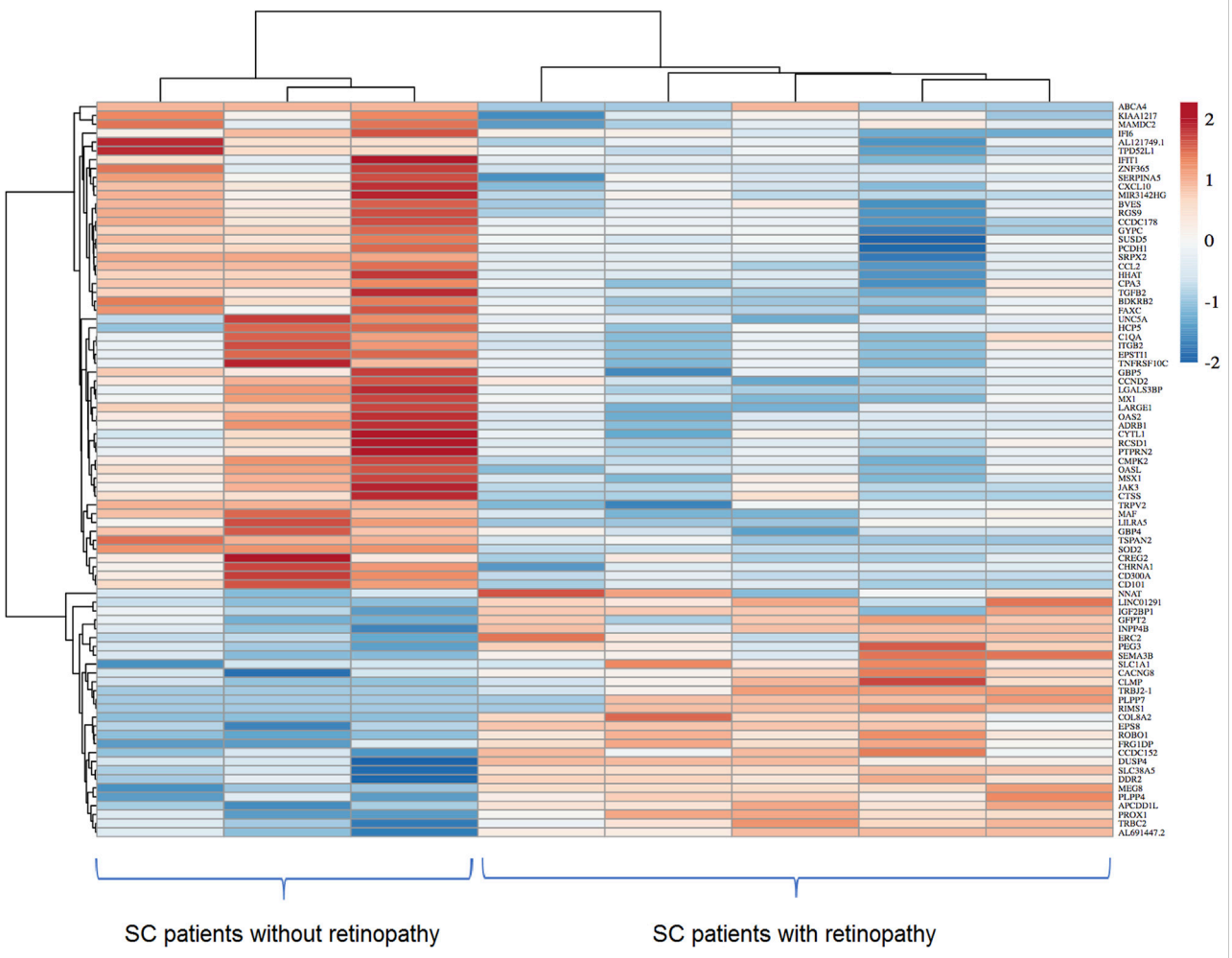

FIGURE 1
Heatmap showing differentially expressed genes identified after the comparison of ECFC transcriptomes of SC patients with and without PSCR. Differential expression threshold criteria of log2FoldChange ≥| +1 ≤|−1| and padj value < 0.05 were applied. Columns represent different samples, whereas rows represent differentially expressed genes. The intensity of the color was used to indicate the level of gene expression. The highest expression is represented by a darker red and the lowest expressions by a darker blue.

ensure single products. Briefly, the PCR amplification was carried out in a 12 µL reaction volume containing 150 or 300 nM specific primers (3 µL), 10 ng cDNA (3 µL), and 6 µL SYBR Green PCR Master Mix (Applied Biosystems, United States). All samples were run in triplicate with the following cycling conditions: 1 cycle of 95°C for 10 min, 40 cycles of 95°C for 15s, and 40 cycles of 60°C for 1 min. Results were quantified using the "delta-delta Ct" method and normalized to the constitutive genes *ACTB* and *GAPDH* transcript levels. Relative expression for each sample was calculated using the standard equation $[2^{(-\Delta Ct)}]$, as previously described by Schmittgen [31]. Delta CT values between genes of interest and GAPDH were analyzed for statistical significance using a t-test by GraphPad Prism version 5.00 for Windows (GraphPad Software, La Jolla, CA, United States).

Results

In the present study, RNA-Seq was used to characterize the ECFC transcriptomes of SC patients with (5) and without PSCR (3). After sequencing, RNAseq produced an average of 70 million 101-base pair paired-end reads per library. GC content was approximately 49%. A minimum of 88% of the bases reached a Q score of 30 (Q30), indicating low probability that a base was erroneously sequenced. A high number of reads (85%–94%) mapped exclusively to the human genome. Raw Illumina RNA-Seq FASTQ files are available in the Gene Expression Omnibus (GEO) database (Accession Number: GSE240446). All transcripts found in the comparison of the group 1 versus group 2 (26,299 variables) were depicted in a volcano plot (See Supplementary Figure S1).

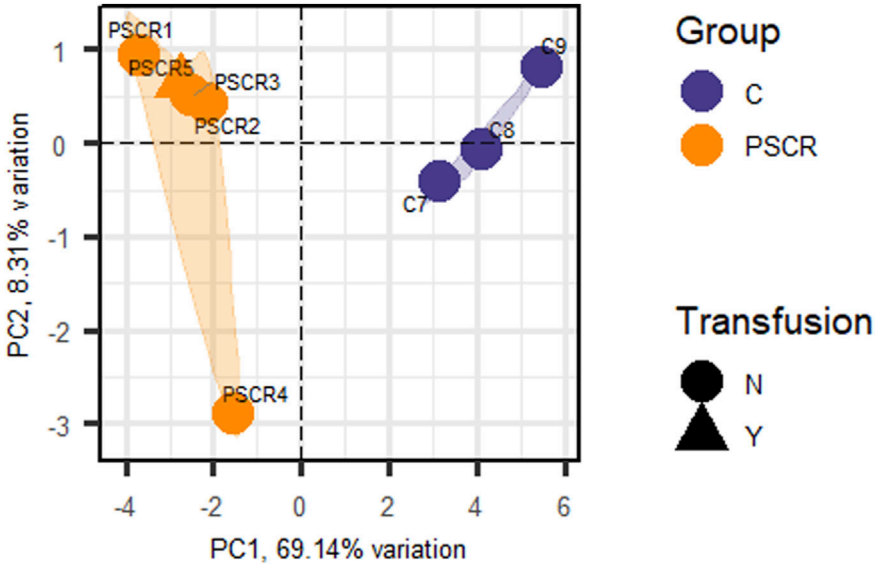

FIGURE 2
Principal Component Analysis (PCA) of the patients obtained from the DEGs (FDR <0.05) identified by RNA sequencing. Principal Component 1 (PC1) represents 69.14% of group variation, and Principal Component 2 (PC2), 8.31%. The triangular shape corresponds to individuals under transfusion treatment. PSCR, Proliferative sickle cell retinopathy; C, Controls; N, No; Y, Yes.

Identification of DEGs

Considering statistically significant FDR < 0.1, a total of 134 DEGs were found when comparing SC patients with and without PSCR. Among these genes, 36 were up-regulated and 98 were down-regulated (Supplementary Tables S6, S7). Volcano plots and GO Functional Enrichment Analysis using Panther tools were generated from FDR < 0.1. A less conservative FDR threshold was used to illustrate the general gene expression pattern detected by DESeq2 and for a broader investigation of potential interactions. When a more stringent significance threshold (FDR<0.05) was used a total of 83 DEGs were found; 28 were up-regulated and 55 were down-regulated. A graphic overview of the differential status of gene expression is represented by the heatmap in Figure 1. A distinct clustering between groups with and without PSCR is also shown in the Principal Component Analysis (PCA) (Figure 2), in which the presence or absence of PSCR explains 69.14% of total group variance.

GO functional enrichment analysis

To gain further insights into the biological functions associated with genes that were differentially expressed in SC patients with PSCR, when compared with SC patients without retinopathy, we used the Panther online tool. GO terms were assigned to 98 down-regulated and 36 up-regulated DEGs. Biological process analysis includes significantly enriched gene ontology terms associated with vasodilation, such as regulation of tube size (FDR = 3.51e-02), regulation of tube diameter (FDR = 3.56e-02), regulation of blood vessel diameter (FDR = 3.62e-02) and vascular process in circulatory system (FDR = 1.21e-02). DEGs are also enriched in terms associated with immune process such as cellular response to type I interferon (FDR = 4.87e-03), type I interferon signaling (FDR = 5.09e-03), response to type I interferon (FDR = 6.96e-03), negative regulation of viral genome replication (FDR = 3.55e-02). GO terms associated with angiogenesis as blood vessel morphogenesis (FDR = 1.64e-03) and vasculature development (FDR = 9.77e-03) are also represented (Figure 3).

Protein-protein interaction (PPI) network analysis

To better understand interactions among the DEGs, PPI network analysis was performed. All the DEGs with corresponding known protein names were analyzed using the StringApp of the Cytoscape software. After filtering the nodes without connection, the main network was generated containing 64 nodes and 151 edges (Supplementary Figure S2). To group the proteins in the clusters based on their interactions from STRING we used the Cytoscape MCL plugin. Ten clusters with three nodes or more and six clusters with only two nodes were generated and the top six clusters are shown in Figure 4. Additionally, functional enrichment analysis and enrichment maps were performed for these six clusters (Supplementary

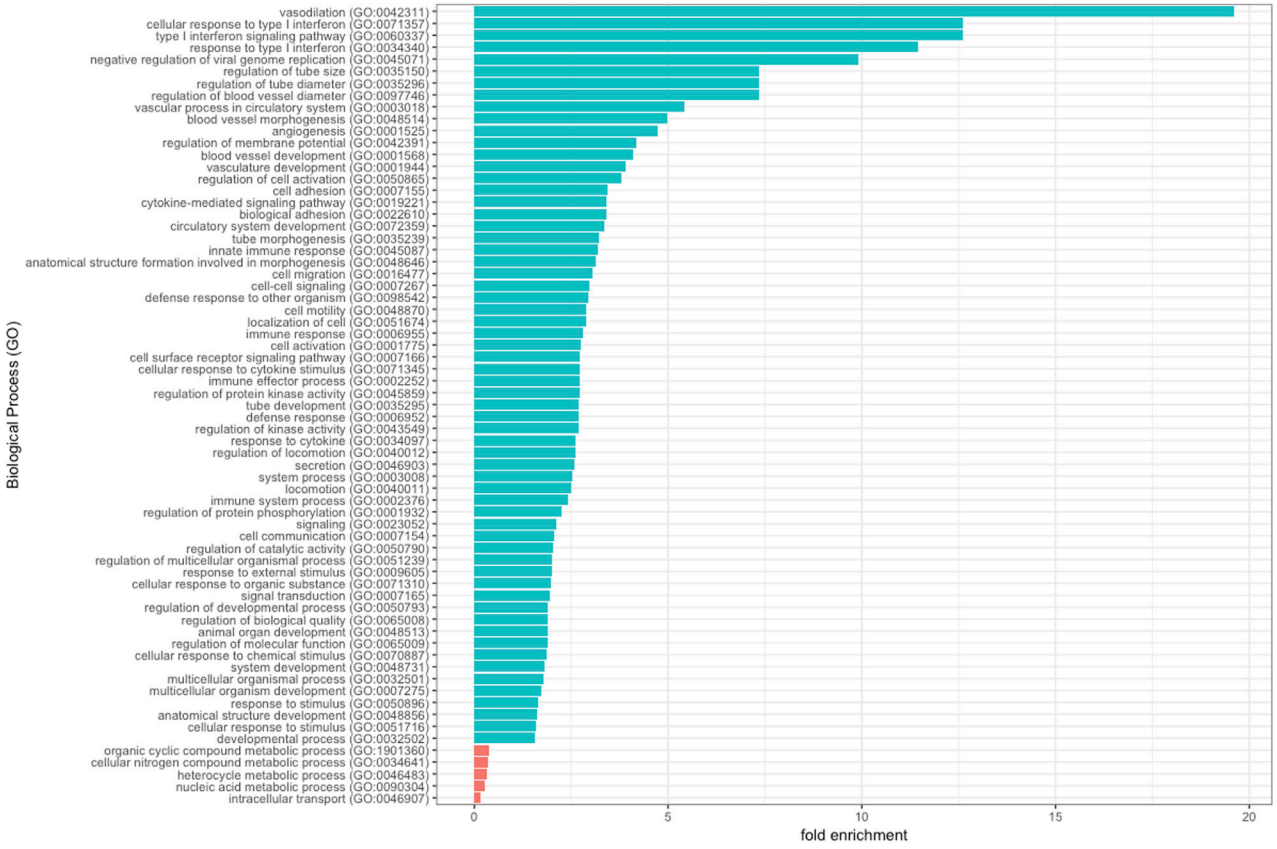

FIGURE 3
Significantly enriched GO terms of DEGs are shown. The 134 DEGs (36 up-regulated and 98 down-regulated) were enriched in biological process.

Figure S3). In these clusters, six hub genes included *IFIT1*, *ITGB2*, *ROBO1*, *BDKRB2*, *CCL2* and *COL4A1* after analysis by the Cytohubba plugin. Pathway enrichment analysis showed that Cluster 1 is mainly associated with type I interferon signaling (FDR = 1.3e-10), innate immune response (FDR = 7.72E-9), response to other organism (FDR = 7.72E-9) and cellular response to cytokine stimulus (FDR = 7.46E-7). Cluster 2 is mainly relevant with tertiary granule (FDR = 3.35E-5), immune system process (FDR = 3.79E-5) and immune response (FDR = 6.24E-5). Cluster 3 is mainly associated with axon guidance (FDR = 4.31E-5), axon guidance receptor activity (FDR = 1.1E-4), cell development (FDR = 1.2E-4) and negative chemotaxis (FDR = 9.5E-4). Cluster 4 shows the main association with G protein-coupled receptor signaling pathway (FDR = 0.0075), regulation of anatomical structure size (FDR = 0.0075) and vasoconstriction (FDR = 0.0075). Cluster 5 shows that the most significant pathways are associated with homeostatic processes (FDR = 0.0202), regulation of endothelial cell apoptotic process (FDR = 0.0202), regulation of developmental processes (FDR = 0.0292). Cluster 6: the most significant terms are extracellular matrix organization (FDR = 1.17E-5), basement membrane (FDR = 1.93E-5), collagen-activated tyrosine kinase receptor signaling pathway (FDR = 1.2E-4) and angiogenesis (6.1E-4).

Validation of expression level analysis of DEGs by qRT-PCR in HbSC and HbSS patients

To validate the RNA-seq data, the expressions of ten genes in the ECFCs from HbSC patients with and without retinopathy were verified by qRT-PCR. In the present study, we also investigated the expression levels of these same DEGs in groups III and IV (HbSS patients with and without retinopathy, respectively). The expressions of the *ROBO1*, *SLC38A5* and *NNAT* genes were significantly higher in HbSC patients with PSCR, p-value <0.05. However, *NNAT* failed to achieve this threshold value after Benjamini Hochberg (BH) adjustment of the p-value. The statistical results showed no difference in the expression levels of the same genes between HbSS patients with and without retinopathy (Figures 4A–F;

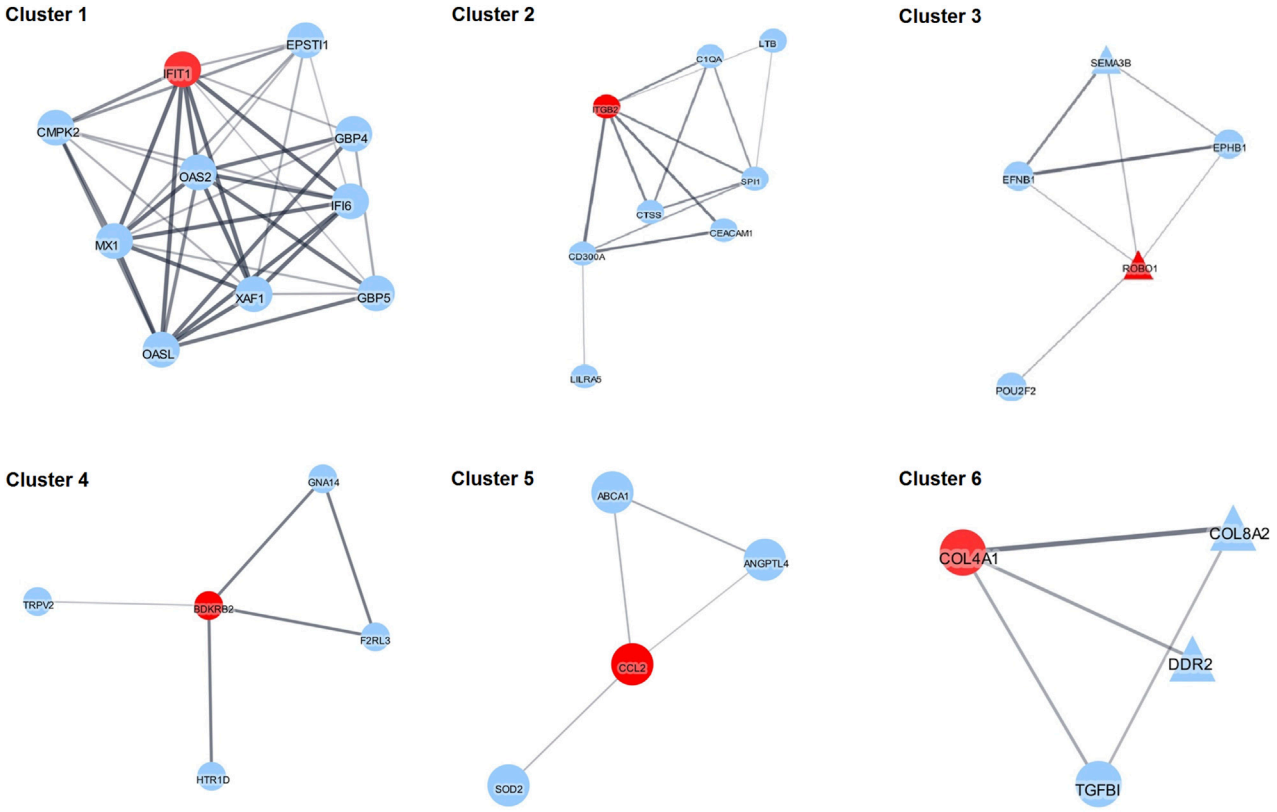

FIGURE 4
The five most significant clusters. Red nodes represent hub genes as inferred by Cytohubba. Triangles represent up-regulated and circles represent down-regulated DEGs.

Supplementary Figure S4). In addition, low levels of expression for the *CCL2, CXCL10, GBP5* and *TGFB2* genes were observed in HbSC patients with PSCR, when compared with HbSC patients without PSCR. On the other hand, no difference was observed among HbSS patients with and without PSCR (Figures 5A–H; Supplementary Figure S4). The differential expressions of the up-regulated genes, *ROBO1* and *SLC38A5,* and the down-regulated genes, *CCL2*, *CXCL10*, *GBP5* and *TGFB2*, observed in qRT-PCR are consistent with the HbSC RNAseq data. However, unlike the RNAseq results, no significant difference was detected for the up-regulated genes, *PROX1*, *SEMA3B* (Figures 5G–J; Supplementary Figure S4), and the down-regulated gene, *OASL* (Figures 6I, J; Supplementary Figure S4), when comparing HbSC patients affected or unaffected by retinopathy by qRT-PCR. Moreover, these latter genes showed no difference in expression levels between groups III and IV.

Discussion

PSCR is considered the most serious ocular complication of SCD, and can potentially result in visual loss due to vitreous hemorrhage or retinal detachment. PSCR is more frequently manifested in patients with HbSC than in other genotypes, and some degree of visual loss can occur in 5%–20% of affected eyes. The mechanisms involved in the higher incidence of ocular alterations in HbSC patients remain unclear. Considering that the neovascularization process involves the recruitment of endothelial progenitor cells, in the present study we compared, for the first time, the transcriptional profiles of ECFCs from patients with HbSC hemoglobinopathy and proliferative retinopathy versus patients without retinopathy. ECFCs, endothelial progenitor cells that circulate in peripheral blood, have a high proliferative capacity [32] and stable phenotype during *in vitro* culture and have been used as a tool for understanding the pathophysiology of vascular diseases and as a model for the study of endothelial function in sickle cell anemia [17, 33]. Emerging pre-clinical evidence underscores the therapeutic potential for ECFCs in ischemic retinopathies, such as diabetic retinopathy and retinopathy of prematurity, promoting vascular repair and revascularization [13–15].

RNA-seq was used to find DEGs, followed by functional enrichment analysis and PPI network, a common workflow in gene expression studies. The functional enrichment analysis for

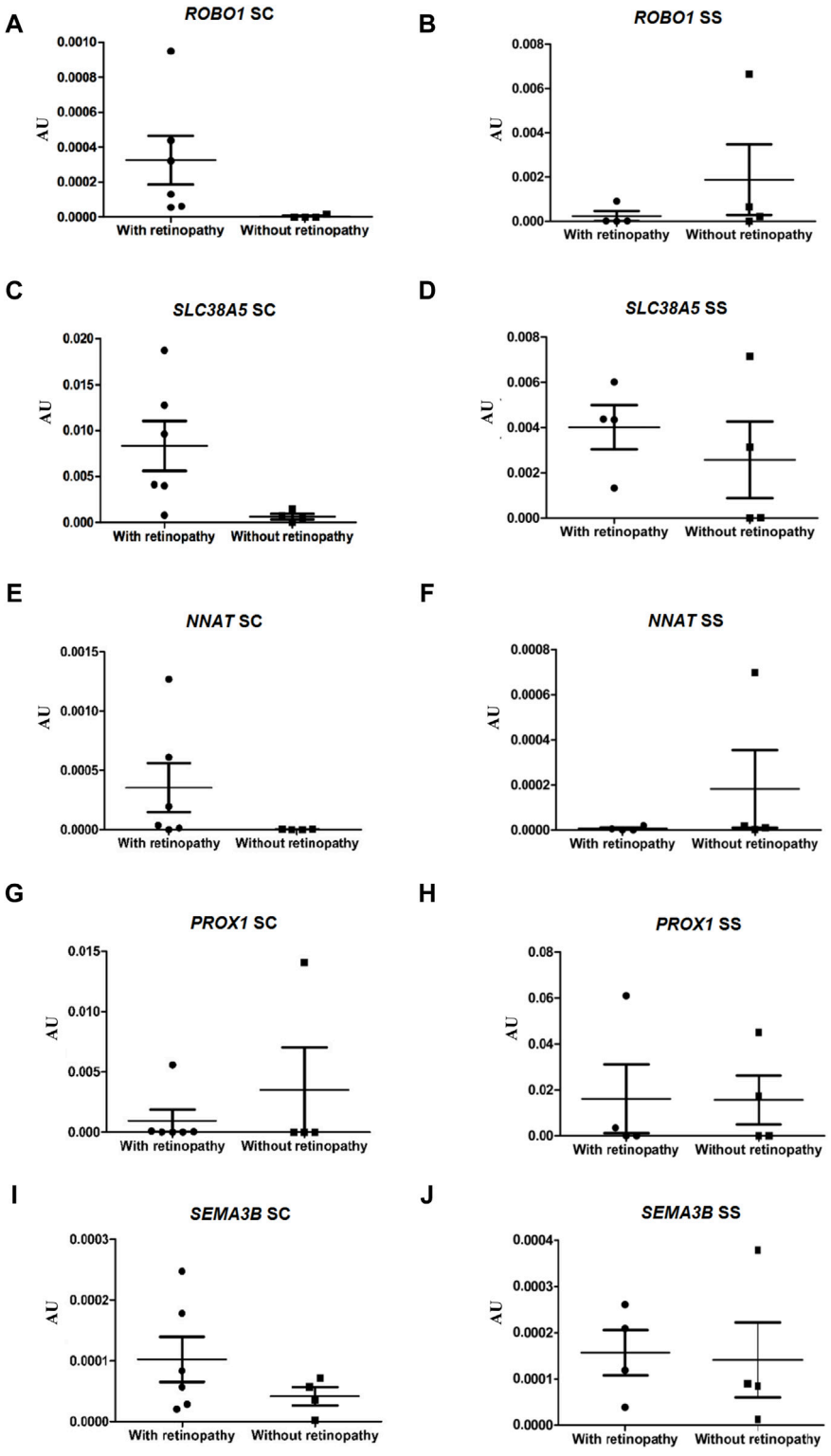

FIGURE 5
Validation of up-regulated genes, *ROBO1*, *SLC38A5*, *NNAT*, *PROX1* and *SEMA3B*, by RT-qPCR in HbSC patients and comparison of relative mRNA levels of the same genes in HbSS patients with and without retinopathy, mRNA expression was normalized to *ACTB* and *GAPDH* mRNA expression levels. Each dot represents the gene expression of an individual. AU (Arbitrary Unit). **(A,C,E,G,I)** HbSC patients. **(B,D,F,H,J)** HbSS patients.

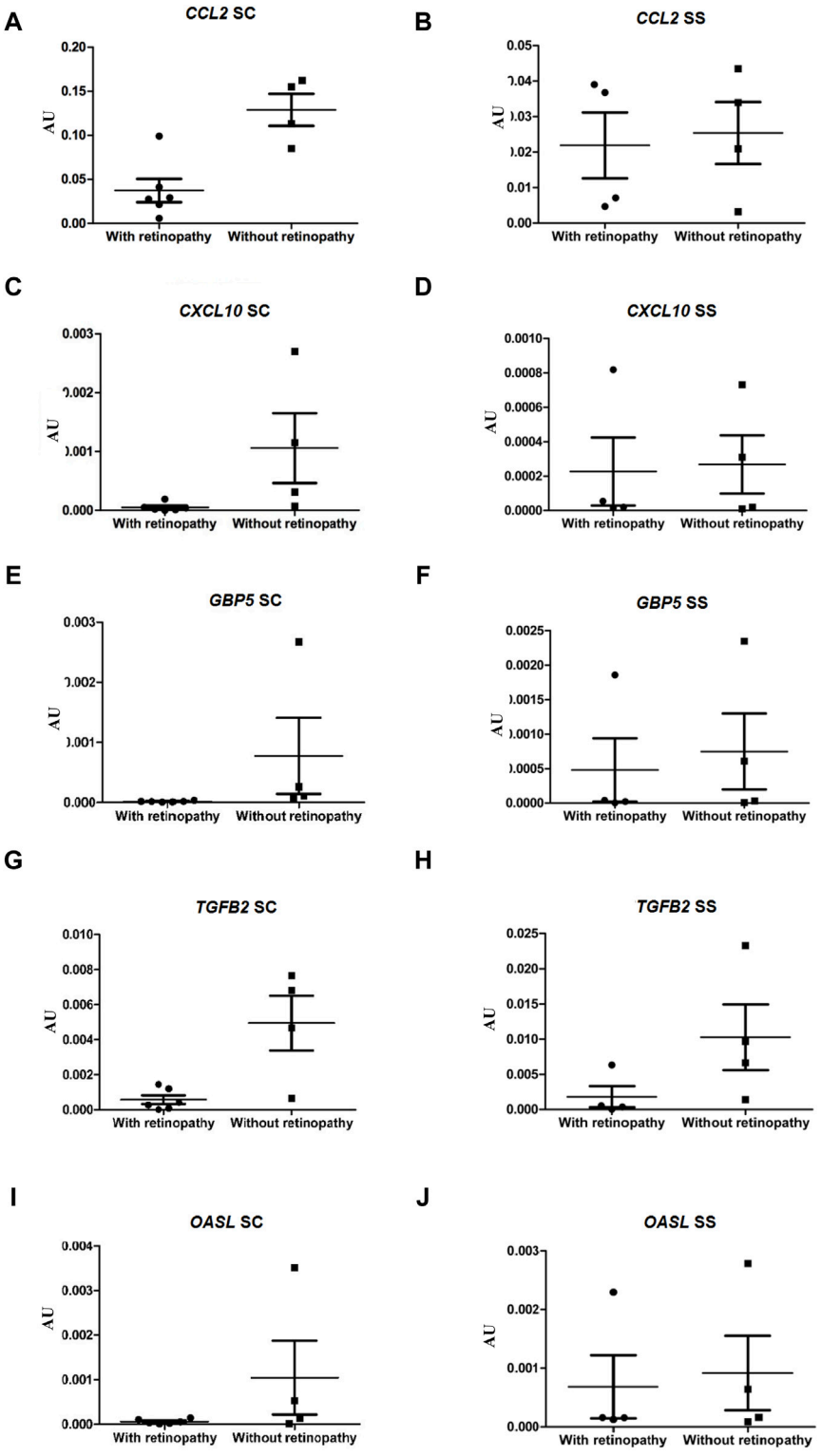

FIGURE 6
Validation of down-regulated genes, *CCL2*, *CXCL10*, *GBP5*, *TGFB2* and *OASL*, by RT-qPCR in HbSC patients and comparison of relative mRNA levels of the same genes in HbSS patients with and without retinopathy. mRNA expression was normalized to ACTB and GAPDH mRNA expression levels. Each dot represents a patient. AU (Arbitrary Unit). **(A,C,E,G,I)** HbSC patients. **(B,D,F,H,J)** HbSS patients.

these DEGs demonstrated that they were significantly enriched in some GO terms that are associated with PSCR, including angiogenesis, cell migration, cell adhesion and innate immune response. Previous studies have demonstrated the important role of pathways associated with the immune system [34] and angiogenesis [35] in the pathogenesis of SCD. Interestingly, our results agree with these findings. Gene ontology analysis showed that the top significant biological terms derived from the list of DEGs included processes like vasodilation, type I interferon signaling, innate immunity and angiogenesis. Moreover, data derived from PPI network analysis reflected a similar pattern. Enrichment analysis of clusters showed that terms associated with type I interferon signaling, innate immune response, axon guidance and angiogenesis were also among the top ranked findings. Results were consistent across different analytical tools. The Cytohubba analysis of the main clusters (1–6) shows that the top six hub genes are *IFIT1*, *ITGB2*, *ROBO1*, *BDKRB2*, *CCL2* and *COL4A1*. The *IFTI1* and *ITGB2* genes play important roles in the immune response and *ROBO1*, *BDKRB2*, *CCL2* and *COL4A1* are associated with angiogenesis. Interestingly, interferon-associated molecular signals, including type I interferon signaling genes such as *IFIT1*, *OASL*, *OAS2*, *IFI6*, *XAF1*, *MX1* are all down-regulated in ECFC of HbSC patients presenting PSCR, when compared with HbSC patients unaffected by PSCR. Likewise, other genes associated with the immune system processes are also downregulated in the ECFC of these patients, such as *CEACAM1*, *CD300A*, *CTSS*, *ITGB2*, *SPI1*, *C1QA*, *LILRA5*, *LTB*.

Several studies, particularly in cancer, have demonstrated the anti-angiogenic activity of type I interferons. This activity has been attributed to various alternative mechanisms [36], including inhibition of basic fibroblast growth factor (*bFGF*) overproduction by tumor cells [37] or down-regulation of *IL-8* and *VEGF* gene expression [38, 39]. IFN-α seems to also have a direct effect on EC, including inhibition of EC proliferation and migration [40–42]. Additionally, IFNs induce the expression of many genes and it has been proposed that the antiangiogenic effects of type 1 interferons may be associated with the up-regulation of angiostatic chemokines, including *CXCL10*, and *CXCL11* [40]. In fact, there is abundant evidence to indicate that CXC chemokines are involved in inhibiting angiogenesis [43]. Guanylate-binding proteins (GBPs) are also a group of IFN-induced proteins that are essential for innate immune responses [44] and can mediate the inhibition of EC proliferation [42] and invasion [45]. The anti-proliferative activity of GBP-1 has been associated with decreased progression in some cancer types, such as breast and colorectal cancer [46]. High expression of *GBP1-5* has been correlated with favorable overall survival in skin cutaneous melanoma (SKCM) patients. In the present study, *CXCL10*, *GBP4* and *GBP5* are downregulated in the ECFC of HbSC patients with PSCR. Since our results revealed reduced expressions of all type I interferon signaling genes, we hypothesized that HbSC patients with PSCR may have an IFNα/β gene signature, which leads to failure in producing significant antiangiogenic effects, contributing to an efficient neovascularization process in these patients.

It is important to emphasize that, considering the notorious clinical heterogeneity of SCD, it is possible that the significantly enriched pathways and the associated genes identified in the analysis of SCR may also be involved in other complications present in the patients studied. In this regard, we highlight the avascular necrosis present in the HbSC patient group with retinopathy (3/6). Avascular necrosis (AVN), also known as osteonecrosis, is a common consequence of vaso-occlusive processes that affect the musculoskeletal system in patients with sickle cell haemoglobinopathy. There is established evidence that angiogenesis, the main pathway identified in this study, and bone formation work closely together in this complication of SCD [47]. The biology of osseointegration involves various processes including inflammation, vascularization, and bone formation [48]. Nevertheless, further studies are necessary to better understand the involvement of DEGs in the cascade of molecular processes that help manage the physiopathology of this complication.

Studies have increasingly indicated that the development of the nervous and vascular systems share similar guidance mechanisms [49, 50]. Among the guidance systems involved in axonal and vascular networks, there are the Slits and Roundabouts (ROBO), Netrins and UNC5 receptors, Semaphorins, and Eph receptors and ephrin ligands. Despite this great complexity of pathways and these already known guidance molecules signaling, interestingly, we identified remarkable overexpression of the *ROBO1* gene in the ECFCs of SC patients with PSCR (log2FoldChange = 4.3, FDR = 1.35E-11) indicating that most likely this receptor is crucial for angiogenesis in sickle cell retinopathy.

ROBO1, a member of the ROBO family, plays key roles in axon guidance receptor regulation and has been reported to mediate tumor angiogenesis [51]. Robo1 may play an important role in cell tube formation, cell attachment, proliferation and promote migration of endothelial cells [51, 52]. Previous studies using monkey choroidal retinal endothelial cells [52], HUVECs [51] and mouse retinal endothelial cells [53] have demonstrated that decreased Robo1 inhibited EC migration. Previous researchers have suggested that *Robo1* is involved in ocular neovascularization. Data show significantly elevated expression levels of Robo1 in the retinas of mice with oxygen-induced retinopathy of prematurity [52–54]. ROP is characterized by local ischemia and preretinal neovascularization. In a comprehensive study, Rama et al. provide clear genetic evidence for the crucial role of Slit2 signaling through Robo1 and Robo2 for promoting pathological and developmental ocular neovascularization [54]. In addition, it has been reported that sprouting angiogenesis, induced by VEGF-A, also requires the presence of Robo1. In the present study, the significant overexpression found in the ECFCs of

HbSC patients with PSCR suggests that Robo1 may play a potential role in the pathophysiology of sickle cell retinopathy.

Among the differentially expressed genes identified, we also highlight the *SLC38A-5* gene (solute carrier family 38, member 5), which encodes an amino acid transporter expressed mainly in Muller cells, ganglion cells and endothelial cells [55]. We found that *SLC38A5* is significantly up-regulated (log2FoldChange = 3.4, FDR = 1,59E-07) in the ECFCs of SC patients with PSCR. *SLC38A5* is a neutral amino acid transporter responsible mostly for glutamine uptake in the retina.

The metabolism of ECs has been recognized as a regulator of angiogenesis and the concept that targeting EC metabolism may represent a novel anti-angiogenic strategy to treat vascular disease is emerging [56, 57]. A growing amount of evidence indicates that endothelial cell glycolysis, fatty acid oxidation and glutamine metabolism are essential in the angiogenic behavior of ECs during vessel formation [58, 59]. Glutamine is the most abundant nonessential amino acid in the human body and contributes to every biosynthetic pathway in proliferating cells [60]. Glutamine is a key carbon and nitrogen source for nucleotide and protein synthesis. Additionally, once transported into the cells, glutamine can be converted to glutamate followed by conversion to ornithine to generate polyamines and nitric oxide (NO), both pro-angiogenic factors [56].

The role of glutamine metabolism in cancer cells has been well characterized. The increased influx of glutamine in cancer is associated with the up-regulation of transporters to satisfy the increased demand for amino acids due to rapid cellular growth and proliferation [60, 61]. Computational analysis focusing on the gene expression data for glutamine and glutamate metabolism in different cancer types showed that the uptake of glutamine is increased by up-regulated *SLC38A5* in breast invasive carcinoma (BRCA), colon adenocarcinoma (COAD), and head and neck squamous cell carcinoma (HNSC) [62]. On the other hand, the role of glutamine metabolism in ECs during angiogenesis is not well known. Nonetheless, studies have demonstrated that depriving ECs of glutamine or inhibiting glutaminase 1 (GLS1) causes impaired EC proliferation, migration and vessel sprouting *in vitro* and *in vivo* [63, 64]. It was reported that endothelial loss of GLS1 diminishes the number of vascular branch points of the vascular plexus and reduces radial expansion of the plexus in the retina of EC-specific GLS1 knockout mice. In addition, pharmacological blockage of glutamine metabolism reportedly reduces pathological ocular angiogenesis in mouse pups with retinopathy (ROP model), which may imply a possible new antiangiogenic strategy [63, 64].

Additionally, in this study we also performed expression level analysis for the ten DEGs in the HbSS samples, with and without retinopathy (groups III and IV). Interestingly, the difference in expression was observed only for the *TGFB2* gene. Therefore, our results indicate that different genes may be involved in sickle cell retinopathy of HbSC and HbSS hemoglobinopathies. We previously employed the present approach to reveal gene expression differences between HbSS patients with and without PSCR [65]. In fact, different sets of genes have been identified coincident with a corresponding increase in endothelial cell expression associated with cell migration, cell adhesion and proliferation signaling. However, further studies with different approaches are necessary to confirm this hypothesis.

This study has some limitations, such as the small number of patients in each group and the lack of quantification of the protein levels of the DEGs. Small sample sizes are not rare in studies employing RNAseq in human samples [66, 67], and can influence the risk of false positives or false negatives results. Additionally, in the present study, five patients (one HbSC patient and four HbSS patients) were undergoing regular blood transfusion. Red blood cell transfusion remains an important therapeutic intervention for improving oxygen carrying capacity and reduce the complications of vaso-occlusion associated with sickle cell disease. Regarding the transfusion treatment and consequent effect on gene expression in circulating ECFCs, it is important to highlight that the peripheral blood samples for isolation of ECFCs were collected immediately before the transfusion of red blood cells. In addition, previous validation study of the present approach demonstrated that alterations in ECFCs gene expression profile as consequence of cell culture stimulation with inflammatory cytokines returned to baseline after one expansion [68]. Since cells from passages 3 to 5 were used for RNA sequencing in our study, we believe that the acquired endothelial phenotypes due transfusion treatment may have been washed out and that therefore, the gene expression of ECFCs reflects only genetic profile of the patients.

Moreover, it is important to emphasize that our approach was based on cultured ECFCs, which are not endothelial cells that reside naturally in the retina. Hence, they are free of tissue specification phenotypes and acquired influences. However, studies have shown that ECFCs demonstrate functional capacity *in vitro* and *in vivo* to both form vessels and integrate into pre-existing vasculature. In this way, evidence from pre-clinical investigations indicates that the administration of ECFCs may present therapeutic efficacy by promoting vascular repair in ischemic disorders, such as ischemic retinopathy [14] and ischemic brain [69]. Therefore, we believe that our strategy has generated data that may provide novel insights for understanding the pathophysiology underlying HbSC sickle cell retinopathy, which remains poorly comprehended.

In conclusion, the results shown here reveal candidate genes involved in HbSC proliferative sickle cell retinopathy, of which we highlight the *ROBO1* and *SLC38A5* genes, which have been previously associated with retinopathy in an animal model and deserve more attention as an alternative strategy to inhibit pathological angiogenesis.

Data availability

The datasets presented in this study can be found in online repositories. The names of the repository/repositories and accession number(s) can be found in the article/Supplementary Material.

Ethics statement

The studies involving humans were approved by the Research Ethics Committees of the Faculty of Medical Sciences, UNICAMP, in accordance with national guidelines (protocol n° 3.960.683) and Declaration of Helsinki. The studies were conducted in accordance with the local legislation and institutional requirements. The participants provided their written informed consent to participate in this study.

Author contributions

All authors participated in the design, interpretation of the study and review of the manuscript; SMSC, MTI participated in sample collection; MGMV conducted the ophthalmological evaluation; SMSC, MTI, SOP and CL conducted the cell isolation and culture; VHB, SMSC, MTI conducted the review of medical records; BBS and PRSC conducted the bioinformatic and statistical analysis; VHB, SMSC, VMR and MBM conducted the interpretation of transcriptome data; PRSC and AMC conducted the gene ontology analysis; VHB, AMC and PRSC conducted the protein-protein interaction analysis; ACLC and DMA conducted validation of expression level analysis of DEGs by qRT-PCR; SMSC wrote the manuscript; FFC, STOS, MCO, and MBM supervised the whole work.

Funding

The authors declare that financial support was received for the research, authorship, and/or publication of this article. This work was supported by Fundação de Amparo à Pesquisa do Estado de São Paulo (FAPESP) (grants 2014/00984-3, 2015/14255-6 and 2019/18886-1) and Conselho Nacional de Desenvolvimento Científico e Tecnológico (CNPq) (grants 305218/2017-4 and 306765/2020-9).

Acknowledgments

We thank all the patients and the research staff at the Human Genetics Laboratory, Center for Molecular Biology and Genetic Engineering, UNICAMP, Campinas, SP, Brazil; and the Hematology and Hemotherapy Center, UNICAMP, Campinas, SP, Brazil. We also thank FAPESP (Fundação de Amparo à Pesquisa do Estado de S. Paulo) and CNPq (Conselho Nacional de Desenvolvimento Científico e Tecnológico).

Conflict of interest

The authors declare that the research was conducted in the absence of any commercial or financial relationships that could be construed as a potential conflict of interest.

Supplementary material

The Supplementary Material for this article can be found online at: https://www.ebm-journal.org/articles/10.3389/ebm.2024.10070/full#supplementary-material

References

1. Moriarty BJ, Acheson RW, Condon PI, Serjeant GR. Patterns of visual loss in untreated sickle cell retinopathy. *Eye (Lond).* (1988) **2**:330–5. doi:10.1038/eye.1988.62

2. Elagouz M, Jyothi S, Gupta B, Sivaprasad S. Sickle cell disease and the eye: old and new concepts. *Surv Ophthalmol* (2010) **55**:359–77. doi:10.1016/j.survophthal.2009.11.004

3. Scott AW. Ophthalmic manifestations of sickle cell disease. *South Med J* (2016) **109**:542–8. doi:10.14423/smj.0000000000000525

4. Campochiaro PA. Ocular neovascularization. *J Mol Med* (2013) **91**:311–21. doi:10.1007/s00109-013-0993-5

5. Lemaire C, Lamarre Y, Lemonne N, Waltz X, Chahed S, Cabot F, et al. Severe proliferative retinopathy is associated with blood hyperviscosity in sickle cell hemoglobin-C disease but not in sickle cell anemia. *Clin Hemorheol Microcirc* (2013) **55**:205–12. doi:10.3233/ch-2012-1622

6. Fox PD, Dunn DT, Morris JS, Serjeant GR. Risk factors for proliferative sickle retinopathy. *Br J Ophthalmol* (1990) **74**:172–6. doi:10.1136/bjo.74.3.172

7. Browne PV, Mosher DF, Steinberg MH, Hebbel RP. Disturbance of plasma and platelet thrombospondin levels in sickle cell disease. *Am J Hematol* (1996) **51**:296–301. doi:10.1002/(sici)1096-8652(199604)51:4<296::aid-ajh8>3.0.co;2-r

8. Stewart MW. The expanding role of vascular endothelial growth factor inhibitors in Ophthalmology. *Mayo Clinic Proc* (2012) **87**:77–88. doi:10.1016/j.mayocp.2011.10.001

9. Jee K, Rodrigues M, Kashiwabuchi F, Applewhite BP, Han I, Lutty G, et al. Expression of the angiogenic mediator, angiopoietin-like 4, in the eyes of patients with proliferative sickle retinopathy. *PLoS One* (2017) **12**:e0183320. doi:10.1371/journal.pone.0183320

10. Ahmed Z, Bicknell R. Angiogenic signalling pathways. *Methods Mol Biol* (2009) **467**:3–24. doi:10.1007/978-1-59745-241-0_1

11. Medina RJ, Barber CL, Sabatier F, Dignat-George F, Melero-Martin JM, Khosrotehrani K, et al. Endothelial progenitors: a consensus statement on nomenclature. *Stem Cells Translational Med* (2017) **6**:1316–20. doi:10.1002/sctm.16-0360

12. Keighron C, Lyons CJ, Creane M, O'Brien T, Liew A. Recent advances in endothelial progenitor cells toward their use in clinical translation. *Front Med* (2018) **5**:354. doi:10.3389/fmed.2018.00354

13. Medina RJ, O'Neill CL, Humphreys MW, Gardiner TA, Stitt AW. Outgrowth endothelial cells: characterization and their potential for reversing ischemic retinopathy. *Invest Ophthalmol Vis Sci* (2010) **51**:5906–13. doi:10.1167/iovs.09-4951

14. Reid E, Guduric-Fuchs J, O'Neill CL, Allen LD, Chambers SEJ, Stitt AW, et al. Preclinical evaluation and optimization of a cell therapy using human cord blood-derived endothelial colony-forming cells for ischemic retinopathies. *Stem Cells Translational Med* (2018) **7**:59–67. doi:10.1002/sctm.17-0187

15. Bertelli PM, Pedrini E, Guduric-Fuchs J, Peixoto E, Pathak V, Stitt AW, et al. Vascular regeneration for ischemic retinopathies: hope from cell therapies. *Curr Eye Res* (2020) **45**:372–84. doi:10.1080/02713683.2019.1681004

16. Goldberg MF. Classification and pathogenesis of proliferative sickle retinopathy. *Am J Ophthalmol* (1971) **71**:649–65. doi:10.1016/0002-9394(71)90429-6

17. Sakamoto TM, Lanaro C, Ozelo MC, Garrido VT, Olalla-Saad ST, Conran N, et al. Increased adhesive and inflammatory properties in blood outgrowth endothelial cells from sickle cell anemia patients. *Microvasc Res* (2013) **90**:173–9. doi:10.1016/j.mvr.2013.10.002

18. Lin Y, Weisdorf DJ, Solovey A, Hebbel RP. Origins of circulating endothelial cells and endothelial outgrowth from blood. *J Clin Invest* (2000) **105**:71–7. doi:10.1172/jci8071

19. Andrews S. *FastQC: a quality control tool for high throughput sequence data* (2010). Available from: http://www.bioinformatics.babraham.ac.uk/projects/fastqc (Accessed October 15, 2021).

20. Dobin A, Davis CA, Schlesinger F, Drenkow J, Zaleski C, Jha S, et al. STAR: ultrafast universal RNA-seq aligner. *Bioinformatics* (2013) **29**:15–21. doi:10.1093/bioinformatics/bts635

21. Anders S, Huber W. Differential expression analysis for sequence count data. *Genome Biol* (2010) **11**:R106. doi:10.1186/gb-2010-11-10-r106

22. Liao Y, Smyth GK, Shi W. FeatureCounts: an efficient general-purpose program for assigning sequence reads to genomic features. *Bioinformatics* (2014) **30**:923–30. doi:10.1093/bioinformatics/btt656

23. Blighe K, Rana S, Lewis M. *Enhanced Volcano: publication-ready volcano plots with enhanced colouring and labeling. R package version 1.16.0* (2022). Available from: https://github.com/kevinblighe/EnhancedVolcano (Accessed April 28, 2024).

24. Metsalu T, Vilo J. ClustVis: a web tool for visualizing clustering of multivariate data using Principal Component Analysis and heatmap. *Nucleic Acids Res* (2015) **43**:W566–70. doi:10.1093/nar/gkv468

25. Blighe K, Lun A. *PCAtools: PCAtools: everything principal components analysis. R package version 2.4.0* (2021). Available from: https://github.com/kevinblighe/PCAtools (Accessed April 28, 2024).

26. Shannon P, Markiel A, Ozier O, Baliga NS, Wang JT, Ramage D, et al. Cytoscape: a software environment for integrated models of biomolecular interaction networks. *Genome Res* (2003) **13**:2498–504. doi:10.1101/gr.1239303

27. Doncheva NT, Morris JH, Gorodkin J, Jensen LJ. Cytoscape StringApp: network analysis and visualization of proteomics data. *J Proteome Res* (2019) **18**:623–32. doi:10.1021/acs.jproteome.8b00702

28. Pundir S, Martin MJ, O'Donovan C, UniProt C. UniProt tools. *Curr Protoc Bioinformatics* (2016) **53**:1.29.21–.29.15. doi:10.1002/0471250953.bi0129s53

29. Rosewicz S, Detjen K, Scholz A, von Marschall Z. Interferon-α: regulatory effects on cell cycle and angiogenesis. *Neuroendocrinology* (2004) **80**:85–93. doi:10.1159/000080748

30. Chin CH, Chen SH, Wu HH, Ho CW, Ko MT, Lin CY. cytoHubba: identifying hub objects and sub-networks from complex interactome. *BMC Syst Biol* (2014) **8**(Suppl. 4):S11. doi:10.1186/1752-0509-8-s4-s11

31. Schmittgen TD, Livak KJ. Analyzing real-time PCR data by the comparative C(T) method. *Nat Protoc* (2008) **3**:1101–8. doi:10.1038/nprot.2008.73

32. Nijmeh H, Balasubramaniam V, Burns N, Ahmad A, Stenmark KR, Gerasimovskaya EV. High proliferative potential endothelial colony-forming cells contribute to hypoxia-induced pulmonary artery vasa vasorum neovascularization. *Am J Physiology-Lung Cell Mol Physiol* (2014) **306**:L661–L671. doi:10.1152/ajplung.00244.2013

33. Ito MT, da Silva Costa SM, Baptista LC, Carvalho-Siqueira GQ, Albuquerque DM, Rios VM, et al. Angiogenesis-related genes in endothelial progenitor cells may Be involved in sickle cell stroke. *J Am Heart Assoc* (2020) **9**:e014143. doi:10.1161/jaha.119.014143

34. de Azevedo JTC, Malmegrim KCR. Immune mechanisms involved in sickle cell disease pathogenesis: current knowledge and perspectives. *Immunol Lett* (2020) **224**:1–11. doi:10.1016/j.imlet.2020.04.012

35. Lopes FC, Traina F, Almeida CB, Leonardo FC, Franco-Penteado CF, Garrido VT, et al. Key endothelial cell angiogenic mechanisms are stimulated by the circulating milieu in sickle cell disease and attenuated by hydroxyurea. *Haematologica* (2015) **100**:730–9. doi:10.3324/haematol.2014.119727

36. Indraccolo S. Interferon-α as angiogenesis inhibitor: learning from tumor models. *Autoimmunity* (2010) **43**:244–7. doi:10.3109/08916930903510963

37. Singh RK, Gutman M, Bucana CD, Sanchez R, Llansa N, Fidler IJ. Interferons alpha and beta down-regulate the expression of basic fibroblast growth factor in human carcinomas. *Proc Natl Acad Sci* (1995) **92**:4562–6. doi:10.1073/pnas.92.10.4562

38. Oliveira IC, Sciavolino PJ, Lee TH, Vilcek J. Downregulation of interleukin 8 gene expression in human fibroblasts: unique mechanism of transcriptional inhibition by interferon. *Proc Natl Acad Sci* (1992) **89**:9049–53. doi:10.1073/pnas.89.19.9049

39. von Marschall Z, Scholz A, Cramer T, Schäfer G, Schirner M, Oberg K, et al. Effects of interferon alpha on vascular endothelial growth factor gene transcription and tumor angiogenesis. *JNCI J Natl Cancer Inst* (2003) **95**:437–48. doi:10.1093/jnci/95.6.437

40. Indraccolo S, Pfeffer U, Minuzzo S, Esposito G, Roni V, Mandruzzato S, et al. Identification of genes selectively regulated by IFNs in endothelial cells. *J Immunol* (2007) **178**:1122–35. doi:10.4049/jimmunol.178.2.1122

41. Lubeseder-Martellato C, Guenzi E, Jörg A, Töpolt K, Naschberger E, Kremmer E, et al. Guanylate-binding protein-1 expression is selectively induced by inflammatory cytokines and is an activation marker of endothelial cells during inflammatory diseases. *Am J Pathol* (2002) **161**:1749–59. doi:10.1016/s0002-9440(10)64452-5

42. Guenzi E, Topolt K, Cornali E, Lubeseder-Martellato C, Jörg A, Matzen K, et al. The helical domain of GBP-1 mediates the inhibition of endothelial cell proliferation by inflammatory cytokines. *EMBO J* (2001) **20**:5568–77. doi:10.1093/emboj/20.20.5568

43. Romagnani P, Lasagni L, Annunziato F, Serio M, Romagnani S. CXC chemokines: the regulatory link between inflammation and angiogenesis. *Trends Immunol* (2004) **25**:201–9. doi:10.1016/j.it.2004.02.006

44. Kim BH, Chee JD, Bradfield CJ, Park ES, Kumar P, MacMicking JD. Interferon-induced guanylate-binding proteins in inflammasome activation and host defense. *Nat Immunol* (2016) **17**:481–9. doi:10.1038/ni.3440

45. Guenzi E, Topolt K, Lubeseder-Martellato C, Jörg A, Naschberger E, Benelli R, et al. The guanylate binding protein-1 GTPase controls the invasive and angiogenic capability of endothelial cells through inhibition of MMP-1 expression. *EMBO J* (2003) **22**:3772–82. doi:10.1093/emboj/cdg382

46. Britzen-Laurent N, Lipnik K, Ocker M, Naschberger E, Schellerer VS, Croner RS, et al. GBP-1 acts as a tumor suppressor in colorectal cancer cells. *Carcinogenesis* (2012) **34**:153–62. doi:10.1093/carcin/bgs310

47. George A, Ellis M, Gill HS. Hypoxia-inducible factor (HIF): how to improve osseointegration in hip arthroplasty secondary to avascular necrosis in sickle cell disease. *EFORT Open Rev* (2019) **4**:567–75. doi:10.1302/2058-5241.4.180030

48. Dimitriou R, Babis GC. Biomaterial osseointegration enhancement with biophysical stimulation. *J Musculoskelet Neuronal Interact* (2007) **7**:253–65.

49. Adams RH, Eichmann A. Axon guidance molecules in vascular patterning. *Cold Spring Harbor Perspect Biol* (2010) **2**:a001875. doi:10.1101/cshperspect.a001875

50. Klagsbrun M, Eichmann A. A role for axon guidance receptors and ligands in blood vessel development and tumor angiogenesis. *Cytokine Growth Factor Rev* (2005) **16**:535–48. doi:10.1016/j.cytogfr.2005.05.002

51. Wang B, Xiao Y, Ding BB, Zhang N, Yuan XB, Gui L, et al. Induction of tumor angiogenesis by Slit-Robo signaling and inhibition of cancer growth by blocking Robo activity. *Cancer Cell* (2003) **4**:19–29. doi:10.1016/s1535-6108(03)00164-8

52. Huang L, Xu Y, Yu W, Li X, Liqun C, He X, et al. Robo1: a potential role in ocular angiogenesis. *Curr Eye Res* (2009) **34**:1019–29. doi:10.3109/02713680903308495

53. Kong Y, Sun B, Han Q, Han S, Wang Y, Chen Y. Slit-miR-218-Robo axis regulates retinal neovascularization. *Int J Mol Med* (2016) **37**:1139–45. doi:10.3892/ijmm.2016.2511

54. Rama N, Dubrac A, Mathivet T, Ní Chárthaigh RA, Genet G, Cristofaro B, et al. Slit2 signaling through Robo1 and Robo2 is required for retinal neovascularization. *Nat Med* (2015) **21**:483–91. doi:10.1038/nm.3849

55. Umapathy NS, Dun Y, Martin PM, Duplantier JN, Roon P, Prasad P, et al. Expression and function of system N glutamine transporters (SN1/SN2 or SNAT3/SNAT5) in retinal ganglion cells. *Invest Ophthalmol Vis Sci* (2008) **49**:5151–60. doi:10.1167/iovs.08-2245

56. Draoui N, de Zeeuw P, Carmeliet P. Angiogenesis revisited from a metabolic perspective: role and therapeutic implications of endothelial cell metabolism. *Open Biol* (2017) **7**:170219. doi:10.1098/rsob.170219

57. Dumas SJ, García-Caballero M, Carmeliet P. Metabolic signatures of distinct endothelial phenotypes. *Trends Endocrinol Metab* (2020) **31**:580–95. doi:10.1016/j.tem.2020.05.009

58. De Bock K, Georgiadou M, Carmeliet P. Role of endothelial cell metabolism in vessel sprouting. *Metab* (2013) **18**:634–47. doi:10.1016/j.cmet.2013.08.001

59. De Bock K, Georgiadou M, Schoors S, Kuchnio A, Wong B, Cantelmo A, et al. Role of PFKFB3-driven glycolysis in vessel sprouting. *Cell* (2013) **154**:651–63. doi:10.1016/j.cell.2013.06.037

60. DeBerardinis RJ, Cheng T. Q's next: the diverse functions of glutamine in metabolism, cell biology and cancer. *Oncogene* (2010) **29**:313–24. doi:10.1038/onc.2009.358

61. Polet F, Feron O. Endothelial cell metabolism and tumour angiogenesis: glucose and glutamine as essential fuels and lactate as the driving force. *J Intern Med* (2013) **273**:156–65. doi:10.1111/joim.12016

62. Tian Y, Du W, Cao S, Wu Y, Dong N, Wang Y, et al. Systematic analyses of glutamine and glutamate metabolisms across different cancer types. *Chin J Cancer* (2017) **36**:88. doi:10.1186/s40880-017-0255-y

63. Huang H, Vandekeere S, Kalucka J, Bierhansl L, Zecchin A, Brüning U, et al. Role of glutamine and interlinked asparagine metabolism in vessel formation. *EMBO J* (2017) **36**:2334–52. doi:10.15252/embj.201695518

64. Wang Z, Yemanyi F, Blomfield AK, Bora K, Huang S, Liu CH, et al. Amino acid transporter SLC38A5 regulates developmental and pathological retinal angiogenesis. *Elife* (2022) **11**:e73105. doi:10.7554/elife.73105

65. Bertozzo VHE, da Silva Costa SM, Ito MT, Cruz PRSD, Souza BB, Rios VM, et al. Comparative transcriptome analysis of endothelial progenitor cells of HbSS patients with and without proliferative retinopathy. *Exp Biol Med (Maywood)* (2023) **248**:677–84. doi:10.1177/15353702231157927

66. Tokuda Y, Okumura N, Komori Y, Hanada N, Tashiro K, Koizumi N, et al. Transcriptome dataset of human corneal endothelium based on ribosomal RNA-depleted RNA-Seq data. *Sci Data* (2020) **7**(1):407. doi:10.1038/s41597-020-00754-1

67. Li X, Chen Y, Fu C, Li H, Yang K, Bi J, et al. Characterization of epigenetic and transcriptional landscape in infantile hemangiomas with ATAC-seq and RNA-seq. *Epigenomics* (2020) **12**(11):893–905. doi:10.2217/epi-2020-0060

68. Chang ML, Wei P, Enenstein J, Jiang A, Hillery CA, Scott JP, et al. Genetic endothelial systems biology of sickle stroke risk. *Blood* (2008) **111**:3872–9. doi:10.1182/blood-2007-06-097188

69. Moubarik C, Guillet B, Youssef B, Codaccioni JL, Piercecchi MD, Sabatier F, et al. Transplanted late outgrowth endothelial progenitor cells as cell therapy product for stroke. *Stem Cel Rev Rep* (2011) **7**:208–20. doi:10.1007/s12015-010-9157-y

EBM Experimental Biology and Medicine

TYPE Original Research
PUBLISHED 31 July 2024
DOI 10.3389/ebm.2024.10090

OPEN ACCESS

*CORRESPONDENCE
Gonzalo M. Rivera,
grivera@tamu.edu
Andreea Trache,
trache@tamu.edu

RECEIVED 24 January 2024
ACCEPTED 09 July 2024
PUBLISHED 31 July 2024

CITATION
Bywaters BC, Trache A and Rivera GM (2024), Modulation of arterial intima stiffness by disturbed blood flow. *Exp. Biol. Med.* 249:10090. doi: 10.3389/ebm.2024.10090

Modulation of arterial intima stiffness by disturbed blood flow

Briana C. Bywaters[1], Andreea Trache[2,3]* and Gonzalo M. Rivera[1]*

[1]Department of Veterinary Pathobiology, Texas A&M University, College Station, TX, United States, [2]Department of Medical Physiology, Texas A&M Health Science Center, Bryan, TX, United States, [3]Department of Biomedical Engineering, Texas A&M University, College Station, TX, United States

Abstract

The intima, comprising the endothelium and the subendothelial matrix, plays a crucial role in atherosclerosis pathogenesis. The mechanical stress arising from disturbed blood flow (d-flow) and the stiffening of the arterial wall contributes to endothelial dysfunction. However, the specific impacts of these physical forces on the mechanical environment of the intima remain undetermined. Here, we investigated whether inhibiting collagen crosslinking could ameliorate the detrimental effects of persistent d-flow on the mechanical properties of the intima. Partial ligation of the left carotid artery (LCA) was performed in C57BL/6J mice, inducing d-flow. The right carotid artery (RCA) served as an internal control. Carotids were collected 2 days and 2 weeks after surgery to study acute and chronic effects of d-flow on the mechanical phenotype of the intima. The chronic effects of d-flow were decoupled from the ensuing arterial wall stiffening by administration of β-aminopropionitrile (BAPN), an inhibitor of collagen crosslinking by lysyl oxidase (LOX) enzymes. Atomic force microscopy (AFM) was used to determine stiffness of the endothelium and the denuded subendothelial matrix in *en face* carotid preparations. The stiffness of human aortic endothelial cells (HAEC) cultured on soft and stiff hydrogels was also determined. Acute exposure to d-flow caused a slight decrease in endothelial stiffness in male mice but had no effect on the stiffness of the subendothelial matrix in either sex. Regardless of sex, the intact endothelium was softer than the subendothelial matrix. In contrast, exposure to chronic d-flow led to a substantial increase in the endothelial and subendothelial stiffness in both sexes. The effects of chronic d-flow were largely prevented by concurrent BAPN administration. In addition, HAEC displayed reduced stiffness when cultured on soft vs. stiff hydrogels. We conclude that chronic d-flow results in marked stiffening of the arterial intima, which can be effectively prevented by inhibition of collagen crosslinking.

KEYWORDS

arterial stiffness, disturbed blood flow, endothelium, subendothelial matrix, atomic force microscopy, lysyl oxidase, collagen crosslinking, BAPN

Impact statement

Although influenced by systemic risk factors, atherosclerotic plaques develop in response to mechanical forces impacting bifurcations and curved segments of the arterial tree. Unraveling the intertwined effects of disturbed blood flow and arterial wall stiffening in the pathogenesis of atherosclerosis remains a challenge. This study provides novel insights into pathological vascular remodeling, emphasizing the significant impact of chronic d-flow on arterial intima stiffening. Our research demonstrates that inhibiting collagen crosslinking effectively prevents the substantial stiffening of the arterial intima induced by chronic exposure to d-flow. Accordingly, modulation of intimal stiffness emerges as a promising avenue for the development of innovative targeted interventions aimed at promoting arterial health.

Introduction

Atherosclerotic lesions develop primarily in areas where arteries branch out or have curved segments [1], despite the influence of systemic risk factors [2]. The mechanical forces exerted by local blood flow patterns play a crucial role in determining the endothelial phenotype and influencing the progression of atherosclerosis [3, 4]. In straight arterial regions, the high-magnitude and unidirectional shear stress resulting from steady blood flow promotes endothelial health and is considered protective against atherosclerosis. On the other hand, in bifurcations and curved arterial segments, the low-magnitude and oscillatory shear stress caused by disturbed blood flow (d-flow) leads to endothelial dysfunction and is deemed prone to atherosclerosis.

The mechanical properties of the arterial wall also play a significant role in the development and progression of atherosclerosis [5]. Factors such as aging [6], metabolic imbalance [7], and hypertension [8], contribute to arterial stiffening by causing changes in the extracellular matrix and vascular cells. Arterial stiffening is also observed in bifurcations and curved segments, which aligns with the localized formation of atherosclerotic lesions due to d-flow [9–11]. However, the specific impact and interplay between chronic exposure to d-flow and arterial wall stiffening on the intimal phenotype, and specifically its biomechanical properties, remain poorly understood.

The mouse model of partial carotid ligation (PCL) has been valuable in uncovering the mechanisms involved in the development of atherosclerosis [12–14]. By surgically inducing d-flow in a previously healthy and straight arterial segment, the development of atherosclerotic lesions can be rapidly stimulated in hyperlipidemic mice [12, 15, 16]. In the presence of physiological levels of cholesterol and triglycerides, however, prolonged exposure (~2 weeks) to PCL-induced d-flow leads to arterial wall remodeling and stiffening, similar to the effects of aging [17]. This model offers, therefore, a unique opportunity to study how mechanical forces contribute to abnormal molecular patterns and cellular phenotypes that drive the progression of atherosclerosis [14]. The objective of this research was to determine the specific contribution of d-flow and arterial wall stiffening to the mechanical phenotype of components of the arterial intima, i.e., the intact endothelium and the denuded subendothelial matrix. This study tested the hypothesis that chronic d-flow initiates a feed forward loop promoting arterial wall stiffening leading to altered endothelial mechanics; hence interventions aimed at reducing arterial wall stiffness have the potential to disrupt this loop and preserve the mechanical homeostasis of the endothelium.

Our findings indicate that reducing arterial wall stiffness can reverse the detrimental effects of prolonged exposure to d-flow on the biomechanical properties of the arterial endothelium.

Materials and methods

Animals

Mice were maintained in the Comparative Medicine Program Laboratory Animal Resources and Research facility at Texas A&M University. Animal handling and experimental procedures were performed according to a protocol (AUP 2019-0184) approved by the Institutional Animal Care and Use Committee of Texas A&M University. Eight-week old male and female C57BL/6J mice (RRID:IMSR_JAX:000664) were used for determinations of stiffness using atomic force microscopy (AFM). The fluorescence reporter mT/mG mouse [18], expressing tamoxifen-inducible Cre recombinase (*Cdh5*-Cre^{ERT2}) in the endothelium [19], was used to verify arterial wall integrity and the subsequent mechanical removal of the endothelium. In these mice, endothelial cells were labeled with EGFP following five intraperitoneal injections, administered every other day, of 75 mg/kg tamoxifen (Sigma-Aldrich) in 100 μL corn oil. All animals were maintained on a 12-h light/dark cycle and fed regular chow ad-libitum.

Experimental design

We performed partial ligation of the left carotid artery (Figure 1A) to determine the acute and chronic effects of d-flow on the mechanical phenotype of the endothelium and subendothelial matrix. Animals were sacrificed and carotid arteries collected 2 days or 2 weeks after surgery. The 2-day time point, which aligns with established experimental design principles in the field [14], captures the initial response to an

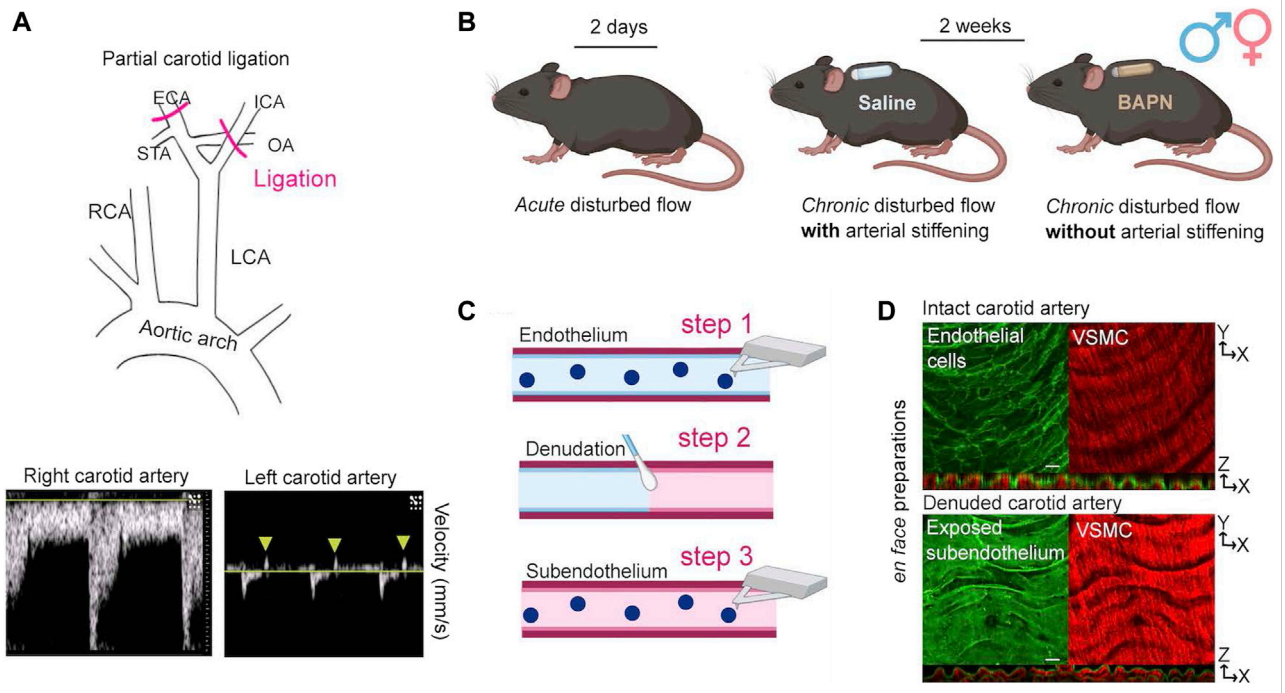

FIGURE 1
Experimental strategy for force decoupling and assessment of the arterial mechanical phenotype. **(A)** At 8 weeks of age, male and female C57B/6J mice underwent PCL of the left carotid artery (LCA) to induce disturbed hemodynamics (top). The intact right carotid artery (RCA) served as an internal control. Successful ligation was verified by ultrasound detection of both decreased blood flow velocity and blood flow reversal (arrowheads) in the ligated LCA (bottom). **(B)** Acute and chronic effects of disturbed hemodynamics were determined 2 days or 2 weeks after PCL (n = 6/sex/time). To decouple the effects of chronic (2 weeks) disturbed hemodynamics from the ensuing stiffening of the arterial wall, mice were affixed at the time of surgery with subcutaneous osmotic minipumps delivering either Saline or 150 mg/kg/day of BAPN, an inhibitor of the collagen crosslinking enzymes of the lysyl oxidase (LOX) family. **(C)** Both carotids were excised and opened *en face* for determination of the elastic modulus of intimal components by AFM. First, AFM measurements were collected from the intact endothelium (step 1). Subsequently, endothelial denudation was performed using a cotton swab (step 2). Following endothelial denudation, AFM measurements were collected from the exposed subendothelial matrix (step 3). **(D)** Successful handling of excised vessels was validated using an endothelial-specific fluorescence reporter mouse (Cdh5-Cre^{ERT2}/mTmG) to confirm integrity (top) and removal (bottom) of the endothelium before and after denudation, respectively. Note apical endothelial fluorescence (top panel) and autofluorescence of elastic fibers (bottom panel) in orthogonal views. Scale bar is 20 μm. VSMC, vascular smooth muscle cells. ICA, internal carotid artery; OA, occipital artery; ECA, external carotid artery; STA, superior thyroid artery.

acute change in hemodynamic forces [20]. To decouple the effects of chronic (2-weeks) d-flow from the ensuing arterial wall stiffening, animals were affixed with subcutaneous osmotic minipumps (ALZET model 1002, capacity: 100 μL, flow rate: 0.25 μL/h) delivering either phosphate buffered saline (Saline) or 150 mg/kg/day of β-aminopropionitrile (BAPN) [21], an inhibitor of the LOX family of enzymes (Figure 1B) [6, 17, 22–24].

Surgical procedures

Partial carotid ligation (PCL)

Mice were anesthetized with isoflurane and hair was chemically removed (Nair, Ewing, NJ) from the chin to the bottom of the sternum. The exposed skin was swabbed alternately with iodine and isopropyl alcohol prior to incision. Sutures (0–6 silk) were used to occlude the external carotid, internal carotid, and occipital branches of the left carotid artery (LCA), leaving the superior thyroid artery unobstructed (Figure 1A). The right carotid artery (RCA) was left intact and served as an internal control. The incision was closed using tissue adhesive (Vetbond, 3M, Saint Paul, MN). Soon after surgery, all mice received a subcutaneous injection of buprenorphine (0.1 mg/kg) to minimize pain and discomfort.

Osmotic minipump insertion

Mice used for the 2-week experiments remained anesthetized after completion of the PCL procedure and were placed in a prone position. Hair was chemically removed from between the shoulder blades and the skin was swabbed with iodine and isopropyl alcohol. A small incision was made to allow the subcutaneous insertion of an osmotic minipump. Following the subcutaneous insertion of the osmotic minipump, the incision was closed using 7 mm wound clips (EZ Clip, Stoelting, Chicago, IL).

Doppler ultrasound

We used ultrasound to confirm successful PCL 1 day after the surgical procedure. Mice were anesthetized using isoflurane and subjected to Doppler ultrasound using a Vevo 3100 system (FUJIFILM VisualSonics, Inc., Bothell, WA) in B-mode. Both flow reversal and decreased flow velocity were recorded in the ligated vessels [12, 13]. The presence of normal flow was confirmed in the intact vessels (Figure 1A, bottom panels).

Tissue collection and handling

Two days or 2 weeks following PCL, mice were euthanized using CO_2 asphyxiation followed by cervical dislocation. The vascular tree was perfused through the apex of the heart with ice-cold Dulbecco's phosphate buffered saline (DPBS, Gibco, Waltham, MA) prior to excision of carotid arteries. Excised vessels were immediately opened *en face* using vannas scissors (Fine Science Tools, Vancouver BC, Canada), affixed to 60 mm plastic dishes (BD Falcon, Franklin Lakes, NJ), and submerged in room temperature DPBS. *En face* vessel preparations were used to determine the stiffness of the intact endothelium and the subendothelial matrix [25]. After measurement of the intact endothelial surface was completed, the endothelial layer was mechanically removed using 10 swipes with a cotton swab (Figure 1C), DPBS was replaced, and measurements of the exposed subendothelial matrix were immediately collected. The integrity of the endothelium and exposure of the subendothelial matrix before and after mechanical removal of the endothelium, respectively, were confirmed by microscopic imaging of arteries harvested from the fluorescence reporter mT/mG mouse (Figure 1D).

Culture, immunofluorescence staining, and imaging of endothelial cells

Human aortic endothelial cells (HAECs; ATCC, Manassas, VA) were cultured in EGM-2 culture media (Lonza Walkersville, Basel, Switzerland) on 0.1% gelatin-coated plastic dishes until ~80% confluence. Cells were then seeded (passage 5) on soft (4 kPa) or stiff (50 kPa) polyacrylamide hydrogels coated with 0.2% collagen I (Matrigen, San Diego, CA) at a density of $40 \times 10^4/18$ mm^2 and cultured for 24 h. HAECs were fixed with 4% paraformaldehyde for 15 min at 37°C in phosphate-buffered saline (PBS). Fixed cells were permeabilized with 0.1% Triton X-100 and nonspecific binding was blocked using 3% bovine serum albumin (BSA) in PBS. Coverslips were incubated with primary mouse monoclonal anti-paxillin antibody (BD Biosciences, 1:1000) in blocking solution for 1 hour at room temperature, followed by Alexa Fluor 488 goat anti-mouse secondary antibody (Life Technologies, 1:500) for 1 hour at room temperature. To visualize actin filaments, cells were stained with Alexa Fluor 647 phalloidin (Life Technologies, 1:200). Images were acquired on an Olympus FV3000 confocal microscope using a PlanApoN SC2 60 × 1.4NA objective at 0.414 μm/px and Z-step of 0.31 μm. Z-stack images were projected as sum intensity. A cell area mask was created using Auto threshold with Huang method of the actin channel in ImageJ/FIJI [26]. Fluorescence intensity inside the mask was measured for actin and paxillin to determine mean intensity.

Atomic force microscopy

A numerical code, unknown to the experimenter, was used to deidentify samples and treatments. To determine the stiffness of the intact endothelium and subendothelial matrix, atomic force microscopy (AFM) measurements were performed as previously described [25]. The AFM probes used were unsharpened silicon nitride cantilevers with a spring constant of 12.2 ± 0.4 pN/nm (MLCT Bio, Bruker Nano-Surfaces, Billerica, MA). The AFM was operated in force mode, setting the cantilever to touch and retract from the tissue surface at 0.8 μm/s in the z-axis. An average of 4–6 separate sites were measured on the common carotid artery along the segment between the aortic arch (proximal) and the internal/external carotid artery bifurcation (distal) with approximately 60 force curves acquired at each site. Care was taken to avoid obtaining measurements at the edges of the tissue due to eventual damage during handling and immobilization in the dish.

In the case of HAEC cultured on hydrogels, measurements of cells stiffness and integrin α5β1 adhesion force to fibronectin were conducted using AFM tips functionalized with fibronectin [27, 28]. Individual cells were measured midway between the nucleus and the edge of the cell [29]. A minimum of 10 cells were measured in each independent experiment, for a total of 1330–1344 force curves per condition. Experiments were performed in triplicates.

AFM data processing

Stiffness at the point of contact was evaluated as Young's modulus of elasticity (E), by fitting the approach curve between the initial point of tissue contact and point of maximum probe displacement with Sneddon's modified Hertz model [30]. Kernel density plots of the distribution of stiffness at the point of contact for both *ex vivo* vessels and cultured cells, as well as kernel density plots of the distribution of integrin adhesion force measurements for cultured cells, were generated using NForceR software [31].

Second harmonic generation imaging

Vessels were mounted on glass slides prior to imaging. Collagen was visualized by second harmonic generation

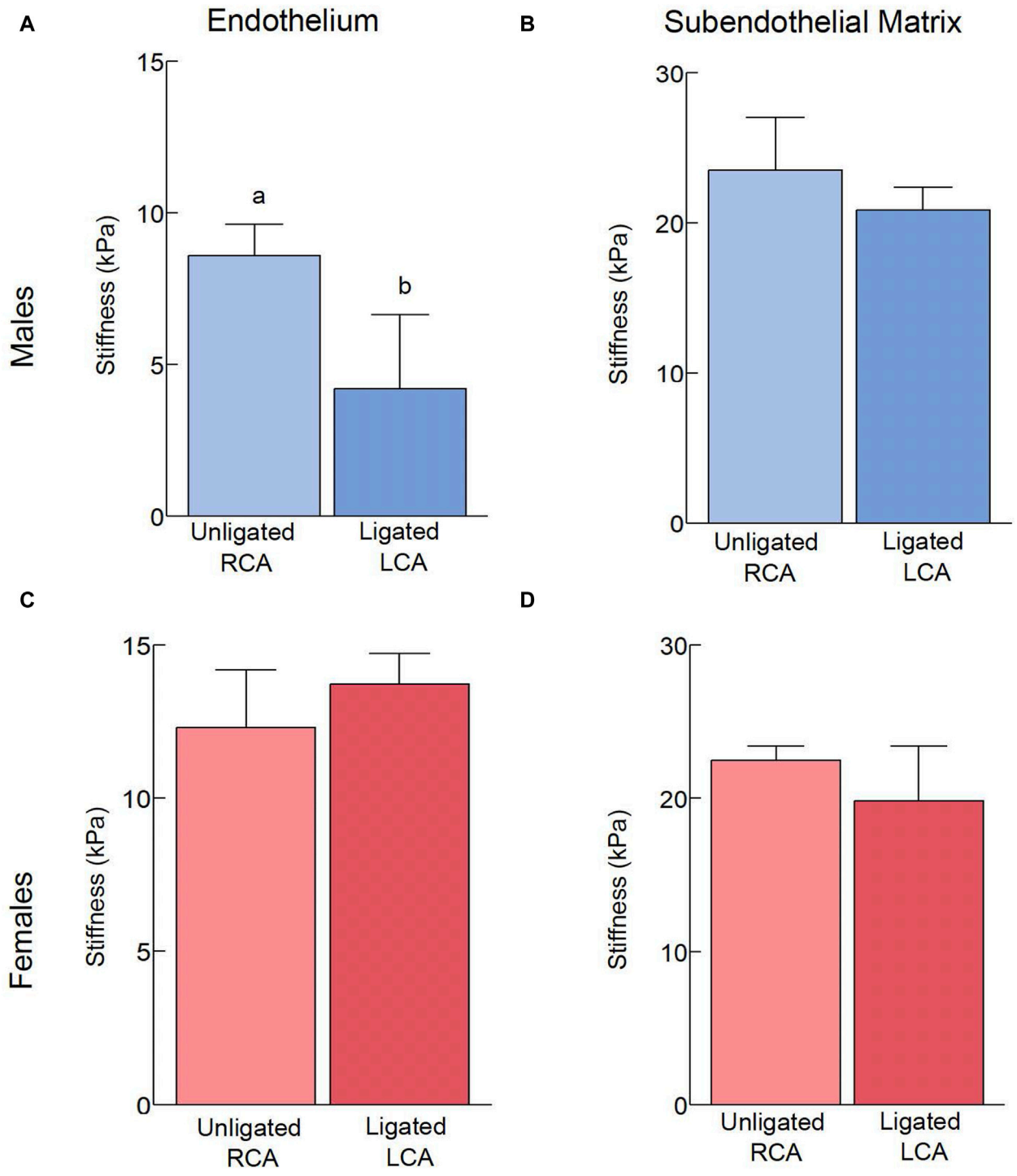

FIGURE 2
Effects of acute, 2-day exposure to disturbed blood flow on the mechanical properties of the carotid intima. The elastic modulus of the endothelium **(A,C)** and subendothelial matrix **(B,D)** was measured using AFM in male **(A,B)** and female **(C,D)** mice 2 days after PCL (n = 6/sex). The number of force curves acquired per vessel type is indicated in parentheses as follows: **(A)** Unligated RCA (1451), Ligated LCA (2609). **(B)** Unligated RCA (890), Ligated LCA (1370). **(C)** Unligated RCA (1103), Ligated LCA (1295). **(D)** Unligated RCA (852), Ligated LCA (902). Bars with different letters, $p < 0.05$.

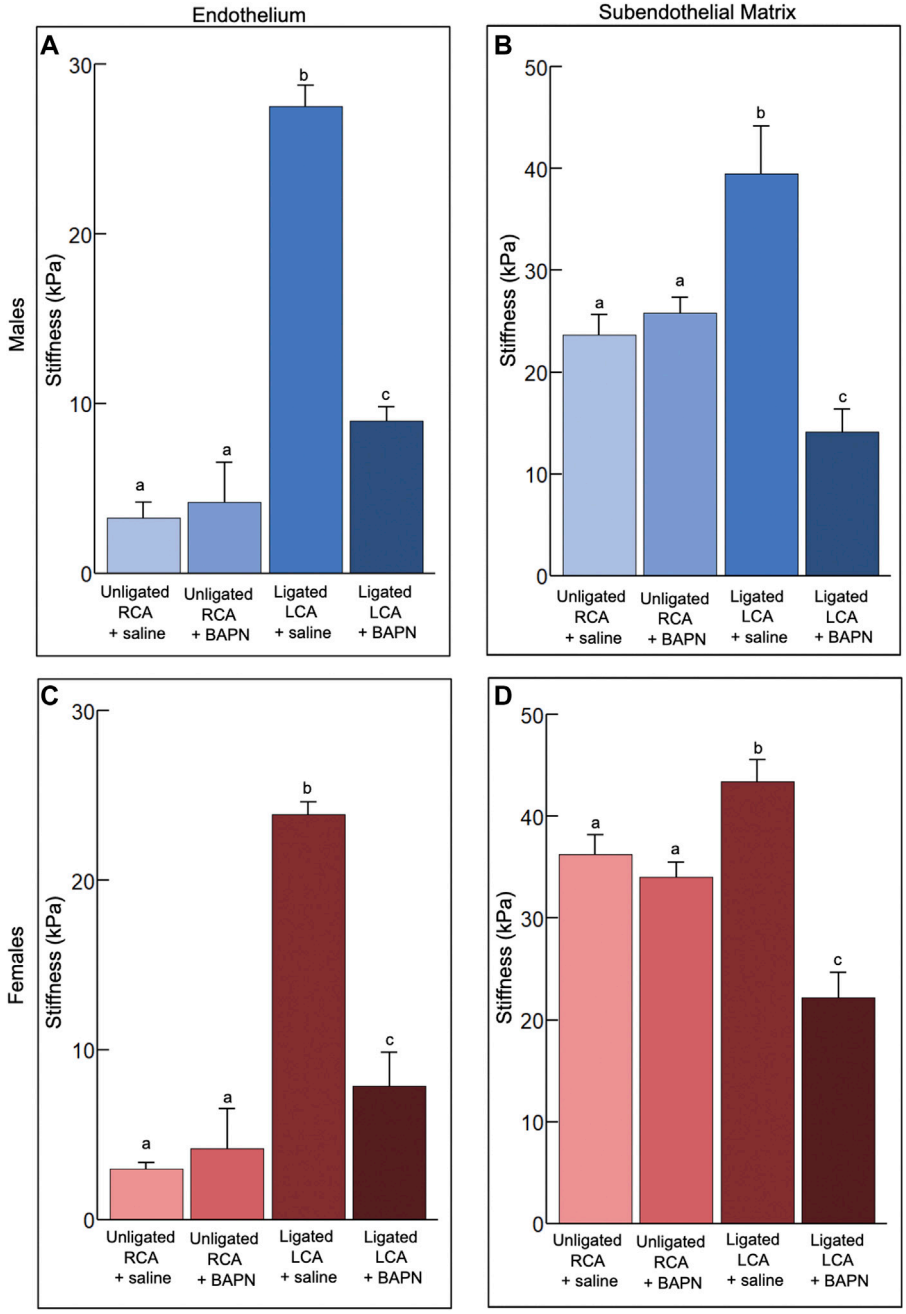

FIGURE 3
Effects of chronic, 2-week exposure to disturbed blood flow on the mechanical properties of the carotid intima. The elastic modulus of the endothelium **(A,C)** and subendothelial matrix **(B,D)** was measured using AFM in male **(A,B)** and female **(C,D)** mice 2 weeks after PCL and treatment with either Saline or 150 mg/kg/day of BAPN, an inhibitor of the collagen crosslinking enzymes of the LOX family (n = 6/sex/group). The number of force curves acquired per vessel type is indicated in parentheses as follows: **(A)** Unligated RCA + saline (1350), Unligated RCA + BAPN (3517), Ligated LCA + saline (2273), Ligated LCA + BAPN (2664). **(B)** Unligated RCA + saline (1995), Unligated RCA + BAPN (1007), Ligated LCA + saline (2251), Ligated LCA + BAPN (1716). **(C)** Unligated RCA + saline (831), Unligated RCA + BAPN (1675), Ligated LCA + saline (1592), Ligated LCA + BAPN (1421). **(D)** Unligated RCA + saline (1570), Unligated RCA + BAPN (1542), Ligated LCA + saline (1817), Ligated LCA + BAPN (890). Bars with different letters, $p < 0.05$.

(SHG) using an Olympus Fluoview FVMPE-RS Multiphoton Laser Scanning Microscope equipped with a XLPLN25XWMP2 25x water immersion objective and 1045 nm excitation laser. Images were processed using in ImageJ/FIJI [26]. All images were subjected to a 50 pixel rolling ball background subtraction and maximum intensity projections of z-stacks were generated.

Statistical analysis

We followed previously established guidelines for determining sample size in experiments involving laboratory animals [32]. Using data from preliminary studies, we estimated standardized effect sizes of 2.09 and 2.46 (stiffness, kPa), respectively, for males and females. To estimate the number of biological replicates, power analysis using G*Power (version 3.1.9.7.0) [33] was performed. Thus, it was determined that a sample size of n = 6 would have a 90% power to detect an effect size ≥2.09 assuming a 5% significance level and a two-sided test.

We analyzed stiffness distribution at the point of contact in blood vessels using kernel density plots and Lorentzian fitting using Fityk software [34]. We generated 95% confidence intervals for peak stiffness values (see Figures 2, 3) for each vessel type [29, 35]. Statistically significant differences were identified based on non-overlapping confidence intervals ($p < 0.05$). Additionally, we introduced a stiffness variability index calculated from half-width half-max (HWHM) values of each fitted distribution. This index represents half the distance between the two points on the x-axis where the probability density function of the distribution drops to half of its maximum value. The stiffness variability index quantifies the spread of elastic modulus measurements for a given vessel type, combining data from approximately 60 force curves per site across 4–6 sites per sample and six independent biological replicates. Thus, a higher numerical value of the stiffness variability index corresponds to a broader range of elastic modulus measurements.

Results

Effects of acute exposure to d-flow on the mechanical properties of the carotid intima

To determine how acute d-flow affects the mechanical properties of the carotid intima, we harvested carotid arteries from male and female mice (n = 6/sex) 2 days following PCL. We used AFM to measure the stiffness of the intact endothelium and subendothelial matrix in both the intact RCA and ligated LCA. Acute exposure to d-flow in males slightly decreased ($p < 0.05$) the endothelial stiffness (Figure 2A) but had no effect on the stiffness of the subendothelial matrix (Figure 2B). Acute exposure to d-flow in females, on the other hand, did not affect ($p > 0.05$) the endothelial (Figure 2C) or subendothelial (Figure 2D) stiffness. Regardless of sex, the intact endothelium was softer ($p < 0.05$) than the subendothelial matrix.

To assess the spread of elastic modulus measurements for a given vessel type, the stiffness variability index was compared (Table 1). In males, the ligation induced a decrease in endothelial stiffness variability but no changes were observed in the subendothelial matrix. In females, the stiffness variability index remained unchanged and increased ~3 fold, respectively, in the endothelium and the subendothelial matrix.

TABLE 1 Stiffness variability index in intact vessels (Unligated RCA) or vessels exposed to acute (2 days) d-flow post-ligation (ligated LCA).

		Unligated RCA	Ligated LCA
Endothelium	Males	23.9	11.1
	Females	22.3	20.6
Subendothelium	Males	33.7	32.4
	Females	13.1	40.1

In conclusion, acute exposure to d-flow slightly reduces endothelial stiffness in males but not in females, with the endothelium being softer than the subendothelial matrix regardless of sex.

Effects of chronic exposure to d-flow on the mechanical properties of the carotid intima

How chronic (2 weeks) d-flow affects the mechanical properties of the carotid intima in male and female mice treated with saline or BAPN (n = 6/sex/condition) was also determined. Treatment with BAPN was implemented to decouple the effects of chronic d-flow from the ensuing stiffening of the arterial wall.

Treatment with BAPN did not affect ($p > 0.05$) the endothelial stiffness in unligated arteries. In saline-treated mice, regardless of sex, chronic d-flow induced a ~8-fold increase ($p < 0.05$) in the stiffness of the endothelium (Figures 3A, C). Such response was reduced largely by the administration of BAPN ($p < 0.05$). Although BAPN effectively prevented ligation-induced endothelial stiffening, the endothelial stiffness of ligated LCA + BAPN carotids was ~2 fold higher than that of unligated RCA counterparts. Treatment with BAPN increased the stiffness variability index in the endothelium of unligated arteries (Table 2).

Treatment with BAPN did not affect ($p > 0.05$) the subendothelial stiffness in unligated arteries. Chronic exposure to d-flow stiffened the subendothelial matrix in both sexes, an effect that was fully counteracted ($p < 0.05$) by concurrent BAPN treatment (Figures 3B, D). Consistent with these results, second harmonic generation (SHG) imaging shows more prominent collagen fibrils in the wall of LCA + saline compared to LCA + BAPN or unligated RCA arteries (Supplementary Figure S1). In both sexes, treatment with BAPN blocked the increase in the stiffness variability index of the subendothelial matrix induced by chronic d-flow (Table 2).

TABLE 2 Stiffness variability index in intact carotids (Unligated RCA) and carotids exposed to chronic (2 weeks) d-flow (Ligated LCA) in the absence (saline) or presence of the LOX family inhibitor β-aminopropionitrile (BAPN).

		Unligated RCA + saline	Unligated RCA + BAPN	Ligated LCA + saline	Ligated LCA + BAPN
Endothelium	Males	5.1	21.4	24.9	13.3
	Females	2.1	15.7	19.0	19.3
Subendothelium	Males	34.7	18.4	64.8	19.8
	Females	30.1	41.9	56.9	38.1

We conclude that chronic exposure to d-flow significantly increases endothelial and subendothelial stiffness in saline-treated mice, an effect largely prevented by BAPN treatment.

The mechanical properties and morphology of endothelial cells depend on substrate stiffness

To determine the effect of substrate stiffness on human aortic endothelial cells (HAEC) *in vitro*, cells were seeded on collagen-coated polyacrylamide hydrogels. Soft (4 kPa) and stiff (50 kPa) hydrogels were used to mimic, respectively, the mechanical properties of the healthy and diseased arterial wall. Twenty-four hours after seeding, stiffness and α5β1 integrin-fibronectin adhesion force at the point of contact were measured in live cells. HAEC cultured on stiff hydrogels were stiffer ($p < 0.05$) than those cultured on soft hydrogels (Figure 4A). Cells cultured on stiffer hydrogels also exhibited increased stiffness variability, as reflected by the variability index (4 kPa: 3.0; 50 kPa: 5.6). In addition, integrin adhesion force was higher ($p < 0.05$) in cells cultured on stiff vs. soft hydrogels (Figure 4B). Consistent with this data, the development of focal adhesions, revealed by the clustering of the focal adhesion-associated protein paxillin, was significantly increased ($p < 0.05$) in endothelial cells cultured on stiff vs. soft matrices (Figures 4C, D). A similar trend was also observed in the organization of the actin cytoskeleton (Figures 4C, D).

In conclusion, endothelial cells cultured on stiffer substrates exhibit increased cell stiffness, greater integrin adhesion force, enhanced focal adhesion formation, and more organized actin cytoskeleton compared to those cultured on softer substrates.

Discussion

A major finding of this study is that pharmacological inhibition of collagen crosslinking by targeting LOX enzymes ameliorates intimal stiffening induced by chronic exposure to d-flow. Of note, these effects were consistently observed in arteries from male and female mice. Thickening and stiffening of the intima in areas where the arterial tree undergoes geometric transitions (such as bifurcations, branch vessels, and curvatures) may constitute an initially adaptive response to changes in local hemodynamics. However, when combined with additional stressors such as metabolic imbalance, hypertension, or aging, altered blood flow patterns in these areas can lead to the formation of atherosclerotic plaque [36, 37]. Therefore, identifying targets that are uniquely sensitive to arterial wall stiffening induced by persistent d-flow, in the absence of confounding atherogenic factors, could potentially advance the development of new therapeutic approaches. These new strategies would complement existing cholesterol-lowering therapies for arterial disease.

Measurements performed just 2 days after PCL provided insights into the effects of acute exposure to d-flow in the absence of changes in the stiffness of the subendothelial matrix. Overall, our results suggest that a) acute, short-duration exposure to disturbed flow *in vivo* has limited effects on the mechanical phenotype of the endothelium and sub-endothelial matrix, b) there is a consistent difference in endothelial stiffness between females and males, regardless of the flow regime, even in the absence of differences in sub-endothelial matrix properties, and c) irrespective of sex or flow regime, the sub-endothelial matrix is consistently stiffer than the endothelium.

Unexpectedly, the endothelium was softer in acutely ligated arteries of males. Acute exposure to oscillatory shear stress was shown to induce transient endothelial dysfunction, assessed by sustained stimulus flow-mediated dilation, in men but not in women [38]. Studies *in vitro* have also identified sex-dependent responses of endothelial cells exposed to combinations of shear stress and substrate stiffness; overall endothelial cells from males were more sensitive than those from females to changes in the mechanical microenvironment [39]. Further studies coupling analysis of mechanical and functional properties of the arterial wall will eventually elucidate the significance of sex-differences in the endothelial response to short-term disturbed blood flow *in vivo*.

Enzymes of the LOX family play a key role in collagen and elastin crosslinking, thereby contributing to their mechanical properties, i.e., tensile strength and elasticity. The LOX family of

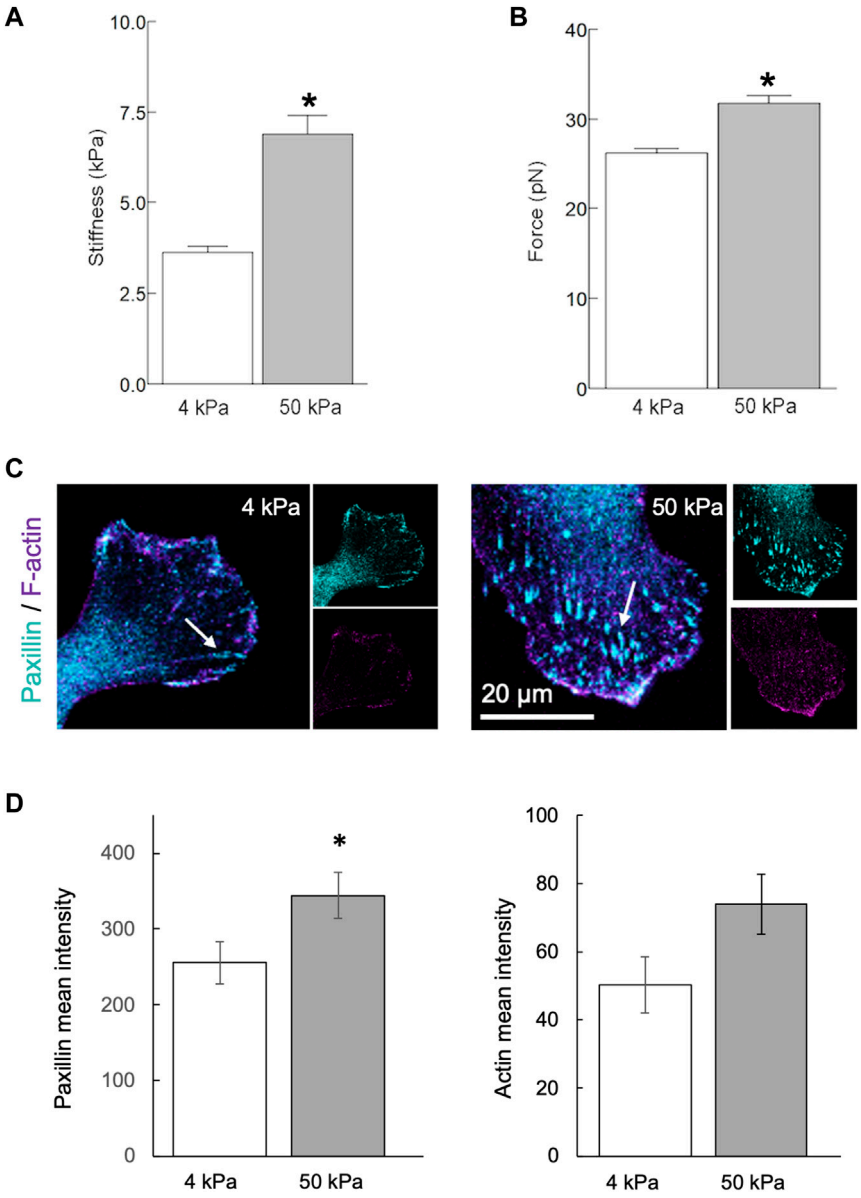

FIGURE 4
Matrix stiffness modulates the endothelial phenotype *in vitro*. Human aortic endothelial cells were cultured on polyacrylamide hydrogels with stiffnesses of 4 or 50 kPa for 24 h. **(A,B)** AFM measurements using a fibronectin-coated pyramidal tip enabled acquisition of integrin-to-fibronectin adhesion forces and cells stiffness at the point of contact. Data summarizing three independent experiments including a minimum of 10 cells examined per experiment. The number of force curves acquired for each condition is indicated in parentheses as follows: 4 kPa (1344), 50 kPa (1330). **(C,D)** Recruitment of paxillin at focal adhesions [arrows, **(C)**] was significantly increased ($p < 0.05$) in endothelial cells cultured on stiff (4 kPa) vs. soft matrices (50 kPa). A similar trend was also observed in the organization of actin cytoskeleton **(D)**. Data shown as mean ± sem. *$p < 0.05$.

enzymes catalyze the oxidative deamination of lysine and hydroxylysine residues to generate highly reactive lysyl-aldehyde (allysine) which, in turn, undergoes spontaneous reactions with other lysine, hydroxylysine or allysine residues to create crosslinks. Previous research showed that a feed-forward loop involving extracellular matrix deposition and LOX-dependent collagen crosslinking promotes atherosclerosis progression in hyperlipidemic, ApoE-deficient mice [40]. In such context, arterial wall softening by the LOX family inhibitor BAPN attenuated atherosclerotic plaque formation. Here, we combined 2 weeks of PCL with continuous delivery of BAPN in wild type (C57BL/6J) mice fed regular chow. Our study, therefore, examined the direct contribution of LOX activity to arterial wall stiffening induced by chronic d-flow without confounding effects of hypercholesterolemia or ApoE inactivation. In line with previous findings [40], our results showing prevention of d-flow-induced

intimal stiffening by BAPN administration suggests that extracellular matrix-targeted approaches that preserve or restore the mechanical homeostasis of the arterial wall may prove effective in reducing the burden of cardiovascular disease.

Alterations in the mechanical characteristics of the arterial wall can potentially influence the communication between endothelial cells and smooth muscle cells. For example, compared to the healthy endothelium of compliant arteries in young mice, the compromised nitric oxide release by the dysfunctional endothelium of stiff arteries in aged mice results in increased synthesis and secretion of LOX enzymes by smooth muscle cells [6]. These observations align with those of Jo and colleagues [12] who used the PCL model to demonstrate that persistent but not short-term exposure to d-flow impairs endothelium-dependent, nitric oxide-mediated arterial relaxation. The present observations, in conjunction with those of others [12, 17], suggest the existence of a mechanically driven feedback loop. This loop entails the disruption of endothelial homeostasis by prolonged exposure to d-flow, which fosters stiffening of the arterial wall. This, in turn, exacerbates endothelial dysfunction. Significantly, links between endothelial stiffening and various indicators of endothelial dysfunction, including decreased release of nitric oxide, increased permeability [41, 42], elevated expression of cell adhesion molecules [43], and augmented leukocyte adhesion [44], have been well documented. In agreement with previous studies [42, 45, 46], our results from *in vitro* experiments show that higher substrate stiffness strengthens focal adhesion formation and binding to the matrix, which in turn, increases the organization of the actin cytoskeleton and cell stiffness. Endothelial cell stiffening, resulting from increased actin reorganization, was shown to promote a pro-inflammatory state linked to increased ICAM-1-mediated leukocyte trans-endothelial migration [43].

The process of elastic fiber formation spans embryonic development and ceases in early postnatal life [47]. Stiffening and remodeling of mature arteries, on the other hand, are accompanied by elastin fragmentation and increased collagen deposition. Given that the activity of enzymes of the LOX family is primarily directed towards the newly deposited collagen, particularly in response to d-flow, we suggest that the observed softer nature of the sub-endothelial matrix in LCA + BAPN compared to control RCA + saline arteries likely results from reduced collagen crosslinking. This is supported by the presence of more prominent collagen fibers in ligated arteries treated with saline vs. those treated with BAPN, as shown by SHG imaging. In addition, BAPN restored, to a significant extent, the mechanical homeostasis of the endothelium. Nonetheless, we observed that the endothelium of ligated, BAPN-treated carotids was ~2-fold stiffer than that of unligated, saline treated counterparts. Thus, in the absence of subendothelial matrix stiffening, chronic stress from d-flow may be sufficient to induce subtle changes in the mechanical phenotype of the endothelium. This mechanism is supported by recent work suggesting that endothelial stiffening may occur without changes in the stiffness of the arterial wall [48] or the subendothelial matrix [25, 49]. Of clinical significance, Levitan and colleagues demonstrated that endothelial stiffening and dysfunction, arising from the combined effects of d-flow and dyslipidemia or aging, leads to early stages of atherogenesis.

While the deliberate inclusion of sex as a biological variable of importance in cardiovascular research has increased in recent years, much of the literature is built on studies excluding females or presenting results combining observations from males and females without rigorous testing for sex specific effects [50, 51]. Our study shows comparable intimal stiffening in arteries from male and female mice exposed to persistent d-flow, an effect that was substantially mitigated by BAPN treatment in both sexes.

Pharmacological inhibition of LOX enzymes to reduce collagen crosslinking is well-supported by multiple lines of evidence as follows: *i*) wild-type mice subjected to partial carotid ligation (PCL) exhibit increased collagen deposition and arterial wall stiffening [17], *ii*) a rat model of intimal hyperplasia demonstrates elevated LOX expression [22], *iii*) hypercholesterolemic, ApoE-deficient mice [40], as well as aged wild-type mice [6], exhibit increased LOX activity associated with arterial stiffening, and *iv*) various preclinical models of hypertension show LOX up-regulation linked to enhanced oxidative stress and vascular stiffness [23]. Furthermore, low shear stress induces increased LOX expression in endothelial and vascular smooth muscle cells [24]. The collective evidence highlights the central role of LOX family activity as a prominent target for addressing arterial stiffening across diverse etiologies. It is worth noting that administration of BAPN, an irreversible inhibitor of enzymes of the LOX family [52], does not cause aortic pathology when administered alone in adult mice [53].

The present investigation underscores the potential of inhibiting collagen crosslinking by LOX enzymes as an effective strategy to offset intimal stiffening. Future studies examining changes in molecular profiles and cellular phenotypes linked to persistent d-flow, coupled with strategies aimed at preserving or restoring the mechanical homeostasis of the arterial wall, hold the potential to unveil novel targeted interventions aimed at promoting arterial health.

Conclusion

This study was primarily designed to test the hypothesis that chronic d-flow initiates a feed forward loop promoting arterial wall stiffening leading to altered endothelial mechanics; hence interventions aimed at reducing arterial stiffness have the potential to disrupt this loop and preserve the mechanical hemostasis of the endothelium. Whereas acute d-flow appears to exert minimal effects on the mechanical properties of the arterial intima, persistent d-flow leads to remarkable stiffening of both the endothelium and the subendothelial matrix. Intimal stiffening induced by persistent d-flow can be averted through pharmacological inhibition of collagen crosslinking by enzymes of the LOX family.

Author contributions

BB: Conceptualization, Data curation, Formal Analysis, Funding acquisition, Investigation, Methodology, Validation, Visualization, Writing–review and editing. AT: Data curation, Formal Analysis, Methodology, Resources, Supervision, Validation, Writing–review and editing. GR: Writing–review and editing, Conceptualization, Formal Analysis, Funding acquisition, Investigation, Methodology, Project administration, Resources, Supervision, Writing–original draft.

Data availability

The raw data supporting the conclusions of this article will be made available by the authors, without undue reservation.

Ethics statement

Ethical approval was not required for the studies on humans in accordance with the local legislation and institutional requirements because only commercially available established cell lines were used. The animal study was approved by Texas A&M University Institutional Animal Care and Use Committees (IACUC), Research Compliance's Animal Welfare Office (AWO). The study was conducted in accordance with the local legislation and institutional requirements.

Funding

The author(s) declare that financial support was received for the research, authorship, and/or publication of this article. BB was supported by Texas A&M University GREAT funds, and a predoctoral fellowship from the American Heart Association (AHA829815). This work was partly funded by the American Heart Association under Grant Numbers AHA17GRNT33680067 and AHA19IPLOI34620007 to GR. Article Processing Costs were partly paid by a Team Building Grant from the Department of Veterinary Pathobiology, Texas A&M University.

Acknowledgments

We thank the laboratory of Dr. Hanjoong Jo at Emory University for training in the partial carotid ligation surgical technique. We also thank the laboratory of Dr. Irena Levitan at The University of Illinois at Chicago for guidance on establishing the splayed vessel preparation for AFM. The authors acknowledge the assistance of Dr. Malea M. Murphy and the Integrated Microscopy and Imaging Laboratory at Texas A&M College of Medicine (RRID: SCR_021637). This work is dedicated to the memory of our colleague Dr. Qinglei Li.

Conflict of interest

The authors declare that the research was conducted in the absence of any commercial or financial relationships that could be construed as a potential conflict of interest.

Supplementary material

The Supplementary Material for this article can be found online at: https://www.ebm-journal.org/articles/10.3389/ebm.2024.10090/full#supplementary-material

SUPPLEMENTARY FIGURE S1
Second harmonic generation images of collagen in unligated (RCA) and ligated (LCA) carotid arteries obtained from male mice treated with saline or BAPN. The light grey traces represent collagen fibrils in the arterial wall. The images show more prominent collagen fibrils in the wall of LCA + saline compared to LCA + BAPN or unligated RCA arteries.

References

1. Dai G, Kaazempur-Mofrad MR, Natarajan S, Zhang Y, Vaughn S, Blackman BR, et al. Distinct endothelial phenotypes evoked by arterial waveforms derived from atherosclerosis-susceptible and -resistant regions of human vasculature. *Proc Natl Acad Sci* (2004) **101**:14871–6. doi:10.1073/pnas.0406073101

2. Libby P, Buring JE, Badimon L, Hansson GK, Deanfield J, Bittencourt MS, et al. Atherosclerosis. *Nat Rev Dis Primers* (2019) **5**:56. doi:10.1038/s41572-019-0106-z

3. Davies PF, Civelek M, Fang Y, Fleming I. The atherosusceptible endothelium: endothelial phenotypes in complex haemodynamic shear stress regions *in vivo*. *Cardiovasc Res* (2013) **99**:315–27. doi:10.1093/cvr/cvt101

4. Tamargo IA, Baek KI, Kim Y, Park C, Jo H. Flow-induced reprogramming of endothelial cells in atherosclerosis. *Nat Rev Cardiol* (2023) **20**:738–53. doi:10.1038/s41569-023-00883-1

5. Mitchell GF, Hwang SJ, Vasan RS, Larson MG, Pencina MJ, Hamburg NM, et al. Arterial stiffness and cardiovascular events: the framingham heart study. *Circulation* (2010) **121**:505–11. doi:10.1161/circulationaha.109.886655

6. Steppan J, Wang H, Bergman Y, Rauer MJ, Tan S, Jandu S, et al. Lysyl oxidase-like 2 depletion is protective in age-associated vascular stiffening. *Am J Physiol Heart circulatory Physiol* (2019) **317**:H49–H59. doi:10.1152/ajpheart.00670.2018

7. Badhwar S, Chandran DS, Jaryal AK, Narang R, Deepak KK. Regional arterial stiffness in central and peripheral arteries is differentially related to endothelial dysfunction assessed by brachial flow-mediated dilation in metabolic syndrome. *Diabetes Vasc Dis Res* (2018) **15**:106–13. doi:10.1177/1479164117748840

8. Steppan J, Jandu S, Savage W, Wang H, Kang S, Narayanan R, et al. Restoring blood pressure in hypertensive mice fails to fully reverse vascular stiffness. *Front Physiol* (2020) **11**:824. doi:10.3389/fphys.2020.00824

9. Polak JF, Person SD, Wei GS, Godreau A, Jacobs DR, Jr, Harrington A, et al. Segment-specific associations of carotid intima-media thickness with cardiovascular risk factors: the Coronary Artery Risk Development in Young Adults (CARDIA) study. *Stroke* (2010) **41**:9–15. doi:10.1161/strokeaha.109.566596

10. Gallo D, Bijari Payam B, Morbiducci U, Qiao Y, Xie Y, Etesami M, et al. Segment-specific associations between local haemodynamic and imaging markers of early atherosclerosis at the carotid artery: an *in vivo* human study. *J R Soc Interf* (2018) **15**:20180352. doi:10.1098/rsif.2018.0352

11. Bijari PB, Wasserman BA, Steinman DA. Carotid bifurcation geometry is an independent predictor of early wall thickening at the carotid bulb. *Stroke* (2014) **45**: 473–8. doi:10.1161/strokeaha.113.003454

12. Nam D, Ni CW, Rezvan A, Suo J, Budzyn K, Llanos A, et al. Partial carotid ligation is a model of acutely induced disturbed flow, leading to rapid endothelial dysfunction and atherosclerosis. *Am J Physiol Heart circulatory Physiol* (2009) **297**: H1535–43. doi:10.1152/ajpheart.00510.2009

13. Nam D, Ni CW, Rezvan A, Suo J, Budzyn K, Llanos A, et al. A model of disturbed flow-induced atherosclerosis in mouse carotid artery by partial ligation and a simple method of RNA isolation from carotid endothelium. *J visualized experiments: JoVE* (2010):1861. doi:10.3791/1861

14. Andueza A, Kumar S, Kim J, Kang DW, Mumme HL, Perez JI, et al. Endothelial reprogramming by disturbed flow revealed by single-cell RNA and chromatin accessibility study. *Cell Rep* (2020) **33**:108491. doi:10.1016/j.celrep.2020.108491

15. Achner L, Klersy T, Fels B, Reinberger T, Schmidt CX, Gross N, et al. AFM-based nanoindentation indicates an impaired cortical stiffness in the AAV-PCSK9(DY) atherosclerosis mouse model. *Pflügers Archiv - Eur J Physiol* (2022) **474**:993–1002. doi:10.1007/s00424-022-02710-x

16. Kumar S, Kang DW, Rezvan A, Jo H. Accelerated atherosclerosis development in C57Bl6 mice by overexpressing AAV-mediated PCSK9 and partial carotid ligation. *Lab Invest* (2017) **97**:935–45. doi:10.1038/labinvest.2017.47

17. Kim CW, Pokutta-Paskaleva A, Kumar S, Timmins LH, Morris AD, Kang DW, et al. Disturbed flow promotes arterial stiffening through thrombospondin-1. *Circulation* (2017) **136**:1217–32. doi:10.1161/circulationaha.116.026361

18. Muzumdar MD, Tasic B, Miyamichi K, Li L, Luo L. A global double-fluorescent Cre reporter mouse. *Genesis* (2007) **45**:593–605. doi:10.1002/dvg.20335

19. Sorensen I, Adams RH, Gossler A. DLL1-mediated Notch activation regulates endothelial identity in mouse fetal arteries. *Blood* (2009) **113**:5680–8. doi:10.1182/blood-2008-08-174508

20. Kant S, Tran KV, Kvandova M, Caliz AD, Yoo HJ, Learnard H, et al. PGC1α regulates the endothelial response to fluid shear stress via telomerase reverse transcriptase control of heme oxygenase-1. *Arteriosclerosis, Thromb Vasc Biol* (2022) **42**:19–34. doi:10.1161/atvbaha.121.317066

21. Izawa-Ishizawa Y, Imanishi M, Zamami Y, Toya H, Nagao T, Morishita M, et al. Development of a novel aortic dissection mouse model and evaluation of drug efficacy using in-vivo assays and database analyses. *J Hypertens* (2019) **37**:73–83. doi:10.1097/hjh.0000000000001898

22. Nuthakki VK, Fleser PS, Malinzak LE, Seymour ML, Callahan RE, Bendick PJ, et al. Lysyl oxidase expression in a rat model of arterial balloon injury. *J Vasc Surg* (2004) **40**:123–9. doi:10.1016/j.jvs.2004.02.028

23. Martinez-Revelles S, Garcia-Redondo AB, Avendano MS, Varona S, Palao T, Orriols M, et al. Lysyl oxidase induces vascular oxidative stress and contributes to arterial stiffness and abnormal elastin structure in hypertension: role of p38MAPK. *Antioxid Redox signaling* (2017) **27**:379–97. doi:10.1089/ars.2016.6642

24. Qi Y-X, Jiang J, Jiang X-H, Wang X-D, Ji S-Y, Han Y, et al. PDGF-BB and TGF-β1 on cross-talk between endothelial and smooth muscle cells in vascular remodeling induced by low shear stress. *Proc Natl Acad Sci* (2011) **108**:1908–13. doi:10.1073/pnas.1019219108

25. Le Master E, Fancher IS, Lee J, Levitan I. Comparative analysis of endothelial cell and sub-endothelial cell elastic moduli in young and aged mice: role of CD36. *J Biomech* (2018) **76**:263–8. doi:10.1016/j.jbiomech.2018.06.007

26. Schindelin J, Arganda-Carreras I, Frise E, Kaynig V, Longair M, Pietzsch T, et al. Fiji: an open-source platform for biological-image analysis. *Nat Methods* (2012) **9**:676–82. doi:10.1038/nmeth.2019

27. Trache A, Meininger GA. Atomic force microscopy (AFM). *Curr Protoc Microbiol* (2008) **Chapter 2**:Unit 2C.2. doi:10.1002/9780471729259.mc02c02s8

28. Sun Z, Martinez-Lemus LA, Trache A, Trzeciakowski JP, Davis GE, Pohl U, et al. Mechanical properties of the interaction between fibronectin and $\alpha_5\beta_1$-integrin on vascular smooth muscle cells studied using atomic force microscopy. *Am J Physiol Heart circulatory Physiol* (2005) **289**:H2526–35. doi:10.1152/ajpheart.00658.2004

29. Chaki SP, Barhoumi R, Berginski ME, Sreenivasappa H, Trache A, Gomez SM, et al. Nck enables directional cell migration through the coordination of polarized membrane protrusion with adhesion dynamics. *J Cell Sci* (2013) **126**:1637–49. doi:10.1242/jcs.119610

30. Trache A, Trzeciakowski JP, Gardiner L, Sun Z, Muthuchamy M, Guo M, et al. Histamine effects on endothelial cell fibronectin interaction studied by atomic force microscopy. *Biophysical J* (2005) **89**:2888–98. doi:10.1529/biophysj.104.057026

31. Trzeciakowski PJ, Meininger GA NForceR: nanoscale force reader and AFM data analysis package (2004). (copyrighted).

32. Festing MF. On determining sample size in experiments involving laboratory animals. *Lab Anim* (2018) **52**:341–50. doi:10.1177/0023677217738268

33. Faul F, Erdfelder E, Lang AG, Buchner A. G*Power 3: a flexible statistical power analysis program for the social, behavioral, and biomedical sciences. *Behav Res Methods* (2007) **39**:175–91. doi:10.3758/bf03193146

34. Wojdyr M. Fityk: a general-purpose peak fitting program. *J Appl Crystallogr* (2010) **43**:1126–8. doi:10.1107/s0021889810030499

35. Venables W, Ripley B. *Modern applied statistics with S-plus. Statistics and computing*. 2nd ed. New York: Springer (1997).

36. Ohyama Y, Ambale-Venkatesh B, Noda C, Chugh AR, Teixido-Tura G, Kim JY, et al. Association of aortic stiffness with left ventricular remodeling and reduced left ventricular function measured by magnetic resonance imaging: the multi-ethnic study of atherosclerosis. *Circ Cardiovasc Imaging* (2016) **9**:e004426. doi:10.1161/circimaging.115.004426

37. Irace C, Cortese C, Fiaschi E, Carallo C, Sesti G, Farinaro E, et al. Components of the metabolic syndrome and carotid atherosclerosis: role of elevated blood pressure. *Hypertension* (2005) **45**:597–601. doi:10.1161/01.hyp.0000158945.52283.c2

38. Tremblay JC, Stimpson TV, Pyke KE. Evidence of sex differences in the acute impact of oscillatory shear stress on endothelial function. *J. Appl. Physiol.* (2019) **126**:314–21.

39. James BD, Allen JB. Sex-specific response to combinations of shear stress and substrate stiffness by endothelial cells *in vitro*. *Adv. Healthc. Mater.* (2021) **10**: e2100735.

40. Kothapalli D, Liu SL, Bae YH, Monslow J, Xu T, Hawthorne EA, et al. Cardiovascular protection by ApoE and ApoE-HDL linked to suppression of ECM gene expression and arterial stiffening. *Cell Rep* (2012) **2**:1259–71. doi:10.1016/j.celrep.2012.09.018

41. Liu Z, Tan JL, Cohen DM, Yang MT, Sniadecki NJ, Ruiz SA, et al. Mechanical tugging force regulates the size of cell-cell junctions. *Proc Natl Acad Sci* (2010) **107**: 9944–9. doi:10.1073/pnas.0914547107

42. Huynh J, Nishimura N, Rana K, Peloquin JM, Califano JP, Montague CR, et al. Age-related intimal stiffening enhances endothelial permeability and leukocyte transmigration. *Sci translational Med* (2011) **3**:112ra122. doi:10.1126/scitranslmed.3002761

43. Schaefer A, Te Riet J, Ritz K, Hoogenboezem M, Anthony EC, Mul FP, et al. Actin-binding proteins differentially regulate endothelial cell stiffness, ICAM-1 function and neutrophil transmigration. *J Cell Sci* (2014) **127**:4985–2. doi:10.1242/jcs.164814

44. Martinelli R, Zeiger AS, Whitfield M, Sciuto TE, Dvorak A, Van Vliet KJ, et al. Probing the biomechanical contribution of the endothelium to lymphocyte migration: diapedesis by the path of least resistance. *J Cell Sci* (2014) **127**: 3720–34. doi:10.1242/jcs.148619

45. van Geemen D, Smeets MW, van Stalborch AM, Woerdeman LA, Daemen MJ, Hordijk PL, et al. F-actin-anchored focal adhesions distinguish endothelial phenotypes of human arteries and veins. *Arteriosclerosis, Thromb Vasc Biol* (2014) **34**:2059–67. doi:10.1161/atvbaha.114.304180

46. Byfield FJ, Reen RK, Shentu TP, Levitan I, Gooch KJ. Endothelial actin and cell stiffness is modulated by substrate stiffness in 2D and 3D. *J Biomech* (2009) **42**: 1114–9. doi:10.1016/j.jbiomech.2009.02.012

47. Wagenseil JE, Mecham RP. Elastin in large artery stiffness and hypertension. *J Cardiovasc Translational Res* (2012) **5**:264–73. doi:10.1007/s12265-012-9349-8

48. Padilla J, Ramirez-Perez Francisco I, Habibi J, Bostick B, Aroor Annayya R, Hayden Melvin R, et al. Regular exercise reduces endothelial cortical stiffness in western diet–fed female mice. *Hypertension* (2016) **68**:1236–44. doi:10.1161/hypertensionaha.116.07954

49. Le Master E, Paul A, Lazarko D, Aguilar V, Ahn SJ, Lee JC, et al. Caveolin-1 is a primary determinant of endothelial stiffening associated with dyslipidemia, disturbed flow, and ageing. *Scientific Rep* (2022) **12**:17822. doi:10.1038/s41598-022-20713-7

50. Kim JY, Min K, Paik HY, Lee SK. Sex omission and male bias are still widespread in cell experiments. *Am J Physiology-Cell Physiol* (2021) **320**:C742–C749. doi:10.1152/ajpcell.00358.2020

51. Man JJ, Beckman JA, Jaffe IZ. Sex as a biological variable in atherosclerosis. *Circ Res* (2020) **126**:1297–319. doi:10.1161/circresaha.120.315930

52. Jung ST, Kim MS, Seo JY, Kim HC, Kim Y. Purification of enzymatically active human lysyl oxidase and lysyl oxidase-like protein from *Escherichia coli* inclusion bodies. *Protein Expr Purif* (2003) **31**:240–6. doi:10.1016/s1046-5928(03)00217-1

53. Kanematsu Y, Kanematsu M, Kurihara C, Tsou TL, Nuki Y, Liang EI, et al. Pharmacologically induced thoracic and abdominal aortic aneurysms in mice. *Hypertension* (2010) **55**:1267–74. doi:10.1161/hypertensionaha.109.140558

EBM Experimental Biology and Medicine

TYPE Original Research
PUBLISHED 27 June 2024
DOI 10.3389/ebm.2024.10129

OPEN ACCESS

*CORRESPONDENCE
Jihua Zou,
zoujihua@smu.edu.cn
Qing Zeng,
zengqingyang203@126.com

†These authors have contributed equally to this work and share first authorship

RECEIVED 25 January 2024
ACCEPTED 12 June 2024
PUBLISHED 27 June 2024

CITATION
Hu J, Fu J, Cai Y, Chen S, Qu M, Zhang L, Fan W, Wang Z, Zeng Q and Zou J (2024), Bioinformatics and systems biology approach to identify the pathogenetic link of neurological pain and major depressive disorder. *Exp. Biol. Med.* 249:10129. doi: 10.3389/ebm.2024.10129

Bioinformatics and systems biology approach to identify the pathogenetic link of neurological pain and major depressive disorder

Jinjing Hu[1,2†], Jia Fu[3†], Yuxin Cai[1,2†], Shuping Chen[1,2], Mengjian Qu[4,5], Lisha Zhang[6,7], Weichao Fan[1], Ziyi Wang[8], Qing Zeng[1,2*] and Jihua Zou[1,2,6*]

[1]Department of Rehabilitation Medicine, Zhujiang Hospital, Southern Medical University, Guangzhou, China, [2]School of Rehabilitation Medicine, Southern Medical University, Guangzhou, China, [3]Department of Rehabilitation Sciences, Hong Kong Polytechnic University, Kowloon, Hong Kong SAR, China, [4]Department of Rehabilitation, The First Affiliated Hospital, Hengyang Medical School, University of South China, Hengyang, China, [5]Rehabilitation Laboratory, The First Affiliated Hospital, Hengyang Medical School, University of South China, Hengyang, China, [6]Faculty of Health and Social Sciences, Hong Kong Polytechnic University, Kowloon, Hong Kong SAR, China, [7]Department of Clinical Medicine, Suzhou Vocational Health College, Suzhou, China, [8]The First School of Clinical Medicine, Southern Medical University, Guangzhou, China

Abstract

Neurological pain (NP) is always accompanied by symptoms of depression, which seriously affects physical and mental health. In this study, we identified the common hub genes (Co-hub genes) and related immune cells of NP and major depressive disorder (MDD) to determine whether they have common pathological and molecular mechanisms. NP and MDD expression data was downloaded from the Gene Expression Omnibus (GEO) database. Common differentially expressed genes (Co-DEGs) for NP and MDD were extracted and the hub genes and hub nodes were mined. Co-DEGs, hub genes, and hub nodes were analyzed for Gene Ontology (GO) and Kyoto Encyclopedia of Genes and Genomes (KEGG) enrichment. Finally, the hub nodes, and genes were analyzed to obtain Co-hub genes. We plotted Receiver operating characteristic (ROC) curves to evaluate the diagnostic impact of the Co-hub genes on MDD and NP. We also identified the immune-infiltrating cell component by ssGSEA and analyzed the relationship. For the GO and KEGG enrichment analyses, 93 Co-DEGs were associated with biological processes (BP), such as fibrinolysis, cell composition (CC), such as tertiary granules, and pathways, such as complement, and coagulation cascades. A differential gene expression analysis revealed significant differences between the Co-hub genes ANGPT2, MMP9, PLAU, and TIMP2. There was some accuracy in the diagnosis of NP based on the expression of ANGPT2 and MMP9. Analysis of differences in the immune cell components indicated an abundance of activated dendritic cells, effector memory $CD8^+$ T cells, memory B cells, and regulatory T cells in both groups, which were statistically significant. In summary, we identified 6 Co-hub

genes and 4 immune cell types related to NP and MDD. Further studies are needed to determine the role of these genes and immune cells as potential diagnostic markers or therapeutic targets in NP and MDD.

KEYWORDS

neurological pain, gene expression omnibus (GEO), major depressive disorder (MDD), bioinformatics, receiver operating characteristic (ROC)

Impact statement

There is a close relationship between Neuropathic Pain (NP) and major depressive disorder (MDD). The underlying molecular pathology of NP and MDD is complex and drug treatments have not yielded satisfactory results, thus further studies are needed to identify biomarkers and therapeutic targets. In this study, we identified common differentially expressed genes (Co-DEGs) for NP and MDD using several available datasets. Co-DEGs, hub genes, and hub nodes were analyzed for GO and KEGG enrichment. We also identified the immune-infiltrating cell component by ssGSEA and analyzed the relationship. We identified 6 co-hub genes, which included ANGPT2, EPO, HGF, MMP9, PLAU, and TIMP2. There were also significant differences in the abundance of activated dendritic cells, effector memory CD8 T cells, memory B cells, and regulatory T cells. Overall, this study may lead to new diagnostic markers and/or therapeutic targets for NP and MDD diseases.

Introduction

Neuropathic Pain (NP) is caused by a somatic sensory neurological condition and may be divided into central and peripheral NP [1, 2]. The prevalence of NP accounts for 6.9%–10.0% of the general population and significantly affects physical and mental health [3]. However, the underlying mechanism of NP is complex and clinical drug treatment has not yet achieved satisfactory results, thus further in-depth exploration of NP is needed [4, 5].

There is a close relationship between NP and major depressive disorder (MDD) [6]. Most patients with NP also have depression and NP may promote adaptive changes in the expression of depression-related brain network genes [7]. Identifying the common pathological factors for NP and depression comorbidities will help to identify effective treatments. Some studies that have examined NP and MDD have shown that synaptic plasticity and the synaptic microenvironment may be important to the pathogenesis of NP and depression [8], where plastic changes in corticolimbic structures have been shown to be a consequence of the association of emotion with painful stimuli [9]. Additionally, the functional and structural changes in neurons due to this neural plasticity may in turn serve as biomarkers of NP [8]. Growing evidence indicates that neuroinflammation is closely related to both NP and depression [10, 11], and that immune system abnormalities mediated by cytokines are strongly linked to the development of NP [10, 12]. Increasing neurodifferentiation and restoring the typical morphology of neonatal dendrites may improve depression-like symptoms in NP [13]. In addition, NP-induced emotional disorders are associated with hippocampal (HC) neuroinflammation [14], whereas abnormal regulation of HC dendritic spines may explain the link between chronic NP and depression [15, 16]. A potential therapeutic focus for managing complicated depressive symptoms in NPs may be the LA/BLA-CeA synapse in the amygdala [17]. Glial cells significantly affect synaptic plasticity and have a significant impact on the progression of coexisting NP and depression [18]. Regulating the P2X7-ROS signaling pathway to inhibit ferroptosis in spinal cord microglia alleviates rats with pain and depressive behavioral changes [19]. Although some progress has been made, much remains unclear regarding the co-pathogenesis of NP and depression co-morbidities. Therefore, an in-depth study of the relationship between these two diseases is needed to identify effective treatments.

We hypothesize that in the pathogenesis of NP and MDD, the expression and activity of specific co-hub genes and immune cells may exhibit significant differences between disease and healthy states, and may play a key role in the common pathological processes of these two diseases. Identifying diagnostic markers and treatment targets for NP and MDD will increase our understanding of the relationship between these two diseases and guide future clinical practice and scientific research. It will also assist doctors in accurately diagnosing NP and MDD comorbidities and provide more effective treatment options for patients. A biomarker is a measurable indicator of a biological state, providing information about disease prognosis and progression [20]. Bioinformatics will facilitate the identification of the co-occurrence mechanism of NP and depression and identify potential biomarkers and prognostic indicators to accurately diagnose and treat NP and depression comorbidities. A recent analysis screened a set of genes associated with NP-induced depression; however, it was done with a single dataset associated with a high false-positive rate [21]. Small sample sizes and different microarray platforms can introduce significant bias in the results. Therefore, finding new therapeutic targets and robust diagnostic markers is required.

TABLE 1 List of GEO datasets Information.

	GSE98793	GSE32280	GSE24982	GSE30691
Platform	GPL570	GPL570	GPL1355	GPL85
Species	*Homo sapiens*	*Homo sapiens*	*Rattus norvegicus*	*Rattus norvegicus*
Tissue	whole blood	peripheral blood lymphocytes	L4 and L5 Dorsal Root Ganglion	Dorsal Root Ganglion
Samples in Case group	128	8	20	11
Samples in Control group	64	8	20	9
Reference	Replicable and Coupled Changes in Innate and Adaptive Immune Gene Expression in Two Case-Control Studies of Blood Microarrays in Major Depressive Disorder	Blood-based gene expression profiles models for classification of subsyndromal symptomatic depression and major depressive disorder	Dynamic changes in the microRNA expression profile reveal multiple regulatory mechanisms in the spinal nerve ligation model of neuropathic pain	Multiple chronic pain states are associated with a common amino acid-changing allele in KCNS1

GEO, gene expression omnibus; MDD, major depressive disorder; NP, neuropathic pain.

In this study, we screened for Co-hub genes between NP and MDD by integrating 4 databases and identified the immune cells associated with the co-morbidity of NP and MDD by analyzing the differences in the immune cell signatures.

Materials and methods

Data downloads

The Gene Expression Omnibus (GEO) is a public repository that archives and distributes high-throughput gene expression and other functional genomics data sets, with web-based tools for data visualization and analysis [22]. We downloaded the gene expression datasets, GSE98793 [23] and GSE32280 [24], which are associated with major depressive disorder (MDD) patients from the GEO database using the R package GEOquery [25] The species source for both the GSE98793 and GSE32280 datasets was *Homo sapiens* and the data platform was GPL570 [HG-U133_Plus_2] Affymetrix Human Genome U133 Plus 2.0 Array. We also downloaded the GSE24982 [26] and GSE30691 [27] gene expression profiles of Neuropathic Pain (NP) patients, in which the species source for both was *Rattus norvegicus*. The data platform for the GSE24982 dataset was GPL1355 [Rat230_2] Affymetrix Rat Genome 230 2.0 Array, whereas the data platform for the GSE30691 dataset was the GPL85 [RG_U34A] Affymetrix Rat Genome U34 Array.

The chip GPL platform file was used for all dataset probe name annotations. We selected data from 128 patients with major depressive disorder (MDD) (MDD group, group: MDD) and 64 healthy controls (control group, group: Control) from the GSE98793 datasets of whole blood samples for inclusion in the analysis. A total of 16 subjects from the GSE32280 datasets were analyzed, including 8 examples of peripheral blood lymphocytes from matched healthy controls (control group, group: Control) and 8 peripheral blood lymphocyte samples from MDD patients. In addition, in the Neuropathic Pain (NP) dataset, GSE24982, we used a total of 40 mRNA data samples based on the L4 and L5 Dorsal Root Ganglion (DRG), including 20 control (group: Control) mRNA samples and 20 mRNA samples from the spinal nerve ligation model of neuropathic pain in rats (NP group, group: NP). The GSE30691 dataset contains mRNA samples from 11 rat neuropathic pain spinal nerve ligation (Ch) models (NP group, group: NP) and 9 Sham (SH) control (group: Control) mRNA data samples. The specific grouping of the information from these datasets is listed in Table 1. The datasets we selected are all expression profiling by array, and the sample size is sufficient to meet our analysis requirements. In addition, to ensure that our control samples match the experimental conditions, the healthy control samples and diseased samples in these datasets are as consistent as possible in terms of sample collection methods, time, and other experimental conditions to minimize the impact of confounding factors.

Editing of raw data and differential gene analysis

The MDD (GSE98793, GSE32280) and NP (GSE24982, GSE30691) datasets were combined for analysis. To minimize the variance in sample combinations across batches, we first standardized the datasets internally using the ControlizeBetweenArrays function of the R limma package [28]. We corrected the combined data for batch effects using the remove batch effect function, which enabled us to obtain the combined MDD and NP datasets. The MDD datasets contained 136 cases (disease group, group: Case/MDD) and 72 controls

(control group, group: Control). The NP datasets contained 31 cases (disease group, group: Case/NP) and 29 controls (control group, group: Control). The expression values for the samples in the MDD and NP datasets were then analyzed using Principal Component Analysis (PCA) before and after correction [29].

Differentially expressed genes (DEGs) are a subset of genes that express differently among experimental conditions, used to determine biological functions or predict therapeutic outcomes. To identify the potential mechanism of action of DEGs in MDD and NP and the associated biological features and pathways, we performed a differential expression analysis on the case and control groups using the R limma package. Genes that met the criteria |logFC| >0 and p-value <0.05 were considered DEGs for subsequent studies. |logFC| represents the absolute log2 value of the fold change in gene expression. To obtain the common differentially expressed genes (Co-DEGs) associated with MDD and NP, we selected the DEGs from the differential analysis of the MDD and NP datasets DEGs and constructed a Venn diagram. A volcano plot was generated using ggplot2 of the R package and a heat map was used to display the results.

Protein-protein interaction network analysis

A protein-protein interaction (PPI) network is made up of different proteins that engage with one another to function in a variety of biological processes, including signaling, regulation of gene expression, substance metabolism, energy production, and cell cycle regulation. A database for identifying known proteins and predicting protein interactions is the STRING database [30]. We constructed a PPI network of Co-DEGs linked to both NP and MDD disease [minimum required interaction score: middle confidence (0.400)], which was visualized with Cytoscape [31] (version 3.9.1). Using the MCODE plugin, we mined the hub nodes with connections to other PPI network nodes (K score: 2, Cutoff degree: 2, Cutoff node score: 0.2) [32]. These nodes were highly interconnected with one another and may play a role in regulating various biological processes associated with NP and MDD.

A molecular complex with a particular biological activity may be represented by closely connected local areas in the PPI network. We also used four algorithms to mine the scores of Co-DEGs in PPI networks that are connected to other PPI network nodes, which included MCC (Matthews Correlation Coefficient metric) [33], MNC (the maximal neighborhood coefficient), EPC (edge percolated component), and Closeness. According to our rankings of the Co-DEGs. The top 20 Co-DEGs across the four algorithms were considered as hub genes (hub genes, mRNA).

GO and KEGG enrichment analysis

Large-scale functional enrichment studies, including biological process (BP), molecular function (MF), and cellular component (CC), are frequently carried out using the Gene Ontology (GO) database [34]. The Kyoto Encyclopedia of Genes and Genomes (KEGG) is a widely used database that genomic data for biological pathways, diseases, and drugs [35]. We conducted GO and KEGG enrichment analyses for MDD and NP disease-associated Co-DEGs, PPI network hub nodes, and hub genes in the PPI network using the clusterProfiler [36]. p values < 0.05 and FDR values (q value) < 0.05, which were considered statistically significant as a criteria for selection and Benjamini-Hochberg was used to correct p values.

Identification and correlation analysis of immune-infiltrating cells

To more precisely measure the percentage of various immune cells in samples associated with MDD and NP. Single-sample gene-set enrichment analysis (ssGSEA) was used to identify highly sensitive and specific differentiation of the various human immune cells in the tumor microenvironment (TME). The algorithm generated a set of 28 genes to mark different tumor-infiltrating resistant cell types from a study of published tumor immune infiltration articles [37, 38]. The degree of immune cell infiltration in each sample was represented by an enrichment score computed by ssGSEA in the GSVA tool of R. The varying abundance of infiltrating immune cells between the Case (MDD/NP) group and the Control group are shown using a heat map and a boxplot for the MDD and NP datasets. We then calculated the correlation between immune cells and Co-hub genes in different disease samples by combining the gene expression matrix of both disease samples. The correlation heat map was displayed using the R package heatmap.

Co-hub gene correlation analysis and differential expression analysis

Finally, the expression of Co-hub genes in the MDD and NP datasets was examined using the Spearman method. The results of the correlation analysis were presented by plotting the correlation heat map. Next, we selected the results for the Co-hub genes with the same trend and displayed them by plotting the correlation scatter graph with the R package ggplot2.

We then established a group comparison graph for the Co-hub genes in various groups (Case/Control) of the MDD and NP

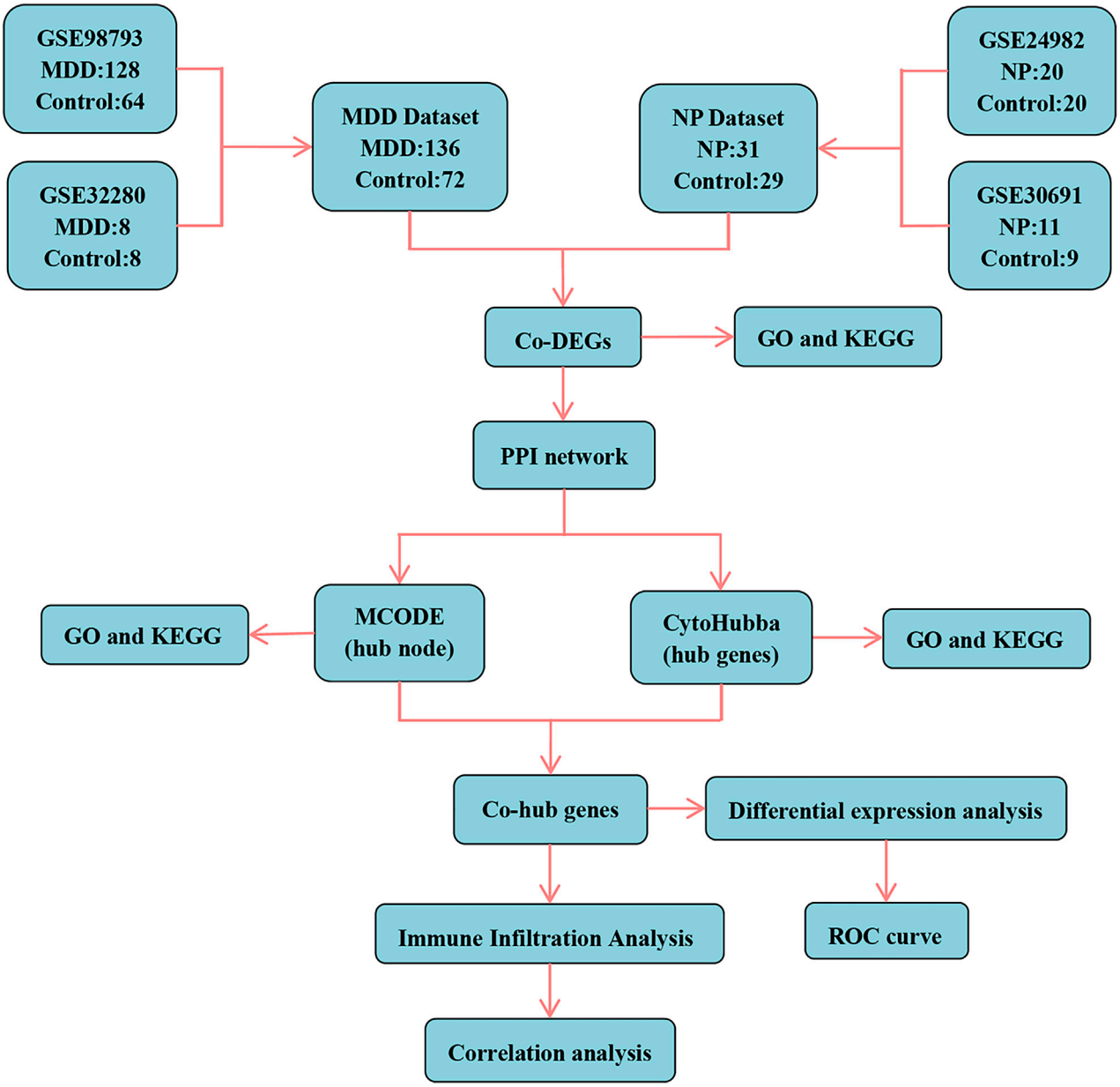

FIGURE 1
Technology roadmap. MDD, major depressive disorder; NP, Neuropathic Pain; Co-DEGs, Common differentially expressed genes; PPI network, Protein-protein interaction network; MCODE, Molecular Complex Detection; GO, Gene Ontology; KEGG, Kyoto Encyclopedia of Genes and Genomes; Co-hub genes, Common hub genes; ROC, Receiver operating characteristic curve.

datasets. The Receiver operating characteristic (ROC) Curve [39] is a composite indicator that represents continuous variables of sensitivity and specificity. We used the R package pROC program to plot the ROC curves of the Co-hub genes in the MDD and NP datasets and calculated the Area Under the Curve (AUC) of the ROC curve to determine the diagnostic significance of the Co-hub genes. The Receiver operating characteristic (ROC) curve AUC typically falls between 0.5 and 1. The diagnostic impact increases as the AUC gets near 1. The AUC exhibits low accuracy in the range of 0.5–0.7, some accuracy in the range of 0.7–0.9, and high accuracy in the range of 0.9 or above.

Statistical analysis

R software was used for data processing and analysis in this paper (Version 4.2.2). We calculated the normally distributed variables using an independent Student t-test to compare two sets

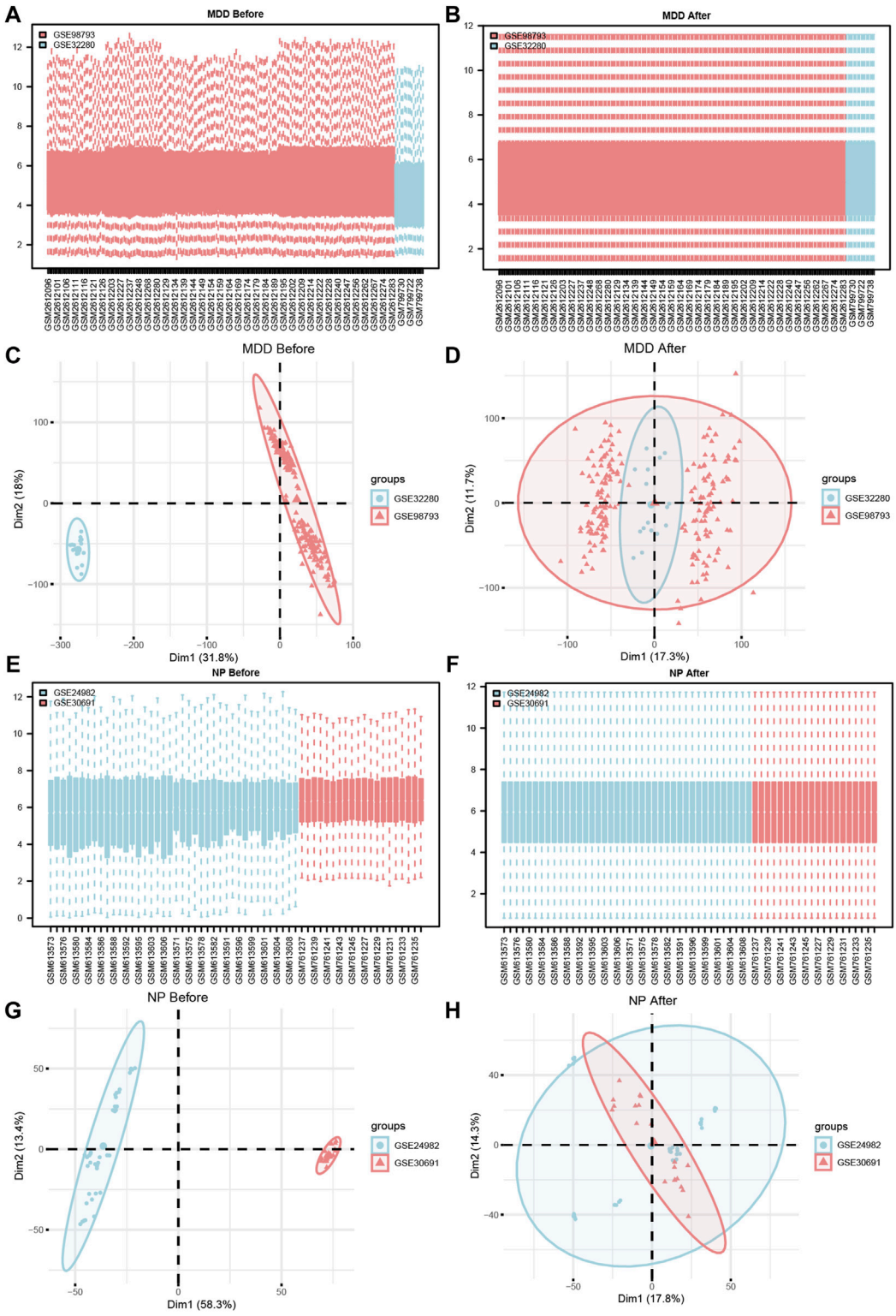

FIGURE 2
Datasets de-batch processing. **(A,B)** The boxplot before **(A)** and after **(B)** the MDD datasets removes the batch effect treatment. **(C,D)** The PCA plots before **(C)** and after **(D)** of the MDD datasets removes the batch effect treatment. **(E,F)** The boxplot before **(E)** and after **(F)** of the NP datasets removes the batch effect treatment. **(G,H)** The PCA plots before **(G)** and after **(H)** of the NP datasets removes the batch effect treatment. MDD, major depressive disorder; NP, Neuropathic Pain; PCA, Principal Component Analysis.

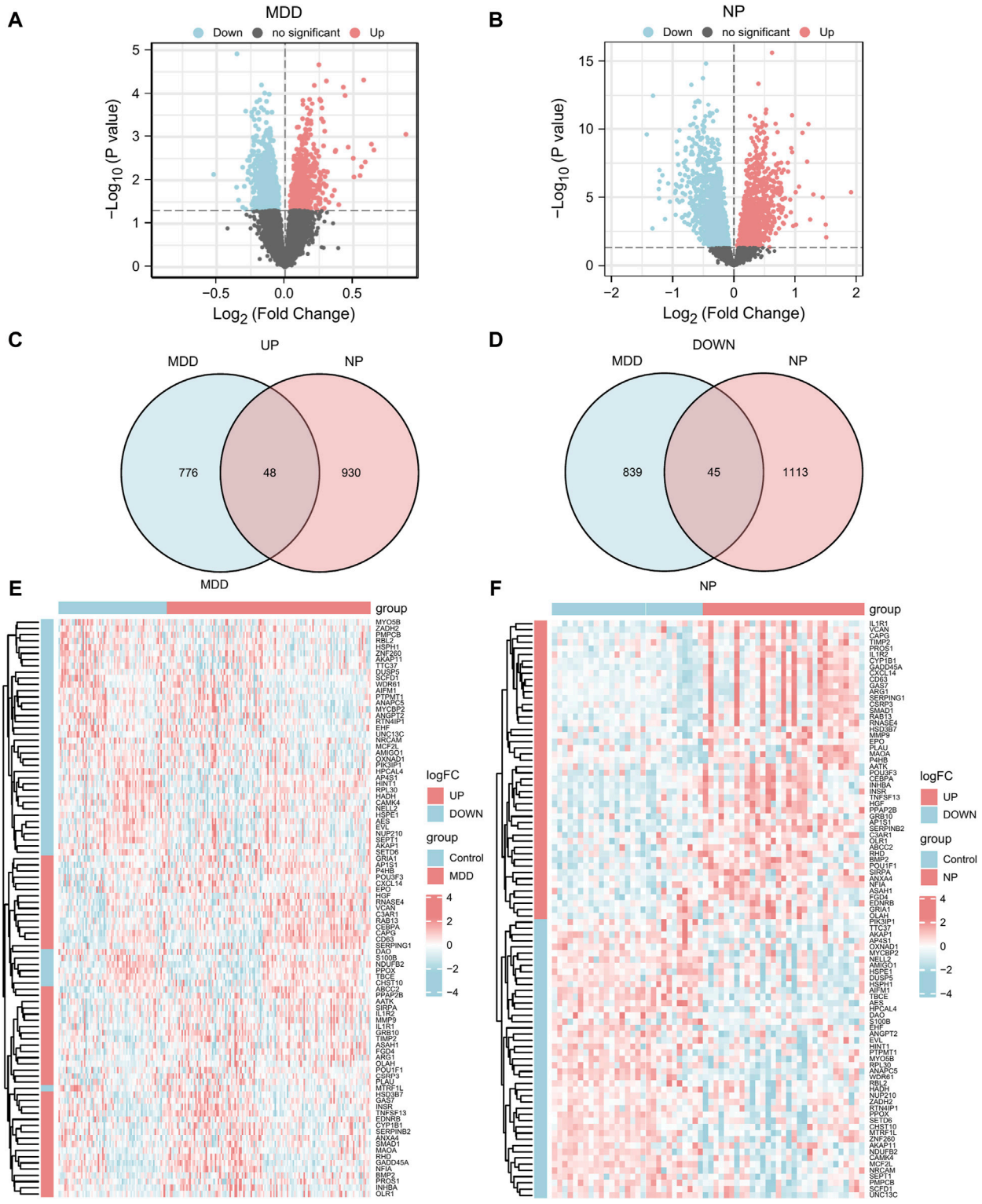

FIGURE 3
DEGs analysis of MDD datasets and NP datasets. **(A,B)** The volcano map of DEGs analysis between the disease group (group: Case/MDD/NP) and control group (group: Control) in the MDD datasets **(A)** and NP datasets **(B)**. **(C,D)** The Venn map of the up-regulation **(C)** and down-regulation **(D)** DEGs in the MDD and NP datasets. **(E,F)** The complex numerical heat map of Co-DEGs in the MDD datasets **(E)** and NP datasets **(F)**. MDD, major depressive disorder; NP, Neuropathic Pain; DEGs, differentially expressed genes; Co-DEGs, Common differentially expressed genes.

TABLE 2 List of Common differentially expressed genes in MDD datasets and NP datasets.

Common differentially expressed genes					
UP			DOWN		
AATK	FGD4	P4HB	AES	HINT1	PPOX
ABCC2	GADD45A	PLAU	AIFM1	HPCAL4	PTPMT1
ANXA4	GAS7	POU1F1	AKAP1	HSPE1	RBL2
AP1S1	GRB10	POU3F3	AKAP11	HSPH1	RPL30
ARG1	GRIA1	PPAP2B	AMIGO1	MCF2L	RTN4IP1
ASAH1	HGF	PROS1	ANAPC5	MTRF1L	S100B
BMP2	HSD3B7	RAB13	ANGPT2	MYCBP2	SCFD1
C3AR1	IL1R1	RHD	AP4S1	MYO5B	SEPT1
CAPG	IL1R2	RNASE4	CAMK4	NDUFB2	SETD6
CD63	INHBA	SERPINB2	CHST10	NELL2	TBCE
CEBPA	INSR	SERPING1	DAO	NRCAM	TTC37
CSRP3	MAOA	SIRPA	DUSP5	NUP210	UNC13C
CXCL14	MMP9	SMAD1	EHF	OXNAD1	WDR61
CYP1B1	NFIA	TIMP2	EVL	PIK3IP1	ZADH2
EDNRB	OLAH	TNFSF13	HADH	PMPCB	ZNF260
EPO	OLR1	VCAN			

MDD, major depressive disorder; NP, neuropathic pain.

of continuous variables. We used the Mann-Whitney *U* test to examine differences among factors with non-normal distributions (i.e., Wilcoxon rank sum test). If not explicitly indicated, a Spearman correlation was used to calculate the correlation coefficients between different molecules. The p values were two-sided with $p < 0.05$ being the threshold for statistical significance.

Results

Dataset pre-processing and differential gene analysis

The technical route of this study is shown in Figure 1. Using the ControlizeBetweenArrays function of the limma package, we normalized the two major MDD datasets (GSE98793 and GSE32280) and the two NP datasets (GSE24982 and GSE30691), respectively. The MDD datasets (Figures 2A, B) and the NP datasets (Figures 2E, F) were obtained through a batch effect correction of the combined data using the "remove batch effect" function. The MDD datasets include 136 MDD samples (group: MDD) and 72 control samples (group: Control). The NP datasets consist of 31 NP samples (group: NP) and 29 control samples (group: Control). In addition, to convert mouse to human genes for subsequent analysis, the R package homologene was used to conduct an ID transformation of the NP datasets.

To verify the effect of removing the batch effect (Figures 2C, D, G, H), we grouped the MDD, and NP datasets according to the source of the samples. For the dataset expression matrix, before, and after the batch effect was eliminated, we performed a Principal Component Analysis (PCA). The results indicated that after the batch removal process, the batch effect was essentially eliminated from the MDD and NP datasets.

Following Principal Component Analysis (PCA), we obtained DEGs between different groups of the MDD and NP datasets. The MDD datasets yielded 21,655 DEGs, of which 1708 met the criteria. For the Case/MDD group, there were 824 upregulated DEGs and 884 downregulated DEGs. The NP datasets yielded 4076 DEGs, of which 2,136 met the criteria. For the Case/NP group, 978 exhibited high expression (low expression in the Control group with positive logFC), and 1,158 genes exhibited low expression (high expression in the Control group with negative logFC). The results for the MDD and NP datasets are depicted in volcano plots (Figures 3A, B).

TABLE 3 GO and KEGG enrichment analysis results of 93 Common differentially expressed genes.

Ontology	ID	Description	GeneRatio	BgRatio	P-value	p.adjust	qvalue
BP	GO:0042730	fibrinolysis	4/90	28/18,670	9.46e-06	0.021	0.018
BP	GO:0050727	regulation of inflammatory response	11/90	485/18,670	2.12e-05	0.023	0.020
BP	GO:0021700	developmental maturation	8/90	284/18,670	6.85e-05	0.045	0.040
BP	GO:0070301	cellular response to hydrogen peroxide	5/90	99/18,670	1.17e-04	0.045	0.040
BP	GO:0030195	negative regulation of blood coagulation	4/90	53/18,670	1.23e-04	0.045	0.040
BP	GO:1900047	negative regulation of hemostasis	4/90	54/18,670	1.33e-04	0.045	0.040
BP	GO:0034614	cellular response to reactive oxygen species	6/90	168/18,670	1.62e-04	0.045	0.040
BP	GO:0050819	negative regulation of coagulation	4/90	57/18,670	1.64e-04	0.045	0.040
CC	GO:0070820	tertiary granule	6/90	164/19,717	1.06e-04	0.026	0.022
KEGG	hsa04610	Complement and coagulation cascades	5/57	85/8,076	3.13e-04	0.048	0.046

GO, gene ontology; BP, biological process; CC, cellular component; MF, molecular function; KEGG, kyoto encyclopedia of genes and genomes.

To obtain Co-DEGs for MDD and NP, we focused on the intersection of 48 upregulated and 45 downregulated Co-DEGs that were presented in a Venn diagram (Figures 3C, D). The data and annotation for these Co-DEGs is listed in Table 2. We examined differential expression of 93 Co-DEGs from the MDD and NP datasets in various groups. Heat maps were used to display the results of the differential analysis using the R package heatmap (Figures 3E, F). As shown in Figure 3, 93 Co-DEGs showed significant differences in expression between the groups based on the MDD and NP datasets.

GO and KEGG enrichment analysis of the Co-DEGs

For the 93 Co-DEGs, we performed a functional enrichment analysis using the Gene Ontology (GO) and the Kyoto Encyclopedia of Genes and Genomes (KEGG) pathway databases (Table 3). The results indicated that 93 Co-DEGs were primarily enriched in biological processes (BP), such as fibrinolysis, regulation of inflammatory response, and developmental maturation. They were also enriched in cellular component (CC) tertiary granules and complement and coagulation cascade from the KEGG pathway database. The results are shown in the form of bubble plots and a network diagram (Figures 4A, B). We then combined the logFC values with the enrichment analysis, which generates a z score by providing the logFC values for the 93 Co-DEGs. The effects of GO and KEGG enrichment analysis by joint logFC are shown as circle plots (Figure 4C) and bubble plots (Figure 4D). The results indicated that the 93 Co-DEGs from the MDD dataset were primarily located in the BP pathway (Figures 4C, D).

The MCODE plug-in identifies the hub nodes

After excluding the Co-DEGs that did not have a connection with other nodes, we constructed a PPI network (Figure 5A) consisting of 54 Co-DEGs using the STRING database. We analyzed the nodes that have connections with other nodes in the PPI network using the MCODE plugin. We then used the genes in cluster1 and cluster2 of the results as hub nodes for the Co-DEG PPI network, in which we obtained an MCODE cluster network consisting of 6 Co-DEGs (PLAU, TIMP2, HGF, ANGPT, MMP9, EPO) (Score = 4.8) (Figure 5B) and an MCODE cluster network (Score = 3) (Figure 5C) consisting of 3 Co-DEGs (RPL30, TTC37, WDR61). The 9 (hub node) genes included PLAU, TIMP2, HGF, ANGPT, MMP9, EPO, RPL30, TTC37, and WDR61. These nodes warrant additional study as they may be important in regulating the entire BP.

On the 9 hub nodes (PLAU, TIMP2, HGF, ANGPT, MMP9, EPO, RPL30, TTC37, WDR61), we performed GO and KEGG enrichment analyses (Supplementary Table S1). The results indicated that the BP, negative regulation of the apoptotic signaling pathway, was largely abundant in the 9 hub nodes. Enrichment in CC, such as tertiary granules, and transcriptionally active chromatin as well as MF, such as serine-type endopeptidase activity, was observed. The KEGG pathways, including proteoglycans in cancer, PI3K-Akt signaling pathway, and RNA degradation, were also enriched. The results are presented using bar graphs in Figure 5D. In addition, the GO analysis outcomes are shown for the BP pathway (Figure 5E), CC pathway (Figure 5F), and MF pathway (Figure 5G) as a network diagram, whereas the results of KEGG pathway enrichment analysis are displayed as a circular network diagram (Figure 5H).

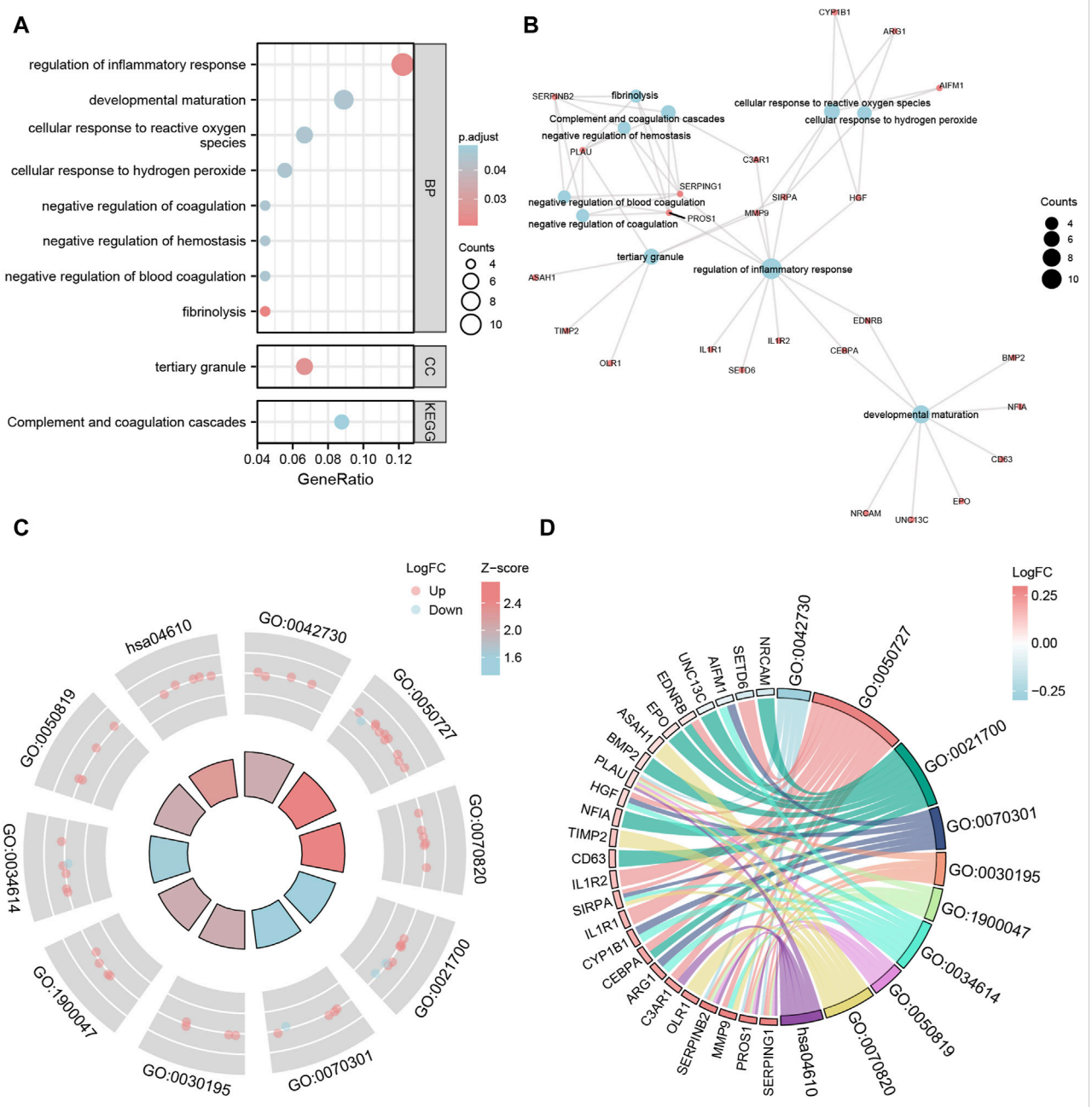

FIGURE 4
GO and KEGG enrichment analysis of Co-DEGs. **(A,B)** The bubble plot **(A)** and network plot **(B)** of GO/KEGG enrichment analysis results of Co-DEGs. **(C,D)** The circle plot **(C)** and chord plot **(D)** of GO function enrichment of Co-DEGs combined with logFC analysis results. The ordinate in the bubble chart **(A)** is GO/KEGG terms, and the length of the bubble distance to the Y axis represents the GeneRatio of GO terms. Co-DEGs, Common differentially expressed genes; GO, Gene Ontology; BP, biological process; CC: cellular component; MF: molecular function; KEGG, Kyoto Encyclopedia of Genes and Genomes. The screening criteria for GO/KEGG-enriched entries were *p* value < 0.05 and FDR value (*q*.value) < 0.05.

CytoHubba plug-in identifies the hub genes

We calculated the PPI network using the cytoHubba plugin for Cytoscape using four algorithms: MCC (Matthews Correlation Coefficient metric), MNC, EPC (edge percolated component), and Closeness. The top 20 Co-DEGs with the best scores were selected to further identify the hub genes in the Co-DEGs PPI network (Figures 6A–D). The color of the dotted blocks in the graph, from yellow to red, represents a gradual increase in rating. Next, we focused on the intersection of the top 20 Co-DEGs obtained by each of the four algorithms

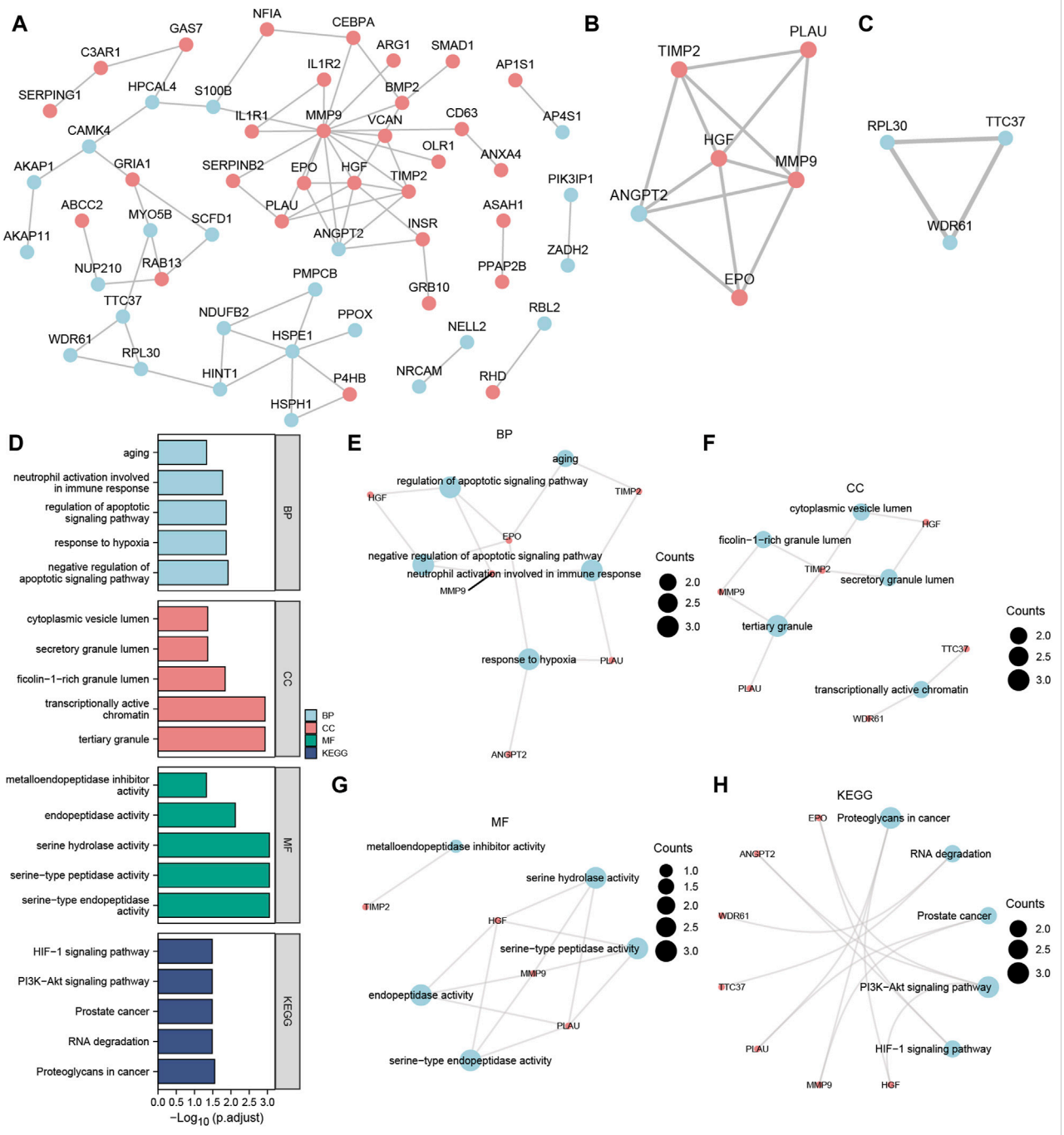

FIGURE 5
MCODE plug-in identifies the hub nodes of GO, and KEGG enrichment analysis and the PPI network. **(A)** PPI network of Co-DEGs. **(B,C)** The MCODE cluster 1 **(B)** and MCODE cluster 2 **(C)** networks of the PPI network of Co-DEGs. **(D)** Histogram of GO/KEGG enrichment analysis results of hub node. **(E–G)** The GO function enrichment analysis of Co-DEGs BP pathway **(E)**, CC pathway result **(F)**, MF pathway **(G)** result network diagram. **(H)** Ring network diagram of KEGG pathway enrichment analysis results of Co-DEGs. The ordinate in the histogram **(D)** is GO/KEGG terms, and the length of the bar distance from the Y axis represents the padj value of GO terms. Co-DEGs, Common differentially expressed genes; PPI network, Protein-protein interaction network; MCODE, Molecular Complex Detection; GO, Gene Ontology; BP, biological process; CC, cellular component; MF, molecular function; KEGG, Kyoto Encyclopedia of Genes and Genomes. The screening criteria for GO/KEGG-enriched entries were p value < 0.05 and FDR value (q.value) < 0.05.

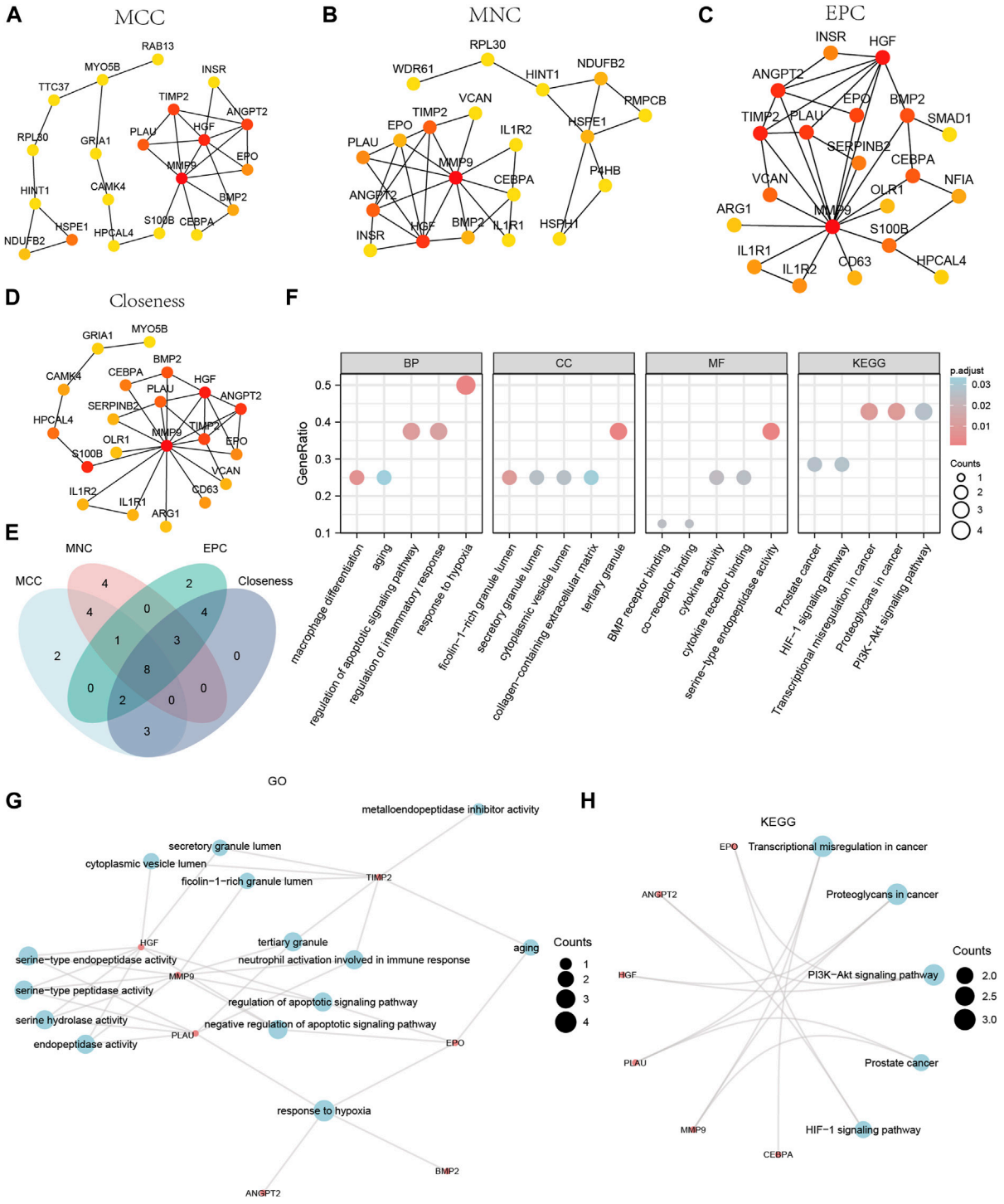

FIGURE 6
CytoHubba plug-in node network for Co-DEGs PPI network and GO and KEGG enrichment analysis. The top 20 node network of the MCC **(A)**, MNC **(B)**, EPC **(C)**, Closeness **(D)** algorithm of the PPI network of Co-DEGs. **(E)** The top 20 nodes of the Venn diagram result from the four algorithms of MCC, MNC, EPC, and Closeness in the Co-DEGs PPI network. **(F)** The bubble plot of GO/KEGG enrichment analysis results of 8 hub genes. **(G)** The network diagram of GO enrichment analysis results of Co-DEGs. **(H)** The ring network diagram of KEGG pathway enrichment analysis results of Co-DEGs. The abscissa in the bubble chart **(F)** is GO/KEGG terms, and the length of the bubble distance from the X-axis represents the GeneRatio value of GO terms. Co-DEGs, Common differentially expressed genes; PPI network, Protein-protein interaction network; MCC, Matthews Correlation Coefficient metric; MNC, the maximal neighborhood coefficient; EPC, edge percolated component; GO, Gene Ontology; BP, biological process; CC, cellular component; MF, molecular function; KEGG, Kyoto Encyclopedia of Genes and Genomes. The screening criteria for GO/KEGG-enriched entries were p value < 0.05 and FDR value (q.value) < 0.05.

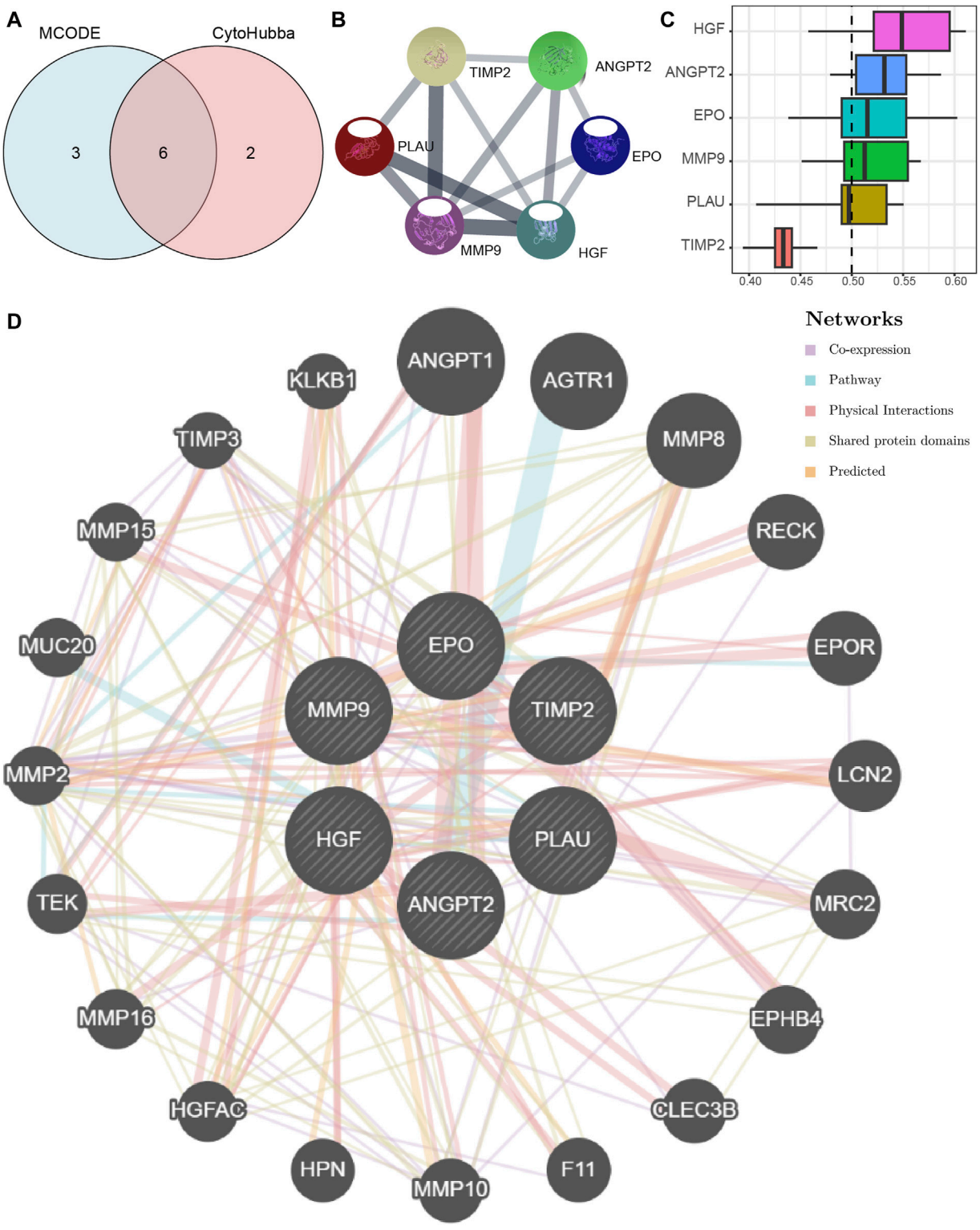

FIGURE 7
The PPI network of Co-hub genes. **(A)** The Venn diagram of the analysis results of the PPI network MCODE plugin and the cytoHubba plug-in analysis results. **(B)** The PPI network of Co-hub genes. **(C)** The histogram of functional similarity analysis results of Co-hub genes. **(D)** The PPI network of Co-hub genes based on the GeneMANIA database. PPI network, Protein-protein interaction network; MCODE, Molecular Complex Detection; Co-hub genes, Common hub genes.

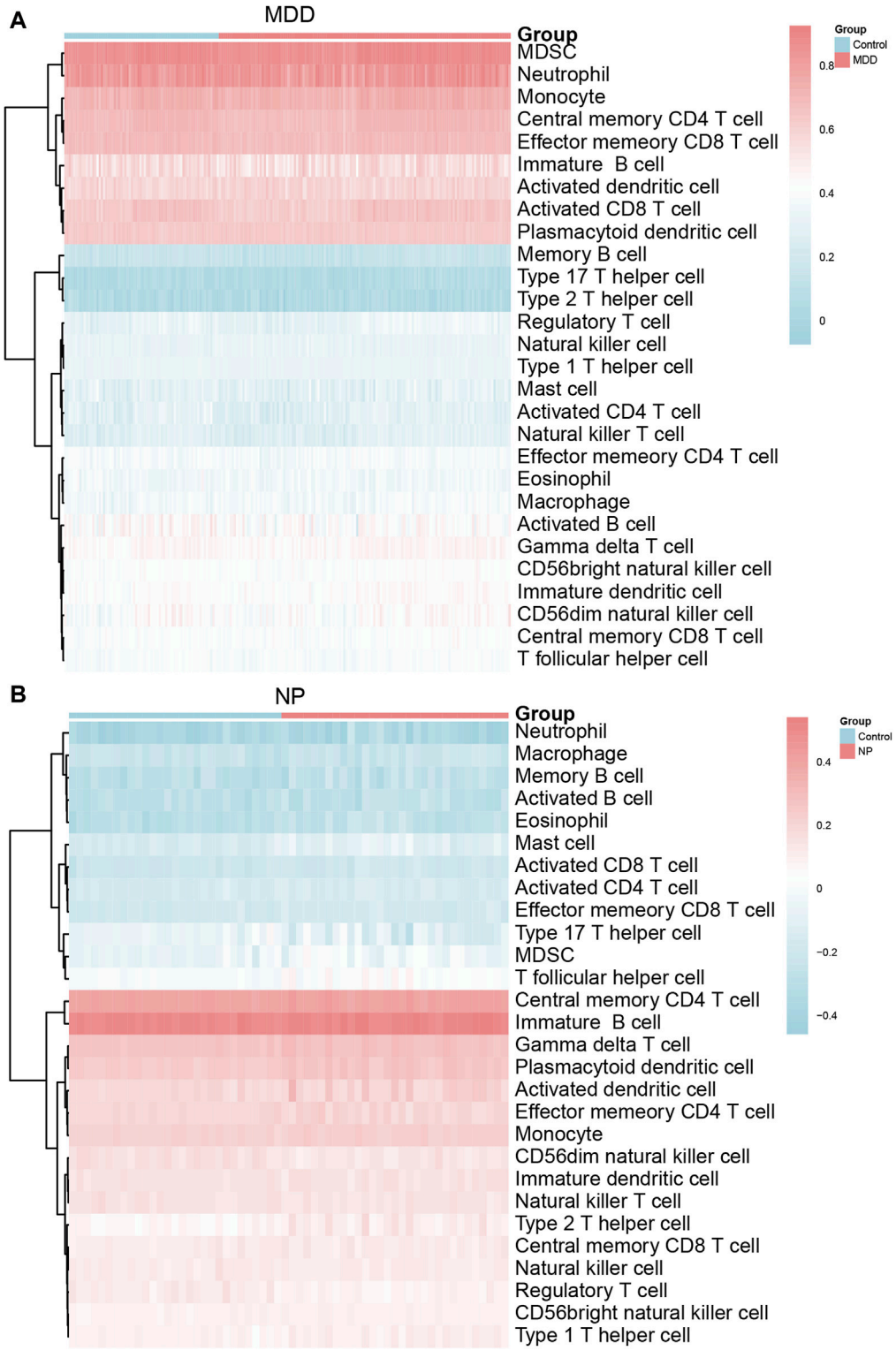

FIGURE 8
Immune characteristics difference analysis of MDD datasets samples and NP datasets samples. **(A,B)** Complex heatmap of ssGSEA immunoinfiltration analysis results for MDD datasets samples **(A)** and NP datasets samples **(B)** MDD, major depressive disorder; NP, Neuropathic Pain; ssGSEA: single-sample gene-set enrichment analysis.

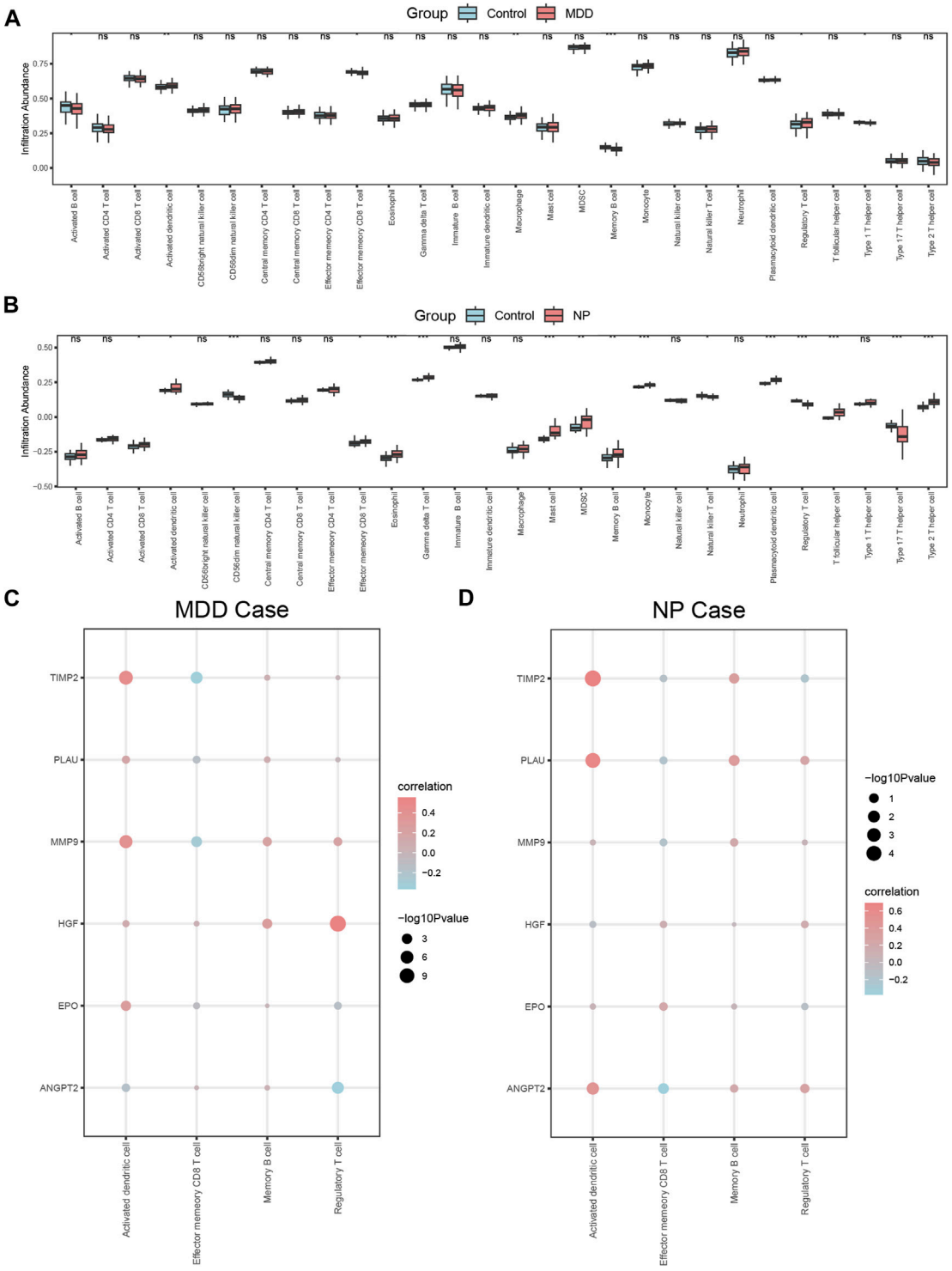

FIGURE 9
Correlation analysis of immune characteristics of MDD datasets disease samples and NP datasets disease samples. **(A,B)** Complex heatmap of ssGSEA immunoinfiltration analysis results for MDD datasets samples **(A)** and NP datasets samples **(B)** MDD, major depressive disorder; NP, Neuropathic Pain; ssGSEA: single-sample gene-set enrichment analysis. **(A,B)** Grouped comparison plot of ssGSEA immunoinfiltration analysis results for MDD datasets samples **(A)** and NP datasets samples **(B)**. **(C,D)** Correlation heat map of immune cell infiltration abundance and Co-hub genes expression in MDD datasets disease samples **(C)** and NP datasets disease samples **(D)**. The symbol ns is equivalent to $p \geq 0.05$, which is not statistically significant; The symbol * is equivalent to $p < 0.05$; the symbol ** is equivalent to $p < 0.01$; and the symbol *** is equivalent to $p < 0.001$. MDD, major depressive disorder; NP, Neuropathic Pain; ssGSEA, single-sample gene-set enrichment analysis.

(MCC, MNC, EPC, Closeness) to obtain the hub genes and drew Venn diagrams to display the results (Figure 6E). We obtained a total of 8 hub genes, which included ANGPT2, BMP2, CEBPA, EPO, HGF, MMP9, PLAU, and TIMP2.

We performed GO and KEGG enrichment analyses for the hub genes (Supplementary Table S2). The results indicated that the 8 hub genes were primarily enriched in BP, such as response to hypoxia. They were also enriched in CC, such as tertiary granules, and MF, such as serine-type endopeptidase activity. The KEGG pathways identified included transcriptional misregulation in cancer. We displayed the findings of the GO and KEGG enrichment analyses using bubble plots (Figure 6F). We also displayed the GO gene functional enrichment analysis findings (Figure 6G) as a network diagram and the KEGG pathway enrichment analysis results (Figure 6H) as a circular network diagram.

The PPI network of Co-hub genes

We first obtained Co-hub genes by taking the intersection of the 9 hub nodes (PLAU, TIMP2, HGF, ANGPT, MMP9, EPO, RPL30, TTC37, WDR61) and the 8 hub genes (ANGPT2, BMP2, CEBPA, EPO, HGF, MMP9, PLAU, TIMP2) (Figure 7A). As shown in Figure 7A, we obtained 6 Co-hub genes, which included ANGPT2, EPO, HGF, MMP9, PLAU, and TIMP2. We analyzed their interaction using the STRING database and visualized them with Cytoscape (Figure 7B). Next, the 6 Co-hub genes (ANGPT2, EPO, HGF, MMP9, PLAU, TIMP2) were analyzed for functional similarity. We calculated the semantic similarity among GO terms, sets of GO terms, gene products, and gene clusters using the R package GOSemSim. The results of this functional similarity analysis between the 6 Co-hub genes are presented as a boxplot in Figure 7C. HGF had the highest value of functional similarity with the other Co-hub genes among the 6 Co-hub genes.

Using the GeneMANIA database, we constructed a Co-hub gene PPI network after retaining the nodes with links to the 6 Co-hub genes (Figure 7D). As shown in Figure 7D, there are five types of interactions between the nodes of our constructed Co-hub genes PPI network and the 6 Co-hub genes, including Co-expression, Pathway, Physical Interactions, Shared protein domains, and Predicted.

Differences in immune characteristics between the MDD and NP datasets

The relative infiltration of 28 immune cell types in the disease group (Case/MDD/NP) and control group samples in the MDD and NP dataset expression matrix were determined using the ssGSEA algorithm. We presented the findings for both datasets using a complex heat map (Figures 8A, B). The results indicated that among the disease and control group samples of MDD (Figure 8A) and NP (Figure 8B), the infiltration by the 28 cell types varied significantly. Next, we used the Mann-Whitney *U* test to analyze the differential degree of infiltration of these cells among the different groups (Case/Control) in the two datasets and the results are grouped in comparison plots (Figures 9A, B). The control group exhibited a higher abundance of activated B cells, effector memory CD8 T cells, memory B cells, and type 1 T helper cells compared with the disease group. In contrast, the disease group contained a more activated dendritic cells, macrophages, and regulatory T cells compared with the control group (Figure 9A).

CD56dim natural killer cells, natural killer T cells, regulatory T cells, and type 17 T helper cells had higher infiltration in the NP dataset control group compared with that in the disease group. In contrast, the disease group had higher infiltration of activated CD8 T cells, activated dendritic cells, effector memory CD8 T cells, eosinophils, gamma delta T cells, mast cells, MDSCs, memory B cells, monocyte neutrophils, plasmacytoid dendritic cells, T follicular helper cells, and type 2 T helper cells (Figure 9B).

Figures 9A, B shows that there were statistically significant differences ($p < 0.05$) between the relative immune infiltration of the MDD and NP dataset samples compared with control group (Case/Control) samples for activated dendritic cells, effector memory CD8 T cells, memory B cells, and regulatory T cells.

We also calculated the correlation for these 4 immune cell types with the expression of the 6 Co-hub genes (ANGPT2, EPO, HGF, MMP9, PLAU, TIMP2) in the MDD and NP dataset disease samples (Figures 9C, D). The results indicated that the expression of these 6 genes and the relative abundance of the four immune cells tended to be significantly positive and less negatively correlated ($p < 0.05$) in the MDD dataset samples (Figure 9C). The results of the correlation analysis between the infiltration of the 4 immune cells and the expression of 6 the Co-hub genes in the NP dataset disease samples revealed that there was a significant positive correlation ($p < 0.05$) between these infiltrating cells and the 6 genes. Activated dendritic cells showed the highest correlation with the expression of these genes (Figure 9D).

Finally, the expression of activated dendritic immune cells, memory B cells and the 6 Co-hub genes had a significant positive correlation in the MDD and NP dataset disease samples (Figures 9C, D). In contrast, the expression of the 6 Co-hub genes was significantly negatively correlated with the infiltration abundance of effector memory CD8 T immune cells in these datasets (Figures 9C, D).

Correlation analysis of the Co-hub genes

The correlation in expression between the 6 Co-hub genes (ANGPT2, EPO, HGF, MMP9, PLAU, TIMP2) was analyzed in

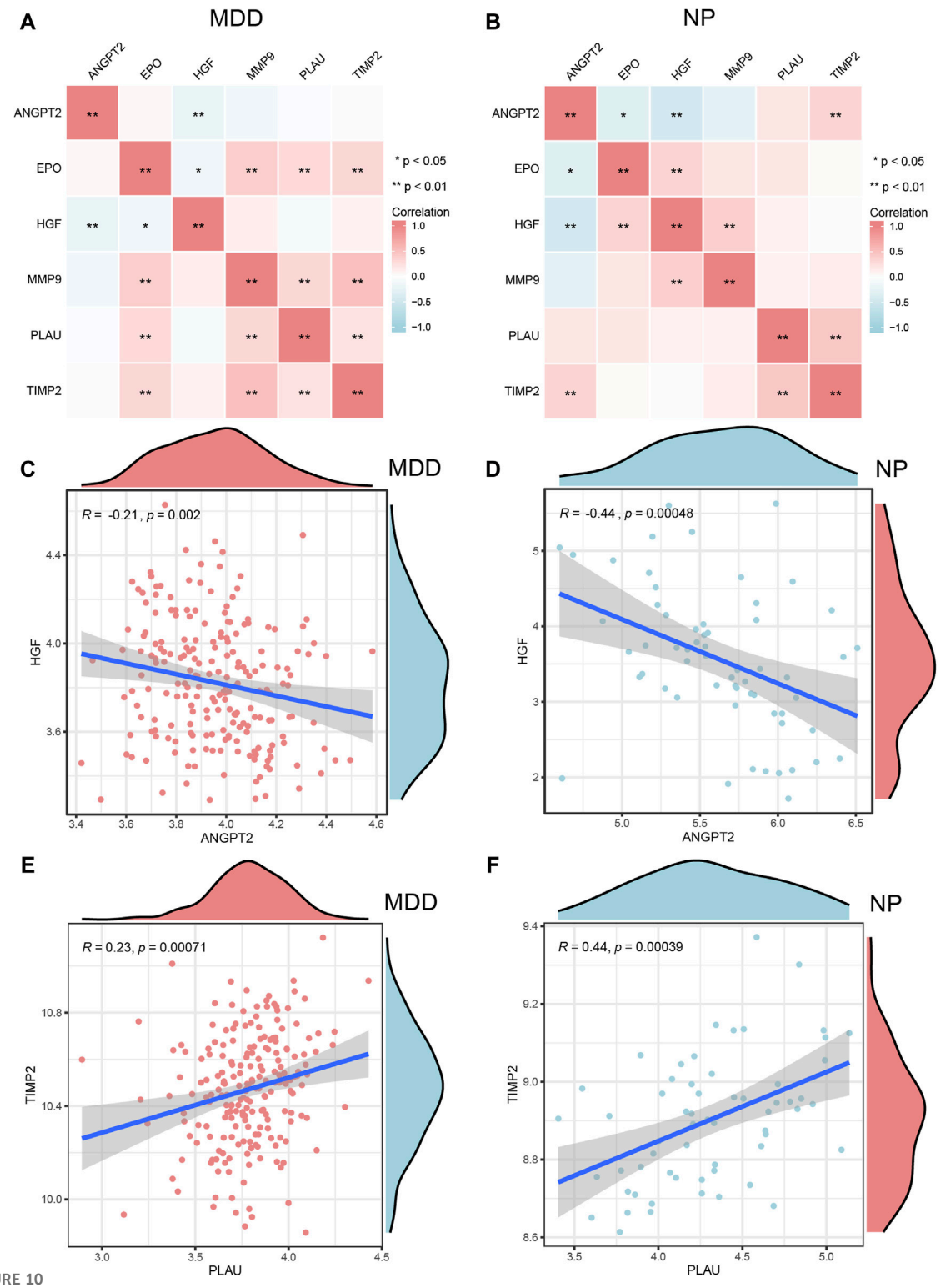

FIGURE 10
Correlation analysis of Co-hub genes. **A,B,** The correlation heat map results of Co-hub genes in MDD datasets **(A)**, NP datasets **(B)**. **(C,D)** The correlation scatterplot results of Co-hub genes ANGPT2 and HGF in MDD datasets **(C)** and NP datasets **(D)**. **(E,F)** The correlation scatterplot results of Co-hub genes PLAU and TIMP2 in the MDD datasets **(E)** and NP datasets **(F)**. $p \geq 0.05$, not statistically significant; $p < 0.05$, statistically significant; $p < 0.01$, which was highly statistically significant; $p < 0.001$, which is exceedingly statistically significant. The correlation coefficient (r) in the correlation scatterplot is strongly correlated if the absolute value is above 0.8; the absolute value is 0.5–0.8 is moderately correlated; Absolute value of 0.3–0.5 is weakly correlated; absolute values below 0.3 are weak or uncorrelated. MDD, major depressive disorder; NP, Neuropathic Pain.

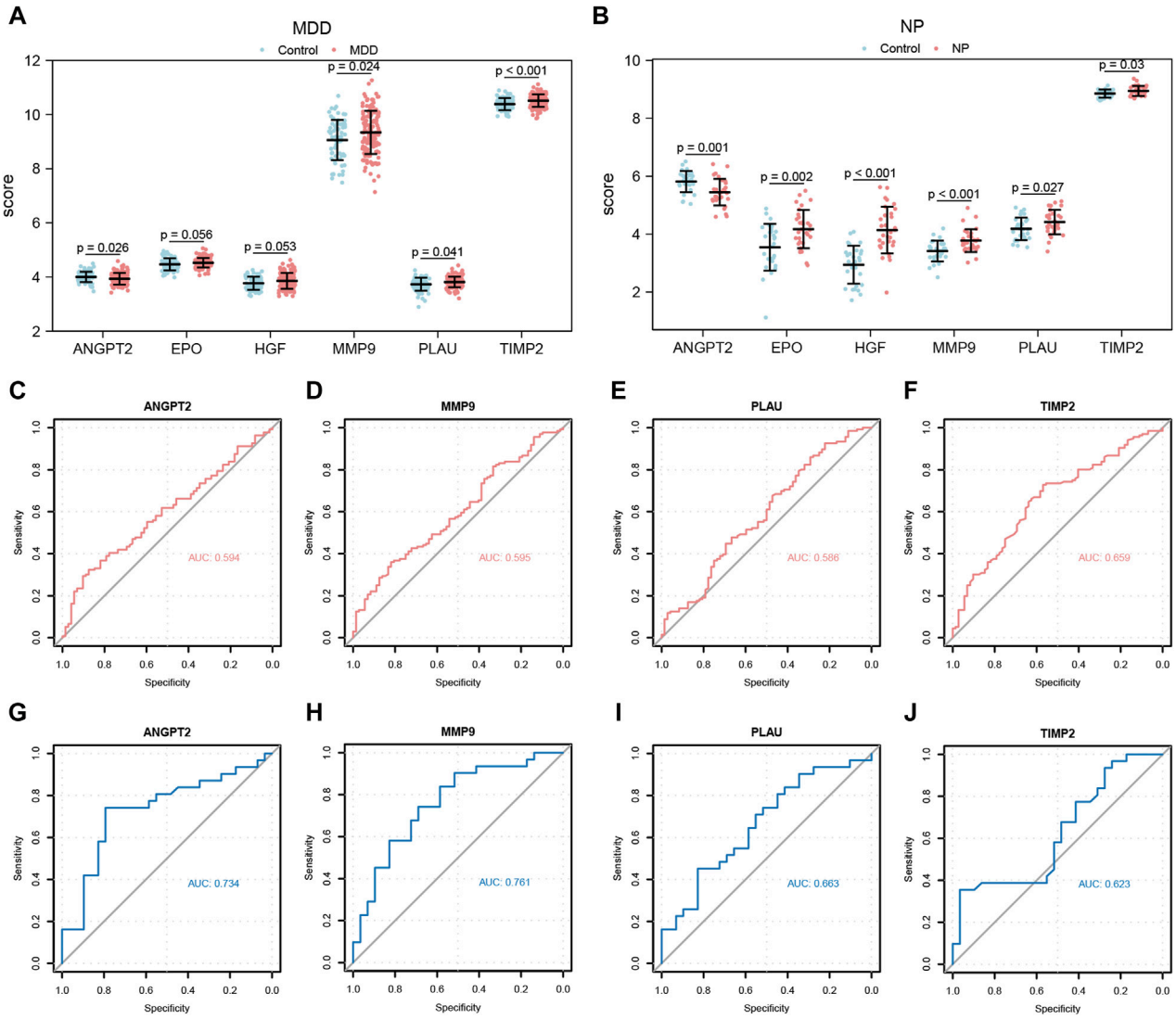

FIGURE 11
Expression differences analysis of Co-hub genes in MDD datasets and NP datasets. **(A,B)** The correlation heat map results of Co-hub genes in MDD datasets **(A)**, NP datasets **(B)**. **(C,D)** The correlation scatterplot results of Co-hub genes ANGPT2 and HGF in MDD datasets **(C)** and NP datasets **(D)**. **(E,F)** The correlation scatterplot results of Co-hub genes PLAU and TIMP2 in the MDD datasets **(E)** and NP datasets **(F)**. $p \geq 0.05$, not statistically significant; $p < 0.05$, statistically significant; $p < 0.01$, which was highly statistically significant; $p < 0.001$, which is exceedingly statistically significant. The correlation coefficient (r) in the correlation scatterplot is strongly correlated if the absolute value is above 0.8; the absolute value is 0.5-0.8 is moderately correlated; Absolute value of 0.3-0.5 is weakly correlated; absolute values below 0.3 are weak or uncorrelated. MDD, major depressive disorder; NP, Neuropathic Pain. **(A,B)** Grouped comparison plot of Co-hub genes in MDD datasets **(A)**, NP datasets **(B)** in different groups (Case/Control). **(C–F)** ROC curves of Co-hub genes ANGPT2 **(C)**, MMP9 **(D)**, PLAU **(E)**, TIMP2 **(F)** in different groups of the MDD datasets. **(G–J)** ROC curves of Co-hub genes ANGPT2 **(G)**, MMP9 **(H)**, PLAU **(I)**, TIMP2 **(J)** in different groups of NP datasets. $p \geq 0.05$, not statistically significant; $p < 0.05$, statistically significant; $p < 0.01$, which was highly statistically significant; $p < 0.001$, which is exceedingly statistically significant. The closer the AUC in the ROC curve is to 1, the better the diagnosis. AUC has low accuracy at 0.50.7; AUC has a certain accuracy at 0.70.9; AUC has high accuracy above 0.9. MDD, major depressive disorder; NP, Neuropathic Pain; ROC, receiver operating characteristic curve; AUC, Area Under the Curve.

the MDD and NP datasets by Spearman correlation analysis and presented as a correlation heat map (Figures 10A, B). There was a positive correlation among most Co-hub genes in both datasets; however, quite a few correlations of Co-hub genes in the NP datasets did not show a statistical difference ($p > 0.05$) (Figures 10A, B).

We selected interaction pairs that were statistically different ($p < 0.05$) with the same trend in the MDD and NP datasets for further analysis. Based on the Spearman algorithm, we generated scatter plots to show the correlation analysis results for the Co-hub genes, ANGPT2 and HGF, in the MDD and NP datasets as well as the correlation analysis result of PLAU and TIMP2 in the

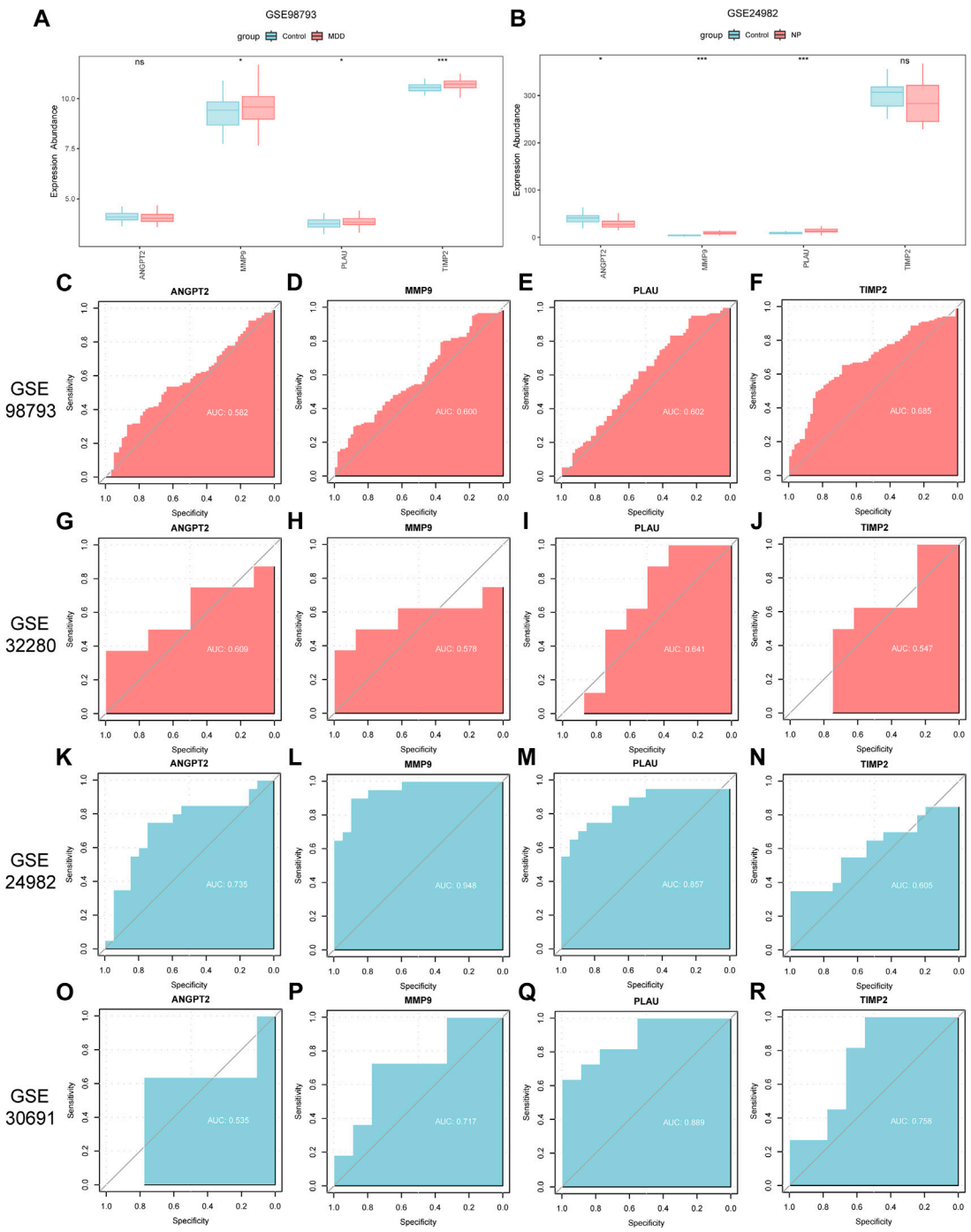

FIGURE 12
Differential expression analysis of co-hub genes in independent disease datasets. **(A,B)** Group comparison charts of co-hub genes in different groups (Case/Control) in the GSE98793 dataset **(A)** and the GSE24982 dataset **(B)**. **(C–F)** ROC curves of ANGPT2 **(C)**, MMP9 **(D)**, PLAU **(E)**, and TIMP2 **(F)** in different groups of the GSE98793 dataset. **(G–J)** ROC curves of ANGPT2 **(G)**, MMP9 **(H)**, PLAU **(I)**, and TIMP2 **(J)** in different groups of the GSE32280 dataset. **(K–N)** ROC curves of ANGPT2 **(K)**, MMP9 **(L)**, PLAU **(M)**, and TIMP2 **(N)** in different groups of the GSE24982 dataset. **(O–R)** ROC curves of ANGPT2 **(O)**, MMP9 **(P)**, PLAU **(Q)**, and TIMP2 **(R)** in different groups of the GSE30691 dataset. The symbol ns is equivalent to $p \geq 0.05$, without statistical significance; the symbol * is equivalent to $p < 0.05$, with statistically significant meaning; the symbol ** is equivalent to $p < 0.01$, with highly statistically significant meaning; the symbol *** is equivalent to $p < 0.001$, with extremely statistically significant meaning. In the ROC curve, the closer the AUC is to 1, the better the diagnostic effect. When the AUC is between 0.5 and 0.7, there is low accuracy; when the AUC is between 0.7 and 0.9, there is certain accuracy; when the AUC is above 0.9, there is high accuracy. MDD, major depressive disorder; NP, Neuropathic Pain; ROC, receiver operating characteristic curve; AUC, Area Under the Curve.

two datasets (Figures 10C–F). Among them, there were negative correlations between the expression of ANGPT2 and HGF (R = −0.21, Figure 10C), (R = 0.44, Figure 10D) in both datasets. Conversely, the expression of PLAU and TIMP2 (R = 0.23, Figure 10E), (R = 0.44, Figure 10F) had a positive correlation in both datasets.

Differential expression analysis of the Co-hub genes

For both datasets, we also examined the expression differences for the 6 Co-hub genes (ANGPT2, EPO, HGF, MMP9, PLAU, and TIMP2) between the disease group (group: Case/MDD/NP) and the control group (group: Control). The results are presented through grouped comparison plots (Figures 11A, B). Of the 6 common hub genes, only ANGPT2, MMP9, PLAU, and TIMP2 were statistically significantly different ($p < 0.05$) in the different groups of the MDD datasets. Although MMP9, PLAU, and TIMP2 expression were all significantly higher in the disease group of the MDD datasets compared with the control group, ANGPT2 expression was significantly lower in the disease group compared with the control group (Figure 11A). The 6 common hub genes in the NP datasets were all statistically significantly ($p < 0.05$) different in the different groups. Among them, ANGPT2 gene expression was upregulated in the normal group, whereas EPO, HGF, MMP9, PLAU, and TIMP2 were upregulated in the disease group (Figure 11B).

Next, we plotted the ROC curves for the four Co-hub genes (ANGPT2, MMP9, PLAU, TIMP2) in both datasets (Figures 11C–J). As shown in Figures 11C–F, the expression of ANGPT2 (AUC = 0.594, Figure 11C), MMP9 (AUC = 0.595, Figure 11D), PLAU (AUC = 0.586, Figure 11E), and TIMP2 (AUC = 0.659, Figure 11F) all had low accuracy for the diagnosis of MDD disease, whereas the expression of the Co-hub genes, ANGPT2 (AUC = 0.734, Figure 11G) and MMP9 (AUC = 0.761, Figure 11H), exhibited a certain accuracy for the diagnosis of NP disease. In contrast, the expression of PLAU (AUC = 0.663, Figure 11I) and TIMP2 (AUC = 0.623, Figure 11J) all had low accuracy for the diagnosis of NP disease.

Differential expression analysis of the Co-hub genes in independent datasets

To verify the expression differences of 4 co-hub genes (ANGPT2, MMP9, PLAU, TIMP2) in MDD and NP datasets, we also used the Wilcoxon rank sum test to analyze the expression levels of these 4 co-hub genes in GSE98793 and GSE24982 datasets. The differences between the disease group (group: Case/MDD/NP) and the control group (group: Control) were shown through comparison charts (Figures 12A, B). As shown in Figures 12A, 11B, MMP9, PLAU, and TIMP2 all had statistically significant differences ($p < 0.05$) in different groups of the MDD datasets. The expression levels of MMP9, PLAU, and TIMP2 in the disease group of GSE98793 dataset were significantly higher than those in the control group (Figure 12A). In the NP dataset, ANGPT2, MMP9, and PLAU all had statistically significant differences ($p < 0.05$) between different groups. The expression level of ANGPT2 was upregulated in the control group while the expression levels of MMP9 and PLAU were upregulated in the disease group (Figure 12B).

We then plotted the ROC curves of the 4 co-hub genes (ANGPT2, MMP9, PLAU, TIMP2) in GSE98793, GSE32280, GSE24982 and GSE30691 datasets and presented the results (Figures 12C–R). As shown in Figures 12C–F, the expression of co-hub genes ANGPT2 (AUC = 0.582, Figure 12C), MMP9 (AUC = 0.600, Figure 12D), PLAU (AUC = 0.602, Figure 12E), and TIMP2 (AUC = 0.685, Figure 12F) all had low accuracy in diagnosing MDD in the GSE98793 dataset. Similarly, as shown in Figures 12G–J, the expression of co-hub genes ANGPT2 (AUC = 0.609, Figure 12G), MMP9 (AUC = 0.578, Figure 12H), PLAU (AUC = 0.641, Figure 12I), and TIMP2 (AUC = 0.547, Figure 12J) all had low accuracy in diagnosing MDD in the GSE32280 dataset.

As shown in Figures 12K–N, the expression of co-hub gene MMP9 (AUC = 0.948, Figure 12L) had high accuracy in diagnosing NP in the GSE24982 dataset. The expression of ANGPT2 (AUC = 0.735, Figure 12K) and PLAU (AUC = 0.857, Figure 12M) had some accuracy in diagnosing NP in the GSE24982 dataset while the expression of TIMP2 (AUC = 0.605, Figure 12N) had low accuracy in diagnosing NP in the GSE24982 dataset.

As shown in Figures 12O–R, the expression of common hub genes MMP9 (AUC = 0.717, Figure 12P), PLAU (AUC = 0.889, Figure 12Q), and TIMP2 (AUC = 0.758, Figure 12R) had some accuracy in diagnosing NP in the GSE30691 dataset while the expression of ANGPT2 (AUC = 0.535, Figure 12O) had low accuracy in diagnosing NP in the GSE30691 dataset. Finally, we summarized the clinical information of different groups in the GSE98793 dataset and presented the results in a clinical data table (Supplementary Table S3).

Discussion

NP is a common chronic pain with a prevalence ranging from 6.9% to 10.0% [3], which significantly reduces the quality of life for individuals [40]. Approximately 50% of NP patients report having depression [41] and when NP patients are co-depressed, they have poor physical, and psychological functioning, which

results in persistent physical and mental distress [42]. Depression and NP are often accompanied by many overlapping symptoms, and antidepressants are used to treat NP, suggesting that they share many common neural circuits and underlying mechanisms, such as neuroinflammation [43]. Studies have found a correlation between the incidence of NP and depression [44] determining whether NP, and depression share a common pathological and molecular mechanism is important for clinical diagnosis and treatment. An understanding of the molecular pathways of disease initiation and development using microarray and bioinformatics analysis will enable us to examine genetic variations and discover novel diagnostic biomarkers and therapeutic targets.

However, when a single dataset is analyzed, one-sided results may be obtained, resulting in a higher false-positive rate. Therefore, in the present study, we combined two datasets for MMD (GSE98793, GSE32280) and two datasets for NP (GSE24982, GSE30691). The combined MMD datasets contained 136 cases and 72 control samples, whereas the NP datasets contained 31 cases and 29 control samples. In total, after analyzing both datasets, we identified 6 Co-hub genes, which included ANGPT2, EPO, HGF, MMP9, PLAU, and TIMP2. The results indicated that ANGPT2, MMP9, PLAU, and TIMP2 expression variations in both datasets were statistically significant. The ROC curves revealed that ANGPT2 and MMP9 can diagnose NP with some accuracy. In addition, we found that the abundance of infiltrating activated dendritic cells, effector memory $CD8^+$ T cells, memory B cells, and regulatory T cells changed significantly ($p < 0.05$).

The functional similarity analysis results between the 6 Co-hub genes indicated that HGF had the highest value compared with the other Co-hub genes (Figure 7C). HGF is a protein-coding gene that acts as a growth factor by promoting hepatocyte regeneration in stem and progenitor cells, which is activated by binding to the c-MET receptor [45]. As a neurotrophic factor, HGF/c-MET is essential for the growth of axons, the development of the central nervous system, and the defense of neurons [46]. In previous mice studies, HGF was demonstrated to improve the symptoms of NP and induce functional recovery and regeneration of neurons [47–50]. By regulating crucial elements linked to DRG neuropathic pain and lowering the spinal microglia activity, HGF produces analgesic effects. Additionally, in a cross-sectional, multicenter investigation of diabetic individuals with neuropathic pain, HGF was linked to increased pain levels [51]. In MDD, psychiatric symptoms, such as anxiety and depression, are also significantly associated with cerebrospinal fluid HGF levels [52]. Downregulation of HGF/c-MET signaling in the hippocampus may be associated with methylation alterations in MET during MDD pathophysiology [53]. Several studies on depression across various groups have also demonstrated a significant relationship between changes in HGF levels and depression [54, 55], and HGF may be useful in assessing the severity of depression-related symptoms [56]. Combined with our results, neuropathic pain, and melancholy conditions may be significantly influenced by HGF. In both the MDD and NP datasets, we found a negative association between the expression of ANGPT2 and HGF (Figures 10C,D). ANGPT2 belongs to the angiopoietin family of growth factors that are upregulated in a variety of inflammatory diseases and are associated with direct control of inflammation-related signaling pathways. Based on our results, the expression of ANGPT2 has a low accuracy for the diagnosis of MDD (Figure 11C) and a certain degree of accuracy for the diagnosis of NP (Figure 11G); however, there are currently no studies related to ANGPT2 in NP or MDD, thus we are the first to discover that ANGPT2 may also play a key role in these diseases.

In numerous models of central and peripheral nerve damage, EPO exhibits a variety of neuroprotective benefits [57, 58]. EPO can alleviate neuropathic pain brought on by peripheral nerve damage by regulating the production of AQP-2 through the AMPK/mTOR/p70S6K pathway [59]. EPO and non-erythropoietic derivatives have also shown potential pro-cognitive effects in psychiatric disorders [60]. The non-erythropoietic derivative ARA290 can reduce inflammation and depression, which prolongs stress in rodents [61]. Studies have found that MDD may be related to neuronal plasticity damage8. Additionally, the neurotrophic and neuroprotective benefits of EPO and brain-derived neurotrophic factor (BDNF) can restore neural plasticity [62]. EPO and non-erythropoietic compounds, such as carbamoylated EPO, increase the production of BDNF in the hippocampus of rats [63]. Additional evidence indicating that EPO acts on the brain through neurotrophic and synaptic plasticity mechanisms has been derived from a bioinformatics study [64]. These studies are consistent with the results of our data mining in which EPO is a Co-hub gene for NP and MDD.

PLAU is a serine protease that converts plasminogen into plasmin, which is crucial for breaking down the extracellular matrix and encouraging fibrinolysis [65]. UPA, a PLAU expression product, can activate or suppress the inflammatory reaction through the AMPK and PI3K/Akt pathways [66]. A previous study identified PLAU as a hub gene of NP [67], which is consistent with our results; however, no studies have associated PLAU with MDD. Our study is the first to show that PLAU expression has low accuracy for the diagnosis of both NP and MDD (Figures 11I,E).

We found that MMP9 expression had a certain accuracy for the diagnosis of NP disease and low accuracy for the diagnosis of MDD (Figures 11D,H). In addition, TIMP2 expression has low accuracy for the diagnosis of NP and MDD occurrence (Figures 11J, 12F). It also plays a role in angiogenesis, axon growth, and neuroplasticity [68, 69]. MMP9, as a mediator of neuroinflammation, influences the onset and progression of NP by stimulating DRG and microglia in the spinal cord, participates in the regulation of oxidative stress and the inflammatory response, affects the maturation of

inflammatory cytokines and may be directly involved in the development and maintenance of NP [70]. MMP9 may also cause a proBDNF/mBDNF (brain-derived neurotrophic factor) imbalance by influencing the process by which proBDNF is converted into mBDNF, leading to depression [71]. Decreased MMP9 levels result in decreased neuronal differentiation in the hippocampus and may cause increased anxiety in mice [72]. Four TIMPs(TIMP1, TIMP2, TIMP3, TIMP4) are physiological tissue inhibitors of MMPs, of which TIMP2 can indirectly affect NP and MDD processes by inhibiting MMP9 activity [73, 74]. These studies confirm the results of our database analysis that MMP9 and TIMP2 have some diagnostic value for NP and MDD.

Our finding that immune cells are associated with the emergence, maintenance, and cure of NP and MDD is consistent with previous studies [75–77]. As shown in Figures 9A,B, the difference in abundance of infiltrating immune cells, including activated dendritic cells, effector memory $CD8^+$ T cells, memory B cells, and regulatory T cells, in the disease, and control group of the MDD datasets and NP datasets was statistically significant. It is worth noting that, the infiltration abundance of Activated dendritic cells is significantly increased in both NP and MDD disease groups. However, the infiltration abundance of Effector memory $CD8^+$ T cells and Memory B cells is significantly increased in the NP disease group, but significantly decreased in the MDD disease group. Conversely, the infiltration abundance of Regulatory T cells is significantly decreased in the NP disease group, but significantly increased in the MDD disease group. Effector memory $CD8^+$ T cells are a type of memory T cell that can rapidly respond to re-infection and are capable of secreting cytokines and killing target cells [78]. Activated dendritic cells are dendritic cells that have captured and processed antigens and have undergone phenotypic and functional changes [79], they are able to more effectively activate T cells and secrete a variety of cytokines to regulate immune responses. Activated dendritic cells and effector memory $CD8^+$ T cells were found to be significantly upregulated in NP [80], which is consistent with our findings. Sun et al. found that the proportion of $CD8^+$ T cells in MDD patients is low, and they are divided into 2 subtypes: a subtype with a higher proportion of $CD8^+$ T cells and a subtype with a lower proportion of $CD8^+$ T cells. In the subtype with a higher proportion of $CD8^+$ T cells, the expression levels of genes related to autophagy, immune response, and apoptosis are higher. Reducing the apoptosis of $CD8^+$ T lymphocytes can reduce the level of inflammatory factors and improve the immune microenvironment of depressed mice [81]. These results suggest that effector memory $CD8^+$ T cells may play an important role in the pathogenesis of NP and MDD. In this study, activated dendritic cells had the highest infiltration associated with the expression of key genes (Figure 9D). Maganin et al. found that dendritic cells cause NP by promoting the kynurenine metabolic pathway [82]. Wang et al. concluded that dendritic cells cause NP by sensitizing nociceptor sensory neurons through paracrine factors [83]. Stiglbauer et al. found that obesity and MDD patients have fewer dendritic cells and effector memory $CD8^+$ T cells compared with normal-weight patients who were not depressed [84]. Ciaramella et al. found that the decrease in dendritic cells is associated with the severity of depressive symptoms in Alzheimer's disease patients [85]. These studies and our results consistently suggest that changes in the number and function of dendritic cells may be involved in the common pathophysiology of comorbid NP and MDD. Memory B cells are formed within the germinal center after the primary infection and play an important role in the secondary immune response [86]. Combining Figures 9C, D, it is evident that the expression of activated dendritic cells, memory B cells, and the 6 Co-hub genes are positively correlated in the MDD and NP datasets disease samples. A previous bioinformatics analysis also found that memory B cells correlated with MDD diagnostic marker genes [87]. The role of memory B cells in NP is currently unclear, and there is no rigorous evidence to show the relationship between memory B cells and NP. The discovery of increased infiltration abundance of memory B cells in NP is a new finding in this study, and further research is needed to explore the role of memory B cells in the comorbidity of NP and MDD. Regulatory T cells control the body's immune response to harmful invaders and prevent overreaction [88]. A study indicated that regulatory T -cells can prevent pain-induced hypersensitivity reactions caused by microglia [89]. In depressed patients, there is a decrease in regulatory T cells [76]. Taken together, there is an immune-activated microenvironment in NP and MDD comorbidities, and immunity, and inflammation may play an important role in NP and MDD comorbidities. Activated dendritic cells, effector memory $CD8^+$ T cells, memory B cells, and regulatory T cells have the potential to be therapeutic targets for NP and MDD. However, articles researching the relationship between these immune cells and NP or MDD are very limited. Their specific roles in the comorbidity of NP and MDD are not clear, and more research is needed to explore the biological significance behind these immune changes.

There are some limitations to this study. First, the study integrates human whole blood samples and peripheral blood lymphocyte chip data on the same sequencing platform for analysis. While it can provide valuable information regarding cell type comparison, immune response analysis, cellular interactions, disease-related analysis, and the identification of potential biomarkers, contributing to a deeper understanding of immune system functionality and the mechanisms underlying related diseases, this approach also has limitations and challenges such as sample heterogeneity, differential gene expression, signal dilution, and technical variations. To overcome these limitations, future research can consider strategies such as cell sorting, single-cell sequencing, and experimental validation to help overcome

these challenges and provide a more focused and accurate analysis of lymphocyte-specific gene expression changes. Secondly, compared to MDD, the sample size of NP is relatively low. In the future, the reliability of the results should be evaluated through hypothesis testing based on sample size, cross-validation, and other methods. Thirdly, the MDD sample is human-sourced, while the NP sample is animal-sourced, and this species difference may have an impact on the results' generalizability. In addition, although batch-effect correction was performed, it is important to note that residual batch effects may still persist in the analysis due to variations in sample processing, experimental conditions, or other technical factors that could not be entirely eliminated. In the future, Emerging machine learning algorithms, such as deep neural networks, can also be used for data mining and analysis to better understand the relationships and trends between samples. Future studies should also explore the role of various immune cells in the co-morbid mechanisms of NP and MDD, and search for therapeutic targets of NP and MDD through anti-inflammatory pathways.

In conclusion, after screening 93 Co-DEGs, and performing GO and KEGG enrichment analyses, we identified 6 Co-hub genes, which included ANGPT2, EPO, HGF, MMP9, PLAU, and TIMP2. We also found that between the disease group and the control group for NP and MDD, there were significant differences in the abundance of activated dendritic cells, effector memory $CD8^+$ T cells, memory B cells, and regulatory T cells. The possible diagnostic or therapeutic value of these immune cells and genes in NP and MDD warrant further study.

Author contributions

JH: Conceptualization, Data curation, Formal Analysis, Investigation, Methodology, Software, Writing–original draft, Writing–review and editing. JF: Data curation, Methodology, Resources, Validation, Visualization, Writing–original draft, Writing–review and editing. YC: Formal Analysis, Resources, Validation, Visualization, Writing–review and editing. SC: Formal Analysis, Resources, Validation, Visualization, Writing–original draft. MQ: Resources, Visualization, Writing–original draft. LZ: Resources, Visualization, Writing–original draft. WF: Writing–original draft. ZW: Writing–original draft. QZ: Supervision, Writing–review and editing. JZ: Conceptualization, Investigation, Project administration, Software, Writing–original draft, Supervision, Writing–review and editing.

Data availability

The original contributions presented in the study are included in the article/Supplementary Material, further inquiries can be directed to the corresponding authors.

Funding

The author(s) declare that no financial support was received for the research, authorship, and/or publication of this article.

Conflict of interest

The authors declare that the research was conducted in the absence of any commercial or financial relationships that could be construed as a potential conflict of interest.

Supplementary material

The Supplementary Material for this article can be found online at: https://www.ebm-journal.org/articles/10.3389/ebm.2024.10129/full#supplementary-material

References

1. Finnerup NB, Kuner R, Jensen TS. Neuropathic pain: from mechanisms to treatment. *Physiol Rev* (2021) **101**:259–301. doi:10.1152/physrev.00045.2019

2. Treede RD, Jensen TS, Campbell JN, Cruccu G, Dostrovsky JO, Griffin JW, et al. Neuropathic pain: redefinition and a grading system for clinical and research purposes. *Neurology* (2008) **70**:1630–5. doi:10.1212/01.wnl.0000282763.29778.59

3. van Hecke O, Austin SK, Khan RA, Smith BH, Torrance N. Neuropathic pain in the general population: a systematic review of epidemiological studies. *Pain* (2014) **155**:654–62. doi:10.1016/j.pain.2013.11.013

4. Ghazisaeidi S, Muley MM, Salter MW. Neuropathic pain: mechanisms, sex differences, and potential therapies for a global problem. *Annu Rev Pharmacol Toxicol* (2023) **63**:565–83. doi:10.1146/annurev-pharmtox-051421-112259

5. Petroianu GA, Aloum L, Adem A. Neuropathic pain: mechanisms and therapeutic strategies. *Front Cell Develop Biol* (2023) **11**:1072629. doi:10.3389/fcell.2023.1072629

6. Kamoun N, Gazzo G, Goumon Y, Andry V, Yalcin I, Poisbeau P. Long-lasting analgesic and neuroprotective action of the non-benzodiazepine anxiolytic etifoxine in a mouse model of neuropathic pain. *Neuropharmacology* (2021) **182**:108407. doi:10.1016/j.neuropharm.2020.108407

7. Descalzi G, Mitsi V, Purushothaman I, Gaspari S, Avrampou K, Loh YHE, et al. Neuropathic pain promotes adaptive changes in gene expression in brain networks involved in stress and depression. *Sci Signal* (2017) **10**:eaaj1549. doi:10.1126/scisignal.aaj1549

8. Guida F, Iannotta M, Misso G, Ricciardi F, Boccella S, Tirino V, et al. Long-term neuropathic pain behaviors correlate with synaptic plasticity and limbic circuit alteration: a comparative observational study in mice. *Pain* (2022) **163**:1590–602. doi:10.1097/j.pain.0000000000002549

9. Neugebauer V, Galhardo V, Maione S, Mackey SC. Forebrain pain mechanisms. *Brain Res Rev* (2009) **60**:226–42. doi:10.1016/j.brainresrev.2008.12.014

10. Coraggio V, Guida F, Boccella S, Scafuro M, Paino S, Romano D, et al. Neuroimmune-driven neuropathic pain establishment: a focus on gender differences. *Int J Mol Sci* (2018) **19**:281. doi:10.3390/ijms19010281

11. Rivest S. Regulation of innate immune responses in the brain. *Nat Rev Immunol* (2009) **9**:429–39. doi:10.1038/nri2565

12. Austin PJ, Moalem-Taylor G. The neuro-immune balance in neuropathic pain: involvement of inflammatory immune cells, immune-like glial cells and cytokines. *J Neuroimmunology* (2010) **229**:26–50. doi:10.1016/j.jneuroim.2010.08.013

13. Li Y, Liu X, Fu Q, Fan W, Shao X, Fang J, et al. Electroacupuncture ameliorates depression-like behaviors comorbid to chronic neuropathic pain via Tet1-mediated restoration of adult neurogenesis. *Stem Cells* (2023) **41**:384–99. doi:10.1093/stmcls/sxad007

14. Mokhtari T, Yue LP, Hu L. Exogenous melatonin alleviates neuropathic pain-induced affective disorders by suppressing NF-κB/NLRP3 pathway and apoptosis. *Sci Rep* (2023) **13**:2111. doi:10.1038/s41598-023-28418-1

15. Lee HJ, Choi EJ, Nahm FS, Yoon IY, Lee PB. Prevalence of unrecognized depression in patients with chronic pain without a history of psychiatric diseases. *Korean J Pain* (2018) **31**:116–24. doi:10.3344/kjp.2018.31.2.116

16. Tyrtyshnaia A, Manzhulo I. Neuropathic pain causes memory deficits and dendrite tree morphology changes in mouse Hippocampus. *J Pain Res* (2020) **13**:345–54. doi:10.2147/jpr.s238458

17. Jiang H, Liu JP, Xi K, Liu LY, Kong LY, Cai J, et al. Contribution of AMPA receptor-mediated LTD in LA/BLA-CeA pathway to comorbid aversive and depressive symptoms in neuropathic pain. *J Neurosci* (2021) **41**:7278–99. doi:10.1523/jneurosci.2678-20.2021

18. Liu Q, Li R, Yang W, Cui R, Li B. Role of neuroglia in neuropathic pain and depression. *Pharmacol Res* (2021) **174**:105957. doi:10.1016/j.phrs.2021.105957

19. Yang R, Shi L, Si H, Hu Z, Zou L, Li L, et al. Gallic acid improves comorbid chronic pain and depression behaviors by inhibiting P2X7 receptor-mediated ferroptosis in the spinal cord of rats. *ACS Chem Neurosci* (2023) **14**:667–76. doi:10.1021/acschemneuro.2c00532

20. Pinero J, Rodriguez Fraga PS, Valls-Margarit J, Ronzano F, Accuosto P, Lambea Jane R, et al. Genomic and proteomic biomarker landscape in clinical trials. *Comput Struct Biotechnol J* (2023) **21**:2110–8. doi:10.1016/j.csbj.2023.03.014

21. Li L, Su H, Yang Y, Yang P, Zhang X, Su S. Screening key genes related to neuropathic pain-induced depression through an integrative bioinformatics analysis. *Ann Transl Med* (2022) **10**:1348. doi:10.21037/atm-22-5820

22. Barrett T, Troup DB, Wilhite SE, Ledoux P, Rudnev D, Evangelista C, et al. NCBI GEO: mining tens of millions of expression profiles--database and tools update. *Nucleic Acids Res* (2007) **35**:D760–5. doi:10.1093/nar/gkl887

23. Leday GGR, Vertes PE, Richardson S, Greene JR, Regan T, Khan S, et al. Replicable and coupled changes in innate and adaptive immune gene expression in two case-control studies of blood microarrays in major depressive disorder. *Biol Psychiatry* (2018) **83**:70–80. doi:10.1016/j.biopsych.2017.01.021

24. Yi Z, Li Z, Yu S, Yuan C, Hong W, Wang Z, et al. Blood-based gene expression profiles models for classification of subsyndromal symptomatic depression and major depressive disorder. *PLoS One* (2012) **7**:e31283. doi:10.1371/journal.pone.0031283

25. Davis S, Meltzer PS. GEOquery: a bridge between the gene expression Omnibus (GEO) and BioConductor. *Bioinformatics* (2007) **23**:1846–7. doi:10.1093/bioinformatics/btm254

26. von Schack D, Agostino MJ, Murray BS, Li Y, Reddy PS, Chen J, et al. Dynamic changes in the microRNA expression profile reveal multiple regulatory mechanisms in the spinal nerve ligation model of neuropathic pain. *PLoS One* (2011) **6**:e17670. doi:10.1371/journal.pone.0017670

27. Costigan M, Belfer I, Griffin RS, Dai F, Barrett LB, Coppola G, et al. Multiple chronic pain states are associated with a common amino acid-changing allele in KCNS1. *Brain* (2010) **133**:2519–27. doi:10.1093/brain/awq195

28. Ritchie ME, Phipson B, Wu D, Hu Y, Law CW, Shi W, et al. Limma powers differential expression analyses for RNA-sequencing and microarray studies. *Nucleic Acids Res* (2015) **43**:e47. doi:10.1093/nar/gkv007

29. He Z, Jiang Q, Li F, Chen M. Crosstalk between venous thromboembolism and periodontal diseases: a bioinformatics analysis. *Dis Markers* (2021) **2021**:1–16. doi:10.1155/2021/1776567

30. Szklarczyk D, Gable AL, Lyon D, Junge A, Wyder S, Huerta-Cepas J, et al. STRING v11: protein-protein association networks with increased coverage, supporting functional discovery in genome-wide experimental datasets. *Nucleic Acids Res* (2019) **47**:D607–D613. doi:10.1093/nar/gky1131

31. Shannon P, Markiel A, Ozier O, Baliga NS, Wang JT, Ramage D, et al. Cytoscape: a software environment for integrated models of biomolecular interaction networks. *Genome Res* (2003) **13**:2498–504. doi:10.1101/gr.1239303

32. Reddy S, Singh S. Investigation of hub genes and their nonsynonymous single nucleotide polymorphism analysis in Plasmodium falciparum for designing therapeutic methodologies using next-generation sequencing approach. *Indian J Pharmacol* (2019) **51**:389–99. doi:10.4103/ijp.ijp_535_19

33. Boughorbel S, Jarray F, El-Anbari M. Optimal classifier for imbalanced data using Matthews Correlation Coefficient metric. *PLoS One* (2017) **12**:e0177678. doi:10.1371/journal.pone.0177678

34. Yu G. Gene Ontology semantic similarity analysis using GOSemSim. *Methods Mol Biol* (2020) **2117**:207–15. doi:10.1007/978-1-0716-0301-7_11

35. Kanehisa M, Goto S. KEGG: kyoto encyclopedia of genes and genomes. *Nucleic Acids Res* (2000) **28**:27–30. doi:10.1093/nar/28.1.27

36. Yu G, Wang LG, Han Y, He QY. clusterProfiler: an R package for comparing biological themes among gene clusters. *OMICS: A J Integr Biol* (2012) **16**:284–7. doi:10.1089/omi.2011.0118

37. Bindea G, Mlecnik B, Tosolini M, Kirilovsky A, Waldner M, Obenauf AC, et al. Spatiotemporal dynamics of intratumoral immune cells reveal the immune landscape in human cancer. *Immunity* (2013) **39**:782–95. doi:10.1016/j.immuni.2013.10.003

38. Zhang Q, Liu W, Zhang HM, Xie GY, Miao YR, Xia M, et al. hTFtarget: a comprehensive database for regulations of human transcription factors and their targets. *Genomics Proteomics Bioinformatics* (2020) **18**:120–8. doi:10.1016/j.gpb.2019.09.006

39. Park SH, Goo JM, Jo CH. Receiver operating characteristic (ROC) curve: practical review for radiologists. *Korean J Radiol* (2004) **5**:11–8. doi:10.3348/kjr.2004.5.1.11

40. Blyth FM. Global burden of neuropathic pain. *Pain* (2018) **159**:614–7. doi:10.1097/j.pain.0000000000001127

41. Meacham K, Shepherd A, Mohapatra DP, Haroutounian S. Neuropathic pain: central vs. Peripheral mechanisms. *Curr Pain Headache Rep* (2017) **21**:28. doi:10.1007/s11916-017-0629-5

42. Midavaine E, Cote J, Marchand S, Sarret P. Glial and neuroimmune cell choreography in sexually dimorphic pain signaling. *Neurosci Biobehavioral Rev* (2021) **125**:168–92. doi:10.1016/j.neubiorev.2021.01.023

43. Llorca-Torralba M, Camarena-Delgado C, Suarez-Pereira I, Bravo L, Mariscal P, Garcia-Partida JA, et al. Pain and depression comorbidity causes asymmetric plasticity in the locus coeruleus neurons. *Brain* (2022) **145**:154–67. doi:10.1093/brain/awab239

44. Askari MS, Andrade LH, Filho AC, Silveira CM, Siu E, Wang YP, et al. Dual burden of chronic physical diseases and anxiety/mood disorders among São Paulo Megacity Mental Health Survey Sample, Brazil. *J Affective Disord* (2017) **220**:1–7. doi:10.1016/j.jad.2017.05.027

45. Nakamura T, Mizuno S. The discovery of hepatocyte growth factor (HGF) and its significance for cell biology, life sciences and clinical medicine. *Proc Jpn Acad Ser B* (2010) **86**:588–610. doi:10.2183/pjab.86.588

46. Desole C, Gallo S, Vitacolonna A, Montarolo F, Bertolotto A, Vivien D, et al. HGF and MET: from brain development to neurological disorders. *Front Cell Dev Biol* (2021) **9**:683609. doi:10.3389/fcell.2021.683609

47. Kessler JA, Shaibani A, Sang CN, Christiansen M, Kudrow D, Vinik A, et al. Gene therapy for diabetic peripheral neuropathy: a randomized, placebo-controlled phase III study of VM202, a plasmid DNA encoding human hepatocyte growth factor. *Clin Translational Sci* (2021) **14**:1176–84. doi:10.1111/cts.12977

48. Ko KR, Lee J, Lee D, Nho B, Kim S. Hepatocyte growth factor (HGF) promotes peripheral nerve regeneration by activating repair schwann cells. *Sci Rep* (2018) **8**:8316. doi:10.1038/s41598-018-26704-x

49. Nho B, Ko KR, Kim S, Lee J. Intramuscular injection of a plasmid DNA vector expressing hepatocyte growth factor (HGF) ameliorated pain symptoms by controlling the expression of pro-inflammatory cytokines in the dorsal root ganglion. *Biochem Biophysical Res Commun* (2022) **607**:60–6. doi:10.1016/j.bbrc.2022.03.125

50. Tsuchihara T, Nukada H, Nakanishi K, Morishita R, Amako M, Arino H, et al. Efficacy of nonviral gene transfer of human hepatocyte growth factor (HGF) against ischemic-reperfusion nerve injury in rats. *PLoS One* (2020) **15**:e0237156. doi:10.1371/journal.pone.0237156

51. Backryd E, Themistocleous A, Larsson A, Gordh T, Rice ASC, Tesfaye S, et al. Hepatocyte growth factor, colony-stimulating factor 1, CD40, and 11 other inflammation-related proteins are associated with pain in diabetic neuropathy: exploration and replication serum data from the Pain in Neuropathy Study. *Pain* (2022) **163**:897–909. doi:10.1097/j.pain.0000000000002451

52. Hidese S, Hattori K, Sasayama D, Tsumagari T, Miyakawa T, Matsumura R, et al. Cerebrospinal fluid neuroplasticity-associated protein levels in patients with

psychiatric disorders: a multiplex immunoassay study. *Transl Psychiatry* (2020) **10**: 161. doi:10.1038/s41398-020-0843-5

53. Ciuculete DM, Voisin S, Kular L, Welihinda N, Jonsson J, Jagodic M, et al. Longitudinal DNA methylation changes at MET may alter HGF/c-MET signalling in adolescents at risk for depression. *Epigenetics* (2020) **15**:646–63. doi:10.1080/15592294.2019.1700628

54. Arnold SE, Xie SX, Leung YY, Wang LS, Kling MA, Han X, et al. Plasma biomarkers of depressive symptoms in older adults. *Transl Psychiatry* (2012) **2**:e65. doi:10.1038/tp.2011.63

55. Brann E, Fransson E, White RA, Papadopoulos FC, Edvinsson A, Kamali-Moghaddam M, et al. Inflammatory markers in women with postpartum depressive symptoms. *J Neurosci Res* (2020) **98**:1309–21. doi:10.1002/jnr.24312

56. Zhang E, Huang Z, Zang Z, Qiao X, Yan J, Shao X. Identifying circulating biomarkers for major depressive disorder. *Front Psychiatry* (2023) **14**:1230246. doi:10.3389/fpsyt.2023.1230246

57. Wakhloo D, Scharkowski F, Curto Y, Javed Butt U, Bansal V, Steixner-Kumar AA, et al. Functional hypoxia drives neuroplasticity and neurogenesis via brain erythropoietin. *Nat Commun* (2020) **11**:1313. doi:10.1038/s41467-020-15041-1

58. Fuentealba J, Hernández C, Burgos C, Gajardo A, Silva-Grecchi T, Gavilan J, et al. Neuroprotective effects of erythropoietin on neurodegenerative and ischemic brain diseases: the role of erythropoietin receptor. *Neural Regen Res* (2017) **12**: 1381–9. doi:10.4103/1673-5374.215240

59. Huang CT, Chen SH, Lin SC, Chen WT, Lue JH, Tsai YJ. Erythropoietin reduces nerve demyelination, neuropathic pain behavior and microglial MAPKs activation through erythropoietin receptors on Schwann cells in a rat model of peripheral neuropathy. *Glia* (2018) **66**:2299–315. doi:10.1002/glia.23461

60. Newton SS, Sathyanesan M. Erythropoietin and non-erythropoietic derivatives in cognition. *Front Pharmacol* (2021) **12**:728725. doi:10.3389/fphar.2021.728725

61. Xu G, Zou T, Deng L, Yang G, Guo T, Wang Y, et al. Nonerythropoietic erythropoietin mimetic peptide ARA290 ameliorates chronic stress-induced depression-like behavior and inflammation in mice. *Front Pharmacol* (2022) **13**: 896601. doi:10.3389/fphar.2022.896601

62. Lee BH, Park YM, Hwang JA, Kim YK. Variable alterations in plasma erythropoietin and brain-derived neurotrophic factor levels in patients with major depressive disorder with and without a history of suicide attempt. *Prog Neuro-Psychopharmacology Biol Psychiatry* (2021) **110**:110324. doi:10.1016/j.pnpbp.2021.110324

63. Sathyanesan M, Watt MJ, Haiar JM, Scholl JL, Davies SR, Paulsen RT, et al. Carbamoylated erythropoietin modulates cognitive outcomes of social defeat and differentially regulates gene expression in the dorsal and ventral hippocampus. *Transl Psychiatry* (2018) **8**:113. doi:10.1038/s41398-018-0168-9

64. Tiwari NK, Sathyanesan M, Schweinle W, Newton SS. Carbamoylated erythropoietin induces a neurotrophic gene profile in neuronal cells. *Prog Neuro-Psychopharmacology Biol Psychiatry* (2019) **88**:132–41. doi:10.1016/j.pnpbp.2018.07.011

65. Wu M, Wei B, Duan SL, Liu M, Ou-Yang DJ, Huang P, et al. Methylation-driven gene PLAU as a potential prognostic marker for differential thyroid carcinoma. *Front Cell Dev Biol* (2022) **10**:819484. doi:10.3389/fcell.2022.819484

66. Dinesh P, Rasool M. uPA/uPAR signaling in rheumatoid arthritis: shedding light on its mechanism of action. *Pharmacol Res* (2018) **134**:31–9. doi:10.1016/j.phrs.2018.05.016

67. Liu H, Xia T, Xu F, Ma Z, Gu X. Identification of the key genes associated with neuropathic pain. *Mol Med Rep* (2018) **17**:6371–8. doi:10.3892/mmr.2018.8718

68. Fingleton B. Matrix metalloproteinases as regulators of inflammatory processes. *Biochim Biophys Acta (Bba) - Mol Cell Res* (2017) **1864**:2036–42. doi:10.1016/j.bbamcr.2017.05.010

69. Wang XL, Wei X, Yuan JJ, Mao YY, Wang ZY, Xing N, et al. Downregulation of fat mass and obesity-related protein in the anterior cingulate cortex participates in anxiety- and depression-like behaviors induced by neuropathic pain. *Front Cell Neurosci* (2022) **16**:884296. doi:10.3389/fncel.2022.884296

70. Fan YX, Hu L, Zhu SH, Han Y, Liu WT, Yang YJ, et al. Paeoniflorin attenuates postoperative pain by suppressing Matrix Metalloproteinase-9/2 in mice. *Eur J Pain* (2018) **22**:272–81. doi:10.1002/ejp.1116

71. Lin LY, Luo SY, Al-Hawwas M, Herselman MF, Zhou XF, Bobrovskaya L. The long-term effects of ethanol and corticosterone on the mood-related behaviours and the balance between mature BDNF and proBDNF in mice. *J Mol Neurosci* (2019) **69**: 60–8. doi:10.1007/s12031-019-01328-6

72. Spychala A, Ruther U. FTO affects hippocampal function by regulation of BDNF processing. *PLoS One* (2019) **14**:e0211937. doi:10.1371/journal.pone.0211937

73. Kamieniak P, Bielewicz J, Kurzepa J, Daniluk B, Kocot J, Trojanowski T. Serum level of metalloproteinase-2 but not metalloproteinase-9 rises in patients with failed back surgery syndrome after spinal cord stimulation. *Neuromodulation: Technol Neural Interf* (2019) **22**:262–8. doi:10.1111/ner.12915

74. Kamieniak P, Bielewicz J, Kurzepa J, Daniluk B, Kocot J, Trojanowski T. The impact of changes in serum levels of metalloproteinase-2 and metalloproteinase-9 on pain perception in patients with disc herniation before and after surgery. *J Pain Res* (2019) **12**:1457–64. doi:10.2147/jpr.s201199

75. Bethea JR, Fischer R. Role of peripheral immune cells for development and recovery of chronic pain. *Front Immunol* (2021) **12**:641588. doi:10.3389/fimmu.2021.641588

76. Beurel E, Medina-Rodriguez EM, Jope RS. Targeting the adaptive immune system in depression: focus on T helper 17 cells. *Pharmacol Rev* (2022) **74**:373–86. doi:10.1124/pharmrev.120.000256

77. Sorensen NV, Frandsen BH, Orlovska-Waast S, Buus TB, Odum N, Christensen RH, et al. Immune cell composition in unipolar depression: a comprehensive systematic review and meta-analysis. *Mol Psychiatry* (2023) **28**: 391–401. doi:10.1038/s41380-022-01905-z

78. Turner SJ, Bennett TJ, La Gruta NL. CD8(+) T-cell memory: the why, the when, and the how. *Cold Spring Harb Perspect Biol* (2021) 13. doi:10.1101/cshperspect.a038661

79. Liu J, Zhang X, Cheng Y, Cao X. Dendritic cell migration in inflammation and immunity. *Cell Mol Immunol* (2021) **18**:2461–71. doi:10.1038/s41423-021-00726-4

80. Ye Q, Huang Z, Lu W, Yan F, Zeng W, Xie J, et al. Identification of the common differentially expressed genes and pathogenesis between neuropathic pain and aging. *Front Neurosci* (2022) **16**:994575. doi:10.3389/fnins.2022.994575

81. Sun Y, Li J, Wang L, Cong T, Zhai X, Li L, et al. Identification of potential diagnoses based on immune infiltration and autophagy characteristics in major depressive disorder. *Front Genet* (2022) **13**:702366. doi:10.3389/fgene.2022.702366

82. Maganin AG, Souza GR, Fonseca MD, Lopes AH, Guimaraes RM, Dagostin A, et al. Meningeal dendritic cells drive neuropathic pain through elevation of the kynurenine metabolic pathway in mice. *J Clin Invest* (2022) **132**:e153805. doi:10.1172/jci153805

83. Wang Z, Song K, Zhao W, Zhao Z. Dendritic cells in tumor microenvironment promoted the neuropathic pain via paracrine inflammatory and growth factors. *Bioengineered* (2020) **11**:661–78. doi:10.1080/21655979.2020.1771068

84. Stiglbauer V, Gamradt S, Scherzer M, Brasanac J, Otte C, Rose M, et al. Immunological substrates of depressive symptoms in patients with severe obesity: an exploratory study. *Cell Biochem Funct* (2021) **39**:423–31. doi:10.1002/cbf.3608

85. Ciaramella A, Salani F, Bizzoni F, Orfei MD, Caltagirone C, Spalletta G, et al. Myeloid dendritic cells are decreased in peripheral blood of Alzheimer's disease patients in association with disease progression and severity of depressive symptoms. *J Neuroinflammation* (2016) **13**:18. doi:10.1186/s12974-016-0483-0

86. Inoue T, Shinnakasu R, Kawai C, Ise W, Kawakami E, Sax N, et al. Exit from germinal center to become quiescent memory B cells depends on metabolic reprograming and provision of a survival signal. *J Exp Med* (2021) **218**: e20200866. doi:10.1084/jem.20200866

87. He S, Deng Z, Li Z, Gao W, Zeng D, Shi Y, et al. Signatures of 4 autophagy-related genes as diagnostic markers of MDD and their correlation with immune infiltration. *J Affective Disord* (2021) **295**:11–20. doi:10.1016/j.jad.2021.08.005

88. Du Y, Fang Q, Zheng SG. Regulatory T cells: concept, classification, phenotype, and biological characteristics. *Adv Exp Med Biol* (2021) **1278**:1–31. doi:10.1007/978-981-15-6407-9_1

89. Kuhn JA, Vainchtein ID, Braz J, Hamel K, Bernstein M, Craik V, et al. Regulatory T-cells inhibit microglia-induced pain hypersensitivity in female mice. *Elife* (2021) **10**:e69056. doi:10.7554/elife.69056

EBM Experimental Biology and Medicine

TYPE Original Research
PUBLISHED 09 July 2024
DOI 10.3389/ebm.2024.10101

OPEN ACCESS

*CORRESPONDENCE
Wei Xiang,
xiangwei20@hotmail.com

RECEIVED 12 January 2024
ACCEPTED 25 June 2024
PUBLISHED 09 July 2024

CITATION
Zheng H, Zhang D, Gan Y, Peng Z, Wu Y and Xiang W (2024), Identification of potential biomarkers for cerebral palsy and the development of prediction models.
Exp. Biol. Med. 249:10101.
doi: 10.3389/ebm.2024.10101

Identification of potential biomarkers for cerebral palsy and the development of prediction models

Haoyang Zheng[1], Duo Zhang[2], Yong Gan[3], Zesheng Peng[1], Yuyi Wu[1] and Wei Xiang[1]*

[1]Department of Neurosurgery, Union Hospital, Tongji Medical College, Huazhong University of Science and Technology, Wuhan, China, [2]Department of Nursing, Tongji Hospital, Tongji Medical College, Huazhong University of Science and Technology, Wuhan, Hubei, China, [3]Department of Social Medicine and Health Management, School of Public Health, Tongji Medical College, Huazhong University of Science and Technology, Wuhan, China

Abstract

Cerebral palsy (CP) is a prevalent motor disorder originating from early brain injury or malformation, with significant variability in its clinical presentation and etiology. Early diagnosis and personalized therapeutic interventions are hindered by the lack of reliable biomarkers. This study aims to identify potential biomarkers for cerebral palsy and develop predictive models to enhance early diagnosis and prognosis. We conducted a comprehensive bioinformatics analysis of gene expression profiles in muscle samples from CP patients to identify candidate biomarkers. Six key genes (CKMT2, TNNT2, MYH4, MYH1, GOT1, and LPL) were validated in an independent cohort, and potential biological pathways and molecular networks involved in CP pathogenesis were analyzed. The importance of processes such as functional regulation, energy metabolism, and cell signaling pathways in the muscles of CP patients was emphasized. Predictive models of muscle sample biomarkers related to CP were developed and visualized. Calibration curves and receiver operating characteristic analysis demonstrated that the predictive models exhibit high sensitivity and specificity in distinguishing individuals at risk of CP. The identified biomarkers and developed prediction models offer significant potential for early diagnosis and personalized management of CP. Future research should focus on validating these biomarkers in larger cohorts and integrating them into clinical practice to improve outcomes for individuals with CP.

KEYWORDS

cerebral palsy, neurodevelopmental disorder, biomarkers, prediction models, therapeutic targets

Impact statement

The discovery of reliable biomarkers has the potential to revolutionize clinical practice by enabling earlier and more accurate diagnosis of CP, which can lead to timely and targeted therapeutic interventions. Early identification of at-risk individuals allows for the implementation of neuroprotective strategies and tailored rehabilitation programs, potentially mitigating the severity of motor impairments and improving long-term outcomes. This study's findings set the stage for future research to validate and refine these biomarkers in larger, diverse populations. Ultimately, the integration of biomarker-based diagnostics into routine clinical practice could transform the management of cerebral palsy, offering new hope for improved quality of life for affected individuals and their families.

Introduction

Cerebral palsy (CP) remains one of the most prevalent childhood motor disorders, affecting approximately 2–2.5 per 1,000 live births worldwide [1]. It encompasses a heterogeneous group of non-progressive disorders of movement and posture caused by early brain injury or malformation, with implications for motor function throughout an individual's lifespan [2]. Despite extensive research, the etiology of CP often remains elusive, hindering both early diagnosis and the implementation of targeted therapeutic interventions.

Skeletal muscles in patients with CP are altered due to neurological lesions. These brain lesions cause various neurological symptoms, including dystonia, ataxia, athetosis, and particularly spasticity [3, 4]. Loss of upper motor neuron inhibition on the lower motor neurons resulted in spasticity, altered muscle tone, and increased or impaired motor unit firing [5]. Although the mechanism is unknown, spastic muscle often shortens to create muscle contractures, which is a primary disability of CP that leads to further complications. CP is the most prevalent non-genetic cause of secondary dystonia, and its clinical management poses significant challenges [6]. The primary objectives in treating dystonia associated with CP are to mitigate dystonic symptoms, optimize functional capacity, alleviate pain, and enhance overall care convenience [7]. Oral medications, physical therapy techniques, chemical neurectomies with phenol or alcohol, chemodenervation using neurotoxins, and deep brain stimulation have been utilized to decrease spasticity and dystonic symptoms among children with CP, but often yield suboptimal results [8].

Skeletal muscle in patients with CP exhibits distinct characteristics, including muscle tissue and fiber atrophy, decreased cross-sectional area, muscle shortening, and reduced specific tension [9]. Identifying reliable biomarkers associated with CP is crucial for understanding its diverse etiologies, facilitating early diagnosis, prognostication, and targeted therapeutic interventions. However, the identification of reliable biomarkers and their translation into clinical practice remain significant challenges.

This study aimed to address these challenges by systematically identifying potential biomarkers for CP and developing robust prediction models. By leveraging advanced computational algorithms, we sought to uncover biomarkers that could serve as reliable indicators of CP risk and severity. In this study, we provided a detailed description of our methods for the discovery of biomarkers and the development of predictive models. We discussed the implications of the findings for clinical practice and proposed strategies for the future integration of biomarker-based diagnostics in the management of CP.

Materials and methods

Data acquisition and preprocessing

The data used in this article was obtained from the NCBI Gene Expression Integration (GEO) database. The following criteria were used for screening the datasets: (1) inclusion of samples from CP patients and healthy individuals, (2) focus on muscle tissue gene expression profiles, (3) availability of publicly accessible raw or processed data, (4) research conducted on *Homo sapiens*, (5) total sample size greater than 15, and (6) exclusion of samples associated with other diseases. Two different gene expression datasets were analyzed in this study: GSE11686 [10] as the analysis set and GSE31243 [11] as the validation set. Detailed characteristics are shown in Table 1. To ensure an adequate sample size and the generalizability of the results, we included data from different muscle samples and performed quality control, preprocessing, and statistical analysis using the limma package in R Studio. The data analysis workflow is depicted in Figure 1.

Identification of the differentially expressed genes (DEGs)

DEGs between the CP group and the control group were identified using the limma package and visualized with a volcano plot. Genes were selected for further analysis in the network construction based on the significance analysis of microarrays (SAM) with adjusted p-value < 0.05 and |log2 fold change (FC)| ≥ 1.2. A heatmap of the DEGs that were screened was generated in R software.

Gene set enrichment analysis (GSEA)

To provide a clearer representation of the gene expression level of highly enriched functional pathways, we used the GSEA software (version 3.0) and downloaded the sub-aggregate of c2.cp.kegg.v7.4.symbols.gmt. from the Molecular Signatures Database (DOI:10.1093/bioinformatics/btr260[1] [12]. The minimum gene set was 5, the maximum gene set was 5,000, and 1,000 resampling was performed. A p-value of <0.05 was considered statistically significant.

Functional enrichment analysis

The DEGs were subjected to functional enrichment analysis using DAVID[2]. Gene ontology (GO) analysis was performed to identify distinguishing biological characteristics, including molecular functions (MF), biological pathways (BP), and cellular components (CC). Kyoto Encyclopedia of Genes and Genomes (KEGG) enrichment analysis was used to explore the activities of genes and their connections to high-level genomic information.

Evaluation and correlation analysis of infiltration-related immune cells

The infiltration matrix of immune cells was obtained by filtering 22 types of immune cell matrices using the cell-type identification by estimating relative subsets of RNA transcripts (CIBERSORT) website ($p < 0.05$) [13]. The Spearman correlation analysis was conducted between unique diagnostic markers and immune infiltrating cells using the "ggplot2" package to illustrate the results.

Construction of weighted gene co-expression network and identification of significant modules

The weighted gene co-expression network analysis (WGCNA) is a valuable tool for studying gene set expression. Data were processed using R-Studio 4.2.2, and abnormal samples were excluded for reliability. Samples were clustered to identify outliers, and the network was built using the automatic network construction function, which determined the soft threshold power β. Adjacency was calculated based on co-expression similarity. Hierarchical clustering created a tree diagram with modules, which were automatically merged for highly correlated feature genes (TOM type = "unsigned," min module size = 30, merge cut height = 0.25). Genes with similar expression patterns were grouped into modules, each assigned a specific color. Module membership (MM) and gene significance (GS) were calculated for clinically relevant modules. Gene information from these modules was extracted for further analysis, and the characteristic gene network was visualized.

Identification of candidate genes

The Venn diagram shows the intersection of WGCNA brown modular genes and DEGs, representing disease-related genes and differentially expressed genes. In total, 45 genes were identified as candidate genes, and their expression is shown in Table 2.

Protein-protein interaction (PPI) network construction and identification of hub genes

To identify the hub genes of each module, the previously acquired genes were mapped to the STRING database[3], a platform for searching PPI. The protein interactions of each module were then constructed and visualized using the CytoHubba plugin within the Cytoscape software[4]. The hub gene was determined as the one with the highest degree of connection. In this study, the Maximal Clique Centrality (MCC) method in CytoHubba, known for its accuracy in predicting essential proteins, was used [14].

Validation of the hub genes expression and prediction value

To validate the expression differences of the hub genes and their universality, we utilized gene expression data from GSE31243, which consists of 20 CP and 20 non-CP muscle samples. The expression of hub genes in muscle samples from CP and non-CP patients was analyzed using box plots created with the "ggplot2" package in R software. The data were presented as standard deviation. Statistical analysis was

1 http://www.gsea-msigdb.org/gsea/downloads.jsp
2 http://david-d.ncifcrf.gov/
3 https://string-db.org/
4 http://www.cytoscape.org/

TABLE 1 Detailed characteristics of the included data sets.

Sample ID	Cohort	Patients		Controls		Tissue of sample
		Sample size	Age (mean ± SD)	Sample size	Age (mean ± SD)	
GSE11686	Training	6	10.3 ± 3.79	2	8.5 ± 2.1	Wrist muscle extensors and flexors
GSE31243	Validation	10	14.8 ± 1.25	10	12.8 ± 1.5	Gracilis and semitendinosus

Note: SD, standard deviation.

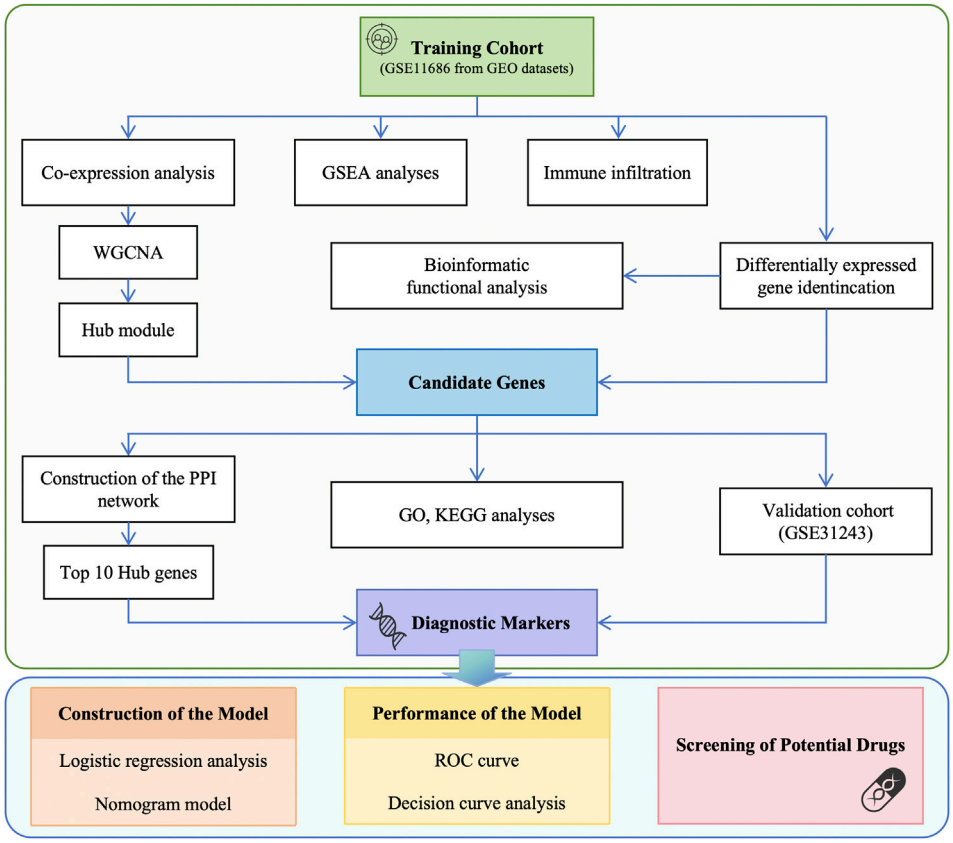

FIGURE 1
Flowchart of data preparation and analysis in this study. GEO, Gene Expression Omnibus; WGCNA, weighted gene co-expression network analysis; GSEA, gene set enrichment analysis; PPI, protein-protein interaction; GO, Gene ontology; KEGG, Kyoto Encyclopedia of Genes and Genomes; ROC, receiver operating characteristic; DCA, decision curve analysis.

performed using an unpaired independent *t*-test, with a significance level set at $p < 0.05$.

Establishment and validation of prediction models and nomogram

To establish the prediction model, we utilized logistic regression analysis. The multivariate model included hub genes that showed differential expression in both the training and validation cohorts. Based on the regression coefficients of the relevant genes in the training cohort, we developed a nomogram. Model covariates were assigned points in the range of 0–100, corresponding to their values. The total points obtained from the predictive model indicated the risk of CP. We assessed the performance of the nomogram using the calibration curve in the training cohort. The predictive ability of the model was evaluated in both the training and validation cohorts using the area under the ROC curve (AUC). We generated ROC curves using SPSS. Genes were considered to have potential clinical significance if their AUC was greater than 0.6.

TABLE 2 The gene expression levels of 45 overlap hub genes.

Gene symbol	*p*-Value	Log FC	Gene title
ACYP1	0.028656	1.273,244	Acylphosphatase-1
ADM	0.017645	−1.225,876	Adrenomedullin
ALCAM	0.018667	1.224,642	Activated leukocyte cell adhesion molecule
AMOT	0.015123	−1.308,099	Angiomotin
ASTN2	0.031953	1.476,799	Astrotactin-2
BDH1	0.033195	−1.561,303	3-hydroxybutyrate dehydrogenase 1
CA8	0.005997	−1.429,715	Carbonic anhydrase VIII
CHAD	0.002794	2.096462	Chondroadherin
CKB	0.008580	−1.320,115	Creatine kinase B-type
CKMT2	0.001798	−1.218,961	Creatine kinase S-type, mitochondrial
CRYM	0.007519	−2.363,445	Crystallin, mu
ESPN	0.006668	−1.604,240	Espin
FABP3	0.009801	−1.800,821	Fatty acid binding protein 3
GOT1	0.013254	−1.301,036	Glutamic-oxaloacetic transaminase 1
GPX3	0.009929	−1.383,203	Glutathione peroxidase 3
HIST1H2BE	0.001751	1.247,343	Histone cluster 1, H2be
KAL1	0.000630	1.337,068	Kallmann syndrome 1 sequence
KCNN2	0.007283	1.591,455	Small conductance calcium-activated potassium channel protein 2
LDHB	0.003401	−1.226,687	Lactate dehydrogenase B
LPL	0.011452	−1.648,013	Lipoprotein lipase
MAP3K7CL	0.010553	1.571,485	MAP3K7 C-terminal like
MMRN1	0.016738	−1.624,806	Multimerin 1
MPC1	0.007283	−1.235,675	Mitochondrial pyruvate carrier 1
MYH1	0.037308	2.365,836	Myosin-1
MYH4	0.001802	2.046775	Myosin-4
NAP1L2	0.005890	1.887,987	Nucleosome assembly protein 1-like 2
NINJ1	0.001699	1.290,459	Ninjurin-1
NKAIN1	0.014994	1.677,495	Na+/K+ transporting ATPase interacting 1
NME3	0.034381	1.597,844	Nucleoside diphosphate kinase 3
NOTCH2NL	0.039355	1.217,319	Notch homolog 2 N-terminal-like protein A
NPTX2	0.019633	−1.319,154	Neuronal pentraxin-2
NSUN5P1	0.028064	1.232,678	Putative NOL1/NOP2/Sun domain family member 5B
OMD	0.008529	1.404,630	Osteomodulin
PEG10	0.006821	1.203,384	Paternally expressed 10
POLI	0.005709	1.571,104	Polymerase (DNA directed) iota
POLM	0.001989	−1.283,703	DNA-directed DNA/RNA polymerase mu

(Continued on following page)

TABLE 2 (*Continued*) The gene expression levels of 45 overlap hub genes.

Gene symbol	*p*-Value	Log FC	Gene title
PPIF	0.004543	−1.211,272	Peptidyl-prolyl cis-trans isomerase F
PREB	0.009929	−1.241,452	Prolactin regulatory element-binding protein
PVALB	0.001802	4.740,443	Parvalbumin alpha
RETSAT	0.000630	−1.540,679	All-trans-retinol 13,14-reductase
SLC12A8	0.036487	−1.651,596	Solute carrier family 12, member 8
SP140L	0.002429	1.601,102	SP140 nuclear body protein like
TGM2	0.001802	−1.509,241	Protein-glutamine gamma-glutamyltransferase 2
TNNT2	0.026367	1.338,269	Troponin T type 2 (cardiac)
TST	0.001802	−1.352,077	Thiosulfate sulfurtransferase

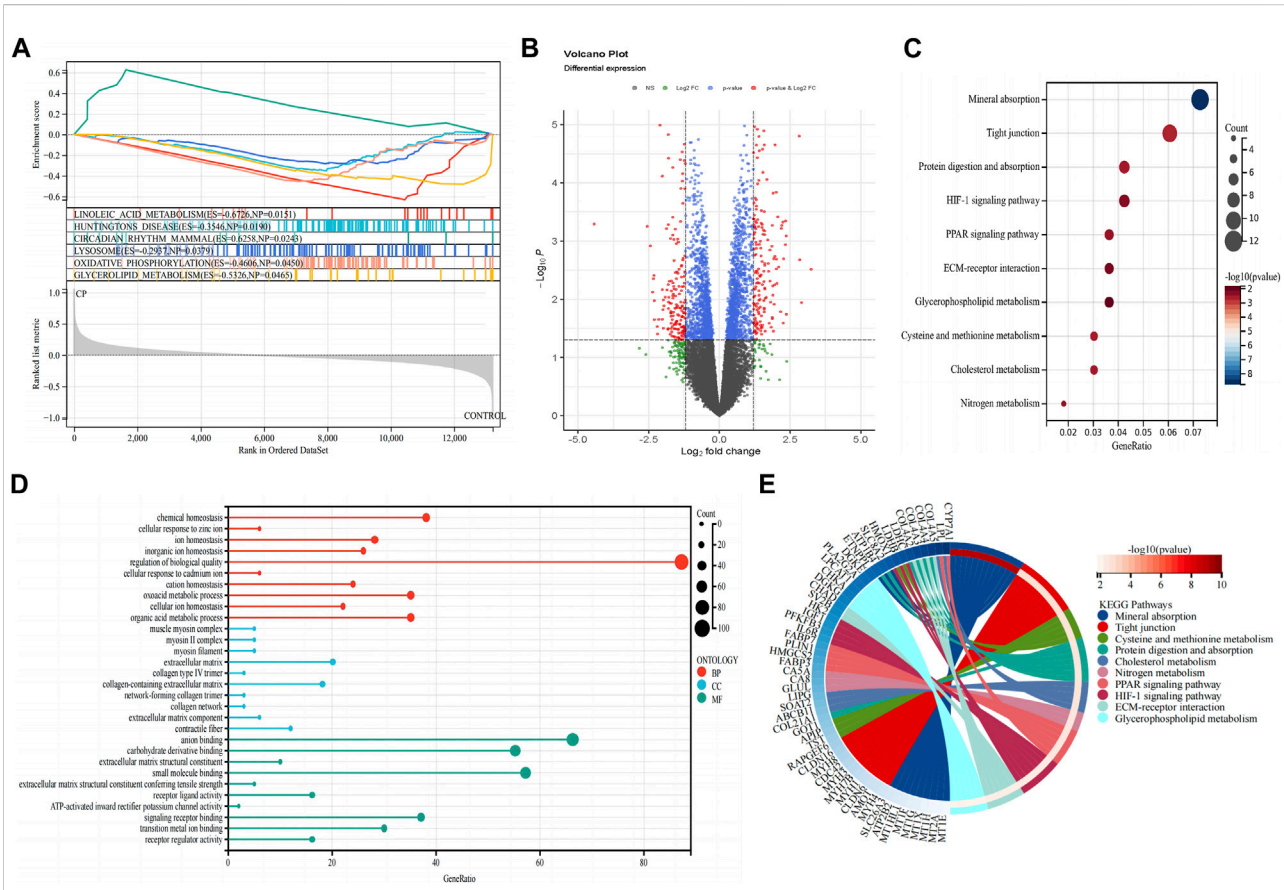

FIGURE 2
Detection of differentially expressed genes and functional enrichment analysis. **(A)** GSEA analysis; **(B)** Volcano plot of the 353 DEGs; **(C)** KEGG pathway enrichment analysis; **(D)** GO enrichment analysis; **(E)** The KEGG-enriched chord diagram shows the genes involved in the KEGG term. DEGs, differentially expressed genes; FC, fold-change; GSEA, gene set enrichment analysis; GO, Gene ontology; KEGG, Kyoto Encyclopedia of Genes and Genomes.

Prediction of potential drugs

Based on the biomarkers of CP, the DGIdb database[5] was utilized to predict potential drugs for the treatment of CP. The network of biomarker-compound pairs was visualized using the Cytoscape software.

Results

GSEA

GSEA was conducted on both patients with CP and healthy control subjects to investigate the biological signaling pathway. The top five terms are shown in Figure 2A. Linoleic acid metabolism, Huntington's disease, circadian rhythm, lysosome, oxidative phosphorylation, and glycerolipid metabolism were significantly enriched in the patients with CP.

Functional enrichment analysis of DEGs

A total of 353 DEGs were identified, including 173 upregulated and 180 downregulated genes (Figure 2B). We performed functional analysis to gain a deeper understanding of the biological functions of the DEGs. In terms of BP, the clusters were significantly associated with the regulation of biological quality, chemical homeostasis, and organic acid metabolic process. In the MF analysis, our results indicate that the DEGs are significantly associated with anion binding, small molecule binding, and carbohydrate derivative binding. In the CC enrichment analysis, the focus was on the extracellular matrix (ECM), collagen-containing ECM, and contractile fiber (Figure 2D). In the KEGG pathway analysis (Figures 2C, E), mineral absorption, tight junction, and protein digestion and absorption were identified as significant pathways in the DEGs.

Infiltration of immune cells results

The assessment of immune infiltration within the sample was conducted using robust bioinformatics methodologies, specifically the CIBERSORT algorithms. Compared to normal samples, samples from patients with CP generally exhibited a higher proportion of mast cells ($p = 0.013$), while Dendritic cells were relatively lower ($p = 0.058$, Figure 3A). In particular, CP patient samples often had a higher proportion of resting mast cells and T cells follicular helper ($p < 0.05$), suggesting a potential regulatory role in the immune response (Figures 3B, C). These findings highlight the complex interplay of various immune cell subsets and emphasize the importance of their interactions in shaping the immune landscape of the analyzed sample.

Identification of co-expression gene modules in CP

In the CP datasets, after excluding any outliers, we used WGCNA to identify co-expression gene modules among multiple genes (Figures 4A, B). To ensure that the network resembled a scale-free network, we calculated the soft-thresholding power, which was found to be 8 based on a scale independence of >0.9 (Figure 4C). By employing hierarchical clustering analysis and dynamic branch cut methods on the gene dendrograms, we grouped the genes into 26 modules (Figure 4F). The clustering dendrogram of the genes is shown in Figure 4E, where genes with similar characteristics are clustered together and represented by the same module color. Importantly, these modules were found to be independent of one another. Figure 4D provides a summary of the significance of all genes in each module with respect to CP. Notably, the brown module exhibited a significant association with CP and was selected for further analysis ($p = 3e\text{-}04$). The scatter plot in Figure 4G illustrated the relationship between CP gene significance and module membership, with a total of 762 genes being significantly associated with CP.

Extract hub genes from DEGs and the hub module in WGCNA

Forty-five candidate genes were identified from the intersection of a venn diagram between two sets of the DEGs and WGCNA brown module (Figure 5A). To explore the biological features and significance of these 45 hub genes, GO and KEGG pathway enrichment analyses were performed (Figures 5D, E). The results of the analysis revealed that these hub genes were significantly related to various biological processes such as muscle contraction, carboxylic acid metabolic process, and phosphocreatine biosynthetic process. In terms of molecular function, the hub genes are associated with creatine kinase activity, DNA-directed DNA polymerase activity, and calcium ion binding. The enrichment analysis of cell component showed a focus on mitochondrion, muscle myosin complex, and neuronal cell body. Additionally, the KEGG pathway analysis indicated that arginine and proline metabolism, cysteine and methionine metabolism, and metabolic pathways were significant pathways in these 45 hub genes. These findings suggest that these genes are significantly enriched in energy metabolism-related pathways, indicating their potential role in muscular movement. For further analysis, a PPI network was constructed among the 45 candidate genes using Cytoscape software (Figure 5C). The MCC method in the CytoHubba plug-in was used to identify potential key genes. The top 10 Hubba nodes were collected for subsequent

5 https://www.dgidb.org/

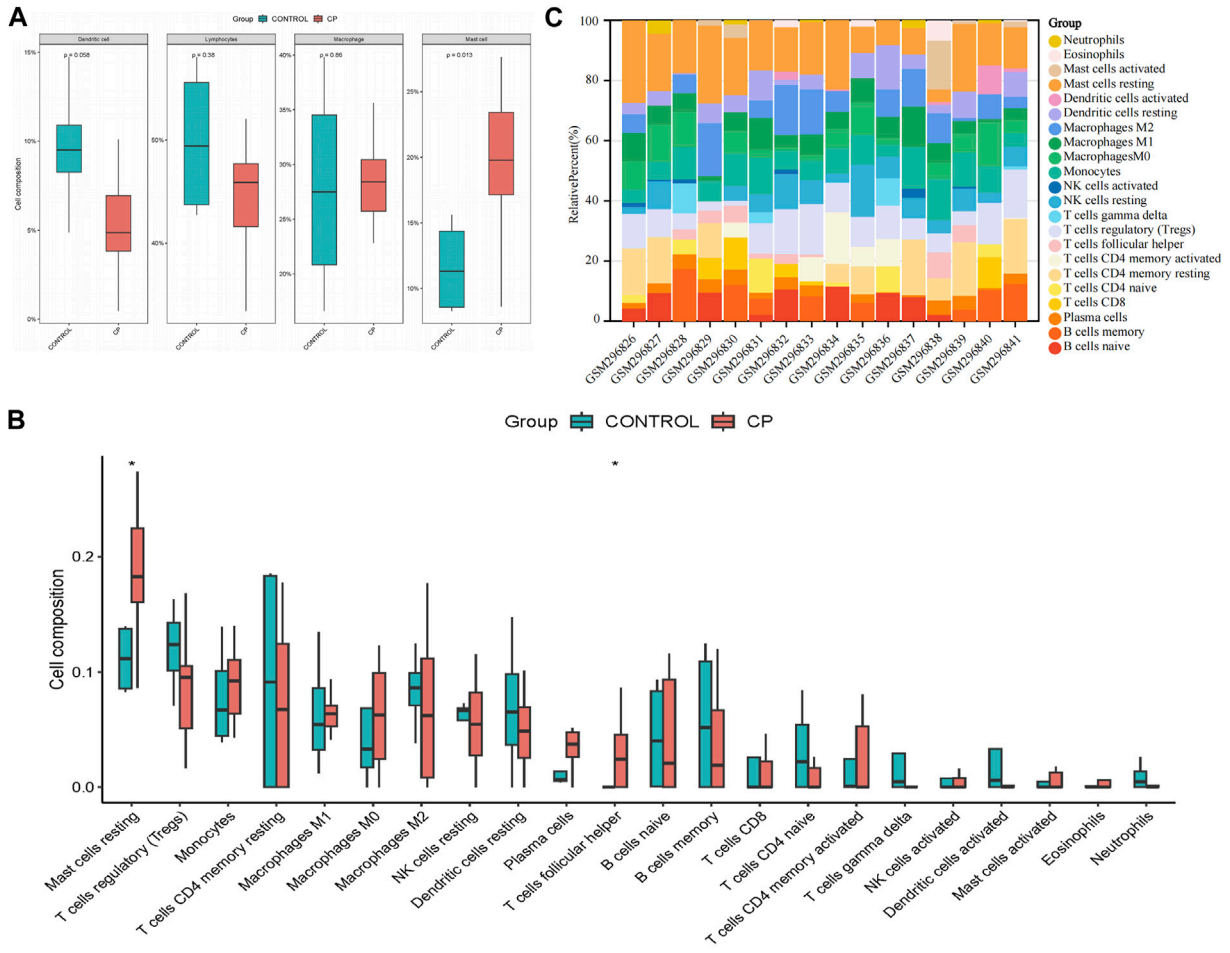

FIGURE 3
Evaluation and visualization of immune cell infiltration. **(A)** Boxplot of the proportion of four classes of immune cells; **(B)** Boxplot of the proportion of 22 types of immune cells; **(C)** Stacked bar graph of the proportion of 22 types of immune cells. NK, natural killer. *$p < 0.05$ compared with the controls.

analysis (Figure 5B). Among the 45 genes, CKMT2, TNNT2, MYH4, MYH1, FABP3, PVALB, GOT1, GPX3, TST, and LPL were identified as the hub genes by the CytoHubba plug-in.

Screening and validation of diagnostic markers

To further demonstrate the significance of the key genes in the module of interest, we assessed the expression of 45 candidate genes using muscle samples from the GSE31243 dataset (Figure 6A). Comparative analysis between the two samples revealed that 14 genes exhibited statistically significant differences in the CP sample. When the top 10 hub genes identified by MCC were analyzed together, we found 6 genes that were statistically different: CKMT2, TNNT2, MYH4, MYH1, GOT1, and LPL. This suggests that these six genes are important in relation to CP. Consequently, we developed a prediction model for CP in the validation cohort based on the expression of these six genes. The final model we obtained was as follows: prediction model = 104.2864 + 0.3745*CKMT2 + 0.8794*TNNT2 + 1.4529*MYH4 − 6.6211*MYH1 − 2.5241*GOT1 + 1.2096*LPL. Additionally, we created a nomogram to visualize the model and used a calibration curve to assess its accuracy. The nomogram is presented in Figure 6B, and the calibration curve is shown in Figure 6E (Mean absolute error = 0.066). The calibration curve of the nomogram for predicting CP risk demonstrated good agreement. Furthermore, the Hosmer-Lemeshow test, which evaluated the model, yielded a Chi-square value of 12.045 ($p = 0.1492 > 0.05$), indicating that the predictive model performed well. In addition, we compared the predictive value of the model with that of the six individual genes. The ROC curves revealed that the combined six-gene prediction had a higher value than the prediction based on a single gene (AUC = 0.905 in the validation cohort) (Figures 6C, D). Finally, according to the results of

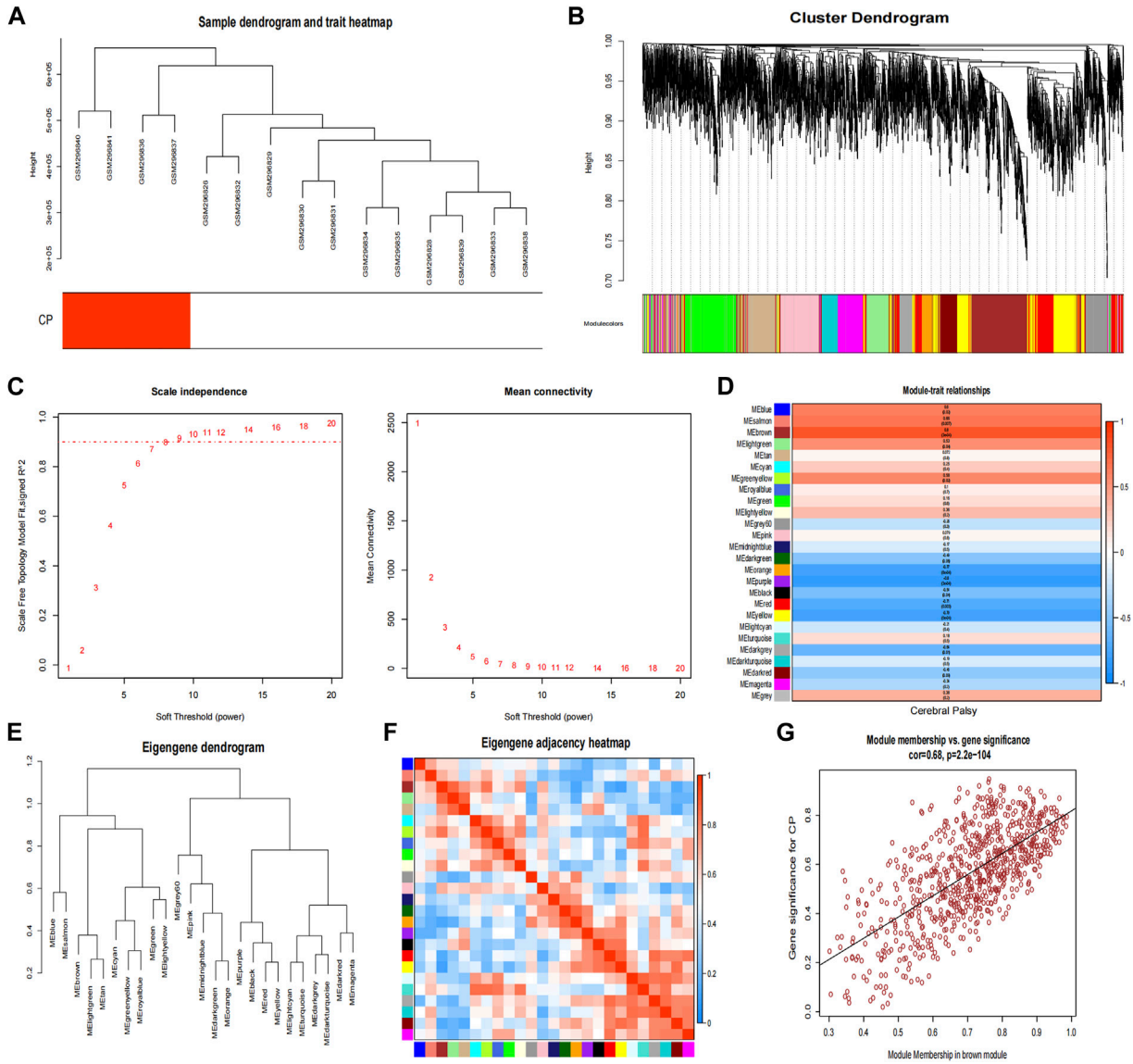

FIGURE 4
Weighted co-expression network related datasets construction. **(A)** Sample dendrogram and trait heatmap; **(B)** Gene dendrograms obtained by average linkage hierarchical clustering; **(C)** Analysis of network topology for various soft thresholds (β); **(D)** Module-trait relationships; **(E)** Clustering dendrogram of genes; **(F)** Module eigengene adjacency heatmap; **(G)** The correlation between the module membership (MM) and gene significance (GS) of the disease group of all genes in the brown module. The correlation value represents the absolute correlation coefficient between GS and MM. CP, cerebral palsy.

the decision curve analysis (DCA), the nomogram model provided a superior clinical benefit (Figure 6F).

Potential drugs targeting the diagnostic genes

To investigate potential drugs for CP therapy, we conducted a search in the DGIdb database for drugs targeting the biomarkers. Our analysis revealed that 28 drugs targeting LPL and 4 drugs targeting TNNT2 were identified. Subsequently, we generated a gene-drug network consisting of 34 nodes, which is presented in Figure 7. Notably, regulatory approval has been granted to 19 drugs targeting LPL and 1 drug targeting TNNT2.

Discussion

This study emphasizes the urgent need for early and accurate identification of biomarkers for CP to enhance diagnostic

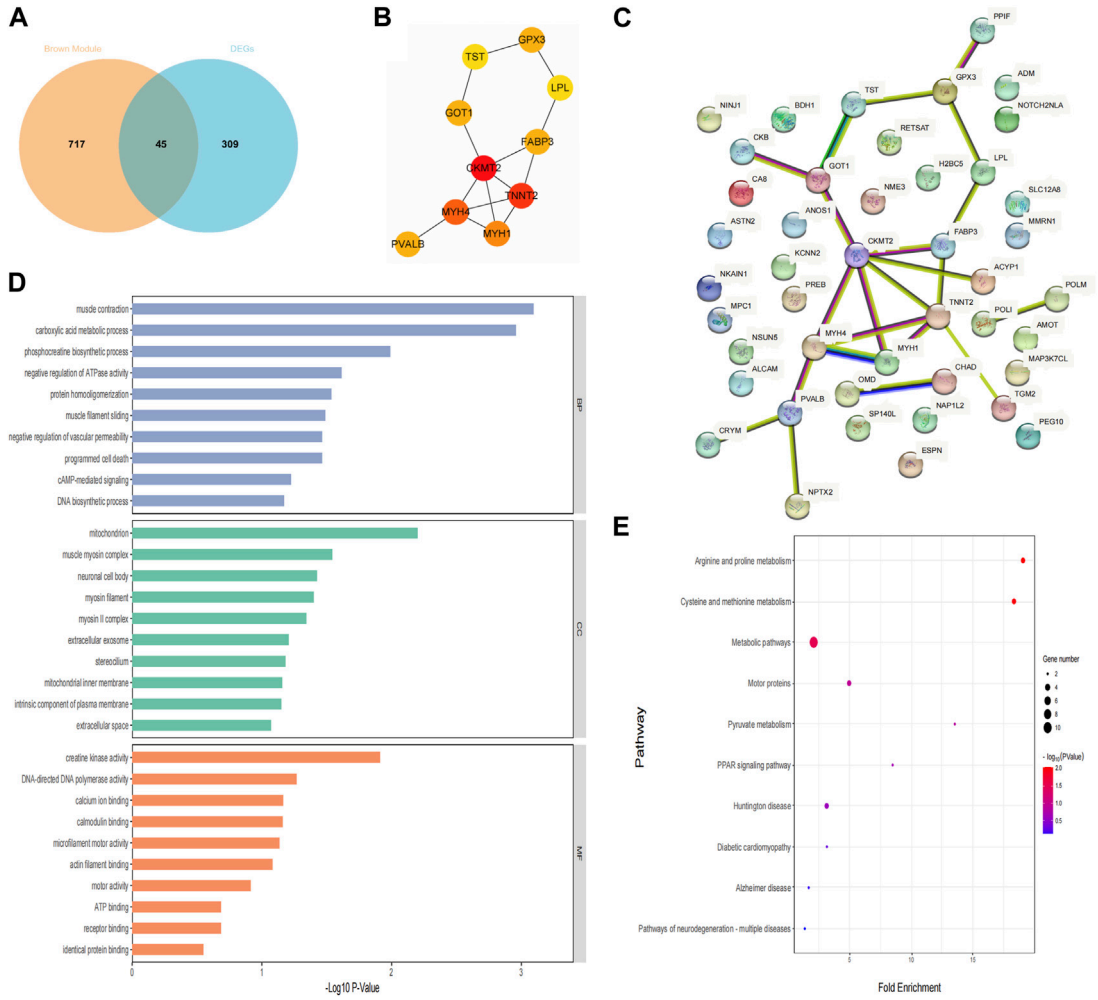

FIGURE 5
Hub genes identification and functional enrichment analysis. **(A)** The overlap of DEGs and module genes was shown as a Venn diagram; **(B)** The top 10 hub genes with the most correlations identified using CytoHubba; **(C)** PPI network of 45 hub genes generated by the Cytoscape software; **(D)** Gene ontology enrichment analysis; **(E)** The Kyoto Encyclopedia of Genes and Genomes pathway enrichment analysis.

precision and improve patient outcomes. Through rigorous analysis, several potential biomarkers were identified, providing insights into the pathophysiological mechanisms related to CP. Developing predictive models based on these biomarkers offers opportunities for early diagnosis and personalized therapeutic interventions for CP. In our research, we identified 45 potential key genes through differential expression and WGCNA. Subsequent GO and KEGG analyses revealed that these genes are primarily involved in energy metabolism-related pathways in the development of CP, underscoring their crucial role in muscle movement. Further dataset validation identified CKMT2 as the key gene most closely associated with CP. Additionally, we established a predictive model for CP by combining five other significantly differentially expressed genes (TNNT2, MYH4, MYH1, GOT1, and LPL).

Previous studies had also identified differential genes and pathways associated with CP, which share many similarities with our research. Our study, along with those by Pingel and Robinson et al., identified genes related to energy production and muscle function as significant in CP [15, 16]. Genes involved in ECM structure and turnover have been emphasized in multiple studies. Increased ECM turnover and net collagen synthesis enable ECM remodeling as an adaptive response to the increased mechanical load and functional demands caused by spasticity [17]. Previous research had shown significantly lower LPL expression and increased intramuscular fat levels in CP patients, which was consistent with our findings [18, 19]. Additionally, Pingel et al.'s study highlighted the importance of calcium homeostasis in skeletal muscle movement and plasticity, finding distorted calcium ion handling in CP [11]. Stress, cell death, and

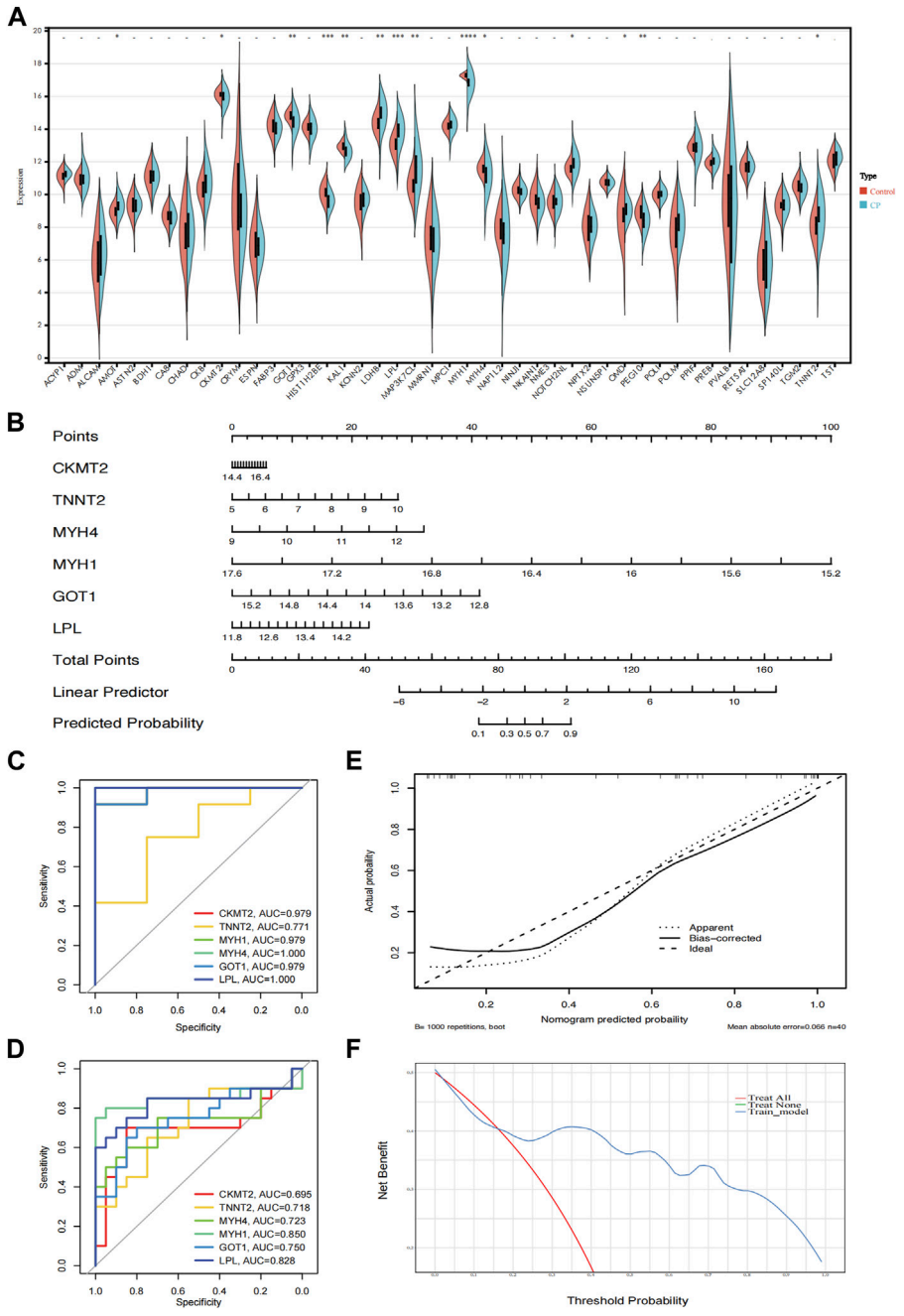

FIGURE 6
Validation of the hub genes. **(A)** The expression of 45 genes in the validation cohort (GSE31243); **(B)** A nomogram estimated CP risk in the training cohort by summing scores from each risk factor and positioning the total on the corresponding bottom line to calculate the probability of CP; **(C)** ROC curves of the training cohort; **(D)** ROC curves of the validation cohort; **(E)** The calibration curve shows the nomogram-predicted CP probability (x-axis) versus actual CP probability (y-axis). The diagonal dotted line represents perfect predictions, while solid lines represent nomogram performance. The closer the solid lines are to the diagonal, the better the prediction accuracy; **(F)** Decision curve analysis shows the prediction model's net benefit (y-axis) against the threshold probability (x-axis), where the harm of false positives exceeds that of false negatives. Higher net benefit at the same probability indicates better clinical usefulness. CP, cerebral palsy. ****: $p < 0.0001$, ***: $p < 0.001$, **: $p < 0.01$, *: $p < 0.05$.

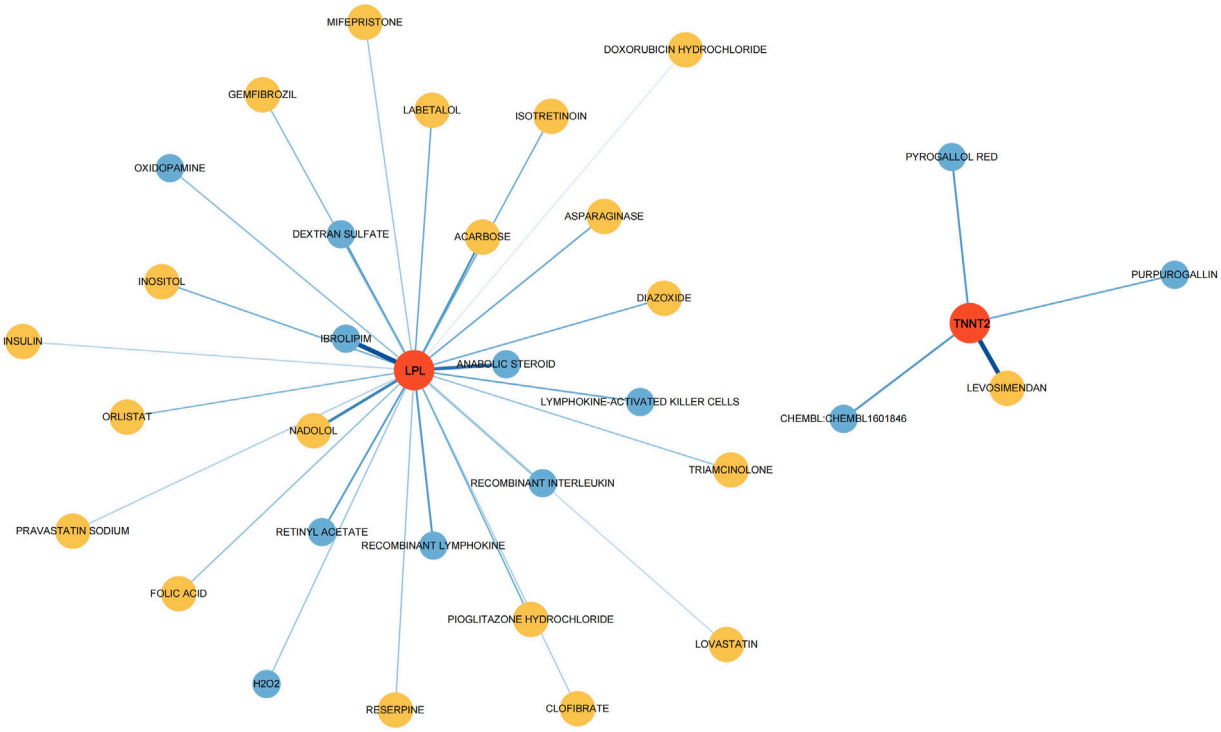

FIGURE 7
Drugs–hub genes interaction network. The red nodes represent genes, yellow nodes represent approved drugs, and blue nodes represent drugs not yet approved.

autophagy also had contributed to the pathology of CP. Each study provided unique insights into the specific genes and mechanisms involved in CP pathology, underscoring the importance of genes related to energy metabolism, muscle function, and ECM structure in CP.

In our diagnostic model, CKMT2 was identified as the key gene most closely related to CP. The CKMT2 gene encodes mitochondrial creatine kinase, an enzyme crucial for energy metabolism in tissues with high and fluctuating energy demands, such as the brain and muscles. CKMT2 plays a primary role in maintaining cellular energy homeostasis by facilitating the reversible transfer of phosphate groups between adenosine triphosphate (ATP) and creatine [20]. This process allows for the storage and transportation of energy within cells, particularly in mitochondria-rich tissues. Additionally, mitochondrial creatine kinase is believed to be essential for maintaining mitochondrial morphology by stabilizing contact sites between the inner and outer mitochondrial membranes. Impaired activity of CKMT2 has been associated with the loss of mitochondrial membrane potential and apoptosis [21]. In the intact rabbit heart, a rapid and irreversible loss of CKMT2 was observed, which was directly related to the duration of ischemia. This loss of CKMT2 correlated with contractile dysfunction during reperfusion [22].

Further studies have demonstrated that CKMT2 overexpression protects against cellular oxidative stress damage, likely due to increased creatine kinase activity and its role in promoting mitochondrial integrity [23, 24]. CKMT2 is crucial for regulating energy production and utilization in the brain, ensuring a constant energy supply essential for neuronal function, neurotransmission, and brain health. Beyond energy provision, CKMT2 maintains cellular energy reserves and buffers against energy fluctuations. Variations or mutations in the CKMT2 gene may contribute to mitochondrial dysfunction, disrupting energy balance in neurons and potentially influencing the onset or severity of CP. Therefore, studying the correlation between CKMT2 variants and CP clinical features (such as severity, motor impairment patterns, or associated comorbidities) can deepen the understanding of disease subtypes and their pathological mechanisms, providing opportunities for personalized treatment. Exploring pathways aimed at regulating mitochondrial function or enhancing energy metabolism may serve as therapeutic strategies to alleviate symptoms or prevent the progression of related damage. Further large-scale genetic studies, functional analyses, and investigations into mitochondrial function will be essential to determine their significance in disease development and identify potential therapeutic targets.

The remaining five genes in the diagnostic model (TNNT2, MYH4, MYH1, GOT1, and LPL) also contribute to the pathology of CP through different mechanisms. TNNT2 encodes a component of the troponin complex critical for muscle contraction regulation, with variants linked to neuromuscular disorders [25]. In CP, TNNT2 variations might affect muscle tone regulation, contributing to motor impairments. MYH4 and MYH1 encode myosin heavy chain proteins, which are essential for muscle contraction. Alterations in these genes may impact muscle fiber composition or contractile properties, potentially leading to abnormalities in motor function and muscle tone observed in CP [26, 27]. GOT1 (Glutamic-Oxaloacetic Transaminase 1) is involved in amino acid metabolism [28]. Although its direct role in CP is not yet clear, disruptions in amino acid metabolism pathways could potentially affect brain development or neural function, thus contributing to the complex etiology of CP. LPL (Lipoprotein Lipase) plays a crucial role in lipid metabolism, affecting neurodevelopment and neuronal health [29]. Dysregulation of LPL may lead to changes in lipid metabolism, which correlates with the previously observed increase in intramuscular fat levels [18]. In conclusion, while the roles of TNNT2, MYH4, MYH1, GOT1, and LPL genes in CP are still under investigation, their involvement in muscle function, metabolic pathways, and potentially neurodevelopmental processes could contribute to the diverse clinical manifestations observed in individuals with CP. Variations in TNNT2, MYH4, and MYH1 may affect muscle structure, contractility, or neuromuscular junction function, contributing to motor impairments and muscle tone abnormalities. Meanwhile, genes such as GOT1 and LPL, involved in amino acid and lipid metabolism respectively, may indirectly affect neurodevelopmental processes and lipogenesis in muscle. Dysregulation of these pathways could impact substance synthesis and neuronal health within muscle, potentially contributing to the multifactorial nature of CP. Further research is needed to validate the differential expression of these genes and their direct impact on the pathogenesis of CP. Experimental models and functional assays are necessary to elucidate their specific contributions to neuronal development or muscle function. Additionally, studying the differential expression of genes and their potential association with birth complications may provide valuable insights into the etiology of CP.

Through the DGIdb database, we obtained potential therapeutic agents targeting the biomarkers. Purpurogallin (PPG) possesses significant antioxidant properties. By inhibiting the TLR4/NF-κB pathway and thereby attenuating endoplasmic reticulum stress and neuroinflammation, PPG demonstrates potential neuroprotective effects against cerebral ischemia-reperfusion injury [30]. Insulin, beyond its role in glucose metabolism, has shown neuroprotective effects and might influence brain development and neuroplasticity, which could be relevant in CP management. Lymphokine-activated killer (LAK) Cells and recombinant lymphokine have cytotoxic activity against tumor cells when activated *in vitro*, but their effects on CP remain unexplored. Levosimendan has a vasodilatory effect, and its potential impact on cerebral circulation and muscle tissue blood supply in CP patients needs further clarification [31]. Statins (Lovastatin, Pravastatin) have shown neuroprotective and anti-inflammatory effects, potentially beneficial in managing neuroinflammation in CP. Diazoxide, a vasodilator and potassium channel opener, does not have well-documented effects on CP but might influence blood flow or neural excitability. Triamcinolone, a corticosteroid, has the potential to suppress inflammation and immune responses, making it a potential option for managing inflammation-related aspects of CP. In a frozen shoulder rat model, the injection of triamcinolone acetonide has shown effective anti-fibrosis, anti-angiogenesis, and anti-inflammatory properties [32]. While these drugs show promise in affecting neurological functions or mechanisms related to CP, their specific impacts on CP patients require extensive clinical studies. Considerations such as dosage, duration, individual variability, and underlying pathology are crucial when evaluating their effects. Some drugs' impacts on CP may not be well-documented or explored in clinical trials specifically for this condition, necessitating targeted research or clinical trials to evaluate their efficacy and safety in this population.

The study used samples from various muscle groups, with tissue collection sites as potential confounders. Different muscle groups exhibited unique gene expression profiles due to their physiological functions and fiber types [33]. Wrist muscles, crucial for fine motor skills and complex hand movements, showed a high gene expression in pathways involved in neuromuscular junctions, muscle contraction, and calcium handling [34, 35]. Conversely, hamstring and quadriceps muscles, involved in gross motor functions, exhibited increased gene expression in ECM tissue and muscle fiber composition for structural integrity and weight-bearing [36]. Additionally, elevated expression related to oxidative phosphorylation, muscle repair, and regeneration supported endurance and adaptive recovery [37, 38]. These differences highlight the unique needs of each muscle group and suggest personalized strategies for treating related diseases. However, obtaining muscle biopsy tissue from high-risk CP patients is an unavoidable challenge. Ethical considerations and strict informed consent procedures, especially for children, must be given primary consideration. The invasiveness of the surgery, along with the risks of postoperative infection, bleeding, and discomfort, may deter participation. Additionally, the medical fragility and anesthesia risks in CP patients complicate the procedure. Despite these challenges, muscle biopsies are crucial for studying the pathophysiology of CP and subsequently developing

targeted therapies to improve muscle function and quality of life. Careful planning and ethical oversight are required, balancing the need for high-quality data with alternative, less invasive methods.

The CP prediction model based on hub genes demonstrates superior predictive power and accuracy compared to utilizing single genes. However, certain limitations related to the data must be acknowledged. The limited size of the cohorts in our dataset was a significant constraint, restricting the statistical power and robustness of our findings. Additionally, differences in age and sex between the control and CP groups represented potential confounding factors. Age-related gene expression differences and sex-specific biological variations can impact results, making it challenging to attribute observed differences solely to CP. Secondly, variability in the severity of CP may exhibit different molecular characteristics. Stratifying CP patients based on detailed clinical data and severity could help elucidate the relationship between CP severity and biomarker expression. It is essential to dynamically monitor changes in gene expression profiles throughout disease progression in longitudinal cohorts. Furthermore, variability among different muscle samples needs further clarification. In CP patients, muscle tissue often exhibits unique pathological changes such as increased ECM, fat infiltration, and heightened inflammation, which can affect gene expression outcomes due to differences in tissue composition. Isolating specific cell types or using single-cell RNA sequencing can provide a more precise understanding of the molecular basis of CP.

Our study highlights the importance of considering demographic variables, repeated measures, and tissue composition in biomarker research. Despite the limitations, our findings provide valuable insights into the molecular underpinnings of CP. Future research should focus on using larger, well-matched cohorts and advanced analytical techniques to improve the accuracy and applicability of biomarker discoveries. By addressing these factors, we can enhance the diagnostic and therapeutic potential of CP biomarkers.

Conclusion

This study provides new insights into identifying potential biomarkers for CP and developing predictive models for early diagnosis and personalized treatment. Using comprehensive bioinformatics approaches, promising biomarkers (CKMT2, TNNT2, MYH4, MYH1, GOT1, and LPL) were identified, and robust predictive models for muscle sample markers specific to CP were developed. The findings highlight the importance of incorporating biomarker-based diagnostics into clinical practice to enable early and accurate diagnosis, leading to timely interventions and improved long-term outcomes. Future research should validate these biomarkers and models in larger cohorts and translate them into practical diagnostic tools and treatment protocols, ultimately enhancing the quality of life for individuals with CP and their families.

Author contributions

HZ: Conceptualization, Data curation, Validation, Visualization, Writing–original draft, Writing–review and editing. DZ: Conceptualization, Data curation, Methodology, Writing–original draft, Writing–review and editing. YG: Writing–review and editing, Methodology, Conceptualization, Supervision, Writing–original draft. ZP: Writing–original draft, Writing–review and editing, Software. YW: Writing–original draft, Writing–review and editing, Validation. WX: Writing–original draft, Writing–review and editing, Methodology, Supervision, Conceptualization.

Data availability

Publicly available datasets were analyzed in this study. This data can be found here: https://doi.org/10.5281/zenodo.12599229.

Ethics statement

Ethical approval was not required for the study involving humans in accordance with the local legislation and institutional requirements. Written informed consent to participate in this study was not required from the participants or the participants' legal guardians/next of kin in accordance with the national legislation and the institutional requirements.

Funding

The author(s) declare that no financial support was received for the research, authorship, and/or publication of this article.

Conflict of interest

The authors declare that the research was conducted in the absence of any commercial or financial relationships that could be construed as a potential conflict of interest.

References

1. Sankar C, Mundkur N. Cerebral palsy-definition, classification, etiology and early diagnosis. *Indian J Pediatr* (2005) **72**:865–8. doi:10.1007/bf02731117

2. Bax M, Goldstein M, Rosenbaum P, Leviton A, Paneth N, Dan B, et al. Proposed definition and classification of cerebral palsy, April 2005. *Dev Med Child Neurol* (2005) **47**:571–6. doi:10.1017/s001216220500112x

3. Pearson TS, Pons R. Movement disorders in children. *CONTINUUM: Lifelong Learn Neurol* (2019) **25**:1099–120. doi:10.1212/con.0000000000000756

4. Sanger TD. Toward a definition of childhood dystonia. *Curr Opin Pediatr* (2004) **16**:623–7. doi:10.1097/01.mop.0000142487.90041.a2

5. Graham HK, Selber P. Musculoskeletal aspects of cerebral palsy. *The J Bone Jt Surg Br volume* (2003) **85-B**:157–66. doi:10.1302/0301-620x.85b2.14066

6. Koy A, Hellmich M, Pauls KA, Marks W, Lin JP, Fricke O, et al. Effects of deep brain stimulation in dyskinetic cerebral palsy: a meta-analysis. *Mov Disord* (2013) **28**:647–54. doi:10.1002/mds.25339

7. Graham HK, Rosenbaum P, Paneth N, Dan B, Lin JP, Damiano DL, et al. Cerebral palsy. *Nat Rev Dis Primers* (2016) **2**:15082. doi:10.1038/nrdp.2015.82

8. Koman LA, Smith BP, Shilt JS. Cerebral palsy. *The Lancet* (2004) **363**:1619–31. doi:10.1016/s0140-6736(04)16207-7

9. Elder GC, Bsc GS, Pt KC, Msc DW, Marshall A, Leahey L, et al. Contributing factors to muscle weakness in children with cerebral palsy. *Dev Med Child Neurol* (2003) **45**:542–50. doi:10.1111/j.1469-8749.2003.tb00954.x

10. Smith LR, Ponten E, Hedstrom Y, Ward SR, Chambers HG, Subramaniam S, et al. Novel transcriptional profile in wrist muscles from cerebral palsy patients. *BMC Med Genomics* (2009) **2**:44. doi:10.1186/1755-8794-2-44

11. Smith LR, Chambers HG, Subramaniam S, Lieber RL. Transcriptional abnormalities of hamstring muscle contractures in children with cerebral palsy. *PLoS One* (2012) **7**:e40686. doi:10.1371/journal.pone.0040686

12. Subramanian A, Tamayo P, Mootha VK, Mukherjee S, Ebert BL, Gillette MA, et al. Gene set enrichment analysis: a knowledge-based approach for interpreting genome-wide expression profiles. *Proc Natl Acad Sci U S A* (2005) **102**:15545–50. doi:10.1073/pnas.0506580102

13. Le T, Aronow RA, Kirshtein A, Shahriyari L. A review of digital cytometry methods: estimating the relative abundance of cell types in a bulk of cells. *Brief Bioinform* (2021) **22**:bbaa219. doi:10.1093/bib/bbaa219

14. Baralic K, Jorgovanovic D, Zivancevic K, Antonijevic Miljakovic E, Antonijevic B, Buha Djordjevic A, et al. Safety assessment of drug combinations used in COVID-19 treatment: *in silico* toxicogenomic data-mining approach. *Toxicol Appl Pharmacol* (2020) **406**:115237. doi:10.1016/j.taap.2020.115237

15. Pingel J, Kampmann M-L, Andersen JD, Wong C, Døssing S, Børsting C, et al. Gene expressions in cerebral palsy subjects reveal structural and functional changes in the gastrocnemius muscle that are closely associated with passive muscle stiffness. *Cell Tissue Res* (2021) **384**:513–26. doi:10.1007/s00441-020-03399-z

16. Robinson KG, Crowgey EL, Lee SK, Akins RE. Transcriptional analysis of muscle tissue and isolated satellite cells in spastic cerebral palsy. *Dev Med Child Neurol* (2021) **63**:1213–20. doi:10.1111/dmcn.14915

17. Nemska S, Serio S, Larcher V, Beltrame G, Portinaro NM, Bang ML. Whole genome expression profiling of semitendinosus tendons from children with diplegic and tetraplegic cerebral palsy. *Biomedicines* (2023) **11**:2918. doi:10.3390/biomedicines11112918

18. Noble JJ, Charles-Edwards GD, Keevil SF, Lewis AP, Gough M, Shortland AP. Intramuscular fat in ambulant young adults with bilateral spastic cerebral palsy. *BMC Musculoskelet Disord* (2014) **15**:236. doi:10.1186/1471-2474-15-236

19. Pingel J, Vandenrijt J, Kampmann ML, Andersen JD. Altered gene expression levels of genes related to muscle function in adults with cerebral palsy. *Tissue and Cell* (2022) **76**:101744. doi:10.1016/j.tice.2022.101744

20. Zervou S, Whittington HJ, Ostrowski PJ, Cao F, Tyler J, Lake HA, et al. Increasing creatine kinase activity protects against hypoxia/reoxygenation injury but not against anthracycline toxicity *in vitro*. *PLoS One* (2017) **12**:e0182994. doi:10.1371/journal.pone.0182994

21. Lenz H, Schmidt M, Welge V, Kueper T, Schlattner U, Wallimann T, et al. Inhibition of cytosolic and mitochondrial creatine kinase by siRNA in HaCaT- and HeLaS3-cells affects cell viability and mitochondrial morphology. *Mol Cel Biochem* (2007) **306**:153–62. doi:10.1007/s11010-007-9565-8

22. Bittl JA, Weisfeldt ML, Jacobus WE. Creatine kinase of heart mitochondria. The progressive loss of enzyme activity during *in vivo* ischemia and its correlation to depressed myocardial function. *J Biol Chem* (1985) **260**:208–14. doi:10.1016/s0021-9258(18)89717-4

23. Akki A, Su J, Yano T, Gupta A, Wang Y, Leppo MK, et al. Creatine kinase overexpression improves ATP kinetics and contractile function in postischemic myocardium. *Am J Physiology-Heart Circulatory Physiol* (2012) **303**:H844–52. doi:10.1152/ajpheart.00268.2012

24. Rojo M, Hovius R, Demel RA, Nicolay K, Wallimann T. Mitochondrial creatine kinase mediates contact formation between mitochondrial membranes. *J Biol Chem* (1991) **266**:20290–5. doi:10.1016/s0021-9258(18)54921-8

25. Wei B, Jin JP. TNNT1, TNNT2, and TNNT3: isoform genes, regulation, and structure-function relationships. *Gene* (2016) **582**:1–13. doi:10.1016/j.gene.2016.01.006

26. Wang M, Yu H, Kim YS, Bidwell CA, Kuang S. Myostatin facilitates slow and inhibits fast myosin heavy chain expression during myogenic differentiation. *Biochem Biophysical Res Commun* (2012) **426**:83–8. doi:10.1016/j.bbrc.2012.08.040

27. Alsaif HS, Alshehri A, Sulaiman RA, Al-Hindi H, Guzmán-Vega FJ, Arold ST, et al. MYH1 is a candidate gene for recurrent rhabdomyolysis in humans. *Am J Med Genet A* (2021) **185**:2131–5. doi:10.1002/ajmg.a.62188

28. Song Z, Yang Y, Wu Y, Zheng M, Sun D, Li H, et al. Glutamic oxaloacetic transaminase 1 as a potential target in human cancer. *Eur J Pharmacol* (2022) **917**:174754. doi:10.1016/j.ejphar.2022.174754

29. Feng L, Sun Y, Liu F, Wang C, Zhang C, Liu J, et al. Clinical features and functions of a novel Lpl mutation C.986A>C (p.Y329S) in patient with hypertriglyceridemia. *Curr Res Translational Med* (2022) **70**:103337. doi:10.1016/j.retram.2022.103337

30. Li X, Cheng Z, Chen X, Yang D, Li H, Deng Y. Purpurogallin improves neurological functions of cerebral ischemia and reperfusion mice by inhibiting endoplasmic reticulum stress and neuroinflammation. *Int Immunopharmacology* (2022) **111**:109057. doi:10.1016/j.intimp.2022.109057

31. Cholley B, Levy B, Fellahi JL, Longrois D, Amour J, Ouattara A, et al. Levosimendan in the light of the results of the recent randomized controlled trials: an expert opinion paper. *Crit Care* (2019) **23**:385. doi:10.1186/s13054-019-2674-4

32. Ahn Y, Moon YS, Park GY, Cho SC, Lee YJ, Kwon DR, et al. Efficacy of intra-articular triamcinolone and hyaluronic acid in a frozen shoulder rat model. *Am J Sports Med* (2023) **51**:2881–90. doi:10.1177/03635465231188524

33. Schiaffino S, Reggiani C. Fiber types in mammalian skeletal muscles. *Physiol Rev* (2011) **91**:1447–531. doi:10.1152/physrev.00031.2010

34. Pereira SC, Benoit B, de Aguiar Junior FCA, Chanon S, Vieille-Marchiset A, Pesenti S, et al. Fibroblast growth factor 19 as a countermeasure to muscle and locomotion dysfunctions in experimental cerebral palsy. *J Cachexia Sarcopenia Muscle* (2021) **12**:2122–33. doi:10.1002/jcsm.12819

35. Tavi P, Westerblad H. The role of *in vivo* Ca(2)(+) signals acting on Ca(2)(+)-calmodulin-dependent proteins for skeletal muscle plasticity. *J Physiol* (2011) **589**:5021–31. doi:10.1113/jphysiol.2011.212860

36. Gumpenberger M, Wessner B, Graf A, Narici MV, Fink C, Braun S, et al. Remodeling the skeletal muscle extracellular matrix in older age-effects of acute exercise stimuli on gene expression. *Int J Mol Sci* (2020) **21**:7089. doi:10.3390/ijms21197089

37. MacInnis MJ, Zacharewicz E, Martin BJ, Haikalis ME, Skelly LE, Tarnopolsky MA, et al. Superior mitochondrial adaptations in human skeletal muscle after interval compared to continuous single-leg cycling matched for total work. *J Physiol* (2017) **595**:2955–68. doi:10.1113/jp272570

38. Kiilerich K, Birk JB, Damsgaard R, Wojtaszewski JFP, Pilegaard H. Regulation of PDH in human arm and leg muscles at rest and during intense exercise. *Am J Physiology-Endocrinology Metab* (2008) **294**:E36–E42. doi:10.1152/ajpendo.00352.2007

EBM Experimental Biology and Medicine

TYPE Original Research
PUBLISHED 22 July 2024
DOI 10.3389/ebm.2024.10196

OPEN ACCESS

*CORRESPONDENCE
Qiu Chen,
chenqiu1005@cdutcm.edu.cn

RECEIVED 10 April 2024
ACCEPTED 12 June 2024
PUBLISHED 22 July 2024

CITATION
Liang Y, Yin S, Chen X, Li C and Chen Q (2024), The causal relationship between autoimmune diseases and rhinosinusitis, and the mediating role of inflammatory proteins: a Mendelian randomization study.
Exp. Biol. Med. 249:10196.
doi: 10.3389/ebm.2024.10196

The causal relationship between autoimmune diseases and rhinosinusitis, and the mediating role of inflammatory proteins: a Mendelian randomization study

Yanjing Liang[1], Shao Yin[1], Xiangyan Chen[1,2], Chengen Li[1] and Qiu Chen[1,2]*

[1]Chengdu University of Traditional Chinese Medicine, Chengdu, China, [2]Hospital of Chengdu University of Traditional Chinese Medicine, Chengdu, China

Abstract

Observational studies have linked autoimmune diseases (ADs) with rhinosinusitis (RS) manifestations. To establish a causal relationship between ADs and RS, and to explore the potential mediating role of inflammatory mediators between ADs and RS, we utilized Mendelian randomization (MR) analysis. Using a two-sample MR methodology, we examined the causality between multiple sclerosis (MS), rheumatoid arthritis (RA), ankylosing spondylitis (AS), psoriasis (PsO), type 1 diabetes (T1D), Sjogren's syndrome (SS), celiac disease (CeD), Crohn's disease (CD), hypothyroidism (HT), Graves' disease (GD), and Hashimoto's thyroiditis and their association with chronic and acute rhinosinusitis (CRS and ARS, respectively).To achieve this, we employed three distinct MR techniques: inverse variance weighting (IVW), MR-Egger, and the weighted median method. Our analysis also included a variety of sensitivity assessments, such as Cochran's Q test, leave-one-out analysis, MR-Egger intercept, and MR-PRESSO, to ensure the robustness of our findings. Additionally, the study explored the role of inflammation proteins as a mediator in these relationships through a comprehensive two-step MR analysis. Among the ADs, MS, RA, T1D, CeD, and HT were determined as risk factors for CRS. Only CeD exhibited a causal relationship with ARS. Subsequent analyses identified interleukin-10 (IL-10) as a potential mediator for the association of MS, RA and HT with CRS, respectively., while C-X-C motif chemokine 10 levels (CXCL10) and T-cell surface glycoprotein CD6 isoform levels (CD6) were found to influence HT's effect on CRS. Our findings demonstrate a causative link between specific autoimmune diseases and rhinosinusitis, highlighting IL-10, CXCL10, and CD6 as potential mediators in this association.

KEYWORDS

autoimmune diseases, rhinosinusitis, inflammatory factors, mediating role, Mendelian randomization

Impact statement

This study establishes a causal link between several autoimmune diseases (ADs)—specifically multiple sclerosis, rheumatoid arthritis, type 1 diabetes, celiac disease, and hypothyroidism—and rhinosinusitis, employing Mendelian randomization (MR) techniques, including inverse variance weighting, MR-Egger, and weighted median methods, alongside a variety of sensitivity assessments. By demonstrating that several ADs are risk factors for chronic rhinosinusitis and identifying celiac disease as a causal factor for acute rhinosinusitis, this work advances understanding of the interplay between autoimmune disorders and sinusitis. Crucially, it identifies inflammatory mediators such as interleukin-10, C-X-C motif chemokine 10, and CD6 isoform levels as key components in these relationships, offering new insights into potential therapeutic targets. These findings significantly impact the field by providing updated clues of the pathological links between autoimmune conditions and sinus health, with implications for treatment strategies.

Introduction

Autoimmune diseases (ADs), characterized by the immune system's disarray leading to self-directed tissue and organ damage, include diseases like multiple sclerosis (MS), rheumatoid arthritis (RA), type 1 diabetes (T1D), systemic lupus erythematosus (SLE), celiac disease (CeD), Crohn's Disease (CD), and autoimmune thyroid diseases (AITD). Their development is tightly linked to genetics, environmental influences, and shifts in the microbiota [1–3]. Epidemiologically, the escalating incidence of ADs is recognized as a significant global health menace, posing a formidable challenge to public health systems [4, 5]. While treatment approaches have evolved, there's a continuing need for tailored treatment plans and profound investigations into the mechanisms of these complex diseases.

Divided into acute and chronic categories, rhinosinusitis (RS) adversely affects the sinus mucous membranes [6]. The acute rhinosinusitis (ARS) presents with symptoms such as nasal congestion, secretion of mucoid or purulent material, facial discomfort, and olfactory reduction, not exceeding 4 weeks in duration [6, 7]. Chronic rhinosinusitis (CRS), lasting over 12 weeks, invariably involves nasal inflammation, often with preceding rhinitis symptoms [6, 8]. Its occurrence is tightly linked with factors including bacterial, viral, genetic, immune deficiency, environmental components, and air quality [8, 9], with nasal polyps and turbinate enlargement also contributing to the severity [10, 11]. Management options range from antibiotics, vasoconstrictors, antihistamines, and hypertonic saline for symptomatic relief to surgical procedures, with treatment efficacy potentially influenced by factors such as weather and emotional states [9, 12].

Inflammation is a key player in the progression of diseases, holding significant importance for both science and public health. Triggered by bacteria such as *Streptococcus* pneumoniae and viruses like coronaviruses, ARS involves the activation of various inflammatory cytokines, including IFN-α, IL-1β, and IL-6 [13, 14]. CRS, mirroring the complexity of chronic diseases, poses a significant challenge in finding a cure. The expression and regulation of cytokines are paramount in its etiology. CRS inflammation is differentiated into three categories based on the elevation of specific lymphocyte cytokines: Types 1, 2, and 3 [15, 16]. The complexity of interactions between immune cells and cytokines plays a critical role in CRS-related inflammation and tissue remodeling [17]. As mediators of communication among immune cells, cytokines are crucial in the regulation of immune responses and inflammation [18]. Aberrant cytokine levels in autoimmune diseases can result in sustained inflammation, leading to tissue damage and advancement of the disease [18, 19]. It has been indicated that autoimmune diseases could heighten the risk of CRS, influencing its prognosis [20, 21]. While the direct causal link remains to be established, the association between immune dysfunctions and inflammatory responses directs future research towards understanding the interplay between these conditions and enhancing therapeutic approaches.

Mendelian randomization (MR) utilizes genetic variants as instruments to investigate the causal relationships between particular exposures and outcomes, leveraging single nucleotide polymorphisms (SNPs) from genome-wide association studies (GWAS) to bypass traditional study confounders and enhance causal inference accuracy. This study is centered on exploring the Mendelian causality between ADs and RS, specifically focusing on the role of inflammatory mediators. Employing large GWAS datasets from European populations, through dual-sample MR analysis and a two-phase mediation approach, our aim is to reveal both the direct and indirect causal links between ADs and RS, contributing to a deeper biological understanding of their mutual influences.

Materials and methods

Study design

To delineate the causal dynamics and possible mediating roles between ADs and RS, chronic and acute, this study embarked on a two-phased Mendelian randomization approach. The initial phase employed univariable MR (UVMR) to explore the causal relationships between ADs and RS. Only exposures with a significant causal link to RS, and where reverse causation was excluded, were subjected to further scrutiny. The subsequent phase was dedicated to identifying and measuring the influence of

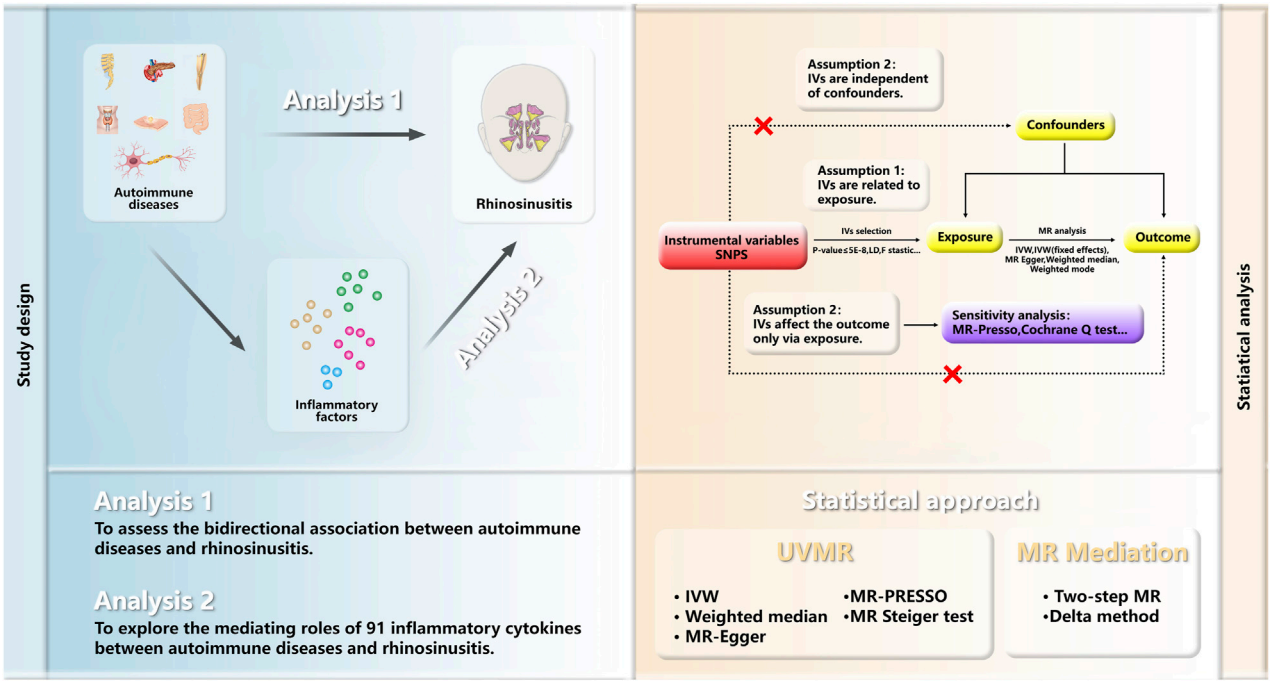

FIGURE 1
Overview of the MR Study Design. The study is structured into two analytical phases. Analysis 1 employed UVMR to investigate the causal links between ADs and RS. Analysis 2 utilized a two-step MR approach to explore the potential mediation effect of inflammatory proteins on the causal association between ADs and RS. MR, Mendelian randomization; UVMR, univariable Mendelian randomization analyses; IVs, Instrumental variables; SNPs, single-nucleotide polymorphisms; LD, linkage disequilibrium; WM, weighted median; IVW, inverse variance weighted; PRESSO pleiotropy residual sum and outlier.

circulating inflammatory proteins as mediators in the causal pathway from ADs to RS. Conducted in accordance with the "Strengthening the Reporting of Observational Studies in Epidemiology Using Mendelian Randomization," this investigation required no additional ethical approvals or informed consent, leveraging publicly accessible GWAS data. The design and analytical procedure are summarized in Figure 1 (All references in the Methods section are listed in Supplementary Table S1).

Data sources

Employing publicly accessible GWAS summary datasets, this MR study assessed designated traits (refer to Table 1). For T1D, genetic tools were sourced from a meta-analysis involving UK and Sardinian participants (7,467 cases versus 10,218 controls). The RA dataset originated from a meta-analysis involving 14,361 cases and 43,923 controls, while genetic instrument variables (IVs) for MS were furnished by a German study (4,888 cases and 10,395 controls). Data for Ankylosing spondylitis (AS) were contributed by the International Genetics of Ankylosing Spondylitis Consortium (IGAS) (9,069 cases and 13,578 controls), and IVs for Psoriasis (PsO) came from research involving 15,967 cases and 28,194 controls. Systemic lupus erythematosus (SLE) data involved 5,201 European descent cases and 9,066 controls. The IEU GWAS database provided information for Sjogren's syndrome (407,746 samples), Celiac disease (11,812 cases and 11,837 controls), Hypothyroidism or myxoedema (405,357 samples), and Crohn's disease (17,897 cases and 33,977 controls). Graves' disease (1,678 cases and 456,942 controls) and Hashimoto thyroiditis (15,654 cases and 379,986 controls) data were derived from a meta-analysis of the European population.

Data regarding rhinosinusitis cases were retrieved from the FinnGen project's R10 dataset, involving 412,181 individuals with European descent, documenting 21,311,942 variants. Summary GWAS results for ARS (with 10,916 cases against 182,945 controls) and CRS (8,524 cases compared to 167,849 controls) were acquired from FinnGen[1]. Information on circulating inflammatory proteins, considered as potential mediators, was taken from a recent European study spanning 11 cohorts, which analyzed 91 plasma proteins across 14,824 samples and performed a

1 https://www.finngen.fi/en

TABLE 1 Data source details for our GWAS study.

	Phenotype	Data source	Cases	Control	Sample size	Ancestry	PIMD
Exposures	Type 1 diabetes	Inshaw JRJ et al.	7,467	10,218	17,685	European	33830302
	Rheumatoid arthritis	Ha E et al.	14,361	43,923	58,284	European	33,310,728
	Multiple sclerosis	Andlauer TF et al.	4,888	10,395	15,283	European	27,386,562
	Ankylosing spondylitis	Cortes A et al.	9,069	13,578	22,647	European	23,749,187
	Psoriasis	Stuart PE et al.	15,967	28,194	44,161	European	34,927,100
	Systemic lupus erythematosus	Bentham J et al.	5,201	9,066	14,267	European	26,502,338
	Sjogren's syndrome (SPA correction)	Mbatchou J et al.	NA	NA	407,746	European	34,017,140
	Celiac disease	Trynka G et al.	11,812	11,837	23,649	European	22,057,235
	Crohn's disease	Liu JZ et al.	17,897	33,977	51,874	European	26,192,919
	Hypothyroidism or myxoedema (SPA correction)	Mbatchou J et al.	NA	NA	405,357	European	34,017,140
	Graves' disease	Sakaue S et al.	1,678	456,942	458,620	European	34,594,039
	Hashimoto thyroiditis	Sakaue S et al.	15,654	379,986	395,640	European	34,594,039
outcome	Acute sinusitis	Finngen	10,916	182,945	193,861	European	NA
	Chronic sinusitis	Finngen	8,524	167,849	176,373	European	NA
Mediator	Circulating inflammatory proteins	Zhao JH et al.	NA	NA	14,824	European	26,192,919

comprehensive genome-wide protein quantitative trait loci (pQTL) study. Detailed data on the inflammatory proteins can be found in Supplementary Table S2.

Selection criteria for IVs

When selecting appropriate genetic IVs from GWAS of 12 ADs using the TwoSampleMR package in R studio (default settings), we primarily chose SNPs with *p*-values less than 5.0E-08 to ensure genome-wide significance. Specifically, for Sjogren's syndrome (SS), due to a lack of SNPs meeting the $p < 5.0E-08$ criterion, we lowered the threshold to $p < 5.0E-06$ to secure a sufficient number of valid IVs. MR-Steiger analysis was utilized to assess the direction and validity of causal relationships, with $p > 0.05$ indicating potential reverse causation, prompting reverse MR analysis. Lower significance threshold to consider $p < 5.0E-06$ was also adopted when analyzing the potential mediating effects of inflammatory proteins. Independence of SNPs was ensured using an $r^2 = 0.001$ and a clumping window of 10,000 kb. The validity of all IVs was evaluated based on the F-statistic ($F = \beta 2/se2$), considering IVs effective when F values exceeded 10.

Statistical analysis

Univariable Mendelian randomization

A UVMR approach was used to examine causal links between ADs and RS, including inverse-variance weighted (IVW), weighted median, and MR-Egger analysis. The IVW method, serving as the main approach, offers precise causal estimates under the condition that all IVs are valid. MR-Egger method, which offers adjustments for estimate heterogeneity and an intercept term for evaluating pleiotropy, enhances the robustness of causal inference. The weighted median approach, effective when a majority of SNPs are credible IVs, allows for an unbiased estimation of causality. Additionally, MR-Steiger analysis was utilized to verify causal direction and mitigate reverse causality concerns among SNPs.

Mediation analysis

After conducting UVMR to assess causal links between ADs and RS, significant causations were selected for mediation effect analysis in a two-step approach. The research delved into the potential mediating roles of 91 inflammatory proteins between ADs and RS. The total causal effect of ADs on RS (β) was first identified via UVMR, followed by an evaluation of the causal influences of ADs on 91 inflammatory proteins (β1) and their subsequent effects on RS (β2). Diseases with evidence of reverse causality were excluded from the mediation analysis. The correlation between inflammatory proteins and the risk for ADs or RS was assessed via two step MR analyses, using the IVW method with $p < 0.05$ indicating statistical significance. For inflammatory proteins related to both ADs and RS, the mediation effect was examined, calculated as the product of β1 and β2 divided by β, and the proportion of mediation effect was estimated using the delta method for 95% confidence intervals (CI).

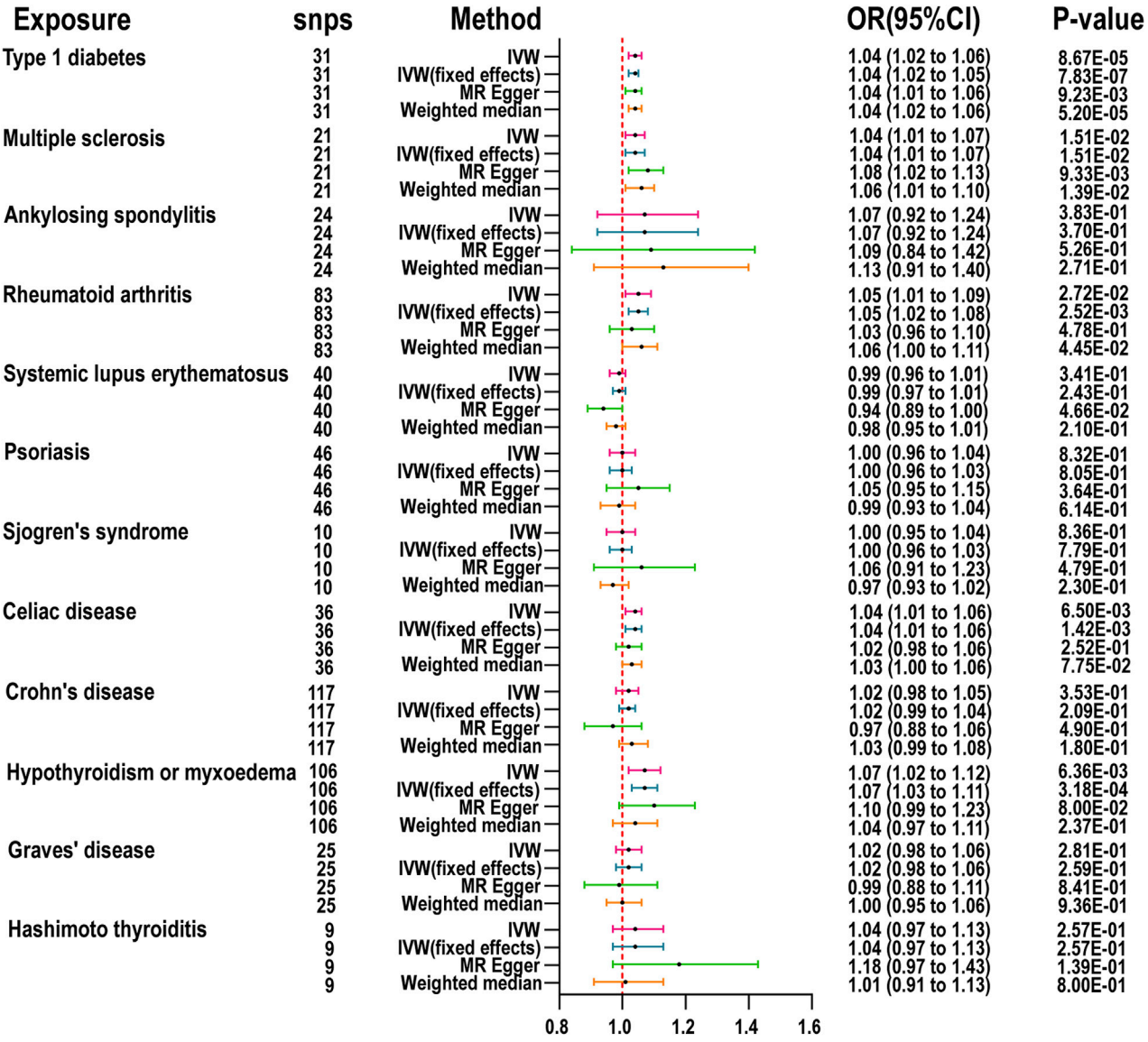

FIGURE 2
MR is used to examine the link between 12 autoimmune diseases and chronic rhinosinusitis. inverse variance weighted (IVW), number of SNPs used in MR (nsnps), odds ratio (OR), confidence interval (CI).

Sensitivity analysis

This research applied MR-Egger and weighted median methods for sensitivity analysis to confirm the UVMR analysis's robustness, additionally utilizing the Cochran Q test to examine IVs heterogeneity. The MR-Egger intercept was deployed to evaluate pleiotropy, depicted in scatter diagrams. High-heterogeneity SNPs were removed through a leave-one-out procedure, with a subsequent reassessment of outcomes. MR-Presso identified and eliminated outlier SNPs, enhancing estimation accuracy. MR-Steiger testing further affirmed causal direction and reliability. The analyses utilized R software (version 4.0.2), specifically through the "TwoSampleMR" (version 0.5.8), "MendelianRandomization" (version 0.9.0), and "MRPRESSO" packages, as detailed in Supplementary Table S1.

Results

Effects of ADs on RS

The MR results for the impact of ADs on CRS are detailed in Figure 2. After rigorous selection and exclusion, the IVs

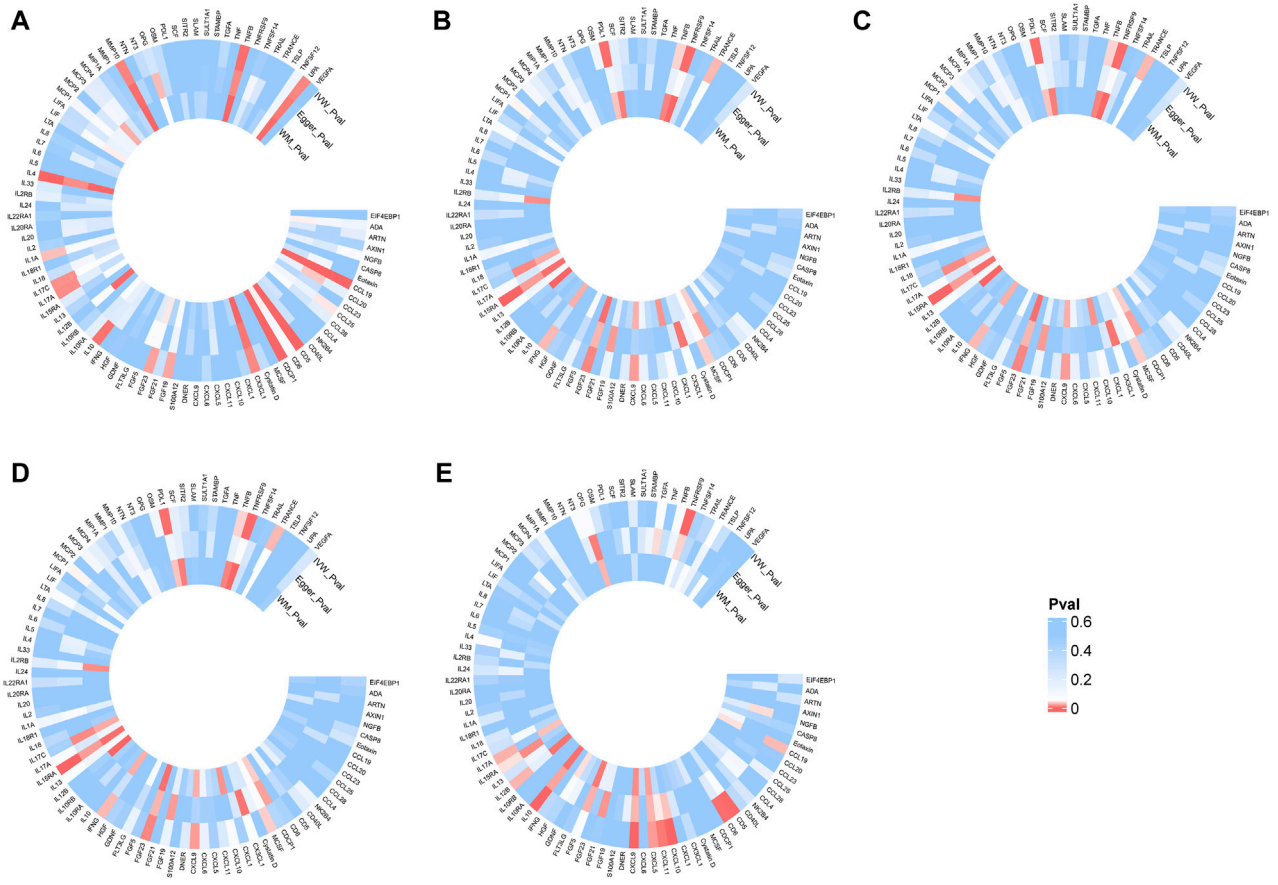

FIGURE 3
Heatmap of the causal relationships between five autoimmune diseases and 91 inflammatory proteins. **(A)**: Effects of multiple sclerosis on inflammatory proteins. **(B)**: Effects of celiac disease on inflammatory proteins. **(C)**: Effects of type 1 diabetes on inflammatory proteins; **(D)**, Effects of rheumatoid arthritis on inflammatory proteins. **(E)**: Effects of hypothyroidism or myxedema on inflammatory proteins. The color gradient from blue to red indicates an increasing significance of the causal relationship.inverse variance weighted (IVW), number of SNPs used in MR (nsnps), odds ratio (OR), confidence interval (CI).

demonstrated F-statistics greater than 10, indicating no weak instrument bias (Supplementary Table S3). If significant heterogeneity was detected (Cochrane Q test p-value <0.05), the random effects model of the IVW method was employed as the primary analytical approach; otherwise, the fixed effects model of IVW was utilized. Two-sample MR (TSMR) revealed that the genetic predisposition to CRS is significantly associated with MS (OR = 1.04, 95% CI: 1.01-1.07, p = 1.51E-02), CeD (OR = 1.04, 95% CI: 1.01-1.06, p = 1.42E-03), RA (OR = 1.05, 95% CI: 1.01-1.09, p = 2.72E-02), T1D (OR = 1.04, 95% CI: 1.02-1.06, p = 8.67E-05), and hypothyroidism or myxedema (OR = 1.07, 95% CI: 1.02-1.12, p = 6.36E-03). The MR-Egger intercept analysis did not demonstrate horizontal pleiotropy, and MR-Steiger testing validated the directionality of our causal inferences (Supplementary Table S4). Scatter plots, funnel plots, and leave-one-out analyses further describe the results (Supplementary Figures S1–12). Similarly, using two-sample MR and the IVW method, only the relationship between CeD and ARS was significant (OR = 1.04, 95% CI: 1.01-1.06, p = 2.07E-03). The MR results for ADs on ARS are presented in Supplementary Figure S13, with sensitivity analyses and MR-Steiger test results in Supplementary Table S4. Scatter plots, funnel plots, and leave-one-out analyses further detail these findings (Supplementary Figures S14–25).

Mediating effect of inflammatory proteins

Following the MR analysis between ADs and RS, we identified five ADs with a close relationship to RS and compared them against 91 circulating inflammatory proteins. Analysis using TSMR and the IVW method revealed that 15, 10, 9, 7, and 12 inflammatory proteins were significantly associated with MS, CeD, RA, T1D, and hypothyroidism (HT), respectively (Figure 3). To investigate which specific inflammatory proteins could serve as potential mediators in the causal relationship

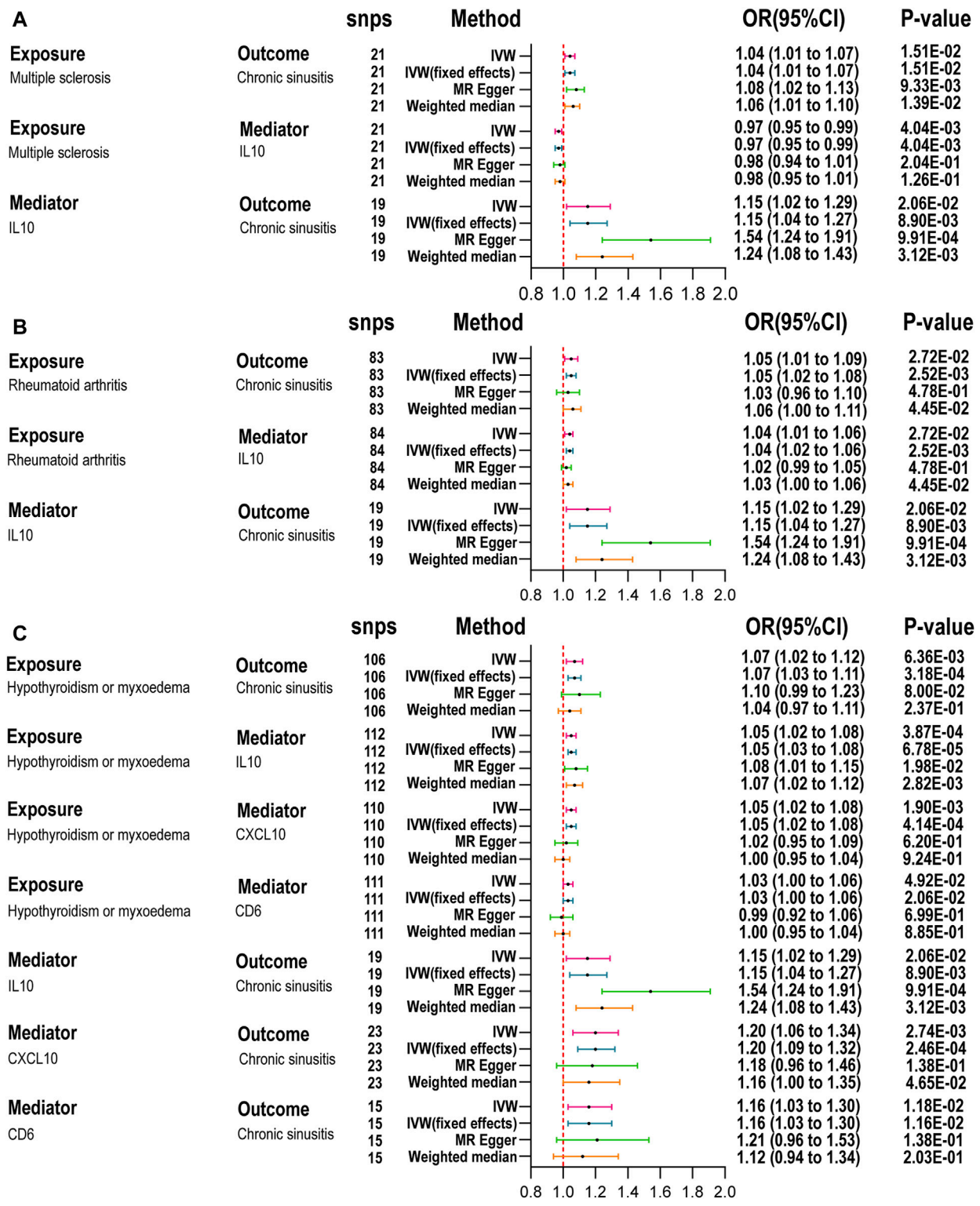

FIGURE 4
Mediation analysis of the effect of autoimmune diseases on chronic rhinosinusitis via inflammatory proteins. **(A)**: Summary MR for the effect of MS on CRS via inflammatory factor. **(B)**: Summary MR for the effect of RA on CRS via inflammatory factor. **(C)**: Summary MR for the effect of HT on CRS via inflammatory factor; inverse variance weighted (IVW), number of SNPs used in MR (nsnps), odds ratio (OR), confidence interval (CI) Table 2. IL-10, nterleukin-10; CXCL10, C-X-C motif chemokine 10; CD6, T-cell surface glycoprotein CD6 isoform.

TABLE 2 Mediation analysis of the effect of ADs on CRS risk via potential mediators.

Exposure	Mediator	The Effect of exposure on outcome β(95%CI)	The Effect of exposure on mediator β1 (95%CI)	The Effect of mediator on outcome β2 (95% CI)	Mediated proportion (%) (95%CI)"
Multiple sclerosis	IL-10	0.0357 (0.0069,0.0647)	−0.0301 (−0.0506,-0.0096)	0.1383 (0.0347, 0.2419)	−11.65% (95% CI: −26.73, 3.44)
Rheumatoid arthritis	IL-10	0.0458 (0.0052,0.0864)	0.0355 (0.0141,0.0569)	0.1383 (0.0347,0.2419)	10.73 (-3.30,24.76)
Hypothyroidism or myxoedema	IL-10	0.0679 (0.0191,0.1167)	0.0515 (0.0230,0.0799 0.1383)	0.1383 (0.0347,0.2419)	10,48 (−1.84, 22.79)
	CXCL10	0.0679 (0.0191, 0.1167)	0.0466 (0.0172, 0.0760)	0.1788 (0.0618, 0.2958)	12.27 (−1.9500, 26.4800)
	CD6	0.0679 (0.0191, 0.1167)	0.0304 (0.0001, 0.0607)	0.1472 (0.0329, 0.2616)	6.59 (−2.99, 16.17)

between ADs and RS, we analyzed those proteins significantly associated with ADs as new exposures in relation to RS. The MR-Steiger test was employed to validate the direction of causality, excluding reverse causal associations from mediation analysis. After SNP filtering and MR analysis, only inflammatory proteins significantly related to both ADs and RS were considered for mediation analysis. The IVW method indicated that interleukin-10 levels (IL-10) were significantly associated with MS (OR = 0.97, 95% CI: 0.95–0.99, p = 4.04E-03), RA (OR = 1.04, 95% CI: 1.01–1.06, p = 1.13E-03), and HT (OR = 1.05, 95% CI: 1.02–1.08, p = 3.87E-04), as detailed in Figure 4. Additionally, T-cell surface glycoprotein CD6 isoform levels (CD6) were significantly related to HT (OR = 1.03, 95% CI: 1.00–1.06, p = 4.92E-02) and CRS (OR = 1.16, 95% CI: 1.03–1.30, p = 1.16E-02), and C-X-C motif chemokine 10 levels (CXCL10) to HT (OR = 1.05, 95% CI: 1.02–1.08, p = 1.90E-03) and CRS (OR = 1.20, 95% CI: 1.06–1.34, p = 2.74E-03), acting as mediators. Weighted median and MR-Egger analyses confirmed the IVW, with heterogeneity and pleiotropy detailed in Supplementary Table S5. Scatter plots, leave-one-out plots, and funnel plots for the relevant instrumental variables provided further evidence (Supplementary Figures S26–S33).

We further quantified the mediating effects of these inflammatory proteins (Table 2), finding IL-10 levels mediated the causal relationship between MS, RA, and HT with CRS. Specifically, the mediation effects were −11.65% (95% CI: −26.73 to 3.44) for MS, 10.73% (95% CI: −3.30–24.76) for RA, and 10.48% (95% CI: −1.84–22.79) for HT. For HT and CRS, the mediation proportions for CXCL10 and CD6 were 12.27% (95% CI: −1.95–26.48) and 6.59% (95% CI: −2.99–16.17), respectively. No inflammatory proteins were identified as mediators between ADs and ARS (Supplementary Figure S34).

Discussion

Employing multiple GWAS datasets, this study leverages Mendelian randomization to shed light on the causal links between ADs and RS. Our genetic analyses identified causal associations between five ADs and CRS: MS, CeD, RA, T1D, and HT. The relationship between CeD and ARS is significant. The role of cytokines has been increasingly recognized in the etiology and progression of ADs and RS, though their exact mechanism within the causal framework between ADs and RS is not fully understood. Given the increased risk of developing RS associated with these ADs, we further employed a large-scale genetic dataset comprising 91 cytokines to explore their role in these relationships.

Evidence suggests a notable link between ADs and CRS, indicating that ADs could serve as risk factors for CRS. A cross-sectional analysis highlighted the disparity in CRS prevalence among various ADs, including multiple sclerosis at 1.4%, ankylosing spondylitis at 6.05%, systemic lupus erythematosus at 3.9%, rheumatoid arthritis at 5.0%, psoriasis at 3.8%, and inflammatory bowel disease at 3.5%. Additionally, this study identified the prevalence of CRS with nasal polyps (CRSwNP) at 9.3% and CRS without nasal polyps (CRSsNP) at 91.7%, analyzing the proportions of CRSwNP and CRSsNP within these ADs [31]. A retrospective study in Asia confirmed the significant correlation between CRS and various ADs, particularly in ankylosing spondylitis, SLE, psoriasis, RA, and Sjögren's syndrome [32]. Our research indicates that, beyond MS and RA, T1D, CeD, and HT are also significantly associated with CRS. It is well recognized that immune dysfunction in diabetes mellitus (DM) patients facilitates infections. A retrospective cohort study of 376 CRS patients found that those with DM were prone to Gram-negative bacterial sinus infections [33]. DM patients are at high risk for mucormycosis, susceptible to severe rhino-orbital-cerebral and pulmonary infections. Hence, prompt diagnosis and management of potential life-threatening fungal infections are crucial for DM patients [22, 23, 34]. Although CeD, as a multisystem autoimmune disease, may cause extraintestinal otolaryngological manifestations [24, 25], current research is insufficient to clarify this relationship, indicating the need for further investigation. Limited studies exist on the relationship between CRS and HT. Existing research has shown that patients

with HT experience prolonged mucociliary clearance times [26, 27], and animal experiments have demonstrated nasal mucosal hypertrophy, cilia loss, and inflammation following thyroidectomy [28]. These findings align with our results, suggesting the importance of close monitoring for respiratory diseases and sinus infections in patients with HT.

The association between inflammatory proteins and ADs involves intricate regulation of the immune system and a disruption in self-tolerance. Studies have indicated that the expression of tumor necrosis factor-alpha (TNF-α), interferon-gamma (IFN-γ), and several interleukins (such as IL-1, IL-6, IL-12, and IL-17) is elevated in autoimmune diseases, driving inflammation and tissue damage [18]. These cytokines activate immune cells, leading to self-tissue destruction and disease progression [19]. Concurrently, regulatory cytokines, such as IL-10, IL-4, and TGF-β, suppress immune responses by promoting immune tolerance and limiting inflammatory reactions, thereby protecting tissues [18]. Rhinosinusitis, involving inflammation of the nasal sinus mucosa, can be triggered by infections, allergies, or environmental factors, with the disease mechanism centrally involving the modulation of immune system responses by inflammatory proteins [29].

When examining inflammatory proteins as mediators between ADs and RS, we identified IL-10 as a mediator in the relationships between MS, RA, and HT with CRS. As a key anti-inflammatory cytokine, IL-10 effectively suppresses the production of pro-inflammatory cytokines, including TNF-α and IL-1, by various immune cells, such as macrophages and dendritic cells. It also enhances the development of regulatory T cells, regulating immune reactions accordingly [30, 35]. In MS patients, serum IL-10 secretion decreases before MS relapse and increases during remission [36], partially aligning with our findings of reduced IL-10 levels in MS patients. In animal models of autoimmune encephalomyelitis (EAE), IL-10 deficiency resulted in more severe disease progression [37, 38]. Studies have shown increased concentrations of IL-10 in the serum and synovial fluid of RA patients [39, 40]. In animal studies, IL-10 reduced symptoms of RA in rats, curbed neutrophil penetration and activation within synovial tissues, and diminished the production of pro-inflammatory cytokines such as TNF, IL-1, and IL-6 [41, 42]. These findings and our results underscore IL-10's undisputed regulatory function as an anti-inflammatory cytokine in arthritis. In patients with autoimmune thyroid disease (AITD), IL-10 mRNA expression was found to increase significantly, decreasing as the autoimmune process subsided [43]. IL-10 mitigates inflammation in early thyroiditis by inhibiting Th1 cytokines like TNF-α and IL-1, while in later stages, Th2 cell activation promotes humoral responses [44, 45]. Changes in IL-10 levels among CRS patients remain contentious [46–49]. Moreover, viral and bacterial infections play a crucial role in exacerbating CRS, where IL-10 demonstrates potential therapeutic value in regulating inflammation and ADs by modulating M2 macrophages and mitigating bacterial inflammatory responses triggered by Toll-like receptor signaling [29, 50, 51]. Therefore, these immunoregulatory functions of IL-10 suggest its potential therapeutic role in preventing inflammatory and autoimmune diseases.

The IL-10 cytokine family, which includes IL-19, IL-20, IL-22, IL-24, and IL-26, is integral to regulating anti-inflammatory, pro-inflammatory, and antiviral responses. Although they were not found to act as mediators in our study, they remain key targets for immunomodulatory therapy [52]. Elevated IL-19 expression has been observed in the mononuclear cells within the synovial fluid of RA sufferers [53]. Antibodies targeting IL-19 have prevented arthritis and osteolysis in animal models by diminishing the secretion of pro-inflammatory cytokines, including TNF-α, IL-1β, IL-6, and RANKL [54]. In psoriasis (PsO), elevated levels of IL-19 have been observed, which induce dysplasia and activation of keratinocytes [55, 56], and also prompts $CD8^+$ T cells to generate Keratinocyte Growth Factor [57]. IL-20 is linked with increased inflammatory activity in RA joints, and its antagonists may offer therapeutic benefits [58]; its overexpression causes psoriasis-like skin conditions [59], while blocking its pathway reduces psoriasis symptoms [60]. IL-22 is enhanced during active MS, affecting T cell function and participating in the disease process [61], and by regulating keratinocyte differentiation, it influences the mechanisms of PsO [62]. IL-24 aggravates inflammation in RA and PsO, yet it plays a protective role in inflammatory bowel disease by sustaining epithelial and mucosal integrity, thus displaying a bidirectional regulatory capacity in inflammation [63]. In summary, through their complex pro-inflammatory and anti-inflammatory functions, members of the IL-10 family play a crucial regulatory role in ADs.

Our investigation also reveals a causal connection between CXCL10 and the relationship between HT and CRS, highlighting CXCL10's critical function in immune cell migration to areas of inflammation or damage, thus contributing to the progression of ADs. Elevated CXCL10 expression in conditions such as RA and AITD is closely associated with disease severity and inflammation levels [64, 65]. By interacting with its receptor, CXCR3, CXCL10 triggers Th1 immune responses, promoting infiltration by inflammatory cells and increasing the production of inflammatory mediators, which aggravates tissue damage [64, 66]. Moreover, airway epithelial cells increase the secretion of inflammatory mediators such as IL-1, IL-6, IL-8, and CXCL10 following infections [67, 68], recruiting inflammatory cells to the inflammation site and intensifying the response [69]. Thus, CXCL10, and its receptor CXCR3, are pivotal in enhancing immune responses and inflammation, presenting new avenues for therapeutic intervention in inflammatory diseases and ADs. Additionally, our study identified CD6 as a significant mediator. Primarily found on T and some B cells, CD6 is integral to the immunoglobulin superfamily [70]. It significantly influences

T cell activation by interacting with its ligand ALCAM (CD166) [71], bolstering TCR signal transmission and encouraging T cell activation and proliferation [70]. CD6's role in immune cell adhesion and migration is vital for inflammation and immune surveillance. With CD6 anomalously expressed in multiple ADs, including MS, SLE, and RA [72], its dysregulated activity could exacerbate inflammatory symptoms and tissue damage. Despite limited direct research on CD6 in HT and CRS, its role in autoimmune processes suggests potential underlying connections that merit further exploration.

Beyond the aforementioned mediatory inflammatory proteins, the significance of other inflammatory proteins in ADs should not be overlooked. For instance, IL-17 levels are elevated in patients with MS, and its inhibitors can mitigate brain damage, underscoring the role of IL-17 in promoting inflammation in the nervous system and exacerbating demyelination and axonal damage [73]. Synovitis in RA is characterized by the continuous influx of immune cells and the production of various pro-inflammatory cytokines such as TNF, IL-1, IL-17, and IL-22, which stimulate bone and cartilage inflammation and damage [74]. In T1D, IL-10, TGF-β, and IL-33 aid in reinstating immune tolerance and shielding β-cells from harm, whereas IL-6, IL-17, IL-21, and TNF accelerate the disease's advancement [75]. Th17 cells, along with their associated inflammatory cytokines IL-17 and IL-23, play a role in the development of autoimmune thyroid (AITD) [44]. IL-15 levels correlate positively with active lesions in patients with celiac disease (CeD), highlighting its importance in CeD [76]. In multiple sclerosis, CC chemokines such as CCL2 and CCL5 promote central nervous system inflammation by regulating immune cell migration [77]. In autoimmune diseases, fibroblast growth factors (FGFs) and their receptors play key roles in inflammatory responses and tissue repair, such as FGF-23, which promotes pro-inflammatory responses of M1 macrophages during infections [78].

Through the application of Mendelian randomization, this research has adeptly navigated confounders and the issue of reverse causation, achieving credible causal effect estimations from observational data [79]. The use of mixed data MR models, incorporating substantial GWAS datasets, has notably increased the efficiency of the analysis compared to smaller-scale, single data models [80]. The study, however, faces significant limitations, notably its sample composed entirely of European individuals, which narrows the generalizability of its findings, and the persistent heterogeneity that could not be fully eradicated, despite thorough attempts with multiple sensitivity analyses, leaving a risk of diversity. Certain Mendelian randomization findings lack empirical backing and thus necessitate careful interpretation, yet they provide a logical foundation for further research. Summarily, the MR analysis elucidated the causal connections between autoimmune diseases and rhinosinusitis, and the mediating influence of inflammatory proteins between ADs and CRS, offering essential biomarkers and potential targets for deciphering disease mechanisms and crafting therapeutic strategies.

Author contributions

YL: Conceptualization, Methodology, Resources, Writing–original draft. SY: Formal Analysis, Data curation, Writing–review and editing. XC: Data curation, Validation, Writing–review and editing. CL: Software, Visualization, Writing–review and editing. QC: Project administration, Supervision, Writing–review and editing.

Data availability

The original contributions presented in the study are included in the article/Supplementary Material, further inquiries can be directed to the corresponding author.

Ethics statement

The data used in this study are derived from publicly available aggregated data, and the ethical approval for each individual study can be found in the original publications, thus no additional ethical approval is required.

Funding

The author(s) declare that no financial support was received for the research, authorship, and/or publication of this article.

Conflict of interest

The authors declare that the research was conducted in the absence of any commercial or financial relationships that could be construed as a potential conflict of interest.

Supplementary material

The Supplementary Material for this article can be found online at: https://www.ebm-journal.org/articles/10.3389/ebm.2024.10196/full#supplementary-material

References

1. Rose NR. Prediction and prevention of autoimmune disease in the 21st century: a review and preview. *Am J Epidemiol* (2016) **183**(5):403–6. doi:10.1093/aje/kwv292

2. Jörg S, Grohme DA, Erzler M, Binsfeld M, Haghikia A, Müller DN, et al. Environmental factors in autoimmune diseases and their role in multiple sclerosis. *Cell Mol Life Sci* (2016) **73**(24):4611–22. doi:10.1007/s00018-016-2311-1

3. Chen B, Sun L, Zhang X. Integration of microbiome and epigenome to decipher the pathogenesis of autoimmune diseases. *J Autoimmun* (2017) **83**:8331–42. doi:10.1016/j.jaut.2017.03.009

4. Ngo ST, Steyn FJ, Mccombe PA. Gender differences in autoimmune disease. *Front Neuroendocrinology* (2014) **35**(3):347–69. doi:10.1016/j.yfrne.2014.04.004

5. Conrad N, Verbeke G, Molenberghs G, Goetschalckx L, Callender T, Cambridge G, et al. Autoimmune diseases and cardiovascular risk: a population-based study on 19 autoimmune diseases and 12 cardiovascular diseases in 22 million individuals in the UK. *The Lancet* (2022) **400**(10354): 733–43. doi:10.1016/S0140-6736(22)01349-6

6. Bleier BS, Paz-Lansberg M. Acute and chronic sinusitis. *Med Clin North America* (2021) **105**(5):859–70. doi:10.1016/j.mcna.2021.05.008

7. Meltzer EO, Hamilos DL, Hadley JA, Lanza DC, Marple BF, Nicklas RA, et al. Rhinosinusitis: establishing definitions for clinical research and patient care. *Otolaryngology–Head Neck Surg* (2004) **131**(6 Suppl. l):S1–62. doi:10.1016/j.otohns.2004.09.067

8. Benninger MS, Ferguson BJ, Hadley JA, Hamilos DL, Jacobs M, Kennedy DW, et al. Adult chronic rhinosinusitis: definitions, diagnosis, epidemiology, and pathophysiology. *Otolaryngology-Head Neck Surg* (2003) **129**(3 Suppl. l):S1–32. doi:10.1016/s0194-5998(03)01397-4

9. Rosenfeld RM, Piccirillo JF, Chandrasekhar SS, Brook I, Ashok Kumar K, Kramper M, et al. Clinical practice guideline (update): adult sinusitis. *Otolaryngology-Head Neck Surg* (2015) **152**(2 Suppl. l):S1–39. doi:10.1177/0194599815572097

10. Fokkens WJ, Lund VJ, Hopkins C, Hellings PW, Kern R, Reitsma S, et al. European position paper on rhinosinusitis and nasal polyps 2020. *Rhinology J* (2020) **0**(Suppl. S29):1–464. doi:10.4193/Rhin20.600

11. Alsowey AM, Abdulmonaem G, Elsammak A, Fouad Y. Diagnostic performance of multidetector computed tomography (mdct) in diagnosis of sinus variations. *Pol J Radiol* (2018) **82**:82713–725. doi:10.12659/PJR.903684

12. Orlandi RR, Kingdom TT, Smith TL, Bleier B, Deconde A, Luong AU, et al. International consensus statement on allergy and rhinology: rhinosinusitis 2021. *Int Forum Allergy Rhinol* (2021) **11**(3):213–739. doi:10.1002/alr.22741

13. Fokkens WJ, Lund VJ, Mullol J, Bachert C, Alobid I, Baroody F, et al. Epos 2012: european position paper on rhinosinusitis and nasal polyps 2012. A summary for otorhinolaryngologists. *Rhinology J* (2012) **50**(1):1–12. doi:10.4193/Rhino12.000

14. Riechelmann H, Deutschle T, Rozsasi A, Keck T, Polzehl D, Bürner H. Nasal biomarker profiles in acute and chronic rhinosinusitis. *Clin Exp Allergy* (2005) **35**(9):1186–91. doi:10.1111/j.1365-2222.2005.02316.x

15. Stevens WW, Peters AT, Tan BK, Klingler AI, Poposki JA, Hulse KE, et al. Associations between inflammatory endotypes and clinical presentations in chronic rhinosinusitis. *J Allergy Clin Immunol Pract* (2019) **7**(8):2812–20.e3. doi:10.1016/j.jaip.2019.05.009

16. Samitas K, Carter A, Kariyawasam HH, Xanthou G. Upper and lower airway remodelling mechanisms in asthma, allergic rhinitis and chronic rhinosinusitis: the one airway concept revisited. *Allergy* (2018) **73**(5):993–1002. doi:10.1111/all.13373

17. Gong X, Han Z, Fan H, Wu Y, He Y, Fu Y, et al. The interplay of inflammation and remodeling in the pathogenesis of chronic rhinosinusitis: current understanding and future directions. *Front Immunol* (2023) **14**:141238673. doi:10.3389/fimmu.2023.1238673

18. O'Shea JJ, Ma A, Lipsky P. Cytokines and autoimmunity. *Nat Rev Immunol* (2002) **2**(1):37–45. doi:10.1038/nri702

19. Yadav D, Sarvetnick N. Cytokines and autoimmunity: redundancy defines their complex nature. *Curr Opin Immunol* (2003) **15**(6):697–703. doi:10.1016/j.coi.2003.09.006

20. Kwah JH, Somani SN, Stevens WW, Kern RC, Smith SS, Welch KC, et al. Clinical factors associated with acute exacerbations of chronic rhinosinusitis. *J Allergy Clin Immunol* (2020) **145**(6):1598–605. doi:10.1016/j.jaci.2020.01.023

21. Min J, Tan BK. Risk factors for chronic rhinosinusitis. *Curr Opin Allergy Clin Immunol* (2015) **15**(1):1–13. doi:10.1097/ACI.0000000000000128

22. Khoshbayan A, Didehdar M, Chegini Z, Taheri F, Shariati A. A closer look at pathogenesis of cerebral mucormycosis in diabetic condition: a mini review. *J Basic Microbiol* (2021) **61**(3):212–8. doi:10.1002/jobm.202000692

23. Kashyap S, Bernstein J, Ghanchi H, Bowen I, Cortez V. Diagnosis of rhinocerebral mucormycosis by treatment of cavernous right internal carotid artery occlusion with mechanical thrombectomy: special case presentation and literature review. *Front Neurol* (2019) **10**:10264. doi:10.3389/fneur.2019.00264

24. Medina-Banegas A, Pastor-Quirante FA, Osete-Albaladejo J, López-Meseguer E, López-Andreu F. Nasal septal perforation in a patient with subclinical celiac disease: a possible new association. *Eur Arch Otorhinolaryngol* (2005) **262**(11): 928–31. doi:10.1007/s00405-004-0865-2

25. Mohn A, di Ricco L, Magnelli A, Chiarelli F. Celiac disease--associated vertigo and nystagmus. *J Pediatr Gastroenterol Nutr* (2002) **34**(3):317–8. doi:10.1097/00005176-200203000-00019

26. Kulekci Ozturk S, Sakci E, Kavvasoglu C. Rhinitis in patients with acquired hypothyroidism. *Eur Arch Otorhinolaryngol* (2021) **278**(1):87–92. doi:10.1007/s00405-020-06254-7

27. Uysal IO, Gökakın AK, Karakuş CF, Deveci K, Hasbek Z, Sancakdar E. Evaluation of nasal mucociliary activity in iatrogenic hypothyroidism. *Eur Arch Otorhinolaryngol* (2013) **270**(12):3075–8. doi:10.1007/s00405-013-2439-7

28. Proud GO, Lange RD. The effect of thyroidectomy on the nasal mucosa of experimental animals. *The Laryngoscope* (1957) **67**(3):201–7. doi:10.1288/00005537-195703000-00003

29. Tan KS, Yan Y, Ong HH, Chow VTK, Shi L, Wang D. Impact of respiratory virus infections in exacerbation of acute and chronic rhinosinusitis. *Curr Allergy Asthma Rep* (2017) **17**(4):24. doi:10.1007/s11882-017-0693-2

30. Saraiva M, Vieira P, O'Garra A. Biology and therapeutic potential of interleukin-10. *J Exp Med* (2020) **217**(1):e20190418. doi:10.1084/jem.20190418

31. Chandra RK, Lin D, Tan B, Tudor RS, Conley DB, Peters AT, et al. Chronic rhinosinusitis in the setting of other chronic inflammatory diseases. *Am J Otolaryngol* (2011) **32**(5):388–91. doi:10.1016/j.amjoto.2010.07.013

32. Shih L, Hsieh H, Tsay GJ, Lee IT, Tsou Y, Lin C, et al. Chronic rhinosinusitis and premorbid autoimmune diseases: a population-based case-control study. *Sci Rep* (2020) **10**(1):18635. doi:10.1038/s41598-020-75815-x

33. Zhang Z, Adappa ND, Lautenbach E, Chiu AG, Doghramji L, Howland TJ, et al. The effect of diabetes mellitus on chronic rhinosinusitis and sinus surgery outcome. *Int Forum Allergy Rhinol* (2014) **4**(4):315–20. doi:10.1002/alr.21269

34. di Coste A, Costantino F, Tarani L, Savastano V, Di Biasi C, Schiavi L, et al. Rhinocerebral zygomycosis with pansinusitis in a 14-year-old girl with type 1 diabetes: a case report and review of the literature. *Ital J Pediatr* (2013) **39**: 3977. doi:10.1186/1824-7288-39-77

35. Saraiva M, O'Garra A. The regulation of il-10 production by immune cells. *Nat Rev Immunol* (2010) **10**(3):170–81. doi:10.1038/nri2711

36. Ozenci V, Kouwenhoven M, Huang YM, Xiao B, Kivisäkk P, Fredrikson S, et al. Multiple sclerosis: levels of interleukin-10-secreting blood mononuclear cells are low in untreated patients but augmented during interferon-β-1b treatment. *Scand J Immunol* (1999) **49**(5):554–61. doi:10.1046/j.1365-3083.1999.00546.x

37. Bettelli E, Prabhu Das M, Howard ED, Weiner HL, Sobel RA, Kuchroo VK. Il-10 is critical in the regulation of autoimmune encephalomyelitis as demonstrated by studies of il-10- and il-4-deficient and transgenic mice. *J Immunol* (1998) **161**(7): 3299–306. doi:10.4049/jimmunol.161.7.3299

38. Psachoulia K, Chamberlain KA, Heo D, Davis SE, Paskus JD, Nanescu SE, et al. Il4i1 augments cns remyelination and axonal protection by modulating t cell driven inflammation. *Brain* (2016) **139**(Pt 12):3121–36. doi:10.1093/brain/aww254

39. Cush JJ, Splawski JB, Thomas R, Mcfarlin JE, Schulze-Koops H, Davis LS, et al. Elevated interleukin-10 levels in patients with rheumatoid arthritis. *Arthritis Rheum* (1995) **38**(1):96–104. doi:10.1002/art.1780380115

40. Bucht A, Larsson P, Weisbrot L, Thorne C, Pisa P, Smedegård G, et al. Expression of interferon-gamma (IFN-δ), IL-10, IL-12 and transforming growth factor-beta (TGF-β) mRNA in synovial fluid cells from patients in the early and late phases of rheumatoid arthritis (RA). *Clin Exp Immunol* (2007) **103**(3):357–67. doi:10.1111/j.1365-2249.1996.tb08288.x

41. Bober LA, Rojas-Triana A, Jackson JV, Leach MW, Manfra D, Narula SK, et al. Regulatory effects of interleukin-4 and interleukin-10 on human neutrophil function *ex vivo* and on neutrophil influx in a rat model of arthritis. *Arthritis Rheum* (2000) **43**(12):2660–7. doi:10.1002/1529-0131(200012)43:12<2660::AID-ANR5>3.0.CO;2-4

42. Tian S, Yan Y, Qi X, Li X, Li Z. Treatment of type ii collagen-induced rat rheumatoid arthritis model by interleukin 10 (il10)-mesenchymal stem cells (bmscs). *Med Sci Monitor* (2019) **25**:252923–2934. doi:10.12659/MSM.911184

43. de la Vega JR, Vilaplana JC, Biro A, Hammond L, Bottazzo GF, Mirakian R. Il-10 expression in thyroid glands: protective or harmful role against thyroid

autoimmunity? *Clin Exp Immunol* (2001) **113**(1):126–35. doi:10.1046/j.1365-2249.1998.00628.x

44. Mikoś H, Mikoś M, Obara-Moszyńska M, Niedziela M. Rola układu immunologicznego oraz udział cytokin w patomechanizmie autoimmunologicznej choroby tarczycy (AITD). *Endokrynologia Polska* (2014) **65**(2):150–5. doi:10.5603/EP.2014.0021

45. Fallahi P, Ferrari SM, Ragusa F, Ruffilli I, Elia G, Paparo SR, et al. Th1 chemokines in autoimmune endocrine disorders. *J Clin Endocrinol Metab* (2020) **105**(4):1046–60. doi:10.1210/clinem/dgz289

46. Tsybikov NN, Egorova EV, Kuznik BI, Fefelova EV, Magen E. Anticytokine autoantibodies in chronic rhinosinusitis. *Allergy Asthma Proc* (2015) **36**(6):473–80. doi:10.2500/aap.2015.36.3880

47. Li L, Feng J, Zhang D, Yong J, Wang Y, Yao J, et al. Differential expression of mir-4492 and il-10 is involved in chronic rhinosinusitis with nasal polyps. *Exp Ther Med* (2019) **18**(5):3968–76. doi:10.3892/etm.2019.8022

48. Xuan L, Zhang N, Wang X, Zhang L, Bachert C. Il-10 family cytokines in chronic rhinosinusitis with nasal polyps: from experiments to the clinic. *Front Immunol* (2022) **13**:13947983. doi:10.3389/fimmu.2022.947983

49. Han X, Wu D, Sun Z, Sun H, Lv Q, Zhang L, et al. Type 1/type 2 inflammatory cytokines correlate with olfactory function in patients with chronic rhinosinusitis. *Am J Otolaryngol* (2020) **41**(5):102587. doi:10.1016/j.amjoto.2020.102587

50. Mantovani A, Sica A, Sozzani S, Allavena P, Vecchi A, Locati M. The chemokine system in diverse forms of macrophage activation and polarization. *Trends Immunol* (2004) **25**(12):677–86. doi:10.1016/j.it.2004.09.015

51. Mahdavinia M, Keshavarzian A, Tobin MC, Landay AL, Schleimer RP. A comprehensive review of the nasal microbiome in chronic rhinosinusitis (crs). *Clin Exp Allergy* (2016) **46**(1):21–41. doi:10.1111/cea.12666

52. Ouyang W, Rutz S, Crellin NK, Valdez PA, Hymowitz SG. Regulation and functions of the il-10 family of cytokines in inflammation and disease. *Annu Rev Immunol* (2011) **29**:2971–109. doi:10.1146/annurev-immunol-031210-101312

53. Alanärä T, Karstila K, Moilanen T, Silvennoinen O, Isomäki P. Expression of il-10 family cytokines in rheumatoid arthritis: elevated levels of il-19 in the joints. *Scand J Rheumatol* (2010) **39**(2):118–26. doi:10.3109/03009740903170823

54. Hsu Y, Hsieh P, Chang M. Interleukin-19 blockade attenuates collagen-induced arthritis in rats. *Rheumatology (Oxford, England)* (2012) **51**(3):434–42. doi:10.1093/rheumatology/ker127

55. Steiniche T, Kragballe K, Rømer J, Hasselager E, Nørby PL, Thorn Clausen J. Epidermal overexpression of interleukin-19 and -20 mrna in psoriatic skin disappears after short-term treatment with cyclosporine a or calcipotriol. *J Invest Dermatol* (2003) **121**(6):1306–11. doi:10.1111/j.1523-1747.2003.12626.x

56. Otkjaer K, Kragballe K, Funding AT, Clausen JT, Noerby PL, Steiniche T, et al. The dynamics of gene expression of interleukin-19 and interleukin-20 and their receptors in psoriasis. *Br J Dermatol* (2005) **153**(5):911–8. doi:10.1111/j.1365-2133.2005.06800.x

57. Li H, Lin Y, Chen P, Hsiao C, Lee JY, Chen W, et al. Interleukin-19 upregulates keratinocyte growth factor and is associated with psoriasis. *Br J Dermatol* (2005) **153**(3):591–5. doi:10.1111/j.1365-2133.2005.06665.x

58. Wang H, Hsu Y, Chang M. Il-20 bone diseases involvement and therapeutic target potential. *J Biomed Sci* (2018) **25**(1):38. doi:10.1186/s12929-018-0439-z

59. Blumberg H, Conklin D, Xu WF, Grossmann A, Brender T, Carollo S, et al. Interleukin 20: discovery, receptor identification, and role in epidermal function. *Cell* (2001) **104**(1):9–19. doi:10.1016/s0092-8674(01)00187-8

60. Stenderup K, Rosada C, Worsaae A, Dagnaes-Hansen F, Steiniche T, Hasselager E, et al. Interleukin-20 plays a critical role in maintenance and development of psoriasis in the human xenograft transplantation model. *Br J Dermatol* (2009) **160**(2):284–96. doi:10.1111/j.1365-2133.2008.08890.x

61. Marcus R. What is multiple sclerosis? *Jama* (2022) **328**(20):2078. doi:10.1001/jama.2022.14236

62. Hao J. Targeting interleukin-22 in psoriasis. *Inflammation* (2014) **37**(1):94–9. doi:10.1007/s10753-013-9715-y

63. Zhong Y, Zhang X, Chong W. Interleukin-24 immunobiology and its roles in inflammatory diseases. *Int J Mol Sci* (2022) **23**(2):627. doi:10.3390/ijms23020627

64. Ruffilli I, Ferrari SM, Colaci M, Ferri C, Fallahi P, Antonelli A. Ip-10 in autoimmune thyroiditis. *Horm Metab Res* (2014) **46**(9):597–602. doi:10.1055/s-0034-1382053

65. Kuan WP, Tam L, Wong C, Ko FWS, Li T, Zhu T, et al. Cxcl 9 and cxcl 10 as sensitive markers of disease activity in patients with rheumatoid arthritis. *J Rheumatol* (2010) **37**(2):257–64. doi:10.3899/jrheum.090769

66. Godessart N, Kunkel SL. Chemokines in autoimmune disease. *Curr Opin Immunol* (2001) **13**(6):670–5. doi:10.1016/s0952-7915(01)00277-1

67. Spurrell JCL, Wiehler S, Zaheer RS, Sanders SP, Proud D. Human airway epithelial cells produce ip-10 (cxcl10) *in vitro* and *in vivo* upon rhinovirus infection. *Am J Physiology-Lung Cell Mol Physiol* (2005) **289**(1):L85–95. doi:10.1152/ajplung.00397.2004

68. Corne JM, Holgate ST. Mechanisms of virus induced exacerbations of asthma. *Thorax* (1997) **52**(4):380–9. doi:10.1136/thx.52.4.380

69. Förster-Ruhrmann U, Szczepek AJ, Pierchalla G, Fluhr JW, Artuc M, Zuberbier T, et al. Chemokine expression-based endotype clustering of chronic rhinosinusitis. *J Personalized Med* (2022) **12**(4):646. doi:10.3390/jpm12040646

70. Hassan NJ, Simmonds SJ, Clarkson NG, Hanrahan S, Puklavec MJ, Bomb M, et al. Cd6 regulates t-cell responses through activation-dependent recruitment of the positive regulator slp-76. *Mol Cell Biol* (2006) **26**(17):6727–38. doi:10.1128/MCB.00688-06

71. Gonçalves CM, Henriques SN, Santos RF, Carmo AM. Cd6, a rheostat-type signalosome that tunes t cell activation. *Front Immunol* (2018) **9**:92994. doi:10.3389/fimmu.2018.02994

72. Pinto M, Carmo AM. Cd6 as a therapeutic target in autoimmune diseases: successes and challenges. *BioDrugs* (2013) **27**(3):191–202. doi:10.1007/s40259-013-0027-4

73. Havrdová E, Belova A, Goloborodko A, Tisserant A, Wright A, Wallstroem E, et al. Activity of secukinumab, an anti-il-17a antibody, on brain lesions in rrms: results from a randomized, proof-of-concept study. *J Neurol* (2016) **263**(7):1287–95. doi:10.1007/s00415-016-8128-x

74. Mcinnes IB, Schett G. Cytokines in the pathogenesis of rheumatoid arthritis. *Nat Rev Immunol* (2007) **7**(6):429–42. doi:10.1038/nri2094

75. Nepom GT, Ehlers M, Mandrup-Poulsen T. Anti-cytokine therapies in t1d: concepts and strategies. *Clin Immunol (Orlando, Fla.)* (2013) **149**(3):279–85. doi:10.1016/j.clim.2013.02.003

76. Setty M, Discepolo V, Abadie V, Kamhawi S, Mayassi T, Kent A, et al. Distinct and synergistic contributions of epithelial stress and adaptive immunity to functions of intraepithelial killer cells and active celiac disease. *Gastroenterology* (2015) **149**(3):681–91.e10. doi:10.1053/j.gastro.2015.05.013

77. Cui L, Chu S, Chen N. The role of chemokines and chemokine receptors in multiple sclerosis. *Int Immunopharmacology* (2020) **83**:83106314. doi:10.1016/j.intimp.2020.106314

78. Han X, Li L, Yang J, King G, Xiao Z, Quarles LD. Counter-regulatory paracrine actions of fgf-23 and 1,25(oh)2 d in macrophages. *FEBS Lett* (2016) **590**(1):53–67. doi:10.1002/1873-3468.12040

79. Emdin CA, Khera AV, Kathiresan S. Mendelian randomization. *Jama* (2017) **318**(19):1925–6. doi:10.1001/jama.2017.17219

80. Ebrahim S, Davey Smith G. Mendelian randomization: can genetic epidemiology help redress the failures of observational epidemiology? *Hum Genet* (2008) **123**(1):15–33. doi:10.1007/s00439-007-0448-6

EBM Experimental Biology and Medicine

TYPE Original Research
PUBLISHED 25 July 2024
DOI 10.3389/ebm.2024.10123

OPEN ACCESS

*CORRESPONDENCE
Santosh Kumar,
ksantosh@uthsc.edu

RECEIVED 20 June 2023
ACCEPTED 01 July 2024
PUBLISHED 25 July 2024

CITATION
Mirzahosseini G, Sinha N, Zhou L, Godse S, Kodidela S, Singh UP, Ishrat T and Kumar S (2024), LM11A-31, a modulator of p75 neurotrophin receptor, suppresses HIV-1 replication and inflammatory response in macrophages.
Exp. Biol. Med. 249:10123.
doi: 10.3389/ebm.2024.10123

LM11A-31, a modulator of p75 neurotrophin receptor, suppresses HIV-1 replication and inflammatory response in macrophages

Golnoush Mirzahosseini[1,2], Namita Sinha[1], Lina Zhou[1], Sandip Godse[1], Sunitha Kodidela[1], Udai P. Singh[1], Tauheed Ishrat[1,2] and Santosh Kumar[1]*

[1]Department of Pharmaceutical Sciences, College of Pharmacy, The University of Tennessee Health Science Center, Memphis, TN, United States, [2]Department of Anatomy and Neurobiology, College of Medicine, The University of Tennessee Health Science Center, Memphis, TN, United States

Abstract

Antiretroviral drugs have made significant progress in treating HIV-1 and improving the quality of HIV-1-infected individuals. However, due to their limited permeability into the brain HIV-1 replication persists in brain reservoirs such as perivascular macrophages and microglia, which cause HIV-1-associated neurocognitive disorders. Therefore, it is highly desirable to find a novel therapy that can cross the blood-brain barrier (BBB) and target HIV-1 pathogenesis in brain reservoirs. A recently developed 2-amino-3-methylpentanoic acid [2-morpholin-4-yl-ethyl]-amide (LM11A-31), which is a p75 neutrotrophin receptor ($p75^{NTR}$) modulator, can cross the BBB. In this study, we examined whether LM11A-31 treatment can suppress HIV-1 replication, oxidative stress, cytotoxicity, and inflammatory response in macrophages. Our results showed that LM11A-31 (100 nM) alone and/or in combination with positive control darunavir (5.5 μM) significantly suppresses viral replication and reduces cytotoxicity. Moreover, the HIV-1 suppression by LM11A-31 was comparable to the HIV-1 suppression by darunavir. Although $p75^{NTR}$ was upregulated in HIV-1-infected macrophages compared to uninfected macrophages, LM11A-31 did not significantly reduce the $p75^{NTR}$ expression in macrophages. Furthermore, our study illustrated that LM11A-31 alone and/or in combination with darunavir significantly suppress pro-inflammatory cytokines including IL-1β, IL-8, IL-18, and TNF-α and chemokines MCP-1 in HIV-induced macrophages. The suppression of these cytokines and chemokines by LM11A-31 was comparable to darunavir. In contrast, LM11A-31 did not significantly alter oxidative stress, expression of antioxidant enzymes, or autophagy marker proteins in U1 macrophages. The

results suggest that LM11A-31, which can cross the BBB, has therapeutic potential in suppressing HIV-1 and inflammatory response in brain reservoirs, especially in macrophages.

KEYWORDS

LM11A-31, HIV-1, inflammation, macrophages, oxidative stress, cytotoxicity

Impact statement

The current antiretroviral drugs do not adequately cross the blood-brain-barrier (BBB) and suppress neuroHIV leading to persistent HIV-1 replication in brain reservoirs and subsequently leading to HIV-1-associated neurocognitive disorders (HAND). The efficacy of LM11A-31, a $p75^{NTR}$ modulator, has been extensively reported in several neurological diseases including Alzheimer's disease (AD), ischemic stroke, and traumatic brain injury. Our study has shown that LM11A-31 can suppress HIV-1 replication in macrophages, and microglia inflammatory functions, which are the major viral reservoirs in the brain. Owing to its ability to cross the BBB, LM11A-31 can potentially be developed as a novel therapy to suppress HIV-1 neuropathogenesis and HAND. Furthermore, since LM11A-31 can potentially treat AD, which is a common comorbidity in HIV-1 aging populations, it can have a dual benefit in HIV-1-AD comorbid conditions.

Introduction

Human Immunodeficiency Virus- 1 (HIV-1) primarily infects T-cells, peripheral macrophages, and multiple cells in the central nervous system (CNS) including perivascular macrophages, microglia, and astrocytes [1–4]. Combination antiretroviral therapy (ART) has improved the quality of HIV-1-infected individuals by suppressing the virus in the periphery at a controlled level [5]. However, ART drugs poorly cross the blood-brain barrier (BBB) and are unable to suppress the virus in the brain reservoirs, especially perivascular macrophages and microglia [2, 6].

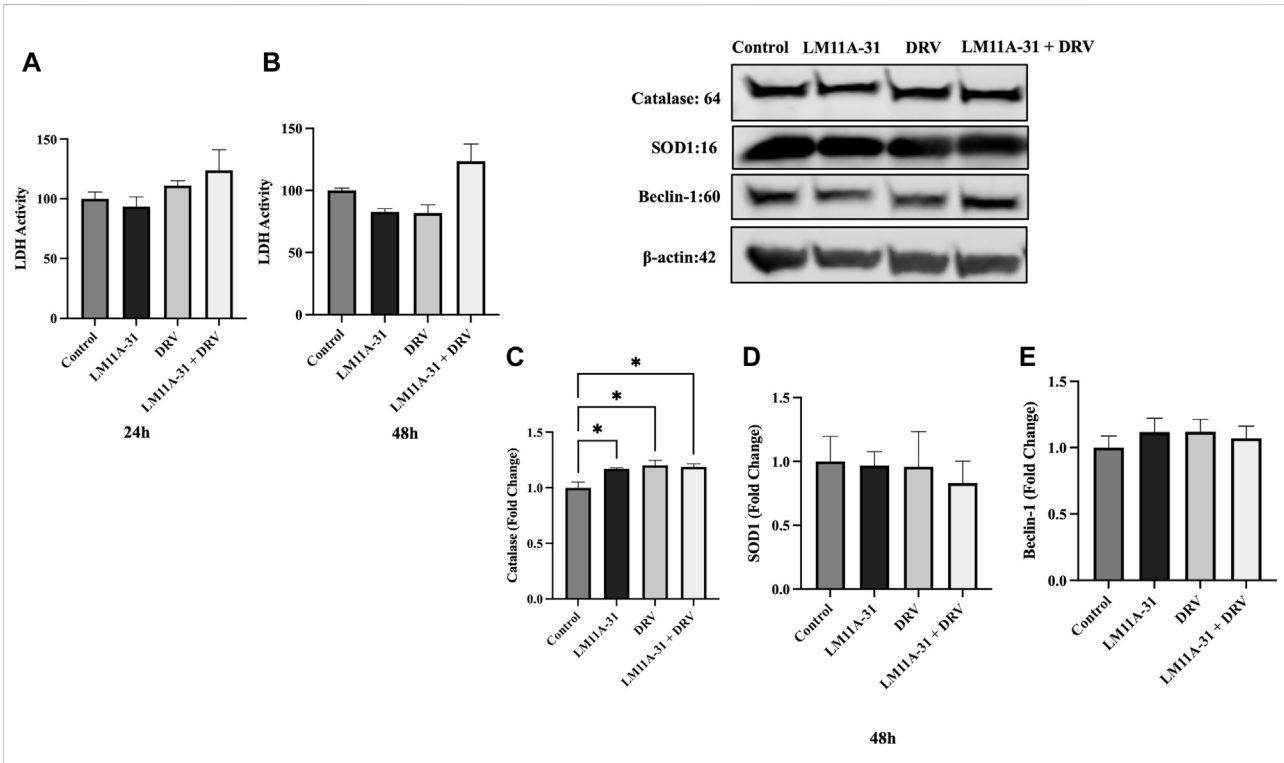

FIGURE 1
The effect of LM11A-31 on cytotoxicity, antioxidant enzymes, and autophagy marker in U937 macrophages. U937 macrophages were differentiated and then treated with DMSO, LM11A-31 (100 nM), DRV (5.5 μM), and LM11A-31 + DRV for 48 h. The cytotoxicity was measured using CyQUANT™ LDH Cytotoxicity Assay Kit. **(A)** LDH measurement at 24 h. **(B)** LDH measurement at 48 h. **(C)** Quantification of protein level of catalase at 48 h. **(D)** Quantification of protein level of SOD1 at 48 h. **(E)** Quantification of protein level of Beclin-1 at 48 h. Values are expressed as mean ± SEM (n = 3), $*p < 0.05$.

Due to the inability of ART drugs to suppress HIV-1 in the CNS viral reservoirs, HIV-1-associated neurocognitive disorder (HAND) is prevalent among HIV-1-infected individuals [7]. Additionally, many ART drugs have been shown to be neurotoxic [7]. Therefore, it is highly desirable to find safe and effective therapeutic agents, which can effectively cross the BBB and suppress HIV-1 in brain reservoirs.

A recently developed water-soluble compound, 2-amino-3-methylpentanoic acid [2-morpholin-4-yl-ethyl]-amide (LM11A-31), is a small molecule, non-peptide $p75^{NTR}$ ligand, which penetrates the BBB [8]. The compound inhibits the binding of precursor nerve growth factor (proNGF) to the p75 neurotrophin receptor ($p75^{NTR}$). Recent attention has been paid to $p75^{NTR}$ as this receptor is upregulated in several CNS diseases [9]. LM11A-31 is orally bioavailable and no systemic toxicity has been reported [10]. Moreover, LM11A-31 is in phase 2 clinical trials for mild-to-moderate Alzheimer's disease (AD)[1] [11]. LM11A-31 activates survival signaling and suppresses degenerative signaling [11]. Recently, the effects of LM11A-31 have been reported in a variety of diseases including but not limited to stroke, AD, Huntington's disease, and traumatic brain injury [8, 12–14]. Additionally, It has been reported that daily treatment of LM11A-31 for 4 months in HIV-1 gp120 transgenic mice reduces microglial activation and dendritic varicosities, and activates microtubule-associated protein-2 (MAP-2) in the hippocampus [15]. LM11A-31 also decreases cell apoptosis and improves mitochondrial movement in cultured rat neurons following exposure to HIV-1 gp120 or conditioned medium from human monocyte-derived macrophages (MDM), which was treated with gp120 [16]. Treatment of 10 nM LM11A-31 to macrophages and microglia upon exposure to HIV-1 gp120 has been shown to inhibit the release of neurotoxic factors from MDM and microglia. Furthermore, the treatment of 10 nM LM11A-31 reduced or eliminated the neuronal pathology as well as the Feline Immunodeficiency Virus (FIV) effect on astrocytes and microglia [17]. However, FIV replication remained unaffected by LM11A-31. These reports illustrate the promising therapeutic effect of LM11A-31 on HIV-1 pathogenesis. Therefore, we hypothesize that LM11A-31 suppresses HIV-1 pathogenesis including inflammatory functions in HIV-1 infected macrophages.

Materials and methods

Cell culture and drug treatment

Human monocyte-derived macrophages (MDM) were prepared as described previously [18]. In brief, peripheral blood mononuclear cells (PBMCs) were obtained from buffy coats (Interstate Blood Bank, Memphis, TN) after density-gradient separation using the established protocol. PBMCs were allowed to adhere to the plastic for 4 h. Then, they were removed and cultured in media supplemented with M-CSF (25 μM) for 7–10 days to promote their differentiation into macrophages. MDM was collected and treated with polybrene for 30 min followed by infection with HIV-1-Ada strain (20 ng/10^6). The HIV-1 Ada-M monocytetropic virus was obtained from the NIH AIDS Reagent Program (Germantown, MD). Infected cells were seeded in 6-well plates and fresh media was added every third day to maintain cell viability. To determine the p24 antigen levels in the culture supernatant, the collected samples were subjected to p24 ELISA analysis according to the protocol. Once the viral infection is confirmed (7–10 days), HIV-1-infected MDM was treated with either control (DMSO) or LM11A-31 (100 nM). We used DMSO as a control because darunavir (DRV), which was used in subsequent treatments, is dissolved in DMSO.

The HIV-1-uninfected U937 monocytic cell line and HIV-1-infected U1 monocytic cell line were obtained from ATCC (Manassas, VA). The cells were cultured in Roswell Park Memorial Institute (RPMI) 1640 media (Sigma Aldrich, St. Louis, MO), containing 10% FBS (Atlanta biologicals, Atlanta, GA) and 1% L-glutamine (Corning Inc, Tewksbury, MA). To assess the chronic effects of LM11A-31, darunavir (DRV), and combination therapy on HIV-1 replication, we used a previously described method [19]. Briefly, U937 and U1 cells were seeded at 0.4×10^6 cells/mL per well containing 100 nM phorbol-12-myristate-13-acetate (PMA) to differentiate into macrophages and induce HIV-1 replication. At 72h, cells were washed using PBS, and media was substituted with fresh RPMI overnight. The next day, cells were treated once daily using DMSO, LM11A-31 (100 nM), DRV (5.5 μM), and LM11A-31 + DRV (100 nM + 5.5 μM) for 72 h. The supernatant was collected daily to measure the concentration of HIV-1 p24 antigen in U1 cells. Lastly, cells were collected at 24 h following the last dose.

Measurement of ROS by flow cytometry

The reactive oxygen species (ROS) was measured using 5-(and-6)-chloromethyl-2′,7′-dichlorodihydrofluorescein diacetate, acetyl ester (CM-H2DCFDA), which was obtained from Thermo Fisher Scientific (Waltham, MA). As previously mentioned [20], the level of ROS in DMSO, LM11A-31, DRV, and LM11A-31 + DRV in U1 cells was assessed. In brief, U1 cells were collected and washed using phosphate buffer saline (PBS) after treatment with DMSO or drugs. Then, cells were incubated using the CM-H2DCFDA dye (2–5 μM) for 30 min at 37°C. After incubation, the cells were washed using PBS and the mean fluorescent intensity (MFI) of samples was analyzed using an Agilent Novocyte flow cytometer (Agilent, Santa Clara, CA). The MFI obtained for DMSO-treated control cells served as 100%.

1 https://clinicaltrials.gov/ct2/show/NCT03069014

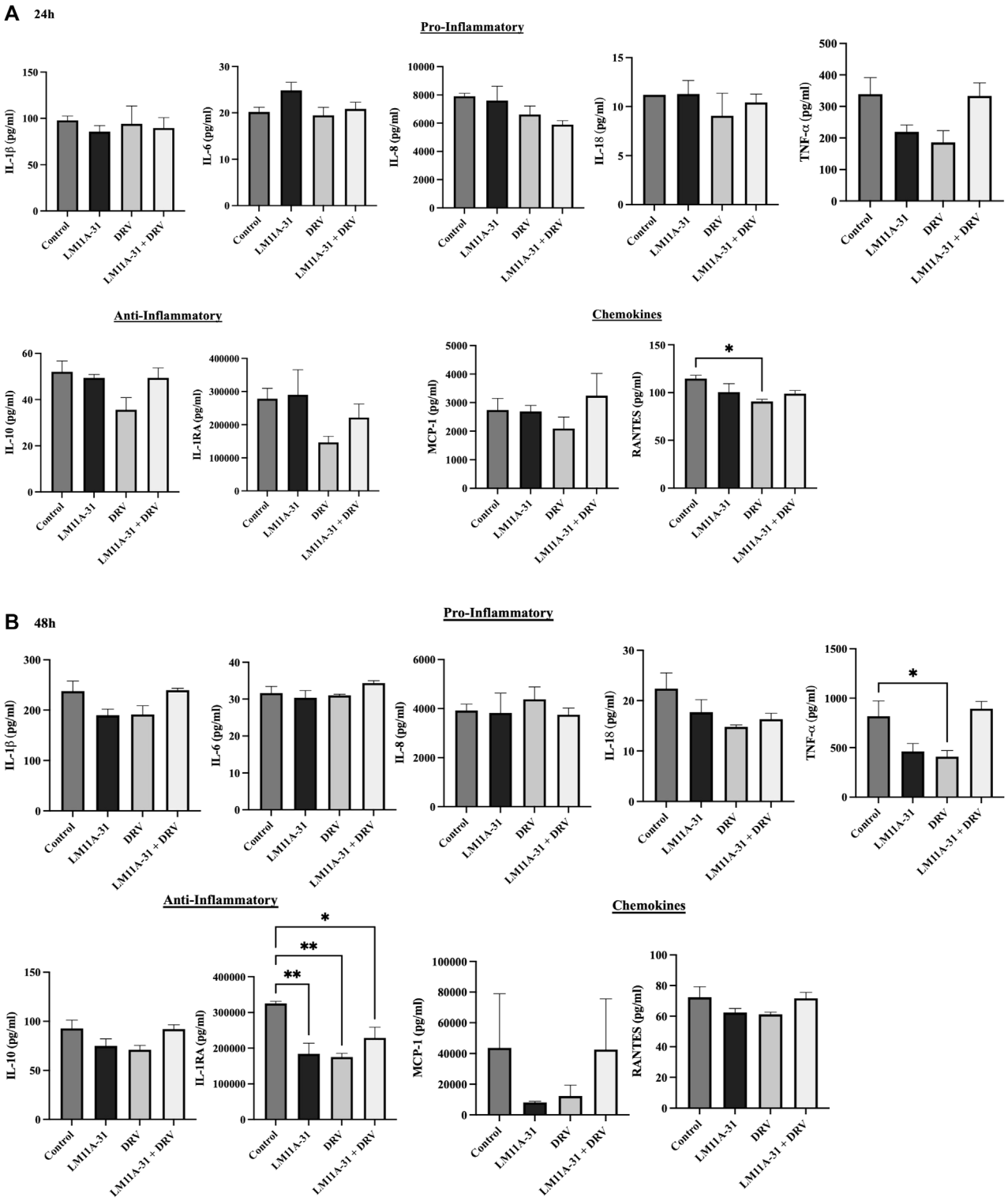

FIGURE 2
The effect of LM11A-31 on inflammatory response in U937 macrophages. U937 macrophages were differentiated and then treated with DMSO, LM11A-31 (100 nM), DRV (5.5 μM), and LM11A-31 + DRV for 48 h. The cytokines and chemokines profile were measured using a customized human 9-Plex ProcartaPlex™ multiplex immunoassay. **(A)** Proinflammatory, chemokines, and anti-inflammatory measurement at 24 h. **(B)** Proinflammatory, chemokines, and anti-inflammatory measurement at 48 h. Values are expressed as mean ± SEM (n = 3). *$p < 0.05$, **$p < 0.01$.

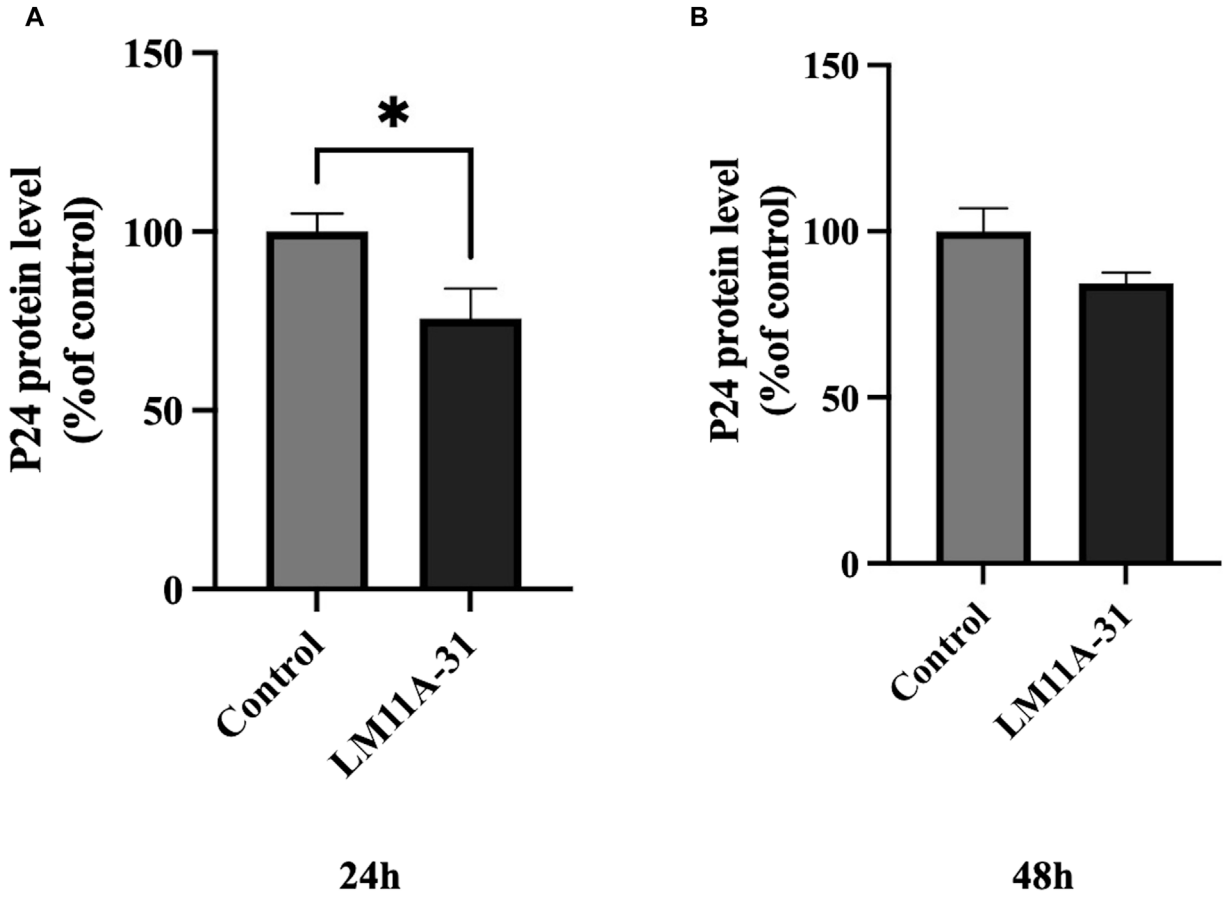

FIGURE 3
The effect of LM11A-31 on HIV-1 replication in MDM. MDM was prepared and infected with HIV-1 as described in Materials and Methods. MDM was treated with DMSO and LM11A-31 (100 nM) for 48 h. The HIV-1 replication was measured using p24 ELISA kit. **(A)** P24 measurement at 24 h. **(B)** P24 measurement at 48 h. Values are expressed as mean ± SEM (n = 3), $*p < 0.05$.

Western blot analysis

Cells were lysed using RIPA buffer and cellular protein was quantified using Pierce BCA Protein Assay Kit (ThermoFisher Scientific). An equal amount of protein (10 μg) obtained from DMSO- and drug-treated U937 and U1 cells was loaded into polyacrylamide gel and electrophoresed, followed by transfer to a PVDF membrane. Then, the membrane was blocked using Li-Cor blocking buffer (LI-COR Biosciences, Lincoln, NE) for 1h. Then, membranes were incubated overnight at 4°C with primary antibodies, including $p75^{NTR}$ (1:500, catalog no. sc-271708, Santa Cruz Biotechnology), SOD1 (1:500, catalog no. sc-101523, Santa Cruz Biotechnology), Catalase (1:500, catalog no. sc-365738, Santa Cruz Biotechnology), Beclin-1 (1:500, catalog no. sc-11427, Santa Cruz Biotechnology), p-Akt (1:1,000, catalog no. S473, Cell Signaling). and β-Actin (1:1,000, catalog no. 3700, Cell Signaling). The next day, membranes were washed three times for 5 min each in PBS containing 0.2% Tween 20 and then incubated with either goat anti-mouse or goat anti-rabbit secondary antibody (1:10,000 dilution, LI-COR Biosciences) for 1 h at room temperature in the dark. Membranes were washed again and scanned using the Li-Cor Scanner (LI-COR Biosciences) for 1h following the secondary antibody. Densitometry analyses of the proteins were conducted using LI-COR Image Studio Software (v.5.2, Nebraska, United States).

Multiplex ELISA

As previously reported [21], the level of cytokines, both pro-inflammatory and anti-inflammatory, and chemokines from cells supernatants were evaluated using customized human 9-Plex ProcartaPlex™ multiplex immunoassay (ThermoFisher Scientific). In brief, U937 and U1 cells were treated with DMSO, LM11A-31, DRV, and LM11A-31 + DRV for 24 and 48 h. Then, supernatants from U937 and U1 cells were collected at 24 and 48 h and transferred to an ELISA plate. Following incubation of samples and standards using a magnetic 96-well

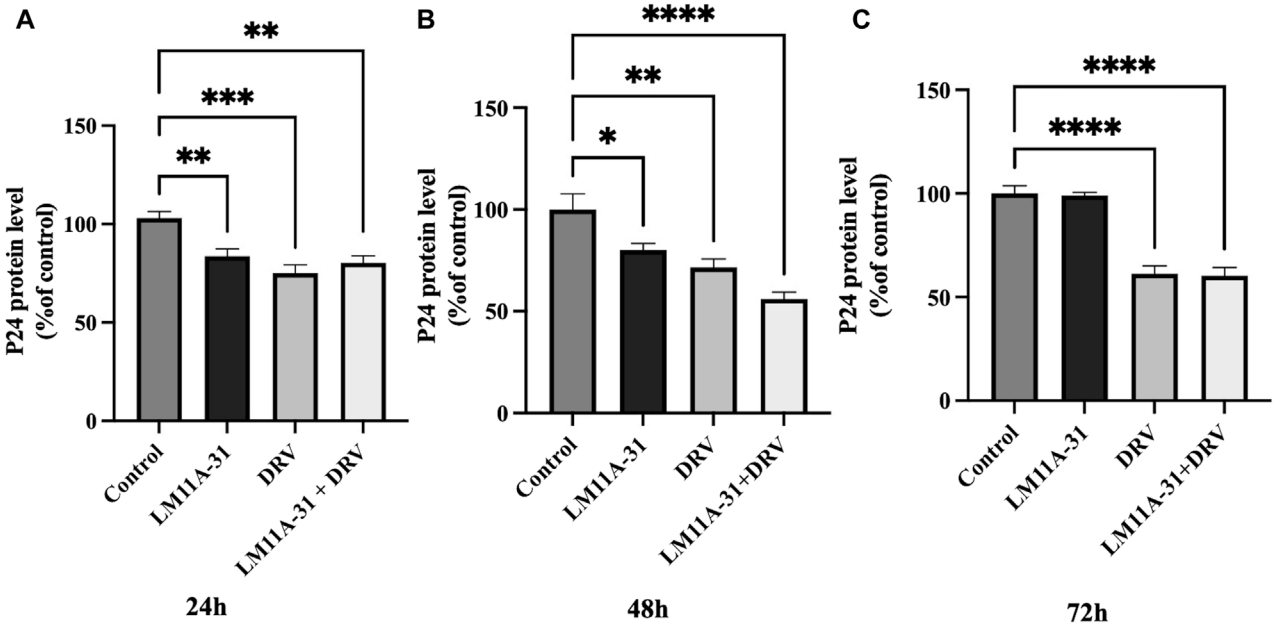

FIGURE 4
The effect of LM11A-31 on HIV-1 replication in U1 macrophages. U1 macrophages were differentiated and then treated with DMSO, LM11A-31 (100 nM), DRV (5.5 μM), and LM11A-31 + DRV for 72 h. The HIV-1 replication was measured using p24 ELISA kit. **(A)** P24 measurement at 24 h. **(B)** P24 measurement at 48 h. **(C)** P24 measurement at 72 h. Values are expressed as mean ± SEM (n = 3–6), $*p < 0.05$, $**p < 0.01$, $***p < 0.001$, $****p < 0.0001$.

ELISA plate for 1 h at room temperature, wells were washed, and then detection antibody, streptavidin-PE, and reading buffer were added. According to the manual, the levels of cytokines/chemokines quantification were measured. The concentration of cytokines and chemokines was reported as pg/mL.

HIV-1 type 1 p24 ELISA

In this study, we used HIV-1 p24 ELISA to measure HIV-1 replication. The majority of HIV-1 p24 assays available in the market utilize a conventional ELISA to capture and identify the p24 antigen. These techniques can detect HIV-1 p24 antigen in the range of 5–25 pg/mL without the need for signal amplification [22, 23]. The HIV-1 Type 1 p24 Antigen ELISA kit was purchased from ZeptoMetrix Corporation (Buffalo, NY). The level of HIV-1 p24 antigen in supernatant collected from U1 macrophages (24, 48, and 72 h post-PMA treatment) and HIV-1-infected MDM (24 and 48 h) was assessed using the enzyme-linked immunoassay (HIV-1 p24 ELISA). Viral antigen in the media is captured into the immobilized monoclonal antibody for p24 coated on microwells in the p24 assay. According to the manufacturer's protocol, the captured viral antigen was sequentially exposed to a biotin-labeled human antibody to HIV-1, streptavidin conjugated to horseradish peroxidase, and tetramethylbenzidine substrate. The optical density of each well was analyzed using a microplate reader at 450 nm and compared against the standard curve to find the concentration of HIV-1 p24 antigen (pg/mL) in the samples. The amount of HIV-1 p24 from DMSO-treated U1 cells was treated as 100%.

LDH activity

To assess the cytotoxic effect of DMSO, LM11A-31, DRV, and combination therapy in U937 and U1 cells, the CyQUANT™ LDH Cytotoxicity Assay Kit (Catalog no. C20300, ThermoFisher Scientific) was used. In brief, U937 and U1 cells were treated using DMSO or drugs for 24, 48, and 72 h. Then, supernatants were collected daily and transferred to a 96-well plate. The reaction mixture was added to the cell culture supernatant for 30 min at room temperature. LDH activity was analyzed using a microplate reader at 680 and 490 nm. Background absorbance of 680 nm was subtracted from 490 nm absorbance to find the LDH activity.

Statistical analysis

The results were expressed as mean ± SEM. Differences among experimental groups were assessed by student's t-test

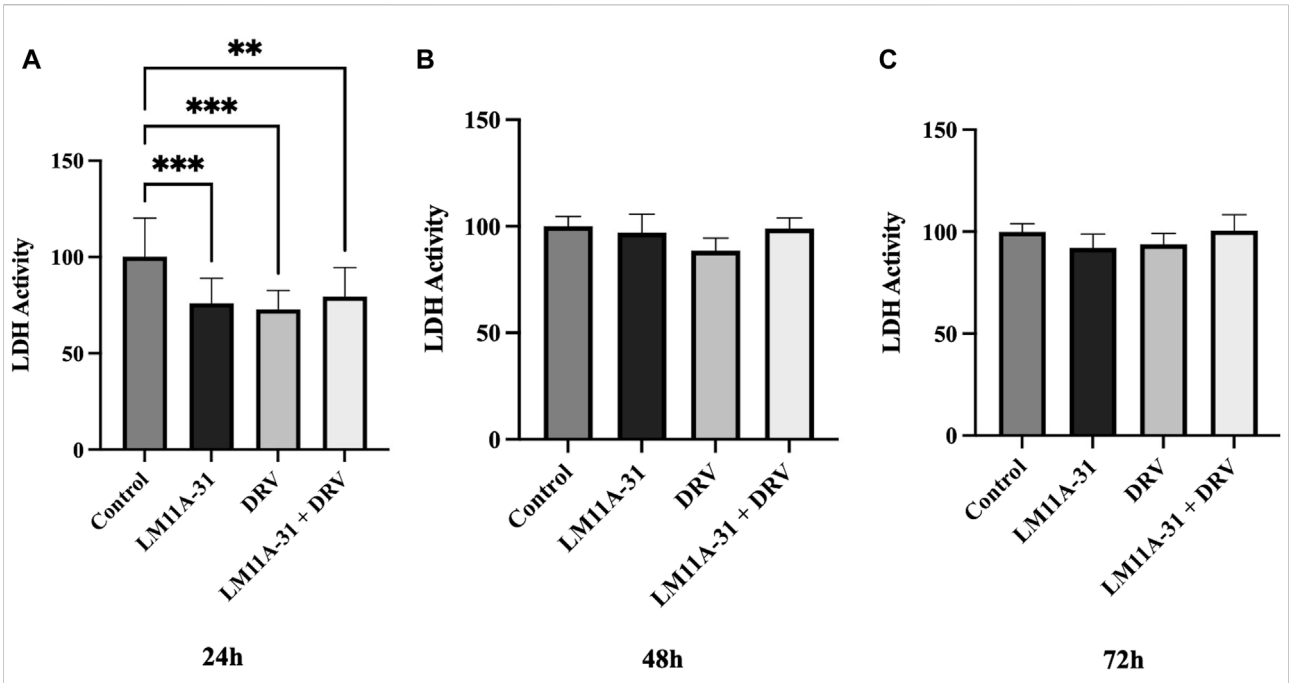

FIGURE 5
The effect of LM11A-31 on cytotoxicity in U1 macrophages. U1 macrophages were differentiated and then treated with DMSO, LM11A-31 (100 nM), DRV (5.5 μM), and LM11A-31 + DRV for 72 h. The cytotoxicity was measured using CyQUANT™ LDH Cytotoxicity Assay Kit. **(A)** LDH measurement at 24 h. **(B)** LDH measurement at 48 h. **(C)** LDH measurement at 72 h. Values are expressed as mean ± SEM (n = 3–6), $*p < 0.05$, $**p < 0.01$, $***p < 0.001$.

or one-way ANOVA followed by Tukey's *post hoc* test. The level of significance was set at $*p < 0.05$, $**p < 0.01$, $***p < 0.001$, $****p < 0.0001$.

Results

The effect of LM11A-31 on cytotoxicity, antioxidant enzymes, and autophagy marker in HIV-1-uninfected U937 macrophages

Before assessing the effect of LM11A-31 in MDM and HIV-1-infected U1 macrophages, we determined whether LM11A-31 is cytotoxic to HIV-1-uninfected U937 macrophages (control cells). U937 macrophages were treated with LM11A-31 (100 nM), DRV, and LM11A-31 + DRV at 24 and 48 h. The results showed that LM11A-31 and DRV are not cytotoxic at 24 and 48 h in U937 macrophages (Figures 1A, B). Furthermore, we determined whether LM11A-31 alters antioxidant enzymes, SOD1 and catalase (markers of oxidative stress), and Beclin-1, a marker of autophagy. Our results demonstrated that LM11A-31, DRV, and combination therapy do not alter the protein levels of catalase (Figure 1C), SOD1 (Figure 1D), and Beclin-1 (Figure 1E) at 24 and 48 h in U937 macrophages.

The effect of LM11A-31 on inflammatory response in U937 macrophages

To evaluate whether LM11A-31 affects inflammatory response in the control U937 macrophages, the cells were treated with LM11A-31, DRV, and LM11A-31 + DRV at 24 and 48 h. We then conducted cytokine assays to measure the levels of key pro-inflammatory, and anti-inflammatory cytokines, and chemokines. The data demonstrated that LM11A-31 and DRV do not alter the levels of pro-inflammatory and anti-inflammatory cytokines at 24 h (Figure 2A). Moreover, no changes were observed in the levels of pro-inflammatory cytokines and chemokines at 48 h by LM11A-31 (Figure 2B). However, DRV significantly reduced the levels of RANTES at 24 h (Figure 2A) and TNF-α at 48 h (Figure 2B). Furthermore, LM11A-31, DRV, and combination therapy significantly decreased the level of IL-1RA at 48 h (Figure 2B). Overall, the results suggest that LM11A-31 does not show a significant inflammatory response in U937 macrophages.

The effect of LM11A-31 on viral replication in MDM

We examined whether LM11A-31 can suppress the viral replication in MDM following 24 and 48 h of acute treatment by measuring the protein level of p24. We found that LM11A-31

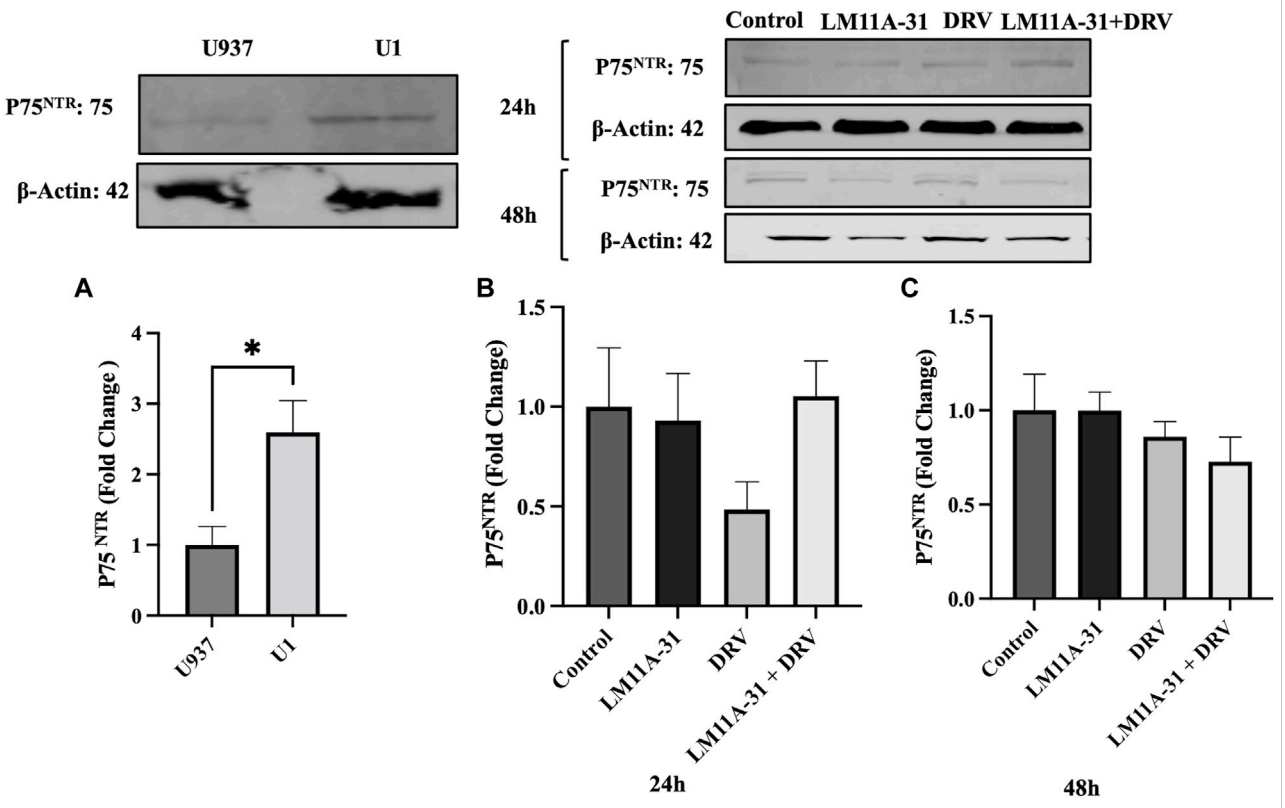

FIGURE 6
The effect of p75^{NTR} in LM11A-31-mediated viral replication in U1 macrophages. U1 macrophages were differentiated and then treated with DMSO, LM11A-31 (100 nM), DRV (5.5 μM), and LM11A-31 + DRV for 48 h. The protein expression was measured using a western blot. **(A)** Quantification of protein level of p75^{NTR} in U1 and U937. **(B, C)** Quantification of protein level of p75^{NTR} at 24 and 48 h. Values are expressed as mean ± SEM (n = 3–4), *$p < 0.05$.

significantly decreased ($p < 0.05$) viral replication compared to the control at 24 h treatment (Figure 3A). In contrast, LM11A-31 did not result in significant change at 48 h treatment (Figure 3B). Following confirmation that LM11A-31 is potentially efficacious in suppressing HIV-1 in primary macrophages, we used HIV-1-infected U1 macrophages for the subsequent studies because the U1 monocytic or HIV-1-infected U937 cell line is the standard model to study HIV-1 pathogenesis [24].

The effect of LM11A-31 on viral replication in U1 macrophages

To examine the effect of LM11A-31, a positive control DRV, and combination on HIV-1 replication in U1 macrophages, we treated the U1 cells at 24, 48, and 72 h. The results showed that LM11A-31 (100 nM) and positive control DRV (5.5 μM) significantly ($p < 0.05$) suppressed the viral replication following 24 and 48 h treatments in U1 macrophages (Figures 4A, B). Interestingly, the HIV-1 suppression by both LM11A-31 and positive control DRV was comparable at both 24 and 48 h treatments. Although both DRV and the combination showed a significant reduction, LM11A-31 did not show a significant change in the viral replication following 72 h treatment (Figure 4C). LM11A-31 may be less stable, or partially metabolized or effluxed out in U1 macrophages at 72 h.

The effect of LM11A-31 on cytotoxicity in U1 macrophages

To examine the effect of LM11A-31, DRV, and combination therapy on cytotoxicity in U1 macrophages, we treated U1 cells at 24 h, 48 h, and 72 h and then assessed cytotoxicity using the LDH assay. Our results showed that LM11A-31, DRV, and combination therapy significantly ($p < 0.05$) reduced cytotoxicity compared to the control group following 24 h treatments (Figure 5A). However, no effect on cytotoxicity was observed after 48 and 72 h treatments in U1 macrophages (Figures 5B, C).

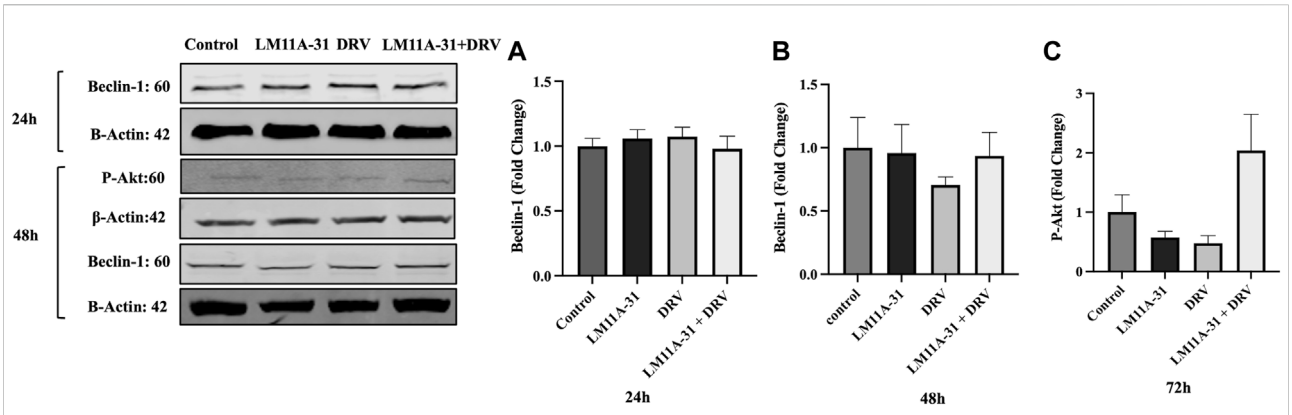

FIGURE 7
The effect of LM11A-31 on autophagy and cell survival pathways in U1 macrophages. U1 macrophages were differentiated and then treated with DMSO, LM11A-31 (100 nM), DRV (5.5 μM), and LM11A-31 + DRV for 48 h. The protein expression was measured using a western blot. **(A, B)** Quantification of protein level of Beclin-1 at 24 and 48 h. **(C)** Quantification of protein level of p-Akt at 48 h.Values are expressed as mean ± SEM (n = 4).

The effect of HIV-1 infection in U1 macrophages on p75^{NTR} regulation

To explore whether p75^{NTR} is altered in HIV-1-infected cells, we seeded U1 and U937 (uninfected) macrophages and then measured the protein level of p75^{NTR} using western blotting. We found that p75^{NTR} expression was significantly upregulated ($p < 0.05$) in U1 compared to U937 macrophages (Figure 6A). This result indicates that HIV-1 infection stimulates protein expression of p75^{NTR}. We then determined whether LM11A-31 and/or DRV suppress p75^{NTR}. Our western blot, data showed that treatment with LM11A-31 and/or DRV does not significantly downregulate p75^{NTR} expression in U1 macrophages at 24 h (Figure 6B). However, there was a trend in the reduction in the level of p75^{NTR} after treatment at 48 h (Figure 6C).

The effect of LM11A-31 on autophagy and cell survival pathways in U1 macrophages

ER stress followed by autophagic dysregulation plays a significant role in the pathogenesis of HIV-1 infection [25]. To determine the role of LM11A-31 on autophagic dysregulation, we performed a western blot for the autophagy marker protein, Beclin-1 in U1 macrophages following 24 and 48 h treatments. Our results showed that LM11A-31 does not change the protein level of Beclin-1 compared to the control at both time points (Figures 7A, B). Further, treatment using DRV alone and in combination with LM11A-31 did not affect the expression of Beclin-1. Since p75^{NTR} has been shown to be involved in cell survival via the p-Akt pathway, we decided to examine whether LM11A-31 alters the protein level of p-Akt in U1 macrophages. However, no change was observed in the protein level of p-Akt following LM11A-31 alone and/or in combination with DRV at 48 h treatment (Figure 7C).

The effect of LM11A-31 on oxidative stress in U1 macrophages

Oxidative stress is one of the major factors in HIV-1 pathogenesis. Therefore, we determined whether LM11A-31 alters ROS and antioxidant enzymes protein level, SOD1, and catalase. For this, U1 macrophages were treated using DMSO, LM11A-31, DRV, and combination therapy for 48 h, and ROS and antioxidant enzymes were assessed. Our results showed that LM11A-31 significantly reduced ROS in U1 macrophages following 48 h treatment Additionally, DRV and combination therapy did not alter the ROS level compared to the control group (Figure 8A). Further, the levels of SOD1 and catalase were also unaltered following treatment of LM11A-31, DRV, and combination at 24 h (Figures 8B, C) and 48 h treatments (Figures 8D, E). Overall, the results showed that LM11A-31 either alone or in combination with DRV did not enhance oxidative stress. This is important because many ART drugs and/or drug combinations are known to increase oxidative stress [26, 27].

The effect of LM11A-31 on inflammatory response in U1 macrophages

Inflammation plays a significant role in the pathogenesis of HIV-1. To determine the impact of LM11A-31 on inflammation, we performed a cytokine assay for the major HIV-1-associated pro-inflammatory and anti-inflammatory cytokines and chemokines on U1 macrophages following 24 and 48 h

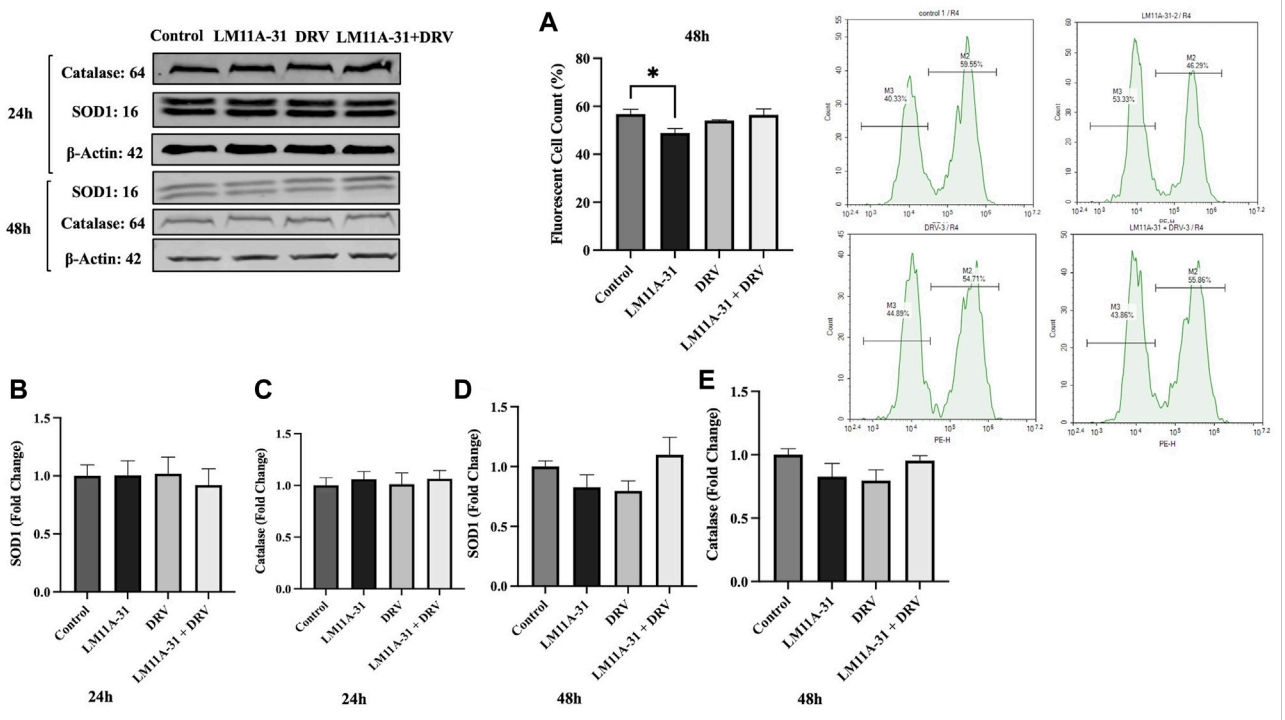

FIGURE 8
The effect of LM11A-31 on oxidative stress in U1 macrophages. U1 macrophages were differentiated and then treated with DMSO, LM11A-31 (100 nM), DRV (5.5 μM), and LM11A-31 + DRV for 48 h. The ROS was measured using flow cytometry. The protein expression was measured using a western blot. **(A)** Measurement of ROS at 48 h, *$p < 0.05$. **(B)** Quantification of protein level of SOD1 at 24 h. **(C)** Quantification of protein level of catalase at 24 h. **(D)** Quantification of protein level of SOD1 at 48 h. **(E)** Quantification of protein level of catalase at 48 h. Values are expressed as mean ± SEM (n = 3–4).

treatments. (Figures 9A, B). For this, we ran a series of pro-inflammatory (IL-1β, IL-6, IL-8, IL-18, and TNF-α), anti-inflammatory cytokines (IL-1RA and I-10), and chemokines (MCP-1 and RANTES) upon treatments with LM11A-31, DRV, and combination at 24 and 48 h treatments. The results showed that treatment of U1 macrophages using LM11A-31 significantly reduced the levels of IL-1β, IL-8, and IL-18 compared to the control at 24 and 48 h (Figures 9A, B; $p < 0.05$). Additionally, DRV significantly reduced the levels of IL-1β and IL-18 at both time points (Figures 9A, B). Combination therapy using LM11A-31 and DRV also significantly downregulated IL-1β, IL-18, and TNF-α at 24 and 48 h (Figures 9A, B; $p < 0.05$). However, the level of anti-inflammatory cytokines IL-1RA, and IL-10, were also significantly reduced in LM11A-31 + DRV and LM11A-31 groups compared to the control at 24 and 48 h, respectively (Figures 9A, B; $p < 0.05$). With regards to proinflammatory chemokine, the level of MCP-1 was significantly reduced in LM11A-31 and LM11A-31 + DRV groups compared to the control at 24 h (Figure 9A; $p < 0.05$). No changes were observed in the level of RANTES for both time points (Figures 9A, B). Overall, the results with LM11A-31 on reducing inflammatory cytokines were comparable to the results obtained by the known ART drug, DRV.

Discussion

Despite freely and widely available ART drugs for HIV-1 treatment, they are unable to suppress the HIV-1 replication in the brain reservoirs. Macrophages express the entry receptor CD4 and co-receptors CCR5 and CXCR4 which interact with the envelope protein of HIV-1 to facilitate entry and infection. They are viral reservoirs and represent a source of infection [28]. In contrast to T cells, productive HIV-1 infection happens in macrophages without relying on the synthesis of cellular DNA, and ART drugs exhibit distinct mechanisms in macrophages and lymphocytes [29]. Pro-inflammatory cytokines have a significant impact on HIV-1 pathogenesis in macrophages [30].

This is the first report that showed that the modulator of $p75^{NTR}$, LM11A-31, suppresses viral replication and reduces cytotoxicity and inflammatory response in macrophages. LM11A-31 can cross the BBB and suppress the virus in CNS reservoirs. Previous reports have shown the potential role of

LM11A-31 in multiple neuronal diseases by modulating $p75^{NTR}$ [15–17]. In this study, we observed that HIV-1-infected U1 macrophages upregulate the expression of $p75^{NTR}$ compared to the uninfected U937 macrophages. Our results are consistent with previous reports, which showed that HIV-1 protein gp120 activates $p75^{NTR}$ expression [15, 31]. Although there is a trend, a lack of significant reduction in the level of $p75^{NTR}$ by LM1A-31 in U1 macrophages suggests that LM11A-31 likely suppresses HIV-1 via multiple pathways.

The current study showed that the effect of LM11A-31 is comparable to the effect caused by positive control DRV. We have previously shown that DRV significantly reduces p24 viral replication in HIV-1-infected monocytic cells including U1 macrophages [32, 33]. HIV-1 RNA, anti-HIV antibodies, and HIV-1 capsid protein (p24 antigen) serve as a primary viral indicator for the identification of HIV-1 infection and for monitoring the advancement of the disease [22]. The p24 antigen becomes detectable approximately 2 weeks following HIV-1 infection due to the initial rapid viral replication phase, which is correlated with viremia elevation.

Our results clearly showed that LM11A-31 suppresses viral replication in both MDM and U1 macrophages, especially at early time points, in acute treatment. It can also be noted that while in MDM its effect is diminished after 24 h, in U1 macrophages the effect continues until 48 h. Although results obtained from U1 macrophages have been replicated in MDM [18, 34], it is possible that MDM is more sensitive to LM11A-31 exposures than U1 macrophages. Primary macrophages and U1 macrophages might have differences in cellular mechanisms and metabolic activities, which can lead to the different effects of LM11A-31 on viral replication [35, 36]. Furthermore, macrophages have different activation states including, M1 or M2 polarization, which may be differentially affected by various drug exposures including LM11A-31 in MDM and U1 macrophages [37, 38].

Further, our results clearly show that the LM11A-31 effect continues for a relatively short period compared to DRV, which sustains the effects until 72 h in U1 macrophages. The findings can be explained by the fact that LM11A-31 is hydrophilic, while DRV is a lipophilic drug [8, 39]. Being hydrophilic, it may be metabolized or destabilized more rapidly than DRV. The findings are also consistent with the literature that LM11A-31 has a relatively lower half-life than DRV (3–4 h vs. 7 h) [10]. LM11A-31 also showed additive effects with DRV at 48 h treatment in U1 macrophages. These findings have significant clinical relevance because LM11A-31 can cross the BBB. Moreover, LM11A-31 has shown the potential to treat several neurological diseases, especially AD, which is a common comorbidity in HIV-1 aging populations [8, 11, 14].

Another interesting observation was that LM11A-31 showed relatively lower cytotoxicity compared to the control and compared to DRV, at 24h in U1 macrophages. Literature has shown that several ART drugs are cytotoxic in brain cells including HIV-1 reservoirs macrophages, microglia, and astrocytes [40]. As expected, LM11A-31 and DRV did not trigger cytotoxicity in control U937 macrophages at 24 and 48 h.

Our study has shown that DRV in combination with ritonavir reduces cell viability [41]. Thus, LM11A-31, being less toxic, could be potentially added with ART treatment to suppress HIV-1 in brain reservoirs. This would also reduce the ART drug load and ART-induced neurotoxicity.

Oxidative stress is one of the hallmarks of HIV-1 pathogenesis, especially in CNS [42]. In our previous report, we have shown that several factors including cigarette smoking trigger oxidative stress and contribute to HIV-1 replication [18, 43]. The present study exhibits that LM11A-31 suppresses ROS in U1 macrophages. While the protein expression of two important antioxidant stress enzymes (SOD1 and catalase) was not altered by LM11A-31 treatment after 24 and 48 h. It is possible that these enzymes in LM11A-31-treated U1 macrophages are at optimum levels to reduce the ROS levels. Additionally, LM11A-31 and DRV did not change the protein expression of these enzymes in U937 macrophages at 48 h, suggesting that LM11A-31 does not cause oxidative stress. Importantly, unlike many drugs including ART drugs [26, 27], LM11A-31 did not increase oxidative stress. Our previous study has shown that DRV in combination with ritonavir enhances oxidative stress by enhancing the levels of ROS and reducing SOD1 [41].

Inflammation is another hallmark of HIV-1 pathogenesis, especially in brain reservoirs [44]. Moreover, recently we have shown that benzo(a)pyrene, which is a major component of cigarettes, induces IL-1β and other cytokines and chemokines in U1 macrophages [45]. Furthermore, we have shown that IL-1β released from HIV-infected U1 macrophages are taken up by neuronal cells leading to neuroinflammation [46]. This phenomenon occurs via extracellular vesicles (EVs) mediated intercellular interactions. Like viral proteins, the inflammatory agents can also be taken up by neurons directly or by packaging in EVs and modulate neuronal inflammation [47]. In this context, cytokines, and chemokines, released from macrophages, can be packaged in EVs, and delivered to neurons reducing neuroinflammation. Therefore, drugs that reduce inflammation in macrophages or neuronal cells are important in reducing HIV-1-induced neuroinflammation. Our results exhibited that LM11A-31 alone and in combination with DRV downregulates many pro-inflammatory cytokines IL-1β, IL-8, IL-18, and TNF-α and chemokine MCP-1. Our results are consistent with the previous report that HIV-1-infected monocytes increase the production of pro-inflammatory cytokines [48]. Importantly, LM11A-31 or DRV did not alter the levels of most pro-inflammatory cytokines and chemokines in U937 macrophages, except for an anti-inflammatory cytokine

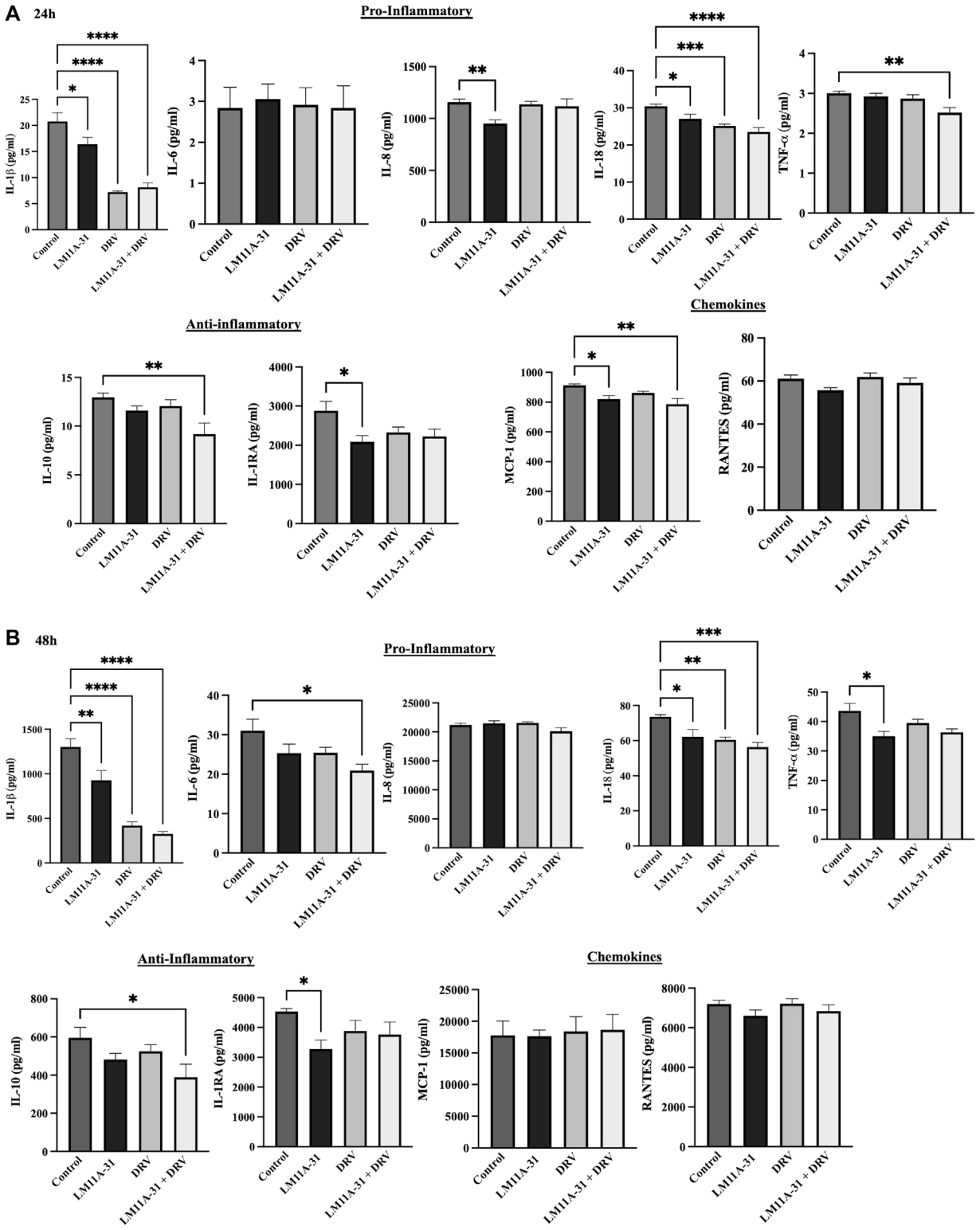

FIGURE 9
The effect of LM11A-31 on inflammatory response in U1 macrophages. U1 macrophages were differentiated and then treated with DMSO, LM11A-31 (100 nM), DRV (5.5 μM), and LM11A-31 + DRV for 48 h. The cytokines and chemokines profile were measured using a customized human 9-Plex ProcartaPlex™ multiplex immunoassay. **(A)** Proinflammatory, chemokines, and anti-inflammatory measurement at 24 h. **(B)** Proinflammatory, chemokines, and anti-inflammatory measurement at 48 h. Values are expressed as mean ± SEM (n = 4–6). *$p < 0.05$, **$p < 0.01$, ***$p < 0.001$, ****$p < 0.0001$.(b)

IL-1RA at 48 h. Taken together, our findings indicate that LM11A-31 reduces HIV-1-induced inflammatory response.

It has been reported that HIV-1 infection increases the level of IL-10 and suppression of IL-10 improves the function of T cells in HIV-1 patients [49]. IL-1RA suppresses IL-1-induced viral replication in U1 macrophages [50]. IL-1 promotes viral replication through IL-1RA [50]. These data demonstrate that LM11A-31 suppresses inflammatory cytokines alone or along with DRV in U1 macrophages. ART drugs, especially protease inhibitors, show increased levels of proinflammatory cytokines in the serum of HIV-1-infected individuals who were treated with different ART drugs [51]. Thus, the addition of LM11A-31 could work effectively as an additive agent with ART drugs without causing drug-induced inflammation.

ER, stress and subsequent autophagic dysregulation by ART drugs are other characteristics of HIV-1 pathogenesis, especially in macrophages [7, 52]. In a study, it has been shown that the ART drug efavirenz dysregulates autophagy by blocking the activity of the Beclin-1/Atg14/PI3KIII complex [53]. Therefore, we determined whether LM11A-31 alone or in combination with DRV also dysregulates autophagy by measuring the levels of Beclin-1. The inability of LM11A-31 to alter the levels of belclin-1 suggests that unlike efavirenz, LM11A-31 is safe with regards to autophagic activity and subsequent autophagic cell death.

A study from Meeker's group in FIV, which is like HIV-1 in producing systemic and CNS disease, has demonstrated the role of LM11A-31 in reducing FIV-induced microglial, astrocytic, and neuronal pathogenesis [17]. LM11A-31 prevented the development of foci of calcium accumulation and beading in the dendrites in feline neurons upon exposure to a conditioned medium from FIV-treated macrophages. The findings from Meeker's study suggest that LM11A-31 may have excellent potential for the treatment of HIV-1-associated neurodegeneration [17]. Our findings from LM11A-31 in U1 macrophages are somewhat consistent with Meeker's FIV study on neuronal pathogenesis. For example, our study suggests that LM11A-31 has the potential to reduce not only HIV-1 replication in myeloid-derived cells (e.g., U1 macrophages) but also oxidative stress and inflammation, which are known to cause HIV-associated neuropathogenesis, including HAND.

Previous reports have shown that HIV-1-infected individuals are susceptible to developing many other neuronal diseases/conditions including cognitive disorders, stroke, AD, and rapid aging in their life [54]. A phase 2a safety and exploratory endpoint trial in AD subjects testing LM11A-31 has recently been completed (EU Clinical Trials Registration: 2015-005263-16, ClinicalTrials.gov registration: NCT03069014). Furthermore, our group found the efficacy of LM11A-31 in a mouse model of ischemic stroke (data not shown). Therefore, LM11A-31 could be relevant to HIV-1-infected individuals who are prone to other neuronal diseases, especially AD and stroke. LM11A-31 along with ART drugs could have a dual role in improving the outcome of comorbidities with HIV-1 and stroke or AD.

In conclusion, we report that LM11A-31 suppresses HIV-1 and has an additive effect on DRV. To some extent, it also decreases cytotoxicity and oxidative stress without causing autophagic dysregulation. More importantly, LM11A-31 alone and in combination with DRV decreases several proinflammatory cytokines and chemokine, resulting in a reduced inflammatory response in macrophages. Due to the inability of ART drugs to cross BBB and suppress HIV-1 in the brain, our present report has clinical relevance as LM11A-31 is hydrophilic and permeable to BBB. However, further studies are needed using an appropriate HIV-1 animal as well as dual (HIV-1+stroke) to fully realize the therapeutic potential of LM11A-31 in HIV-1 and other comorbid conditions.

Author contributions

GM and SaK designed and conceived the idea and the experimental plans. GM, NS, SuK, and SG performed experiments. GM, LZ, SD, and US analyzed the data and prepared the figures. GM and SaK wrote the first draft of the manuscript. TI reviewed and edited the manuscript. All authors have read and agreed to the published version of the manuscript.

Data availability

The original contributions presented in the study are included in the article/Supplementary Material, further inquiries can be directed to the corresponding author.

Ethics statement

Ethical approval was not required for the studies on humans in accordance with the local legislation and institutional requirements because only commercially available established cell lines were used.

Funding

The authors declare that financial support was received for the research, authorship, and/or publication of this article. This work was supported by National Institute of Health grants including DA047178 and AG081140.

Conflict of interest

The authors declare that the research was conducted in the absence of any commercial or financial relationships that could be construed as a potential conflict of interest.

References

1. Kandathil AJ, Sugawara S, Balagopal A. Are T cells the only HIV-1 reservoir? *Retrovirology* (2016) **13**:86–10. doi:10.1186/s12977-016-0323-4

2. Marban C, Forouzanfar F, Ait-Ammar A, Fahmi F, El Mekdad H, Daouad F, et al. Targeting the brain reservoirs: toward an HIV cure. *Front Immunol* (2016) **7**: 397. doi:10.3389/fimmu.2016.00397

3. Bertrand L, Cho HJ, Toborek M. *Blood–brain barrier pericytes as a target for HIV-1 infection*. Oxford University Press (2019).

4. Bertrand L, Méroth F, Tournebize M, Leda AR, Sun E, Toborek M. Targeting the HIV-infected brain to improve ischemic stroke outcome. *Nat Commun* (2019) **10**:2009–14. doi:10.1038/s41467-019-10046-x

5. Ellis R, Langford D, Masliah E. HIV and antiretroviral therapy in the brain: neuronal injury and repair. *Nat Rev Neurosci* (2007) **8**:33–44. doi:10.1038/nrn2040

6. Ash MK, Al-Harthi L, Schneider JR. HIV in the brain: identifying viral reservoirs and addressing the challenges of an HIV cure. *Vaccines (Basel)* (2021) **9**:867. doi:10.3390/vaccines9080867

7. Robertson K, Liner J, Meeker RB. Antiretroviral neurotoxicity. *J Neurovirol* (2012) **18**:388–99. doi:10.1007/s13365-012-0120-3

8. Simmons DA, Knowles JK, Belichenko NP, Banerjee G, Finkle C, Massa SM, et al. A small molecule p75NTR ligand, LM11A-31, reverses cholinergic neurite dystrophy in Alzheimer's disease mouse models with mid-to late-stage disease progression. *PloS one* (2014) **9**:e102136. doi:10.1371/journal.pone.0102136

9. Becker K, Cana A, Baumgärtner W, Spitzbarth I. p75 neurotrophin receptor: a double-edged sword in pathology and regeneration of the central nervous system. *Vet Pathol* (2018) **55**:786–801. doi:10.1177/0300985818781930

10. Knowles JK, Simmons DA, Nguyen T-VV, Vander Griend L, Xie Y, Zhang H, et al. A small molecule p75NTR ligand prevents cognitive deficits and neurite degeneration in an Alzheimer's mouse model. *Neurobiol Aging* (2013) **34**:2052–63. doi:10.1016/j.neurobiolaging.2013.02.015

11. Massa SM, Xie Y, Yang T, Harrington AW, Kim ML, Yoon SO, et al. Small, nonpeptide p75NTR ligands induce survival signaling and inhibit proNGF-induced death. *J Neurosci* (2006) **26**:5288–300. doi:10.1523/jneurosci.3547-05.2006

12. Simmons DA, Mills BD, Butler IIIRR, Kuan J, McHugh TL, Akers C, et al. Neuroimaging, urinary, and plasma biomarkers of treatment response in Huntington's disease: preclinical evidence with the p75NTR ligand lm11a-31. *Neurotherapeutics* (2021) **18**:1039–63. doi:10.1007/s13311-021-01023-8

13. Nguyen T-VV, Crumpacker RH, Calderon KE, Garcia FG, Zbesko JC, Frye JB, et al. Post-stroke administration of the p75 neurotrophin receptor modulator, LM11A-31, attenuates chronic changes in brain metabolism, increases neurotransmitter levels, and improves recovery. *J Pharmacol Exp Ther* (2022) **380**:126–41. doi:10.1124/jpet.121.000711

14. Shi J, Longo FM, Massa SM. A small molecule p75NTR ligand protects neurogenesis after traumatic brain injury. *Stem cells* (2013) **31**:2561–74. doi:10.1002/stem.1516

15. Xie Y, Seawell J, Boesch E, Allen L, Suchy A, Longo FM, et al. Small molecule modulation of the p75 neurotrophin receptor suppresses age-and genotype-associated neurodegeneration in HIV gp120 transgenic mice. *Exp Neurol* (2021) **335**:113489. doi:10.1016/j.expneurol.2020.113489

16. Meeker RB, Poulton W, Clary G, Schriver M, Longo FM. Novel p75 neurotrophin receptor ligand stabilizes neuronal calcium, preserves mitochondrial movement and protects against HIV associated neuropathogenesis. *Exp Neurol* (2016) **275**:182–98. doi:10.1016/j.expneurol.2015.09.012

17. Meeker RB, Poulton W, Feng W-H, Hudson L, Longo FM. Suppression of immunodeficiency virus-associated neural damage by the p75 neurotrophin receptor ligand, LM11A-31, in an *in vitro* feline model. *J Neuroimmune Pharmacol* (2012) **7**:388–400. doi:10.1007/s11481-011-9325-0

18. Rao P, Ande A, Sinha N, Kumar A, Kumar S. Effects of cigarette smoke condensate on oxidative stress, apoptotic cell death, and HIV replication in human monocytic cells. *PloS one* (2016) **11**:e0155791. doi:10.1371/journal.pone.0155791

19. Folks T, Justement J, Kinter A, Schnittman S, Orenstein J, Poli G, et al. Characterization of a promonocyte clone chronically infected with HIV and inducible by 13-phorbol-12-myristate acetate. *J Immunol* (1988) **140**:1117–22. doi:10.4049/jimmunol.140.4.1117

20. Jin M, Arya P, Patel K, Singh B, Silverstein PS, Bhat HK, et al. Effect of alcohol on drug efflux protein and drug metabolic enzymes in U937 macrophages. *Alcohol Clin Exp Res* (2011) **35**:132–9. doi:10.1111/j.1530-0277.2010.01330.x

21. Kumar A, Sinha N, Haque S, Kodidela S, Wang T, Martinez AG, et al. Nicotine self-administration with menthol and audiovisual cue facilitates differential packaging of CYP2A6 and cytokines/chemokines in rat plasma extracellular vesicles. *Scientific Rep* (2021) **11**:17393–13. doi:10.1038/s41598-021-96807-5

22. Bystryak S, Acharya C. Detection of HIV-1 p24 antigen in patients with varying degrees of viremia using an ELISA with a photochemical signal amplification system. *Clinica Chim Acta* (2016) **456**:128–36. doi:10.1016/j.cca.2016.02.022

23. Miedouge M, Grèze M, Bailly A, Izopet J. Analytical sensitivity of four HIV combined antigen/antibody assays using the p24 WHO standard. *J Clin Virol* (2011) **50**:57–60. doi:10.1016/j.jcv.2010.09.003

24. Cassol E, Alfano M, Biswas P, Poli G. Monocyte-derived macrophages and myeloid cell lines as targets of HIV-1 replication and persistence. *J Leukoc Biol* (2006) **80**:1018–30. doi:10.1189/jlb.0306150

25. Nardacci R, Ciccosanti F, Marsella C, Ippolito G, Piacentini M, Fimia GM. Role of autophagy in HIV infection and pathogenesis. *J Intern Med* (2017) **281**: 422–32. doi:10.1111/joim.12596

26. Sharma B. Oxidative stress in HIV patients receiving antiretroviral therapy. *Curr HIV Res* (2014) **12**:13–21. doi:10.2174/1570162x12666140402100959

27. Akay C, Cooper M, Odeleye A, Jensen BK, White MG, Vassoler F, et al. Antiretroviral drugs induce oxidative stress and neuronal damage in the central nervous system. *J Neurovirol* (2014) **20**:39–53. doi:10.1007/s13365-013-0227-1

28. Veenhuis RT, Abreu CM, Shirk EN, Gama L, Clements JE. HIV replication and latency in monocytes and macrophages. *Semin Immunol* (2021) **51**:101472. doi:10.1016/j.smim.2021.101472

29. Verani A, Gras G, Pancino G. Macrophages and HIV-1: dangerous liaisons. *Mol Immunol* (2005) **42**:195–212. doi:10.1016/j.molimm.2004.06.020

30. Herbein G, Varin A. The macrophage in HIV-1 infection: from activation to deactivation? *Retrovirology* (2010) **7**:33–15. doi:10.1186/1742-4690-7-33

31. Speidell A, Asuni GP, Wakulski R, Mocchetti I. Up-regulation of the p75 neurotrophin receptor is an essential mechanism for HIV-gp120 mediated synaptic loss in the striatum. *Brain Behav Immun* (2020) **89**:371–9. doi:10.1016/j.bbi.2020.07.023

32. Midde NM, Gong Y, Cory TJ, Li J, Meibohm B, Li W, et al. Influence of ethanol on darunavir hepatic clearance and intracellular PK/PD in HIV-infected monocytes, and CYP3A4-darunavir interactions using inhibition and *in silico* binding studies. *Pharm Res* (2017) **34**:1925–33. doi:10.1007/s11095-017-2203-6

33. Kodidela S, Sinha N, Kumar A, Kumar S. Anti-HIV activity of cucurbitacin-D against cigarette smoke condensate-induced HIV replication in the U1 macrophages. *Viruses* (2021) **13**:1004. doi:10.3390/v13061004

34. Gong Y, Chowdhury P, Midde NM, Rahman MA, Yallapu MM, Kumar S. Novel elvitegravir nanoformulation approach to suppress the viral load in HIV-infected macrophages. *Biochem Biophys Rep* (2017) **12**:214–9. doi:10.1016/j.bbrep.2017.10.005

35. Mengozzi M, De Filippi C, Transidico P, Biswas P, Cota M, Ghezzi S, et al. Human immunodeficiency virus replication induces monocyte chemotactic protein-1 in human macrophages and U937 promonocytic cells. *Blood* (1999) **93**:1851–7. doi:10.1182/blood.v93.6.1851.406k12_1851_1857

36. Herbein G, Varin A, Larbi A, Fortin C, Mahlknecht U, Fulop T, et al. Nef and TNFα are coplayers that favor HIV-1 replication in monocytic cells and primary macrophages. *Curr HIV Res* (2008) **6**:117–29. doi:10.2174/157016208783884985

37. Cory TJ, He H, Winchester LC, Kumar S, Fletcher CV. Alterations in P-glycoprotein expression and function between macrophage subsets. *Pharm Res* (2016) **33**:2713–21. doi:10.1007/s11095-016-1998-x

38. Kim H, Kim HS, Piao YJ, Moon WK. Bisphenol A promotes the invasive and metastatic potential of ductal carcinoma *in situ* and protumorigenic polarization of macrophages. *Toxicol Sci* (2019) **170**:283–95. doi:10.1093/toxsci/kfz119

39. Daskapan A, Tran QTD, Cattaneo D, Gervasoni C, Resnati C, Stienstra Y, et al. Darunavir population pharmacokinetic model based on HIV outpatient data. *Ther Drug Monit* (2019) **41**:59–65. doi:10.1097/ftd.0000000000000576

40. Liner KJ, Ro MJ, Robertson KR. HIV, antiretroviral therapies, and the brain. *Curr HIV/AIDS Rep* (2010) **7**:85–91. doi:10.1007/s11904-010-0042-8

41. Rao PS, Kumar S. Chronic effects of ethanol and/or darunavir/ritonavir on U937 monocytic cells: regulation of cytochrome P450 and antioxidant enzymes, oxidative stress, and cytotoxicity. *Alcohol Clin Exp Res* (2016) **40**:73–82. doi:10.1111/acer.12938

42. Mollace V, Nottet HS, Clayette P, Turco MC, Muscoli C, Salvemini D, et al. Oxidative stress and neuroAIDS: triggers, modulators and novel antioxidants. *Trends Neurosciences* (2001) **24**:411–6. doi:10.1016/s0166-2236(00)01819-1

43. Ande A, McArthur C, Ayuk L, Awasom C, Achu PN, Njinda A, et al. Effect of mild-to-moderate smoking on viral load, cytokines, oxidative stress, and

cytochrome P450 enzymes in HIV-infected individuals. *PloS one* (2015) **10**: e0122402. doi:10.1371/journal.pone.0122402

44. Yadav A, Collman RG. CNS inflammation and macrophage/microglial biology associated with HIV-1 infection. *J Neuroimmune Pharmacol* (2009) **4**: 430–47. doi:10.1007/s11481-009-9174-2

45. Kumar A, Sinha N, Kodidela S, Zhou L, Singh UP, Kumar S. Effect of benzo (a) pyrene on oxidative stress and inflammatory mediators in astrocytes and HIV-infected macrophages. *Plos one* (2022) **17**:e0275874. doi:10.1371/journal.pone.0275874

46. Kodidela S, Sinha N, Kumar A, Zhou L, Godse S, Kumar S. Extracellular vesicles released from macrophages modulates interleukin-1β in astrocytic and neuronal cells. *Sci Rep* (2023) **13**:3005. doi:10.1038/s41598-023-29746-y

47. Rahimian P, He JJ. Exosome-associated release, uptake, and neurotoxicity of HIV-1 Tat protein. *J Neurovirol* (2016) **22**:774–88. doi:10.1007/s13365-016-0451-6

48. Molina J-M, Schindler R, Ferriani R, Sakaguchi M, Vannier E, Dinarello CA, et al. Production of cytokines by peripheral blood monocytes/macrophages infected with human immunodeficiency virus type I (HIV-I). *J Infect Dis* (1990) **161**:888–93. doi:10.1093/infdis/161.5.888

49. Brockman MA, Kwon DS, Tighe DP, Pavlik DF, Rosato PC, Sela J, et al. IL-10 is up-regulated in multiple cell types during viremic HIV infection and reversibly inhibits virus-specific T cells. *Blood* (2009) **114**:346–56. doi:10.1182/blood-2008-12-191296

50. Granowitz EV, Saget BM, Wang MZ, Dinarello CA, Skolnik PR, Fauci A. Interleukin 1 induces HIV-1 expression in chronically infected U1 cells: blockade by interleukin 1 receptor antagonist and tumor necrosis factor binding protein type 1. *Mol Med* (1995) **1**:667–77. doi:10.1007/bf03401607

51. Maritati M, Alessandro T, Zanotta N, Comar M, Bellini T, Sighinolfi L, et al. A comparison between different anti-retroviral therapy regimes on soluble inflammation markers: a pilot study. *AIDS Res Ther* (2020) **17**:61. doi:10.1186/s12981-020-00316-w

52. Gnanadhas DP, Dash PK, Sillman B, Bade AN, Lin Z, Palandri DL, et al. Autophagy facilitates macrophage depots of sustained-release nanoformulated antiretroviral drugs. *J Clin Invest* (2017) **127**:857–73. doi:10.1172/jci90025

53. Bertrand L, Toborek M. Dysregulation of endoplasmic reticulum stress and autophagic responses by the antiretroviral drug efavirenz. *Mol Pharmacol* (2015) **88**:304–15. doi:10.1124/mol.115.098590

54. Singer EJ, Valdes-Sueiras M, Commins DL, Yong W, Carlson M. HIV stroke risk: evidence and implications. *Ther Adv chronic Dis* (2013) **4**:61–70. doi:10.1177/2040622312471840

EBM Experimental Biology and Medicine

TYPE Review
PUBLISHED 22 July 2024
DOI 10.3389/ebm.2024.10121

OPEN ACCESS

*CORRESPONDENCE
Jianqiang Wu,
wujianqiang_pumch@163.com
Zairong Wei,
zairongwei@163.com
Yuehong Zheng,
zhengyuehong2022@outlook.com

RECEIVED 02 August 2023
ACCEPTED 08 July 2024
PUBLISHED 22 July 2024

CITATION
Zhou L, Wu J, Wei Z and Zheng Y (2024), Legumain in cardiovascular diseases. *Exp. Biol. Med.* 249:10121. doi: 10.3389/ebm.2024.10121

Legumain in cardiovascular diseases

Lei Zhou[1,2], Jianqiang Wu[3]*, Zairong Wei[1]* and Yuehong Zheng[2]*

[1]Department of Burns and Plastic Surgery, Affiliated Hospital of Zunyi Medical University, Zunyi, China, [2]Department of Vascular Surgery, State Key Laboratory of Complex Severe and Rare Diseases, Peking Union Medical College Hospital, Chinese Academy of Medical Sciences and Peking Union Medical College, Beijing, China, [3]Institute of Clinical Medicine, National Science and Technology Key Infrastructure on Translational Medicine, State Key Laboratory of Complex Severe and Rare Diseases, Peking Union Medical College Hospital, Chinese Academy of Medical Sciences and Peking Union Medical College, Beijing, China

Abstract

Cardiovascular diseases (CVDs) are the leading cause of death worldwide, having become a global public health problem, so the pathophysiological mechanisms and therapeutic strategies of CVDs need further study. Legumain is a powerful enzyme that is widely distributed in mammals and plays an important role in a variety of biological processes. Recent research suggests that legumain is associated with the occurrence and progression of CVDs. In this review, we provide a comprehensive overview of legumain in the pathogenesis of CVDs. The role of legumain in CVDs, such as carotid atherosclerosis, pulmonary hypertension, coronary artery disease, peripheral arterial disease, aortic aneurysms and dissection, is discussed. The potential applications of legumain as a biomarker of these diseases are also explored. By understanding the role of legumain in the pathogenesis of CVDs, we aim to support new therapeutic strategies to prevent or treat these diseases.

KEYWORDS

legumain, cardiovascular disease, atherosclerosis, coronary artery disease, aortic disease

Impact statement

CVDs are the leading cause of death globally and remain a heavy unresolved societal burden. The discovery of novel biomarkers and therapeutic targets may improve the situation. Legumain is involved in the occurrence, development, and prognosis of multiple CVDs. This work details the action mechanism of legumain in CVDs to develop new therapeutic targets. It also describes the research progress on legumain as a biomarker for CVDs.

Introduction

Cardiovascular diseases (CVDs) are the leading cause of death worldwide [1]. In recent years, with the continuous development of biomarkers and new drugs, the

secondary prevention of CVDs has made significant progress, but their mortality rate is still high. Therefore, it is still necessary to further explore the pathogenesis of CVDs and find new strategies for diagnosis and treatment.

Cysteine proteases are involved in the degradation of intracellular proteins and the extracellular matrix (ECM), protein processing and cell signal transduction, playing an important role in the pathogenesis of CVDs, and their inhibitors have therapeutic potential for CVDs [2]. As a member of the cysteine protease family, legumain (LGMN) augments the occurrence and development of atherosclerosis, pulmonary hypertension, peripheral vascular disease, aortic aneurysm and dissection, and promotes the outcome of coronary heart disease. In this review, we discuss mechanistic and biomarker-related studies of LGMN in CVDs and explore LGMN as a potential therapeutic target for these diseases.

The origin and regulation of LGMN

Source of LGMN

LGMN, also known as asparaginyl endopeptidase (AEP), belongs to the C13 family of cysteine proteases. It was first identified in the early 1980s and received its name in 1993 for its function in legume seeds [3, 4]. In 1996, LGMN was identified in mammalian tissues, and it is widely distributed in various tissues, including the testes, kidneys, liver, heart, and vasculature [5, 6].

In cells, mature LGMN is located primarily in the lysosome. Prolegumain is translocated from the endoplasmic reticulum and Golgi apparatus to the lysosomal system and activated in the acidic environment of the lysosome. Prolegumain can be secreted extracellularly directly through the Golgi apparatus or via the lysosomal/endosomal system [7], allowing LGMN to be detected in the plasma/serum of patients.

Activation of LGMN

Prolegumain has 433 amino acids and molecular mass of 56 kDa. It has 3 parts: the catalytic domain, activation peptide (AP) and LGMN stabilization and activity-modulating (LSAM) domain. Prolegumain has no protease activity because the LSAM covers the catalytic active site. In an acidic environment, LGMN undergoes a pH-dependent conformational change, and at pH < 4.5, autocatalytic cleavage exposes the active site (Cys189) in the catalytic domain to yield biologically active mature LGMN with a molecular mass of 36 kDa [8, 9]. LGMN is activated primarily in lysosomes and can be delivered extracellularly. According to the latest literature, the secreted protein LGMN can act as a novel signaling molecule to perform biological functions outside the cells [10, 11].

Inducers and inhibitors of LGMN

Hypoxia-inducible factor 1-alpha (HIF1α) is a nuclear transcription factor that directly increases the gene and protein expression levels of LGMN [11, 12]. *In vitro* studies revealed that primary human monocytes polarized to M1 macrophages in response to the proinflammatory factors lipopolysaccharide (LPS) and IFN-γ had 9-fold higher LGMN protein expression levels than IL-4-polarized M2 macrophages, whereas no significant difference in LGMN secretion was observed between M2-type and resting macrophages [13]. Various proinflammatory cytokines, such as Interleukin-1β (IL-1β), interferon-γ (IFN-γ), and tumor necrosis factor-α (TNF-α), can increase the protein expression levels of various cysteine proteases in monocytes and vascular cells [14–16]. The protein expression levels of LGMN may also be regulated by these cytokines and further research is needed.

Currently, several small-molecule substrates, inhibitors, and activity-based probes of LGMN have been developed [17]. The inhibitor RR-11a appears to be a promising agent for disease treatment. RR-11a is a synthetic LGMN-specific inhibitor that irreversibly inhibits LGMN function by forming a covalent bond to the catalytic cysteine Cys189, demonstrating potential therapeutic utility in several CVD disease models [10, 18, 19].

LGMN in CVDs

Carotid atherosclerosis

Atherosclerosis is a common CVD characterized by the accumulation of lipids and other molecules in the walls of arteries and the formation of plaques, resulting in the narrowing and hardening of blood vessels, such as medium and large arteries, throughout the body [20, 21]. LGMN plays a key role in the development of atherosclerosis. LGMN was increased in the plasma and arterial tissue of patients with carotid atherosclerosis as well as in mouse models of atherosclerosis [22, 23]. Carotid artery stenosis, i.e., atherosclerotic narrowing or even occlusion of the carotid arteries, can produce serious or lethal neurological consequences, so identifying potential diagnostic, therapeutic and risk stratification methods for carotid artery stenosis is essential [24]. LGMN protein expression levels are elevated in the plasma and plaques of patients with carotid stenosis [15], suggesting that it may be involved in the occurrence and progression of this disease.

The mechanism of action of LGMN in atherosclerosis is complex. LGMN can indirectly participate in the degradation of the ECM by activating cathepsins B, H, and L, as well as matrix metalloproteinase-2 (MMP-2) [25, 26], enzymes that promote atherogenesis by degrading ECM collagen and elastin [27–29]. LGMN can directly degrade fibronectin in the ECM [30]. Degradation of the ECM allows the accumulation of lipids

and other substances, and facilitates the formation of fatty streaks in the arterial wall, the earliest stage of atherosclerosis. In addition, the protein expression levels of LGMN, MMPs, and cathepsins are higher in unstable than stable plaques. A potential activator of MMPs and cathepsins, LGMN may destabilize plaques by activating these ECM-degrading enzymes.

LGMN is involved in tumor neovascularization [31, 32]. In atherosclerotic plaques, intraplaque angiogenesis enhances deposition but also fragility and instability of plaques [33]. Further studies are necessary to understand the mechanisms of LGMN in plaque stability and to develop effective therapeutic strategies. The increased protein expression levels of LGMN in unstable plaques could be used to identify people at high risk of developing CVDs, allowing for early detection and preventive treatment.

The protein expression level of LGMN is elevated in macrophages of atherosclerosis. LGMN expression, activity and secretion are significantly enhanced during the differentiation of monocytes to macrophages, the major inflammatory cells in atherosclerosis. The protein expression level of LGMN is higher in proinflammatory M1 macrophages than in anti-inflammatory M2 macrophages. These findings suggest that LGMN may regulate monocyte/macrophage inflammatory functions [15, 34]. *In vitro* migration assays revealed that LGMN dose-dependently increased the migration of monocytes and their adhesion to endothelial cells [23], followed by their migration in the subendothelium, where they differentiated into macrophages, initiating the formation of atherosclerotic lesions [35]. LGMN can be secreted extracellularly, and the chemotactic effect of extracellular LGMN on monocytes may contribute to the recruitment of monocytes/macrophages into atherosclerotic lesions and exacerbate inflammation in the vessel wall. *In vitro*, LGMN increases endothelial cell expression of proinflammatory cytokines, such as monocyte chemoattractant protein-1 (MCP-1) [5], which is a multifunctional chemokine that promotes monocyte adhesion, migration, and induction of inflammatory responses.

Foam cells, macrophages that phagocytose large amounts of lipid, are atherosclerotic hallmarks. Stimulation with cholesterol crystals significantly increases the secretion of LGMN by M1-type macrophages, suggesting that LGMN may promote lipid metabolism [15]. LGMN increases the protein expression levels of scavenger receptor class A (SR-A), acyl-coenzyme A: cholesterol acyltransferase-1 (ACAT-1), and neutral cholesterol ester hydrolase (NCEH) in macrophages and may regulate lipid metabolism through this pathway to increase oxidized low-density lipoprotein (oxLDL) induced foam cell formation [5]. SR-A is one of the main receptors responsible for ox-LDL binding and uptake in macrophages [36]. Uncontrolled uptake of ox-LDL leads to impaired intracellular cholesterol metabolism and the accumulation of cytoplasmic lipid droplets, subsequently triggering the formation of foam cells. ACAT1 and NCEH play key roles in cholesterol esterification. ACAT1 esterifies free cholesterol in the endoplasmic reticulum to form cholesteryl esters. NCEH can hydrolyze lipid droplets in the cytoplasm and excrete them from the cell [37]. The balance between ACAT1 and NCEH regulates intracellular lipid metabolism.

The discovery, validation and implementation of novel biomarkers are important for clarifying disease diagnoses, determining disease severity and predicting clinical prognoses. The protein expression levels of LGMN was significantly higher in the plasma and plaques of patients with carotid stenosis than in healthy control individuals and was increased in the carotid plaques of recently symptomatic patients compared to asymptomatic patients. These findings suggest that the protein expression levels of LGMN is elevated in stenotic disease and indicate that LGMN may be a useful atherosclerotic biomarker for diagnosing and assessing the disease [15]. LGMN protein promotes plaque instability, further suggesting that LGMN may be a new therapeutic target for unstable plaques and a biomarker that can predict clinical prognosis to diagnose and assess disease [22].

Peripheral artery disease

Peripheral artery disease (PAD) affects more than 200 million people worldwide and is most commonly caused by atherosclerosis. Atherosclerotic plaques cause arterial stenosis which limits blood supply to distal tissues [38, 39]. Most patients with PAD have no obvious symptoms. When stenosis is severe, it can cause intermittent claudication, resting pain, and even foot ulcers and gangrene, which not only seriously affect the patient's quality of life but may also lead to amputation or even death [39]. Serum LGMN was significantly higher in PAD patients than in non-PAD patients, and high serum LGMN was independently associated with an increased risk of PAD [40]. These findings suggest LGMN could be a blood biomarker and predictor of PAD. The mechanism of action of LGMN and its roles as a therapeutic target and biomarker of atherosclerosis-related diseases deserve further study.

Pulmonary arterial hypertension

Pulmonary arterial hypertension (PAH) is a serious and potentially life-threatening condition characterized by increased vascular stiffness, which can lead to severe symptoms such as progressive dyspnea, fatigue, chest pain, and syncope [41].

LGMN serum concentration paralleled the severity of PAH, suggesting that this protein may be involved in disease progression [19]. LGMN knockdown or inhibition reduces the severity of PAH in animal models. In PAH, elastin degradation,

collagen deposition and cross-linking, and tenascin and fibronectin deposition in the ECM lead to pulmonary vascular wall remodeling and vascular stiffening [42]. The transforming growth factor-β1 (TGF-β1) signaling pathway is a key initiator and driver of ECM protein deposition and fibrotic disease [43, 44], and excessive TGF-β-mediated signaling promotes PAH development [45]. Macrophage-derived LGMN promotes the deposition of collagen I, fibronectin and tenascin-C in the ECM via the MMP2/TGF-β signaling pathway, contributing to the progression of PAH [19]. LGMN promotes the synthesis of ECM components in PAH and the degradation of ECM components in atherosclerosis, further demonstrating the key role of LGMN in tissue remodeling.

The involvement of LGMN in pulmonary vascular wall remodeling has implications for the occurrence and progression of PAH. Targeting LGMN might reduce pulmonary vascular wall remodeling to improve symptoms. In addition, the LGMN inhibitor RR-11a may be used to reduce the risk and progression of PAH [19]. Further studies are needed to fully understand the role of LGMN in the development of PAH and to develop safe and effective treatments.

Coronary artery disease

The global epidemic of coronary artery disease (CAD) is imposing ever-increasing rates of morbidity and mortality [46]. CAD is caused by atherosclerotic plaque accumulation leading to coronary artery stenosis or occlusion, and acute attacks may lead to conditions such as myocardial infarction and angina pectoris. LGMN was overexpressed in the plasma and tissues of acute CAD patients, suggesting that it may play an important role in the occurrence and progression of this disease [18, 47–49]. One study also found plasma LGMN to be independently associated with complex CAD [49], suggesting that LGMN may be a potential biomarker of CAD. Plasma LGMN levels have also been associated with patient outcomes. A study of patients with acute coronary syndrome with a 1-month follow-up showed that plasma LGMN was negatively associated with the incidence of stroke [47]. However, two studies with long-term follow-up of all-cause mortality in the myocardial infarction population yielded opposite results: One showed that low plasma LGMN was associated with increased mortality in the myocardial infarction population [48]. The other showed that all-cause mortality was significantly higher in the high-plasma-LGMN group than in the low-LGMN group [18]. Thus, prospective studies with larger cohorts are needed to clarify the predictive role of LGMN in acute myocardial infarction patients.

A recent study has shown that LGMN colocalized with platelets in arterial plaques and was released in response to platelet activation. Circulating LGMN protein was significantly correlated with plasma levels of the platelet activation markers P-selectin and platelet factor 4 (PF4), further suggesting that LGMN plays an important role in plaque stability and thrombosis [48]. Circulating LGMN is elevated in patients with acute myocardial infarction, a potentially deadly manifestation of CAD [18, 48]. In animal studies, the LGMN inhibitor RR-11a was found to improve myocardial remodeling and reduce the rate of cardiac rupture by inhibiting ECM degradation, demonstrating that LGMN may be a therapeutic target for myocardial infarction.

LGMN is also involved in regulating the efferocytosis of apoptotic cells. Efferocytosis is the phagocytosis and removal of cells that have undergone programmed cell death by macrophages. The timely removal of dead cells is essential to maintain physiological homeostasis or pathological improvements and to avoid further damage to surrounding tissues by the release of intracellular contents from dead cells [50, 51]. Macrophage secretion of LGMN was required to promote the efferocytosis of apoptotic cardiomyocytes in myocardial infarction, and selective overexpression of LGMN by macrophages improved cardiac function in mice after myocardial infarction. LGMN knockout resulted in the accumulation of apoptotic cardiomyocytes and exacerbated myocardial infarction [52].

The development and prognosis of myocardial infarction can be improved by regulating the function of LGMN, which will require more studies to clarify the function of LGMN in disease occurrence, progression, and recovery.

Aortic aneurysm and aortic dissection

Aortic aneurysms and dissection are severely life-threatening, and mortality after aortic rupture can be as high as 85% [53]. The formation of aortic aneurysm and dissection may be related to ECM degradation, vessel wall inflammation, oxidative stress, and vascular smooth muscle cell (VSMC) dysfunction [54, 55]. The exact mechanism of aortic aneurysm and dissection is unknown, but recent studies have identified increased the protein expression levels of LGMN in the plasma and tissue of patients with aortic aneurysm and dissection [10, 56] and have identified a new potential role for LGMN in the pathogenesis of aortic aneurysm and dissection.

LGMN promotes degradation of the ECM components of the aortic wall and alters the structure and integrity of the aortic wall, which may be related to the formation of aortic aneurysms and dissection. Recent studies have shown that LGMN promoted the formation of thoracic aortic dissection by participating in the phenotypic switching of VSMCs [10]. VSMCs in healthy vessel walls exhibited a contractile phenotype to maintain vascular tone, moderating blood pressure and flow through their contractile and diastolic capacities [57]. The loss of VSMC contractile function altered vascular tone, increased aortic wall stress, and decreased vascular elasticity, thereby promoting aneurysm and dissection formation [54]. During thoracic aortic dissection,

TABLE 1 Legumain has potential as a biomarker or therapeutic target for CVDs.

Study	Disease(s)	Result
Papaspyridonos M *et al.*, 2006	unstable atherosclerotic plaque	LGMN may be a novel target for the treatment of unstable plaque or useful diagnostic markers of plaque instability
Lunde NN *et al.*, 2017	atherosclerosis	LGMN was increased in both plasma and plaques of patients with carotid stenosis and might be a new and early biomarker of atherosclerosis
Bai P *et al.*, 2019	pulmonary hypertension	LGMN may serve as a valuable biomarker for evaluating the efficiency of PAH treatment
Fang Y *et al.*, 2019	atherosclerosis	LGMN can be used as a reference marker of atherosclerosis
Lunde NN *et al.*, 2020	acute cardiovascular events	LGMN was upregulated during acute cardiovascular events and was associated with improved outcome
Umei TC *et al.*, 2020	complex coronary lesions	Plasma LGMN level could become a biomarker for complex coronary lesions. High legumain levels in patients with CAD reflected coronary plaque instability
Yang H *et al.*, 2020	acute myocardial infarction	LGMN was not only a serological biomarker for inflammation and cardiac remodeling but also a pathogenic element responsible for the poor prognosis of AMI patients
Wei W *et al.*, 2021	peripheral artery disease	High serum LGMN was correlated with increased risk of PAD in T2DM patients
Wu J *et al.*, 2022	abdominal aortic aneurysm	LGMN is a novel biomarker of AAA with high diagnostic performance
He Y *et al.*, 2024	hypertension	Specifically targeting LGMN in Tregs may be an innovative approach for hypertension treatment

LGMN: legumain; PAH: pulmonary arterial hypertension; CAD: coronary artery disease; AMI: acute myocardial infarction; PAD: peripheral artery disease; T2DM: type 2 diabetes mellitus, AAA: abdominal aortic aneurysm.

LGMN binds and blocks integrin αvβ3, thereby attenuating Rho GTPase activation, downregulating VSMC differentiation markers [10]. This study also showed that LGMN deficiency or inhibition can inhibit ECM degradation and VSMC transformation to synthetic type, reducing the incidence, mortality and degree of aortic dilatation in animal models. The results show that LGMN may be a potential therapeutic target for thoracic aortic dissection.

No diagnostic biomarkers or therapeutic agents are approved for abdominal aortic aneurysm (AAA). A recent study identified potential diagnostic biomarkers through proteomics analysis of AAA patients and healthy control individuals [56]. It identified 39 differentially expressed plasma proteins and subjected them to ROC analysis. LGMN was screened as a key protein that could be used as a diagnostic biomarker for AAA and further validated by ELISA in a larger cohort. LGMN may become a novel biomarker or therapeutic target for AAA [56].

Discussion

Current studies indicate that LGMN may serve as a potential plasma biomarker for the diagnosis, severity, and prognosis of various CVDs (Table 1). Because the sensitivity and specificity of a single biomarker are often inadequate [58], the establishment of diagnostic models combining LGMN with other differentially expressed proteins or traditional biochemical indicators will further improve the diagnostic performance of LGMN for CVDs. Meanwhile, recent evidence suggests that LGMN is a multifunctional protein. In addition to LGMN's well-known lysosomal protease activity, its protease-independent functions have also been increasingly recognized, including regulation of inflammation, ECM remodeling, lipid metabolism, efferocytosis, and VSMC phenotypic transformation in CVDs (Figure 1). Therefore, LGMN is a promising therapeutic target for CVDs.

LGMN knockout inhibits the upregulation of proinflammatory cytokines in ischemia-reperfusion injury (IRI) induced acute kidney injury [59], providing evidence of the involvement of LGMN in the proinflammatory response. *In vitro*, LGMN increases the protein expression levels of Macrophage receptor with collagenous structure (MARCO) in macrophages [5], which may increase the protein expression levels of proinflammatory factors [60, 61]. Some *in vitro* studies findings suggest that LGMN may increase the expression of proinflammatory factors by increasing the expression of MARCO in macrophages. Some *in vitro* studies have shown that LGMN promotes the protein expression levels of anti-inflammatory factors in monocytes, inhibits monocyte activation and facilitates macrophage polarization toward the M2 type [48]. LGMN promotes the protein expression levels of the anti-inflammatory factors IL-10 and CD163 in primary monocytes and inhibits the protein expression levels of the proinflammatory cytokines MCP-1 and MPO. LGMN also inhibits the protein expression levels of CD14, an activation marker of monocytes. LGMN inhibits the protein expression levels of TLR2 and TLR4, which are markers of M1 macrophages, but increases the protein expression levels of MSR1, CD36, and CD163, which are markers of M2 macrophages [48]. These results identify anti-inflammatory mechanisms of LGMN in monocytes.

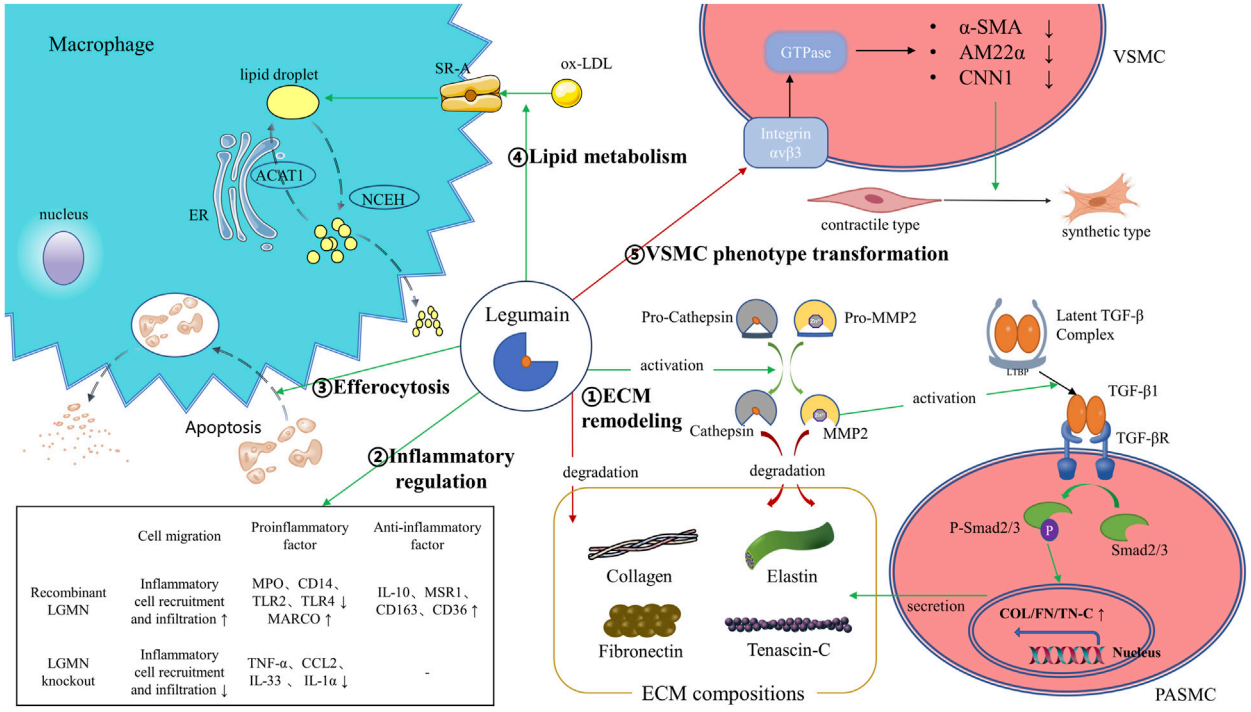

	Cell migration	Proinflammatory factor	Anti-inflammatory factor
Recombinant LGMN	Inflammatory cell recruitment and infiltration ↑	MPO、CD14、TLR2、TLR4 ↓ MARCO ↑	IL-10、MSR1、CD163、CD36 ↑
LGMN knockout	Inflammatory cell recruitment and infiltration ↓	TNF-α、CCL2、IL-33 、IL-1α ↓	-

FIGURE 1
Illustration of the legumain pathway. ①LGMN could promote ECM degradation by activation of proMMP-2, processing of cathepsins or by direct proteolysis of ECM components like fibronectin. Meanwhile, LGMN promotes ECM remodeling by activating the MMP-2/TGF-β1 signaling. ②LGMN is involved in regulating the recruitment and infiltration of inflammatory cells, as well as regulating the expression of intracellular inflammatory factors. ③LGMN promotes clearance and degradation of apoptotic cardiomyocytes by efferocytosis. ④LGMN promotes macrophage uptake of ox-LDL to form lipid droplets by increasing SR-A expression. ⑤LGMN binds and blocks integrin αvβ3, thereby attenuating Rho GTPase activation and downregulating VSMC differentiation markers. ER: endoplasmic reticulum; ACAT1: acyl-coenzyme A: cholesterol acyltransferase-1; NCEH: neutral cholesterol ester hydrolase; SR-A: scavenger receptor class A; ox-LDL: oxidized low-density lipoprotein; α-SMA: α−smooth muscle actin; AM22α: smooth muscle 22α; CNN1: calponin 1; TGF-β: transforming growth factor-β; PASMC: pulmonary artery smooth muscle cell; MARCO: macrophage receptor with collagenous structure; IL: Interleukin; MPO: myeloperoxidase.

LGMN induces monocyte/macrophage recruitment in atherosclerosis, and in animal models of stroke, LGMN promotes inflammatory cell infiltration at sites of cerebral ischemia [62]. The aforementioned reduction of acute IRI-induced kidney injury by LGMN knockout further substantiates LGMN recruitment of monocytes/macrophages [59]. In contrast, during myocardial infarction, LGMN deficiency increases macrophage infiltration and monocyte recruitment [38]. These seemingly contradictory results may be related to the functional differences in LGMN in monocytes/macrophages in different tissues and organs. In addition, LGMN promotes monocyte/macrophage recruitment in inflammatory disease, reduce monocyte/macrophage infiltration and promote inflammation regression by promoting efferocytosis. Further studies are required to clarify the mechanism of LGMN in the occurrence, progression, and regression of CVDs.

Recently, new mechanisms of LGMN have also been discovered. Ferroptosis, an iron-dependent mode of cell death associated with lipid peroxidation [63], is involved in CVDs such as atherosclerosis, PAH, myocardial infarction, and aortic aneurysm and dissection [64–66]. Recent studies of acute kidney injury implicated LGMN in the degradation of glutathione peroxidase 4 (GPX4), a key protective factor against ferroptosis, through molecular chaperone-mediated lysosomal autophagy [59]. LGMN-mediated promotion of ferroptosis may play the same role in CVDs, which warrants further investigation.

Age is an independent risk factor for CVDs, as large and medium-sized arteries in elderly individuals exhibit changes in vascular structure and function that lead to vascular disease [67]. Lysosomes are degradation centers and signaling hubs in cells that participate in aging-related metabolism [68, 69]. LGMN is one of the key proteins involved in lysosome function, promoting the progression of aging. The protein expression levels and activation of LGMN in the brain increased with age and were associated with age-related neurodegenerative diseases [70]. The progression of neurodegenerative diseases was attenuated by pharmacologic inhibition of LGMN [71]. In CVDs, the protein expression levels of LGMN was related to aging in

aortic tissue [23]. More research is needed to elucidate the underlying mechanism of LGMN in vascular aging.

Hypertension is one of the most important risk factors for CVDs. Recent studies have shown that gene expression levels of LGMN is significantly increased in $CD4^+$ T cells from hypertensive patients and mice [72]. LGMN directly interacts with and promotes the degradation of tumor necrosis factor receptor-associated factor 6 (TRAF6) through chaperone-mediated autophagy, thereby inhibiting NF-κB activation and impairing regulatory T-cell (Treg) differentiation and function to prevent hypertension and its complications [72]. LGMN may be an innovative approach for treating hypertension and deserves further study.

Statins reduce cholesterol synthesis by inhibiting hydroxymethylglutaryl coenzyme A reductase of the mevalonate pathway. Statins are effective agents for the treatment of CVDs, and their pleiotropic effects on patients include increased expression of genes involved in monocyte/macrophage apoptosis, inhibition of the inflammatory response, antioxidant effects, prevention of foam cell formation, and stabilization of atherosclerotic plaques [73]. The abundance of LGMN mRNA in circulating monocytes was reduced in patients treated with atorvastatin and was further validated *in vitro* [34, 73]. Additionally, in animal experiments, atorvastatin treatment reduced the abundance of LGMN in macrophages in aortic atherosclerotic plaques [74]. The inhibitory effect of statins on the abundance and activity of LGMN further demonstrates the promise of LGMN as a new therapeutic target for CVDs.

In summary, current evidence shows that LGMN is associated with CVDs such as atherosclerosis, PAD, PAH, CAD, aortic aneurysms and dissection. In most cases, LGMN plays a harmful role in CVDs, and animal experiments show that inhibiting the function or protein expression levels of LGMN can alleviate the development of atherosclerosis, PAH, and aortic dissection. Meanwhile, in specific conditions, LGMN can also play a beneficial effect in myocardial infarction. The platelet-derived LGMN has anti-inflammatory effects and may improve outcomes in ST-elevation myocardial infarction patients [48]. And cardiac resident macrophage-derived LGMN can improve cardiac repair by promoting clearance of apoptotic cardiomyocytes after myocardial infarction through phagocytosis [52]. The underlying mechanism of LGMN in different CVDs needs further study.

Conclusion

LGMN is a promising therapeutic target for CVDs. LGMN has both protease and non-protease functions and plays either deleterious of beneficial roles in different diseases depending on the cell source that secretes LGMN, which deserves further study. By understanding the pathogenesis and biomarker function of LGMN in CVDs, we will develop new strategies to prevent, diagnose, or treat these diseases.

Author contributions

JW proposed the concept; LZ and JW wrote the manuscript; YZ and ZW supervised the project and provided critical reviews on the manuscript. All authors contributed to the article and approved the submitted version.

Funding

The author(s) declare financial support was received for the research, authorship, and/or publication of this article. This work was supported by the Beijing Natural Science Foundation (5244054), the Natural Science Foundation of China (51890894, 82070492), the Chinese Academy of Medical Sciences, Innovation Fund for Medical Sciences (CIFMS 2021-I2M-1-016), and the National High Level Hospital Clinical Research Funding (2022-PUMCH-B-100, 2022-PUMCH-C-062).

Conflict of interest

The authors declare that the research was conducted in the absence of any commercial or financial relationships that could be construed as a potential conflict of interest.

References

1. Dagenais GR, Leong DP, Rangarajan S, Lanas F, Lopez-Jaramillo P, Gupta R, et al. Variations in common diseases, hospital admissions, and deaths in middle-aged adults in 21 countries from five continents (PURE): a prospective cohort study. *The Lancet* (2020) **395**(10226):785–94. doi:10.1016/s0140-6736(19)32007-0

2. Liu CL, Guo J, Zhang X, Sukhova GK, Libby P, Shi GP. Cysteine protease cathepsins in cardiovascular disease: from basic research to clinical trials. *Nat Rev Cardiol* (2018) **15**(6):351–70. doi:10.1038/s41569-018-0002-3

3. Chen JM, Dando PM, Rawlings ND, Brown MA, Young NE, Stevens RA, et al. Cloning, isolation, and characterization of mammalian legumain, an asparaginyl endopeptidase. *J Biol Chem* (1997) **272**(12):8090–8. doi:10.1074/jbc.272.12.8090

4. Kembhavi AA, Buttle DJ, Knight CG, Barrett AJ. The two cysteine endopeptidases of legume seeds: purification and characterization by use of specific fluorometric assays. *Arch Biochem Biophys* (1993) **303**(2):208–13. doi:10.1006/abbi.1993.1274

5. Ozawa N, Sato Y, Mori Y, Masuda H, Yamane M, Yamamoto Y, et al. Legumain promotes atherosclerotic vascular remodeling. *Int J Mol Sci* (2019) **20**(9):2195. doi:10.3390/ijms20092195

6. Tanaka T, Inazawa J, Nakamura Y. Molecular cloning of a human cDNA encoding putative cysteine protease (PRSC1) and its chromosome assignment to 14q32.1. *Cytogenet Genome Res* (1996) **74**(1-2):120–3. doi:10.1159/000134397

7. Dall E, Brandstetter H. Structure and function of legumain in health and disease. *Biochimie* (2016) **122**:126–50. doi:10.1016/j.biochi.2015.09.022

8. Solberg R, Lunde NN, Forbord KM, Okla M, Kassem M, Jafari A. The mammalian cysteine protease legumain in health and disease. *Int J Mol Sci* (2022) **23**(24):15983. doi:10.3390/ijms232415983

9. Zhang W, Lin Y. The mechanism of asparagine endopeptidase in the progression of malignant tumors: a review. *Cells* (2021) **10**(5):1153. doi:10.3390/cells10051153

10. Pan L, Bai P, Weng X, Liu J, Chen Y, Chen S, et al. Legumain is an endogenous modulator of integrin αvβ3 triggering vascular degeneration, dissection, and rupture. *Circulation* (2022) **145**(9):659–74. doi:10.1161/circulationaha.121.056640

11. Pang L, Guo S, Khan F, Dunterman M, Ali H, Liu Y, et al. Hypoxia-driven protease legumain promotes immunosuppression in glioblastoma. *Cell Rep Med* (2023) **4**(11):101238. doi:10.1016/j.xcrm.2023.101238

12. Xuan W, Hsu WH, Khan F, Dunterman M, Pang L, Wainwright DA, et al. Circadian regulator CLOCK drives immunosuppression in glioblastoma. *Cancer Immunol Res* (2022) **10**(6):770–84. doi:10.1158/2326-6066.cir-21-0559

13. Lunde NN, Holm S, Dahl TB, Elyouncha I, Sporsheim B, Gregersen I, et al. Increased levels of legumain in plasma and plaques from patients with carotid atherosclerosis. *Atherosclerosis* (2017) **257**:216–23. doi:10.1016/j.atherosclerosis.2016.11.026

14. Liu J, Sukhova GK, Yang JT, Sun J, Ma L, Ren A, et al. Cathepsin L expression and regulation in human abdominal aortic aneurysm, atherosclerosis, and vascular cells. *Atherosclerosis* (2006) **184**(2):302–11. doi:10.1016/j.atherosclerosis.2005.05.012

15. Sukhova GK, Shi GP, Simon DI, Chapman HA, Libby P. Expression of the elastolytic cathepsins S and K in human atheroma and regulation of their production in smooth muscle cells. *J Clin Invest* (1998) **102**(3):576–83. doi:10.1172/jci181

16. Shi GP, Dolganov GM. Comprehensive transcriptome of proteases and protease inhibitors in vascular cells. *Stroke* (2006) **37**(2):537–41. doi:10.1161/01.str.0000198816.62266.e9

17. Poreba M. Recent advances in the development of legumain-selective chemical probes and peptide prodrugs. *Biol Chem* (2019) **400**(12):1529–50. doi:10.1515/hsz-2019-0135

18. Yang H, He Y, Zou P, Hu Y, Li X, Tang L, et al. Legumain is a predictor of all-cause mortality and potential therapeutic target in acute myocardial infarction. *Cell Death Dis* (2020) **11**(11):1014. doi:10.1038/s41419-020-03211-4

19. Bai P, Lyu L, Yu T, Zuo C, Fu J, He Y, et al. Macrophage-derived legumain promotes pulmonary hypertension by activating the MMP (matrix metalloproteinase)-2/TGF (transforming growth factor)-β1 signaling. *Arteriosclerosis, Thromb Vasc Biol* (2019) **39**(4):e130–e145. doi:10.1161/atvbaha.118.312254

20. Munjal A, Khandia R. Atherosclerosis: orchestrating cells and biomolecules involved in its activation and inhibition. *Adv Protein Chem Struct Biol* (2020) **120**:85–122. doi:10.1016/bs.apcsb.2019.11.002

21. Ruiz-León AM, Lapuente M, Estruch R, Casas R. Clinical advances in immunonutrition and atherosclerosis: a review. *Front Immunol* (2019) **10**:837. doi:10.3389/fimmu.2019.00837

22. Papaspyridonos M, Smith A, Burnand KG, Taylor P, Padayachee S, Suckling KE, et al. Novel candidate genes in unstable areas of human atherosclerotic plaques. *Arteriosclerosis, Thromb Vasc Biol* (2006) **26**(8):1837–44. doi:10.1161/01.atv.0000229695.68416.76

23. Clerin V, Shih HH, Deng N, Hebert G, Resmini C, Shields KM, et al. Expression of the cysteine protease legumain in vascular lesions and functional implications in atherogenesis. *Atherosclerosis* (2008) **201**(1):53–66. doi:10.1016/j.atherosclerosis.2008.01.016

24. Wang W, Wu J, Liu P, Tang X, Pang H, Xie T, et al. Urinary proteomics identifying novel biomarkers for the diagnosis and phenotyping of carotid artery stenosis. *Front Mol Biosci* (2021) **8**:714706. doi:10.3389/fmolb.2021.714706

25. Shirahama-Noda K, Yamamoto A, Sugihara K, Hashimoto N, Asano M, Nishimura M, et al. Biosynthetic processing of cathepsins and lysosomal degradation are abolished in asparaginyl endopeptidase-deficient mice. *J Biol Chem* (2003) **278**(35):33194–9. doi:10.1074/jbc.m302742200

26. Chen JM, Fortunato M, Stevens RA, Barrett AJ. Activation of progelatinase A by mammalian legumain, a recently discovered cysteine proteinase. *Biol Chem* (2001) **382**(5):777–83. doi:10.1515/bc.2001.093

27. Reddy VY, Zhang QY, Weiss SJ. Pericellular mobilization of the tissue-destructive cysteine proteinases, cathepsins B, L, and S, by human monocyte-derived macrophages. *Proc Natl Acad Sci U S A* (1995) **92**(9):3849–53. doi:10.1073/pnas.92.9.3849

28. Mattock KL, Gough PJ, Humphries J, Burnand K, Patel L, Suckling KE, et al. Legumain and cathepsin-L expression in human unstable carotid plaque. *Atherosclerosis* (2010) **208**(1):83–9. doi:10.1016/j.atherosclerosis.2009.07.022

29. Nagase H, Visse R, Murphy G. Structure and function of matrix metalloproteinases and TIMPs. *Cardiovasc Res* (2006) **69**(3):562–73. doi:10.1016/j.cardiores.2005.12.002

30. Morita Y, Araki H, Sugimoto T, Takeuchi K, Yamane T, Maeda T, et al. Legumain/asparaginyl endopeptidase controls extracellular matrix remodeling through the degradation of fibronectin in mouse renal proximal tubular cells. *FEBS Lett* (2007) **581**(7):1417–24. doi:10.1016/j.febslet.2007.02.064

31. Lin Y, Wei C, Liu Y, Qiu Y, Liu C, Guo F. Selective ablation of tumor-associated macrophages suppresses metastasis and angiogenesis. *Cancer Sci* (2013) **104**(9):1217–25. doi:10.1111/cas.12202

32. Wang H, Chen B, Lin Y, Zhou Y, Li X. Legumain promotes gastric cancer progression through tumor-associated macrophages *in vitro* and *in vivo*. *Int J Biol Sci* (2020) **16**(1):172–80. doi:10.7150/ijbs.36467

33. Camaré C, Pucelle M, Nègre-Salvayre A, Salvayre R. Angiogenesis in the atherosclerotic plaque. *Redox Biol* (2017) **12**:18–34. doi:10.1016/j.redox.2017.01.007

34. Solberg R, Smith R, Almlöf M, Tewolde E, Nilsen H, Johansen HT. Legumain expression, activity and secretion are increased during monocyte-to-macrophage differentiation and inhibited by atorvastatin. *Biol Chem* (2015) **396**(1):71–80. doi:10.1515/hsz-2014-0172

35. Fan J, Watanabe T. Atherosclerosis: known and unknown. *Pathol Int* (2022) **72**(3):151–60. doi:10.1111/pin.13202

36. Yu XH, Fu YC, Zhang DW, Yin K, Tang CK. Foam cells in atherosclerosis. *Clinica Chim Acta* (2013) **424**:245–52. doi:10.1016/j.cca.2013.06.006

37. Ghosh S, Zhao B, Bie J, Song J. Macrophage cholesteryl ester mobilization and atherosclerosis. *Vasc Pharmacol* (2010) **52**(1-2):1–10. doi:10.1016/j.vph.2009.10.002

38. Shamaki GR, Markson F, Soji-Ayoade D, Agwuegbo CC, Bamgbose MO, Tamunoinemi BM. Peripheral artery disease: a comprehensive updated review. *Curr Probl Cardiol* (2022) **47**(11):101082. doi:10.1016/j.cpcardiol.2021.101082

39. Morley RL, Sharma A, Horsch AD, Hinchliffe RJ. Peripheral artery disease. *BMJ* (2018) **360**:j5842. doi:10.1136/bmj.j5842

40. Wei W, Chen S, Huang J, Tong Y, Zhang J, Qiu X, et al. Serum legumain is associated with peripheral artery disease in patients with type 2 diabetes. *J Diabetes Res* (2021) **2021**:1–7. doi:10.1155/2021/5651469

41. Poch D, Mandel J. Pulmonary hypertension. *Ann Intern Med* (2021) **174**(4):Itc49–itc64. doi:10.7326/aitc202104200

42. Thenappan T, Chan SY, Weir EK. Role of extracellular matrix in the pathogenesis of pulmonary arterial hypertension. *Am J Physiology-Heart Circulatory Physiol* (2018) **315**(5):H1322–h1331. doi:10.1152/ajpheart.00136.2018

43. Meng XM, Nikolic-Paterson DJ, Lan HY. TGF-β: the master regulator of fibrosis. *Nat Rev Nephrol* (2016) **12**(6):325–38. doi:10.1038/nrneph.2016.48

44. Peng D, Fu M, Wang M, Wei Y, Wei X. Targeting TGF-β signal transduction for fibrosis and cancer therapy. *Mol Cancer* (2022) **21**(1):104. doi:10.1186/s12943-022-01569-x

45. Yung LM, Nikolic I, Paskin-Flerlage SD, Pearsall RS, Kumar R, Yu PB. A selective transforming growth factor-β ligand trap attenuates pulmonary hypertension. *Am J Respir Crit Care Med* (2016) **194**(9):1140–51. doi:10.1164/rccm.201510-1955oc

46. Roth GA, Abate D, Abate KH, Abay SM, Abbafati C, Abbasi N, et al. Global, regional, and national age-sex-specific mortality for 282 causes of death in 195 countries and territories, 1980-2017: a systematic analysis for the Global Burden of Disease Study 2017. *The Lancet* (2018) **392**(10159):1736–88. doi:10.1016/s0140-6736(18)32203-7

47. Gregersen I, Michelsen AE, Lunde NN, Åkerblom A, Lakic TG, Skjelland M, et al. Legumain in acute coronary syndromes: a substudy of the plato (platelet inhibition and patient outcomes) trial. *J Am Heart Assoc* (2020) **9**(17):e016360. doi:10.1161/jaha.120.016360

48. Lunde NN, Gregersen I, Ueland T, Shetelig C, Holm S, Kong XY, et al. Legumain is upregulated in acute cardiovascular events and associated with improved outcome - potentially related to anti-inflammatory effects on macrophages. *Atherosclerosis* (2020) **296**:74–82. doi:10.1016/j.atherosclerosis.2019.12.008

49. Umei TC, Kishimoto Y, Aoyama M, Saita E, Niki H, Ikegami Y, et al. High plasma levels of legumain in patients with complex coronary lesions. *J Atheroscler Thromb* (2020) **27**(7):711–7. doi:10.5551/jat.52027

50. Doran AC, Yurdagul A, Jr, Tabas I. Efferocytosis in health and disease. *Nat Rev Immunol* (2020) **20**(4):254–67. doi:10.1038/s41577-019-0240-6

51. Boada-Romero E, Martinez J, Heckmann BL, Green DR. The clearance of dead cells by efferocytosis. *Nat Rev Mol Cell Biol* (2020) **21**(7):398–414. doi:10.1038/s41580-020-0232-1

52. Jia D, Chen S, Bai P, Luo C, Liu J, Sun A, et al. Cardiac resident macrophage-derived legumain improves cardiac repair by promoting clearance and degradation of apoptotic cardiomyocytes after myocardial infarction. *Circulation* (2022) **145**(20):1542–56. doi:10.1161/circulationaha.121.057549

53. Sakalihasan N, Michel JB, Katsargyris A, Kuivaniemi H, Defraigne JO, Nchimi A, et al. Abdominal aortic aneurysms. *Nat Rev Dis Primers* (2018) **4**(1):34. doi:10.1038/s41572-018-0030-7

54. Qian G, Adeyanju O, Olajuyin A, Guo X. Abdominal aortic aneurysm formation with a focus on vascular smooth muscle cells. *Life* (2022) **12**(2):191. doi:10.3390/life12020191

55. Wang Y, Gao P, Li F, Du J. Insights on aortic aneurysm and dissection: role of the extracellular environment in vascular homeostasis. *J Mol Cell Cardiol* (2022) **171**:90–101. doi:10.1016/j.yjmcc.2022.06.010

56. Wu J, Wang W, Xie T, Chen Z, Zhou L, Song X, et al. Identification of novel plasma biomarkers for abdominal aortic aneurysm by protein array analysis. *Biomolecules* (2022) **12**(12):1853. doi:10.3390/biom12121853

57. Owens GK, Kumar MS, Wamhoff BR. Molecular regulation of vascular smooth muscle cell differentiation in development and disease. *Physiol Rev* (2004) **84**(3):767–801. doi:10.1152/physrev.00041.2003

58. Wu J, Wang W, Chen Z, Xu F, Zheng Y. Proteomics applications in biomarker discovery and pathogenesis for abdominal aortic aneurysm. *Expert Rev Proteomics* (2021) **18**(4):305–14. doi:10.1080/14789450.2021.1916473

59. Chen C, Wang D, Yu Y, Zhao T, Min N, Wu Y, et al. Legumain promotes tubular ferroptosis by facilitating chaperone-mediated autophagy of GPX4 in AKI. *Cell Death Dis* (2021) **12**(1):65. doi:10.1038/s41419-020-03362-4

60. Cai T, Xu L, Xia D, Zhu L, Lin Y, Yu S, et al. Polyguanine alleviated autoimmune hepatitis through regulation of macrophage receptor with collagenous structure and TLR4-TRIF-NF-κB signalling. *J Cell Mol Med* (2022) **26**(22):5690–701. doi:10.1111/jcmm.17599

61. Bowdish DM, Sakamoto K, Kim MJ, Kroos M, Mukhopadhyay S, Leifer CA, et al. MARCO, TLR2, and CD14 are required for macrophage cytokine responses to mycobacterial trehalose dimycolate and *Mycobacterium tuberculosis*. *Plos Pathog* (2009) **5**(6):e1000474. doi:10.1371/journal.ppat.1000474

62. Ishizaki T, Erickson A, Kuric E, Shamloo M, Hara-Nishimura I, Inácio AR, et al. The asparaginyl endopeptidase legumain after experimental stroke. *J Cereb Blood Flow Metab* (2010) **30**(10):1756–66. doi:10.1038/jcbfm.2010.39

63. Dixon SJ, Lemberg KM, Lamprecht MR, Skouta R, Zaitsev EM, Gleason CE, et al. Ferroptosis: an iron-dependent form of nonapoptotic cell death. *Cell* (2012) **149**(5):1060–72. doi:10.1016/j.cell.2012.03.042

64. Chen Y, Li X, Wang S, Miao R, Zhong J. Targeting iron metabolism and ferroptosis as novel therapeutic approaches in cardiovascular diseases. *Nutrients* (2023) **15**(3):591. doi:10.3390/nu15030591

65. Li N, Yi X, He Y, Huo B, Chen Y, Zhang Z, et al. Targeting ferroptosis as a novel approach to alleviate aortic dissection. *Int J Biol Sci* (2022) **18**(10):4118–34. doi:10.7150/ijbs.72528

66. Ren J, Lv Y, Wu L, Chen S, Lei C, Yang D, et al. Key ferroptosis-related genes in abdominal aortic aneurysm formation and rupture as determined by combining bioinformatics techniques. *Front Cardiovasc Med* (2022) **9**:875434. doi:10.3389/fcvm.2022.875434

67. Costantino S, Paneni F, Cosentino F. Ageing, metabolism and cardiovascular disease. *J Physiol* (2016) **594**(8):2061–73. doi:10.1113/jp270538

68. Carmona-Gutierrez D, Hughes AL, Madeo F, Ruckenstuhl C. The crucial impact of lysosomes in aging and longevity. *Ageing Res Rev* (2016) **32**:2–12. doi:10.1016/j.arr.2016.04.009

69. Leeman DS, Hebestreit K, Ruetz T, Webb AE, McKay A, Pollina EA, et al. Lysosome activation clears aggregates and enhances quiescent neural stem cell activation during aging. *Science* (2018) **359**(6381):1277–83. doi:10.1126/science.aag3048

70. Zhang Z, Tian Y, Ye K. δ-secretase in neurodegenerative diseases: mechanisms, regulators and therapeutic opportunities. *Transl Neurodegener* (2020) **9**:1. doi:10.1186/s40035-019-0179-3

71. Wang J, Hu HJ, Liu ZK, Liu JJ, Wang SS, Cheng Q, et al. Pharmacological inhibition of asparaginyl endopeptidase by δ-secretase inhibitor 11 mitigates Alzheimer's disease-related pathologies in a senescence-accelerated mouse model. *Transl Neurodegener* (2021) **10**(1):12. doi:10.1186/s40035-021-00235-4

72. He Y, Zou P, Lu J, Lu Y, Yuan S, Zheng X, et al. CD4+ T-cell legumain deficiency attenuates hypertensive damage via preservation of TRAF6. *Circ Res* (2024) **134**(1):9–29. doi:10.1161/circresaha.123.322835

73. Wang ZH, Liu XL, Zhong M, Zhang LP, Shang YY, Hu XY, et al. Pleiotropic effects of atorvastatin on monocytes in atherosclerotic patients. *J Clin Pharmacol* (2010) **50**(3):311–9. doi:10.1177/0091270009340889

74. Fang Y, Duan C, Chen S, Xie P, Ai W, Wang L, et al. Increased Legumain/Smad3 expression in atherosclerotic plaque of rat thoracic aorta. *Biomed Pharmacother* (2019) **119**:109353. doi:10.1016/j.biopha.2019.109353

EBM Experimental Biology and Medicine

TYPE Retraction
PUBLISHED 25 June 2024
DOI 10.3389/ebm.2024.10275

OPEN ACCESS

*CORRESPONDENCE
EBM Editorial Office,
ebm@ebm-journal.org

RECEIVED 06 June 2024
ACCEPTED 07 June 2024
PUBLISHED 25 June 2024

CITATION
EBM Editorial Office (2024), Retraction: MicroRNA-34a alleviates steroid-induced avascular necrosis of femoral head by targeting Tgif2 through OPG/RANK/RANKL signaling pathway. *Exp. Biol. Med.* 249:10275. doi: 10.3389/ebm.2024.10275

Retraction: MicroRNA-34a alleviates steroid-induced avascular necrosis of femoral head by targeting Tgif2 through OPG/RANK/RANKL signaling pathway

EBM Editorial Office*

A Retraction of the Original Research Article

MicroRNA-34a alleviates steroid-induced avascular necrosis of femoral head by targeting Tgif2 through OPG/RANK/RANKL signaling pathway

by Peng W. X., Ye C., Dong W. T., Yang L. L., Wang C. Q., Wei Z. A., Wu J. H., Li Q., Deng J., and Zhang J. (2017). Experimental Biology and Medicine. 242(12):1234–1243. doi: 10.1177/1535370217703975

Following publication, the authors contacted the Editorial Office to request the retraction of the cited article, stating that concerns were raised on the PubPeer platform regarding the reuse of certain images, as well as concerns over incomplete data. Particularly, in Figure 3, Panels c and d appear to overlap. Those panels also show duplication with Figure 11B from Zhang et al 2017 and Figure 5 from Yu et al 2019 (both retracted sources). Further, in Tables 2, 3 values are shown as means ± standard deviation and no exact measurements are provided. Therefore, the article has been retracted.

Figure 3 appears to show an overlap between panels (c) and (d).

Tables 2, 3 show values as means +/− deviation, no exact measurements provided.

This retraction was approved by the Editor-in-Chief of Experimental Biology and Medicine. The authors received communication regarding the retraction but did not respond. The communication has been recorded by the publisher.

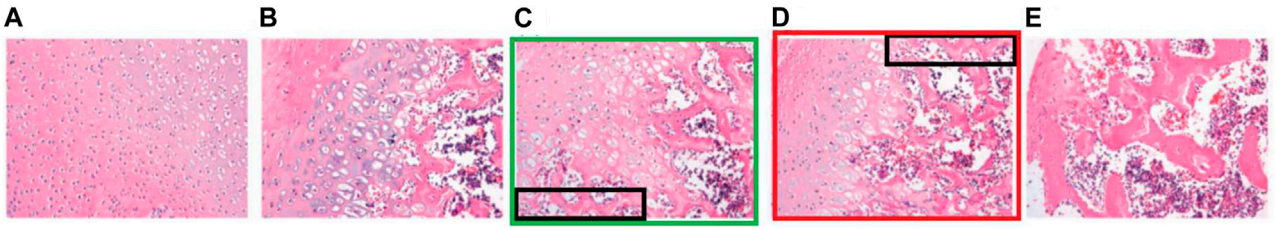

FIGURE 3
Comparison of the morphology changes in the femoral head by HE staining among (x100) among normal control, model control, negative control, miR-34a mimics and miR-34a inhibitor groups. **(A)**, normal control group; **(B)**, model control group; **(C)**, negative control group; **(D)**, miR-34a mimics group; **(E)**, miR-34a inhibitors group; miR-34a, miRNA-34a. (A color version of this figure is available in the online journal).

TABLE 2 Comparison of parameters of trabecular in the cancellous bone within the unit volume of the center of the femoral head between normal control group and model control group.

Group	BV/TV	BS/BV	Tb.Th	Tb.N
Normal control group	0.72 ± 0.07	25.07 ± 2.52	0.14 ± 0.02	6.34 ± 0.63
model control group	0.59 ± 0.06[a]	21.25 ± 2.10[a]	0.13 ± 0.01	5.83 ± 0.58[a]

[a]Compared with the normal control group, $p < 0.05$; BV/TV, bone volume/total volume. BS/BV, bone surface area/bone volume; Tb.Th, trabecular thickness; Tb.N, trabecular number.

TABLE 3 Comparison of parameters of trabecular in the cancellous bone within the unit volume of the center of the femoral head among normal control, model control, negative control, miR-34a mimics and miR-34a inhibitor groups.

Group	BV/TV	BS/BV	Tb.Th	Tb.N
Normal control	0.71 ± 0.07	24.92 ± 2.51	0.14 ± 0.03	7.02 ± 0.69
Model control	0.55 ± 0.05[a]	20.13 ± 2.01[a]	0.13 ± 0.02	5.65 ± 0.56[a]
Negative control	0.52 + 0.05[a]	20.07 ± 2.00[a]	0.13 ± 0.02	5.63 ± 0.56[a]
miR-34a inhibitor	0.46 ± 0.04[a,b]	17.75 ± 1.75[a,b]	0.15 ± 0.04	5.00 ± 0.51[a,b]
miR-34a mimics	0.63 ± 0.06[a,b]	22.39 ± 2.22[a,b]	0.14 ± 0.02	6.39 + 0.63[a,b]

[a]Compared to normal control group, $p < 0.05$.
[b]Compared to model control group, $p < 0.05$. BV/TV, bone volume/total volume; BS/BV, bone surface area/bone volume; Tb.Th, trabecular thickness; Tb.N, trabecular number.

Experimental Biology & Medicine Conference

Orlando, FL - October 13 -16, 2024

Please visit **exbiomedcon.org** or scan the QR code for more info.

Keynote Lecturers

Namandjè Bumpus, Ph.D.
Chief Scientist - US Food and Drug Administration

Advancing Emerging Technologies in Regulatory Science

Michael Friedlander, Ph.D.
Vice President - Health Sciences and Technology at Virginia Tech

All events will take place at the Embassy Suites by Hilton, Orlando Lake Buena Vista South

Cardiovascular

Delphine Gomez, Ph.D.
University of Pittsburgh

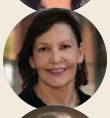

Karen Hirschi, Ph.D.
University of Virginia

Jay Humphrey, Ph.D.
Yale University

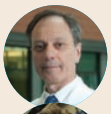

Ali J. Marian, M.D.
The University of Texas Health Science Center at Houston

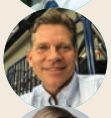

Joseph Miano, Ph.D.
Medical College of Georgia

Dianna Milewicz, M.D., Ph.D.
University of Texas Heath Science Center Houston

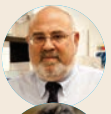

Robert Schwartz, Ph.D.
University of Houston

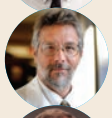

George Taffet, M.D.
Baylor College of Medicine

David Zawieja, Ph.D.
Texas A&M University Health Science Center

Neuroscience

Lique Coolen, Ph.D.
Kent State university

Michael Fehlings, M.D.
University of Toronto

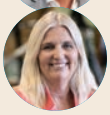

Susan Harkema, Ph.D.
University of Louisville

Maria Lehtinen, Ph.D.
Harvard University

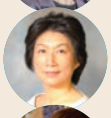

Fang Liu, Ph.D.
NCTR/US Food and Drug Administration

Agnes Luo, Ph.D.
University Cincinnati

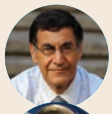

Mervyn Maze, MBChB
University of California San Francisco

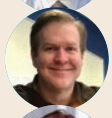

Dorian McGavern, Ph.D.
National Institute of Neurological Diorders and Stroke

Vesna Jevtovic-Todorovic, M.D., Ph.D.
University of Colorado School of Medicine

Regenerative Medicine

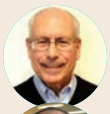

Arnold I. Caplan, Ph.D.
Case Western Reserve

Jian Feng, Ph.D.
State University of New York at Buffalo

Joshua Hare, M.D.
University of Miami

Karen Hasty, Ph.D.
University of Tennessee Health Science Center

Rajasingh Johnson, Ph.D.
University of Tennessee Health Science Center

Y. James Kang, DVM, Ph.D.
Sichuan University

Kwang-Soo Kim,Ph.D.
Harvard University

Joanne Kurtzberg, M.D.
Duke University

Jun Wu, Ph.D.
UT Southwestern

Trainees

Justin Boyd, Ph.D.
Vaxxinity

Udayan Apte, Ph.D.
U of Kansas Medical Center

Ram Kumar, Ph.D.
U of Kansas Medical Center

And More

Career Development
Short Talks
Poster Sessions
Member Blitz

SEBM SOCIETY FOR EXPERIMENTAL BIOLOGY AND MEDICINE

EBM Experimental Biology and Medicine

Scope

Experimental Biology and Medicine (EBM) is a global, peer-reviewed journal dedicated to the publication of multidisciplinary and interdisciplinary research in the biomedical sciences. The journal covers the spectrum of translational research from T0, basic research, to T4, population health. Articles in EBM represent cutting edge research at the overlapping junctions of the biological, physical and engineering sciences that impact upon the health and welfare of the world's population. EBM is particularly appropriate for publication of papers that are multidisciplinary in nature, are of potential interest to a wide audience, and represent experimental medicine in the broadest sense of the term. However, manuscripts reporting novel findings on any topic in the realm of experimental biology and medicine are most welcome.

EBM publishes Research, Reviews, Mini Reviews, and Brief Communications in the following categories.

- Anatomy/Pathology
- Artificial Intelligence/ Machine Learning Applications to Biomedical Research
- Biochemistry and Molecular Biology
- Bioimaging
- Biomedical Engineering
- Bionanoscience
- Cell and Developmental Biology
- Clinical Trials
- Endocrinology and Nutrition
- Environmental Health/Biomarkers/ Precision Medicine
- Genomics, Proteomics, and Bioinformatics
- Immunology/Microbiology/Virology
- Mechanisms of Aging
- Neuroscience
- Pharmacology and Toxicology
- Physiology and Pathophysiology
- Population Health
- Stem Cell Biology
- Structural Biology
- Synthetic Biology
- Systems Biology and Microphysiological Systems
- Translational Research

EBM Experimental Biology and Medicine

EBM is the official journal of the Society for Experimental Biology and Medicine

Led by Dr Steven Goodman, Experimental Biology and Medicine (EBM) is a global, peer-reviewed journal dedicated to the publication of multidisciplinary and interdisciplinary research in the biomedical sciences.

Discover more of our Special Issues

See more →

Contact

development@ebm-journal.org

See more

ebm-journal.org

publishingpartnerships.frontiersin.org/our-partners